ANDREW PETER INCE

THE CULTIVATION OF MARINE MICROALGAE WITHIN A TUBULAR PHOTOBIOREACTOR AS A SOURCE OF POLYUNSATURATED FATTY ACIDS

Liverpool John Moores University
School of Biological & Earth Sciences

2006

Ph.D THESIS

CONTENTS — PAGE

TABLES; FIGURES; PLATES & EQUATIONS ——— PAGE-

TABLES

TABLES *continued...*

FIGURES

FIGURES *continued...*

FIGURES *continued...*

FIGURES *continued...*

PLATES

PLATES *continued...*

EQUATIONS

Preface

The diversely branched field of biotechnology is more often lead by the primordial roots of our evolution. A fact generally overlooked within modern life, yet our ancestral lungs remain ubiquitous throughout nature. As with many parents they remain a continuing source of guidance. The following poem by Lewin (1987) poignantly summarises the founding role played by microalgae from Earth's fruition to our present day advances in biotechnology:

In the beginning

In the beginning the earth was all wet;
We hadn't got life- or ecology- yet.
There were larva and rocks- quite a lot of them both-
And oceans of nutrient Oparin broth.
But then there arose, at the edge of the sea,
Where sugars and organic acids were free,
A sort of a blob in a kind of coat-
The earliest protero- prokaryote.
It grew and divided: it flourished and fed;
From puddle to puddle it rapidly spread.
Until it depleted the ocean's store
And nary an acid was found any more.

Now, if one considered that terrible trend,
One might have predicted that that was the end-
But no! In some sunny wee lochan or slough
Appeared a new creature- we cannot say how.
By some strange transition that nobody knows,
A photosynthetical alga arose.
It grew and it flourished where nothing had been
Till much of the land was a blue shade of green
And bubbles of oxygen started to rise
Throughout the world's oceans, and filled up the skies;
While, off in the antediluvian mists,
Arose a few species with heterocysts
Which, by a procedure which no-one can tell,
Fixed gaseous nitrogen into the cell.

As the gases turned on and the gases turned off,
There emerged a respiring young heterotroph.
It grew in it's turn, and it lived and it throve,
Creating fine structure, genetics and love,
And using its enzymes and oxygen-2,
Produced such fine creatures as coli and you.

This, then is the story of life's evolution
From Oparin broth to the final solution.
So, prokaryologists, dinna forget:
We've come a long way since the world was all wet.
We owe a great deal- you can see from these notes-
To photosynthetical prokaryotes.

ABSTRACT

A helical tubular photobioreactor design was investigated to determine the productivity of two algal strains (*Isochrysis galbana* and *Nannochloropsis oculata*) both rich in PUFAs (mainly DHA and EPA, respectively). The photobioreactor occupied a footprint area of 1.13 m^2 with a working volume of 70 L, 61 % (43 L) of which was attributed to the photostage (with an i.d. of 24 mm). The ratio of cross-sectional area between the downcomer and riser of the air-lift (Ar:Ad) was 0.82, and light intermittency ratio of the recirculating cultures was 9 : 1 (light to dark zones). Cultures grown in the photobioreactor were recirculated using an air-lift at 15 L/min, giving cells a linear fluid velocity of 0.47 m/sec around the photostage and a total system recirculation time of 136 sec (90 % of which was in the photostage), when using a 'standard sparge plate' (69 × 1 mm pores). This sparge plate configuration was found to be the optimum when measuring mass transfer (K_La 19 Hr^{-1}). Reducing pore size was statistically shown to increase fluid flow rates and consequently Reynolds number (~28000 at 15 L/min, air flow), whereas changing pore density had no significant effect. It is estimated that during fed-batch growth of *I. galbana* and *N. oculata* (with average daily harvest volumes of 7.06 and 6.19 $L/m^2/day$, respectively) in the photobioreactor produced an areal volumetric PUFA yield of 2.87 (27 % DHA) and 2.62 (65 % EPA) $mg/L/m^2/day$, respectively.

CHAPTER 1: INTRODUCTION

1.1: MICROALGAE OR PHYTOPLANKTON?

The terms microalgae and phytoplankton are generally used interchangeably, but typically refer to microscopic organisms able to harvest light energy using pigments to provide chemical energy for the building blocks of life (proteins, carbohydrates and lipids). The word 'algae' refers to plant-like organisms that inhabit aquatic environments, lacking any true vascular or root systems, which are still able to convert light into chemical energy via photosynthesis. In fact, because they lack any photosynthetically inactive cells such as roots and trunks, algae are more efficient at utilizing light energy than higher plants (Pulz and Scheibenbogen, 1998). Although algae vary in size they can be generally placed into two distinct groups, known as the seaweeds (macroalgae) and the phytoplankton (microalgae). The word "plankton" originates from a Greek word (πλανκτοζ, pronounced *plun-oonk-tosd*) meaning 'wanderers' or 'drifters' which was first coined in 1887 by the German scientist Victor Heusen, with reference to the microscopic organisms found within any natural body of water (Ghosal *et al.*, 2000). These planktonic micro-organisms were divided into two distinct groups- *phyto*plankton and *zoo*plankton. The former contain pigments which allows them to photosynthesise, whilst the latter are unable to photosynthesise and instead sustain themselves by 'grazing' directly upon phytoplankton.

The term 'phytoplankton' is a generic name used to encompass the numerous sub-species of dinoflagellates, diatoms and microalgae, all of which can usually be found within the top 200 mm of the waters surface. Collectively covering over 70 % of the Earth's surface they act as the primary producers of the world's rivers and oceans and include more than 40,000 separate species of floating or swimming organisms (using simple flagella), responsible for more than 90 % of the total photosynthetic activity in the seas (Pulz and Scheibenbogen, 1998). Phytoplankton have also been estimated to contribute some 40 % of the planets total annual primary (photosynthetic) production (Pileke, 1995), accounting for 30 – 60 % of the global fixation of carbon (approximately 35 - 45 gigatonnes/ year according to Sakshaug *et al.*, 1997). By converting sunlight into vital nutrients they in-turn support the progressive trophic

levels of zooplankton, developing fish larvae, invertebrates, molluscs and coral reefs (Benemann, 1990). These organisms take many forms (unicellular, undifferentiated multicellular filaments or colonies) and yet are individually invisible to the human eye (each being typically less than 30 μm), making-up only 1 – 2 % of the total global biomass (Sakshaug *et al.*, 1997). Yet, in high enough cell densities they can change the colour of the water, which in the case of large algal blooms can become visible from space (Ghosal *et al.*, 2000). The reason for this colouration is due to the pigments contained within the cells chromoplast (see Section 1.9.2), which are used to harvest light energy (photons). Colours can vary from greens, browns, and reds (e.g. Section 4.1, Plate 6).

Although small microalgae represent perhaps the longest living ecosystem on the planet, having been dated as far back as 3.7 billion years ago, in the form of filamentous prokaryotic microalgae (Cyanobacteria) which have been helping to support life on Earth ever since (Graham and Wilcox, 2000; Schopf, 1996). Microalgae go through various morphological changes as a result of both their natural life-cycle, but also in response to abiotic factors. Actively motile cells during exponential growth are called 'zooids'. Cells entering the stationary phase period of their life-cycle become slightly larger and less motile and are often referred to as 'palmella cells'. During periods of adverse conditions or towards cell death cells can form cysts, whereby the cell wall becomes hardened allowing cells to survive extremes. However, perhaps the clearest evidence within the fossil record can be seen in the remnants of calcium carbonate scales called coccoliths (*Kokkos* = berry; *lithos* = rock) produced by some algal strains (Haptophytes) which date back to the late Triassic era (220 million years ago) (Graham and Wilcox, 2000).

1.2: GENERAL HISTORY AND TRENDS OF MICROALGAL PRODUCTS

Whilst alga products, such as the humble agar Plate, have long been used by many scientists (most historically by Alexander Fleming in 1929, in isolating Penicillin), interest in microalgal biotechnology truly began as a means of treating sewage (Oswald, 1963). The application of microalgal products has become increasingly varied (Tramper *et al.*, 2003), from waste treatment to renewable fuel sources (biofuels) (Pulz and Scheibenbogen, 1998; NREL, 1996; Bonalberti and Croatto, 1985). However, the majority of applications today involve human health food supplements (preventative) and pharmaceutical (curative) treatments. Reviews of various microalgal metabolites and their uses have been highlighted by many authors (Olaizola, 2003; Tramper, *et al.*, 2003; Duerr *et al.*, 1998; Borowitzka, 1997; Yamaguchi, 1997; Benemann, 1990; Watanabe *et al.*, 1983). The four main current markets of microalgal products include single-cell protein, food colourings, human health food supplements and as aquaculture feeds.

1.2.1: From single-cell proteins to human health food supplements

Interest in microalage as a potential food source had begun in the late 1800s but ground to a virtual halt during the World War I and II (Pulz and Scheibenbogen, 1998). Post-war Japan, as much of the world, faced a serious food shortage and established non-profit organisations to extensively research and produce the protein-rich *Chlorella* (Yamaguchi, 1997). Certain strains of *Chlorella* are known to accumulate upto 60 % (dry weight) protein and the term 'single-cell protein' was coined (Pulz and Scheibenbogen, 1998). Although cultures could be mass produced in simple ponds or lakes, it was soon realised that the tough cell wall is highly indigestible and so rice and wheat crops were used to solve the post-war global food shortages instead. Subsequently, in 1975, U.S. funded projects finally developed a means of breaking down the tough cell wall in order to allow cells to undergo digestion in the gut (Benemann, 1990), but many considered this too late and an opportunity to establish microalgal biotechnology missed. However, Germany and Czechoslovakia continued research into *Chlorella* as a human food source through the late 1970s, and process developments designed to increase productivities (algal raceways- see Section 1.6.2) were subsequently exported to India, Thailand and Peru as part of a foreign aid program (Benemann, 1990). A major and persistent drawback

with cultivating *Chlorella,* however, was species control, often suffering from predation or competition from other micro-organisms under 'open' conditions (refer to Section 1.6). As a result of which, attention instead switched to a prokaryotic microalga, *Spirulina*, as an alternative source of single-cell protein, since it is fast growing and less prone to contamination due to it's preference for alkaline conditions. *Spirulina* has become an established food source throughout several countries due to it's nutritional composition, 5 g of which is equivalent in terms of vitamin and mineral content to 100 g of vegeTables (Borowitzka, 1994).

As a by-product of *Spirulina* production, water extraction allowed for the recovery of phycocyanin (a blue pigment). As a result of which a new market opened for microalgae pigments, to be used as natural food colourants. Carotenoids are a family of pigments found ubiquitously throughout nature including microalgae, where they act as light harvesting structures in addition to the dominant chlorophylls. There are estimated to be over 600 known carotenoids (Tsavalos *et al.*, 1993; Young and Britton, 1993; Sinnott, 1988) covering a myriad of colours, yet their appearance becomes more apparent during the degradation of chlorophylls (e.g. changes in colouration of autumn leaves (Eugster, 1995)), which normally masks their presence. For many aquatic and terrestrial species, the ingestion and bioaccumulation of these pigments can result in changes in flesh pigmentation (Nickel and Bromage, 1997; Sinnott, 1988). Pigmentation in some marine invertebrates is also the result of *carotenoprotein* complexes. For example, a lobster becomes red when it is boiled because astaxanthin (a red carotenoid pigment) becomes free from the denatured protein (Eugster, 1995). Another example is the pink plumage of flamingos which is directly related to their dietary intake of microalgal carotenoids, the absence of which results in the loss of their colourful plumage (Eugster, 1995; Olson *et al.*, 1989). Even the pigmentation of ornamental fish, such as Koi carp, can be enhanced by the addition of *Spirulina* to their feed (Borowitzka, 1997; Borowitzka, 1994; Shaish *et al.*, 1992). Furthermore, the colouration of egg yolks can be altered by the addition of lutein (a yellow pigment) to poultry-feed supplements in order to meet with consumer preferences which can vary between countries (A. Young, pers. com). *Dunaliella*, a well document microalgal source of ß-carotene (Yamaguchi, 1997; Borowitzka, 1994; Shaish *et al.*, 1992), is used as a colourant in a variety of foodstuffs, but mainly orange squash (Pulz and Scheibenbogen, 1998). Whilst synthetic pigments have been

used in foods, there have been allegations that some have carcinogenic properties and have been linked with various allergic reactions in humans (Bernhard, 1990). European Union legislation states that synthetically pigmented produce be labelled as 'artificially coloured' (Sinnott, 1988). Because microalgae are a natural source pigments, labeling of such products will simply state 'natural ingredients'. The use and demand of microalgal pigments as food colourants has therefore increased substantially.

Aside from their aesthetic roles, pigments have additional properties as anti-oxidants. Photosynthesis can generate highly reactive free radicals (atoms or molecules with unpaired electrons) such as oxygen, as a result of over excitation of chlorophyll (i.e. under high light intensities). These free radicals can damage cell organelles, by a process of lipid peroxidation (Das, *et al.*, 2001; Olson *et al.*, 1989), unless quenched by carotenoids, which act as buffers against photodamage (Wozniak and Dera, 2000; Tsavalos, 1995). Consequently, whilst being used as natural food colourants carotenoids also act to increase the shelf-life of certain foods, slowing down the process of cellular decay. This also demonstrates that pigments have an inherent ability to aid health. Indeed, certain carotenoids are also understood to act as vitamin pre-cursors (Borowitzka, 1991), which regulate immune responses (increasing T and B lymphocyte proliferation). Vitamin A deficiency alone can be responsible for poor growth and high mortality rates, as seen in many third-world countries. Furthermore, conditions such as anaemia, night blindness, reduced haematopoiesis and immuno-suppression, can all result from a reduction of vitamin A within the metabolism. The dietary intake of carotenoids, such as β-carotene and canthaxanthin, which are known to undergo intestinal enzymatic cleavage into vitamin A, are therefore of particular pharmaceutical interest. In fact, the consumption of the microalga *Dunaliella salina* (as powders or pastes) has been linked to vitamin A biosynthesis (from the natural 9-*cis* isomer of ß-carotene as the pre-cursor) in humans, and is a known oral source of treatment for conditions leading to immuno-suppression and photosensitivity in the skin (Olsen, *et al.*, 1989). In addition, the therapeutic properties of *Spirulina* have been used to alleviate hyperlipidemia, hypertension suppression, prevention of renal failure and regulation of serum glucose levels (Yamaguchi, 1997).

1.2.2: Aquaculture

Ecological damage caused by over fishing and the consequences of entrapment of protected species in nets, combined with modern pollution catastrophes within the world's oceans is of growing concern regarding wild fish farming. Furthermore, wild fish farming is time-consuming and the nutritional value of the fish caught can vary depending upon species, season and geographical factors. For example northern waters are known to produce fish richer in monounsaturated fatty acids (MUFAs- refer to Section 1.4.2) compared to those in the southern hemisphere (Bryhn, 2001). A difference that is echoed through the progressive trophic levels, as found when comparing Atlantic and Antarctic baleen whale oils (Ackman and Tocher, 1968). Consequently, there is increasing commercial interest in the field of aquaculture, where fish can be captively 'farmed' under controlled conditions with the additional benefits of quality control, in terms of consistency. Such aquaculture farms however, despite their ideology, bring with them their own inherent problems. Captive bred marine animals, which include molluscs, crustaceans and fish, become isolated from their natural prey (phytoplankton and zooplankton), which can reduce nutritional quality. For example, commercial farming of salmon, can leave the flesh of the salmon grey and discoloured, due to the lack of natural carotenoid rich microalgae from their diet, compared to wild caught salmon (Young and Britton, 1993). Salmon farmers will typically supplement salmon feeds with high levels of astaxanthin (a specific carotenoid pigment) to regain a more natural tone to the flesh of farmed salmon, making it more attractive to the consumer. Whilst artificial supplements do exist (rich in *trans* isomers) they tend to be less soluble and harder to digest than microalgae sources such as *Haematococcus pluvialis* (also contain *cis* isomers) which are often more favourable. Of the 14.5 million metric tons of aquacultured fish and shell-fish (22 % of the world harvest) in 1993, ~90 % were reared on phytoplankton (Duerr *et al.*, 1998). Various feed supplements are added to replace vital components, which would otherwise be missing from their artificial diets, resulting in increased pathologies and possible mortality of livestock (Morris, 2000). Live phytoplankton can be fed directly to fish larvae or indirectly via zooplankton (such as the rotifer, *Brachionus plicatilis* or the brine shrimp, *Artemia salina*) to larger juveniles. Microalgal feeds are also available as either pastes, freeze-dried or spray-dried formulas.

1.3: MICROALGAL POLYUNSATURATED FATTY ACIDS

In 1980 the US Solar Energy Research Institute (SERI, later becoming the National Renewable Energy Laboratory (NREL) in 1990) launched their Aquatic Species Program (ASP), which sought to develop renewable sources of lipids as an alternative combustible fuel (biofuel). This government ran venture, which sponsored both internal and external contracts, aimed to mass produce microalgal triacylglycerols (Behrens and Kyle, 1996), but was setback due to insufficient productivities. Whilst the fruits of this research are still subject to more long-term development, the ASP study had also revealed the fatty acid composition of those microalgal lipids. Showing them to be a source of several essential fatty acids (EFAs) and in particular polyunsaturated fatty acids (PUFAs), a spin-off of this research has been it's application to trends in health food supplements and the growing industry of aquaculture.

1.3.1: Historic discoveries

The beneficial properties of fish oil (lipid) can be dated as far back in history as medieval times, when pregnant women in Nordic coastal regions were deliberately fed cod liver oil. In 1895 a Norwegian scientist (Heyerdahl, P.M.) revealed that the health benefits of cod liver oil was linked to "Therapic acid". This was later isolated/ identified in the 1950 - 60s as Docosahexaenoic acid (DHA) by Professor Notevarp, and was linked with the treatment of cardiovascular disease (Bryhn, 2001). During the 1970's a group of Danish scientists (namely, Drs Hans Olaf Bang and Jørn Dyerberg) discovered that cardiovascular disease amongst native Inuit Eskimos was extremely rare (Bryhn, 2001; GISSI, 1999), which was later attributed to their unique diet of fish (Connor, 1999). Whilst both Eskimo and Danish populations in Greenland both ate high fat diets, the Eskimo diet of oily fish was a richer source of PUFAs, specifically DHA and Eicosapentaenoic acid (EPA) (Connor, 1999), resulting in lower serum cholesterol levels (Harris, 2001). Despite earlier preconceptions of cod liver oil, it was not until the 1970s that pharmaceutical interest gave rise to numerous dietary studies (GISSI, 1999), which continue to highlight the roles of PUFAs in our diets in terms of neurological (linked to EPA) and cardiovascular (linked to DHA) development and maintenance. However, it is now known that fish, like humans, cannot biosynthesise fatty acids longer than 18 carbon atoms and that the presence of DHA and EPA in fish oils (lipids) is simply a result of bioaccumulation from their own diet of microalgae and zooplankton (Sargent *et al.*, 1999b).

1.3.2: Pharmaceutical roles

Fatty acids can be devided into 'families', referred to as omega (or n-) series, on the basis of their molecular structure (more detail is given in Section 1.4.2). Whilst the human body is able to synthesis n-9 fatty acids it is unable to place double bonds in the n-6 or n-3 positions (Stuchlík and Zák, 2002; Parrish, 1999), which are considered to be EFAs required by the body as dietary fats (Bryhn, 2001). EFAs help form important structural components of the brain and myelin sheaths of the central nervous system (Uauy *et al.*, 2001). DHA, an n-3 polyunsaturated EFA, is the main fatty acyl component of electrically active tissues such as the phosphatidyl serine (PS) and phosphatidyl ethanolamine (PE) in both the retina (as much as 50 – 60 %), and in brain's grey matter (20 – 25 %) (Jeffery *et al.*, 2001; Kyle, 1996). It is estimated that an average human brain contains as much as 20 g of DHA (Bryhn, 2001). The body's demand for DHA during certain periods (mainly perinatal growth) is such that our endogenous biosynthesis is unable to supply enough without dietary sustenance. Studies have shown that n-3 fatty acid deficiencies can affect retinal and auditory development in children (Uauy *et al.*, 2001). Feeding of n-3 enriched formula supplements to preterm (premature) human infants have proved to enhance visual acuity, specifically by increasing integrity of the neural pathway from the retina to the occipital cortex (GISSI, 1999). DHA is found in the outer segments of rod cells (highly sensitive to low light) of the retina (Jeffery *et al.*, 2001), where it increases opsin/ rhodopsin expression and mitochondrial activity, preventing photoreceptors from apoptosis (cell death) (Politi *et al.*, 2001). Furthermore, ten-month-old children fed PUFA supplemented feeds were found to score higher in cognitive behavioural tests, measured through simple problem-solving tasks (Uauy *et al.*, 2001). DHA is also responsible for regulating serotonin, the feel-good neurotransmitter, helping to alleviate depression and aggressive behaviour in children (Medev, 2002). Research has also shown low activity/ loss of desaturases within biosynthetic pathways as a result of aging (Kyle, 1997). Furthermore, it has been suggested that the presence of high levels of DHA may in fact help prevent the onset of Alzheimer's disease (Cederholm, 2004), also reflecting the dietary importance of PUFAs for the elderly.

PUFAs are also responsible for regulating a specific group of hormones in humans referred to as eicosanoids. The eicosanoids (produced in almost all tissue types in trace amounts) include a range of C20 paracrine hormones, specifically prostaglandins (PGs); thromboxanes and leukotrienes (LT), produced in response to stress conditions on a cellular and whole body level (Tapiero *et al.*, 2002). Both Arachidonic acid (ARA- an n-6 PUFA) and EPA (an n-3 PUFA) are EFAs which actively compete as precursors for the eicosanoids metabolites (Sargent *et al.*, 1999a; 1999b). Due to the chemical similarities of these two key PUFAs there is significant competition between them for cellular uptake, since they undergo chain elongation and cleavage from the same enzyme complexes (see Figure 1.6). Whilst ARA- derived eicosandoids are pro-inflammatory, EPA has anti-inflammatory effects. EPA, by reducing the presence of pro-inflammatory cytokines, can indirectly help inhibit joint erosion, which can otherwise lead to rheumatoid arthritis (Venkatraman and Meksawan, 2002). Additionally, the presence of dietary PUFAs have been linked with reducing auto-immune diseases (Venkatraman and Meksawan, 2002, Denys *et al.*, 2001), glomerular (kidney) disorders (Das, *et al.*, 2001) and fatal myocardial infarction (Medev, 2002; GISSI, 1999).

The so-called modern 'Western diet' of North America, which has gradually spread across much of Europe, has resulted in a rise in coronary heart disease, now believed to be directly related to the absence of n-3 PUFAs (Connor, 1999). The recommended daily intake of n-3 fatty acids is 0.6 – 1 g/day (Bryhn, 2001), however the 'Western diet' contains only about 0.08 – 0.12 g/day of PUFAs (Kyle, 1997). Whilst n-6 fatty acids are also EFAs (see Table 1.1), the 'Western diet' can also contain up to 30 times more omega-6 than omega-3 fatty acids. Thus the dietary balance is heavily tipped in favour of n-6 fatty acids- three times higher than recommended for a balanced diet. In comparison, the Mediterranean diet has become recognised as 'healthy' since it limits the use of red meats (high in n-6 fatty acids). Consequently, there more dietary awareness and interest in C18 - 20 PUFAs with three or more double bonds (Stuchlík and Zák, 2002).

PUFA formula (omega series)	Systemic name
18:3 (n-6)	γ-linolenic acid (GLA)
20:4 (n-6)	Arachidonic acid (ARA)
18:4 (n-3)	Octadecatetraenoic acid (OTA)
20:5 (n-3)	Eicosapentaenoic acid (EPA)
22:6 (n-3)	Docosahexaenoic acid (DHA)

TABLE 1.1: Major PUFAs for human nutrition. As given by Ratledge (1998), shows both n-6 and n-3 fatty acids to be essential dietary fatty acids. However, a balanced ratio of 4:1 (n-6:n-3) is important. Refer to Section 1.4.2 for explanation of PUFA formulae.

Most dietary n-6 fatty acids can be obtained from red meats, soybean, rape seed and corn oil. Whereas, n-3 fatty acids can be found in fresh fruits, walnuts, garlic, flaxseed or olive oil, whole grain and fatty fish such as herring, mackerel, sardines and salmon (Bryhn, 2001). Diets lacking such foods can be supplemented with a variety of commercially available health foods. The first commercial n-3 supplement to be sold in the 1970s was MaxEPA, which contained 18 % EPA; 12 % DHA, as well as non-essential fatty acids (Bryhn, 2001). With the continuing evidence gathered by medical studies and increasing public awareness, pharmaceutical companies have been driven to produce more PUFA health food supplements. Today refined production has led to microalgal products containing as much as 95 % EPA (EPADEL, sold in Japan) (Bryhn, 2001). Pronova Biocare Omacor™ is marketed throughout the world, also named Esapent or Seacor in Italy, containing an 85 % blend of EPA and DHA (Bryhn, 2001; Harris, 2001). DHASCO (Kyle, 1996) is triacylglycerol oil enriched with 40 % DHA (Behrens and Kyle, 1996) produced from a marine microalga called *Crypthecodinium cohnii* (Kyle, 1997).

1.3.3: Polyunsaturated fatty acids in aquaculture

With continuing legislation against the farming of wild fish, the field of aquaculture (captive bred fish farms) is becoming increasingly commercial. The captive breeding of fish does however bring with it various constraints, with over intensive farming (overcrowding) resulting in increased BOD (biological oxygen demand), causing minor deformities of fins and gills. Perhaps more significant however, is the reduced level of survival rates in fish larvae (Evjemo and Olsen, 1999; Kureshy *et al.*, 1999; Lu and Blake, 1997; Lubzens *et al.* 1985). A model for such conditions can be seen in the marine fish hobbyist sector (home aquariums), where breeders of the common clown fish (*Amphiprion percula*, or the 'false clown', *A.ocellaris*) have reported incidents of 'sudden shock syndrome', now thought to be the result of underdeveloped nervous systems due to a lack of EFAs in their diet leading to hypersensitivity. This has been ascribed to a lack of neurological and cardiac development, resulting from an insufficient supply of DHA and EPA in the diet (Rimmer, 2000; Duray *et al.*, 1997), ultimately impacting upon growth and mortality rates (Reitan *et al.*, 1997; Yamaguchi, 1997). Furthermore, a lack of DHA in rod cells (of the eyes) can impair their ability to capture prey, ultimately affecting growth and survival (Sargent, *et al.*, 1999b). Consequently, much commercial interest in the field of phytoplankton has arisen, specifically focusing on strains high in EPA and DHA, since marine fish specialists and hobbyists alike are becoming increasing educated in the nutritional quality of fish-feeds. Dietary needs are species specific and must also consider the age of the stocks, but provided these needs are met aquaculture can offer greater nutritional consistency over wild-farmed fish (which are subject to geographical and seasonal variations).

Whilst larger juvenile or adult fish may be fed zooplankton or large pellets, smaller fish larvae and fry are unable to ingest and/ or catabolise such foods due to both prey size and underdeveloped digestive tracts (Fernandez-Reiriz and Labarta, 1996). Their natural prey item at such early stages, phytoplankton, must therefore meet the highly demanding nutritional requirements of active growth. Although adult fish may feed upon larger zooplankton, they too indirectly benefit from the bioaccumulation of microalgal nutrients, since phytoplankton are known to trigger digestive enzymes at pancreatic and intestinal level (Kureshy *et al.*, 1999; Sargent *et al.*, 1999). In this respect, zooplankton act as 'pack-horses' for nutrient transport and so should be

equally well nourished with phytoplankton (Ben-Amotz *et al.*, 1987). Whilst zooplankton can be grown on low-cost diets of common baker's yeast (*Saccharomyces cerevisiae*) alone, juvenile fish can suffer from poor survival rates. For example, Watanabe *et al.* (1983) reports survival rates of black sea bream to be as low as 3 %, when reared solely on bakers yeast. Enrichment of rotifers fed with *Nannochloropsis* (see Section 1.5.2) has reported to increase survival rates of juvenile fish towards 70 % (Watanabe *et al.*, 1983). Although phytoplankton feeds are comparatively more expensive (Borowitzka, 1997; Rainuzzo *et al.*, 1994), zooplankton are often 'enriched' with phytoplankton as late as 24 hr prior to harvest (Reitan *et al.*, 1997; Fernandez-Reiriz and Labarta, 1996)- a method referred to as short-term (ST) enrichment (Lavens and Sorgeloos, 1996). Perhaps the most common zooplankton cultures used are rotifers (specifically *Brachionus plicatilis*), which were first used over 40 years ago in Japan and are used in the hatchery production of more than 60 species of marine finfish and 18 species of crustaceans (Sargent *et al.*, 1999b; Lavens and Sorgeloos, 1996).

Much of the research into human health (especially with respect to polyunsaturated fatty acids) is now being applied retrospectively within aquaculture as a means of maintaining our natural food chain supply of essential fatty acids. Since wild fish farming is seen as ecologically damaging, it is in our own interest, in terms of dietary requirements, to increase the captive welfare of animals entering our food chain via commercial aquaculture.

1.4: AN OVERVIEW OF LIPID & FATTY ACID BIOCHEMISTRY

Depending upon the lipid class, lipids can be hydrolysed (broken down) into their components of glycerols, phosphates, saccharides and fatty acids. The hydrocarbon tails of fatty acids can vary considerably in both length and desaturation (Gill and Valivety, 1997). The nutritional profile, and likewise lipid content (including fatty acids), of various microalgal strains is fairly unique with regard to their major groups, as highlighted by Behrens and Kyle (1996). Changes in lipid profile within a species can also reflect the stage within the life cycle of the organism. In addition to which, prevailing environmental parameters (such as nutrient levels, temperature, pH, salinity and irradiance) can play a significant role in regulating lipid class, as well as the fatty acid composition of lipids (Renaud *et al.*, 2002; 1999; Behrens and Kyle, 1996). Regulation of cellular lipid (and inherent fatty acid) profiles is therefore highly dynamic unless environmental conditions can be controlled in order to produce consistency within a species.

1.4.1: Lipid classification

The term lipid (which includes fats, oils and waxes) refers to compounds that are insoluble in water but soluble in organic solvents. Lipids can generally divided as either simple (Figure 1.1) or complex structures (Figures 1.2 – 1.4). 'Simple lipids' include two subclasses, the terpenes and the steroids, which remain unbound (in a free state). Terpene hydrocarbons therefore have molecular formulas $(C_5H_8)_n$. Terpenes are found in essential oils, and include Vitamin A, E and K along with various secondary plant metabolites such as gibberellic acid, ß-carotene and phytol. Phytol is a diterpene, comprising of four isoprene units (CH_2=C(CH_3)-CH=CH_2). Steroids are much more distinctive, and are easily identified by the presence of a cyclic four-ring hydrocarbon nucleus (e.g. hormones, vitamin D, cholesterol).

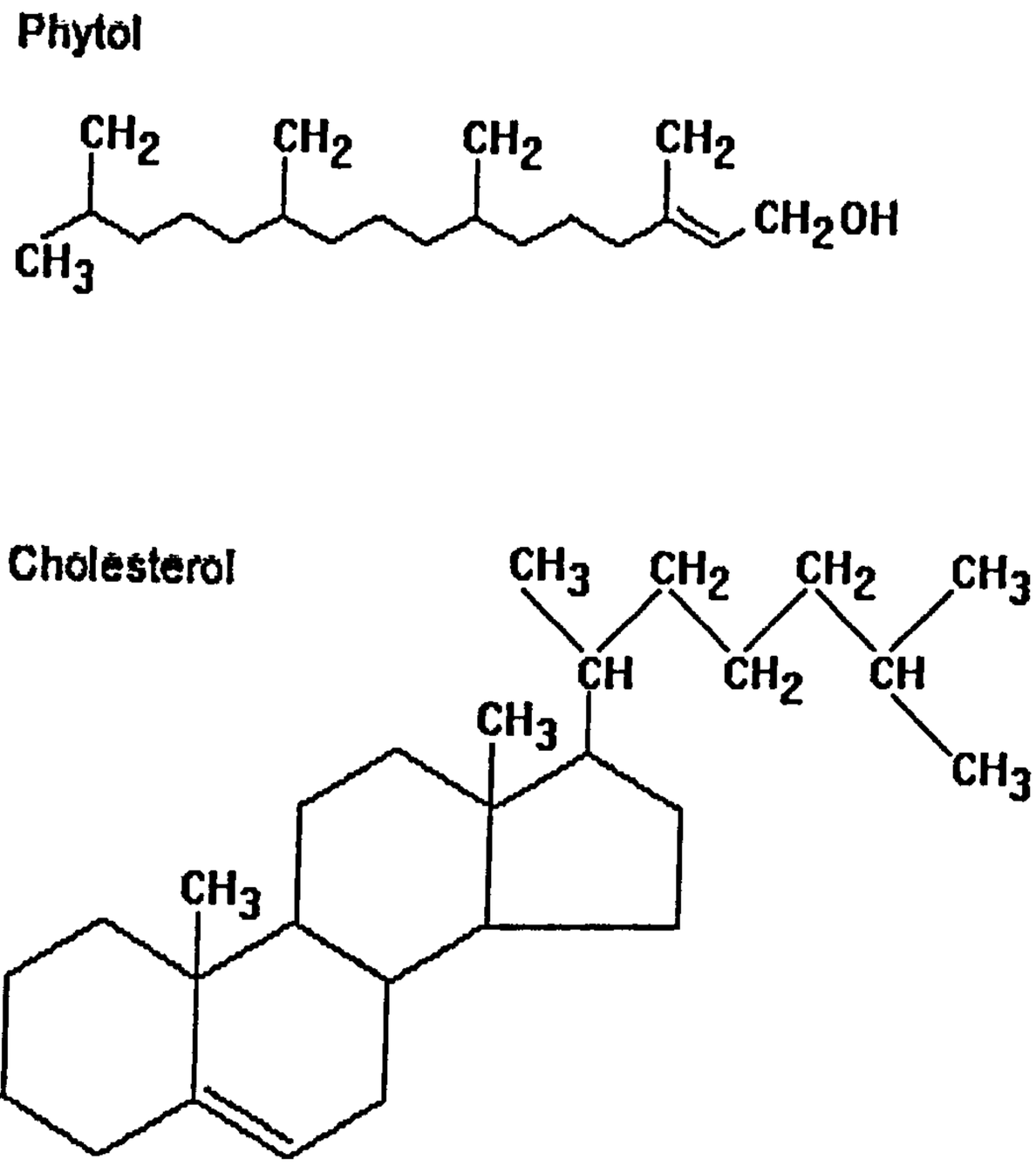

Figure 1.1: Simple lipid structures. Examples include the isoprenoid-based structure of phytol (a terpene lipid) and the cyclic structure of cholesterol (a steroid lipid).

In contrast, 'complex lipids' rarely exist in a free state, and instead have a tendency to interact with proteins (lipoproteins) or carbohydrates (lipopolysaccharides). On a molecular level the complex lipids are constructed primarily from a glycerol or a sphingosine backbone, onto which the various end groups become esterified. These include, phosphates in the case of phospholipids (PLs) and saccharides in the case of glycolipids (GLs), along with fatty acids. Fatty acid hydrocarbon groups can vary in size from 1 to 30 carbon atoms, and are capable of undergoing desaturation. Water solubility of a lipid decreases and melting point is raised as fatty acid chain length increases. The three major classes of complex lipids are as follows:

(1) Triacylglycerols (TAGs) (also known as triglycerides) are non-polar (neutral) lipids, which accumulate within cellular vacuoles and generally act as energy stores. TAGs consist of a glycerol molecule in which all three hydroxyl groups have been esterified with a fatty acid. Fatty acid chain length and saturation can vary. Simple TAGs are formed from three identical fatty acids, whereas this can vary amongst the fatty acid composition of complex TAGs.

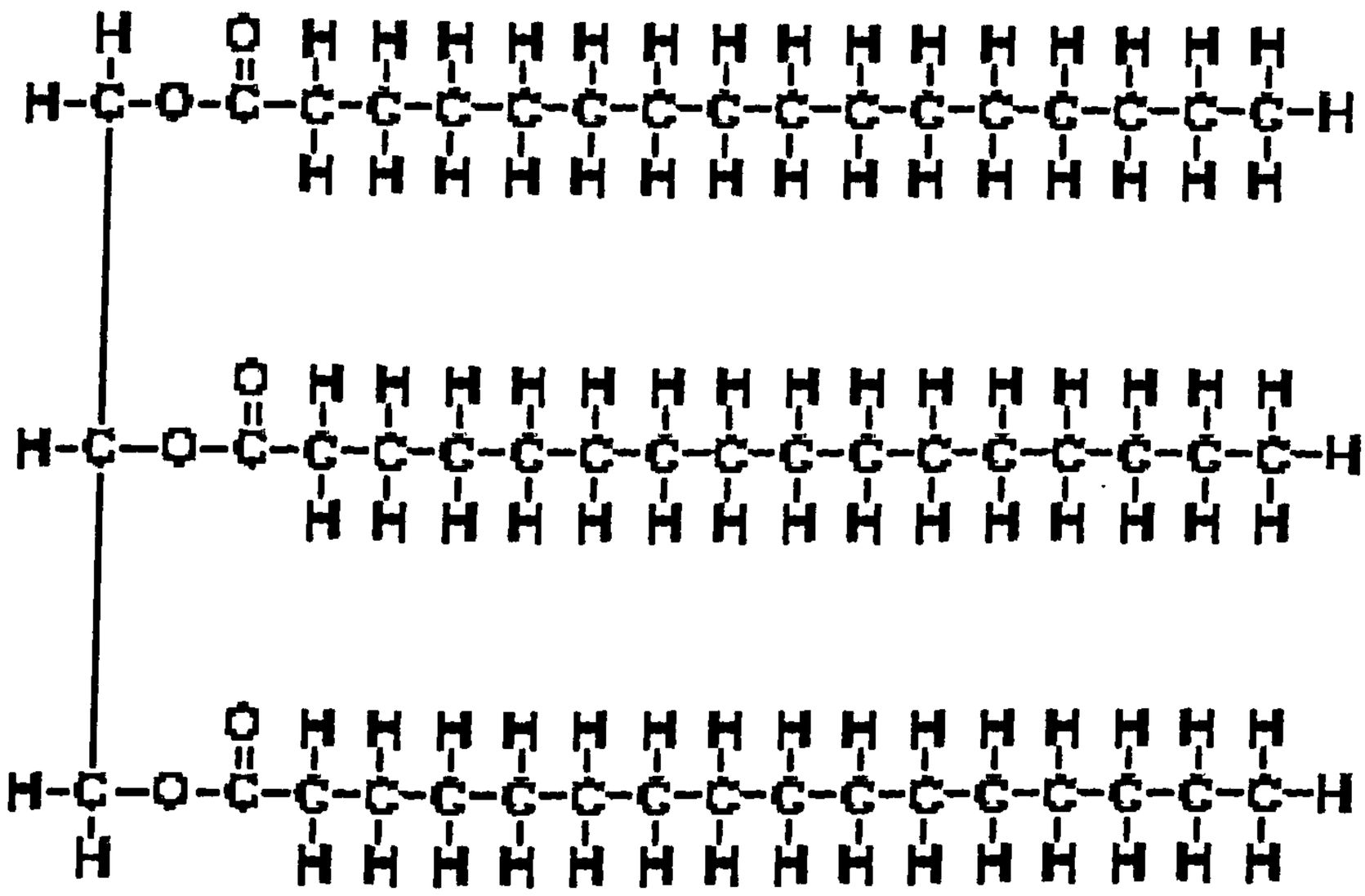

Figure 1.2: Triacylglycerol structure. A simple triacylglycerol consisting of glycerol covalently bonded via ester linkages to 3 × Palmitic acid (PAL), a saturated fatty acid (refer to Section 1.4.2)

(2) Phospholipids (PLs) act as key molecules in the structure of cell membranes due to their unique polarity. Phospholipids are formed from a glycerol backbone, onto which two fatty acid and a phosphoric acid molecule are bound via ester linkages. Two hydrophobic fatty acid chains act as 'tails', whilst the hydrophilic phosphate acts as a head, as commonly established in principles of the lipid bilayer and fluid mosaic model (Guttman, 1999). There are eight phospholipid sub-classes (depending upon the phosphate 'head group'), which can form complexes within membranes responsible for intracellular transport of various metabolites. The introduction of a double bond (unsaturation) in the fatty acid tails causes a kink in the tertiary structure producing gaps between phospholipids within a membrane giving them a degree of fluidity. Heat energy promotes desaturation and so membrane fluidity can increase with temperature.

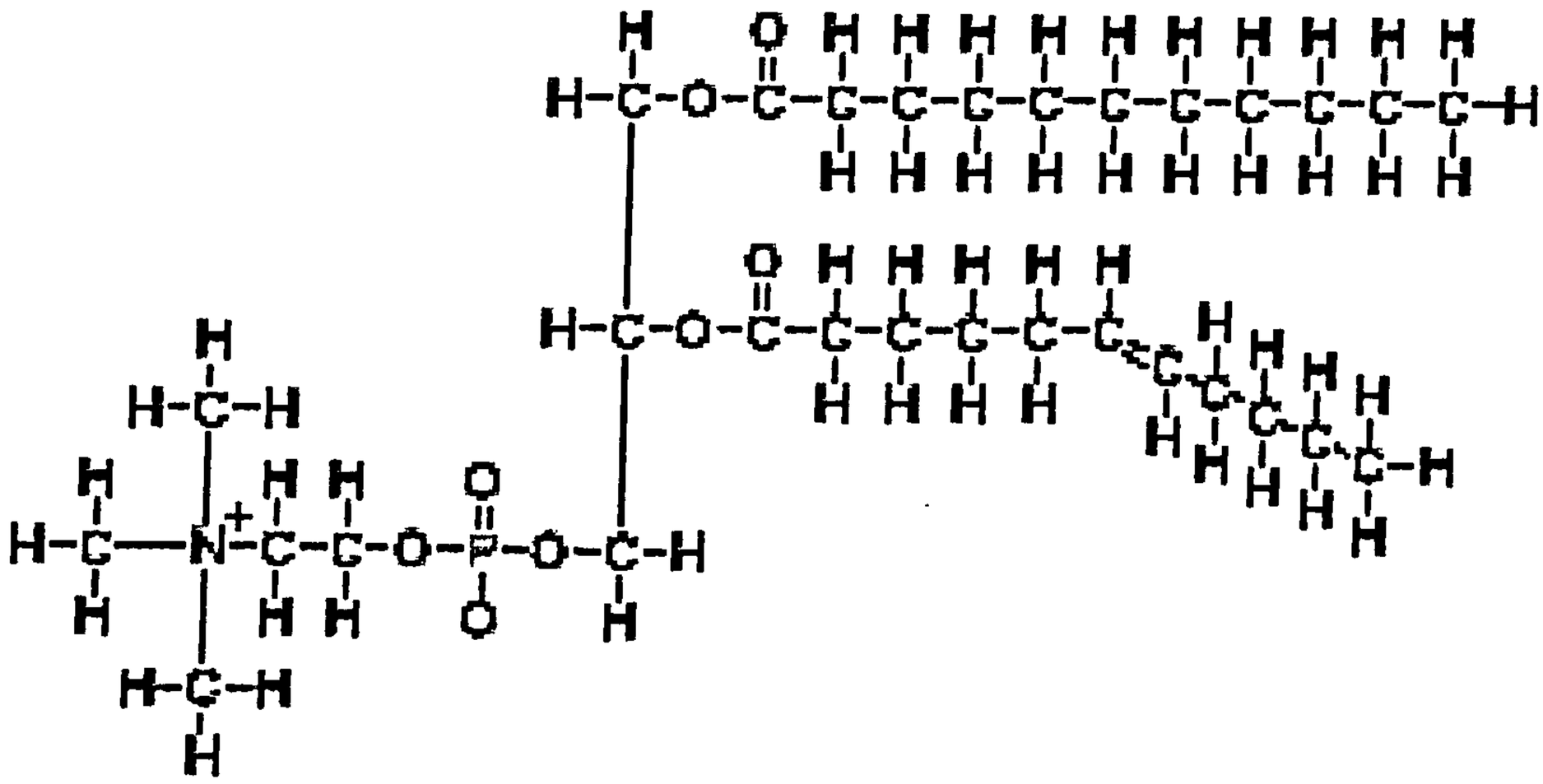

Figure 1.3: Phospholipid structure. Phosphatidylcholine contains two fatty acids: undecanoic (SAT) and undecylenic acid (MUFA) branching from a central glycerol molecule (refer to Section 1.4.2).

(3) Glycolipids (GL) are comprised of a sphingosine backbone (a long chain amino alcohol that bears an approximate similarity to glycerol) with a hydrophilic saccharide 'head' and two hydrophobic fatty acid chains. Glycolipids are highly associated with thylakoid membranes, although their specific function remains largely unknown (Minoda *et al.*, 2002). There are four main classes of glycerolipids: monogalactosyldiacylglycerol (MGDG), digalactosyldiacylglycerol (DGDG), phosphatidylglycerol (PtdG) and sulfoquinovosyldiacylglycerol (SQDG) (Minoda *et al.*, 2002). Both MGDG and DGDG form the dominant components of thylakoid membranes (Alonso *et al.*, 1998).

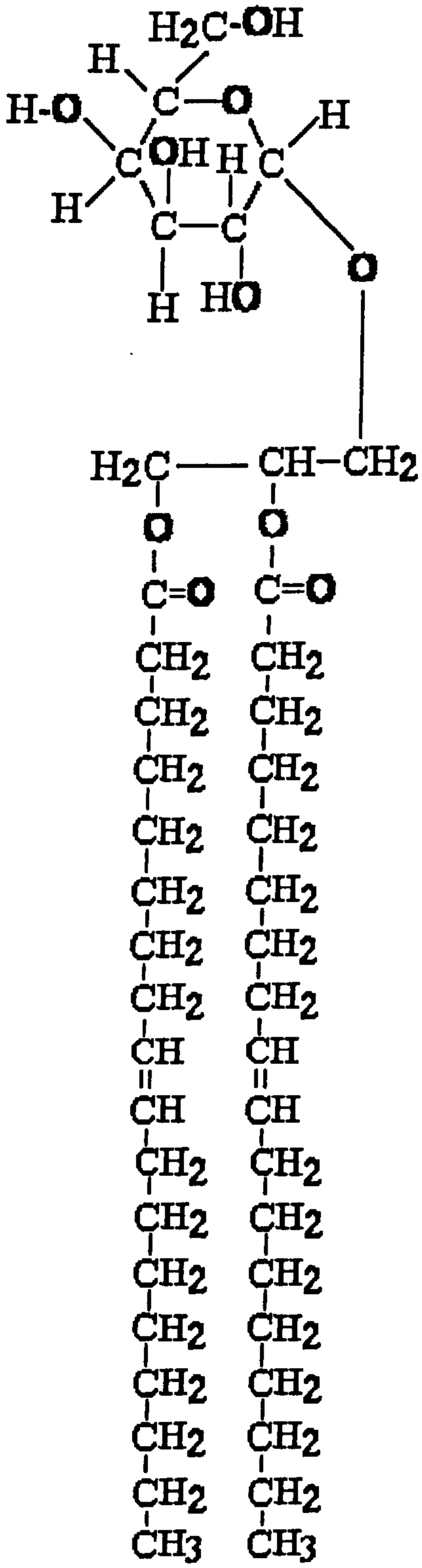

Figure 1.4: Glycolipid structure. Molecular structure of the glycolipid, monogalactosyldiacylglycerol (MGDG), comprising of a hydrophilic saccharide head (galactose), sphingosine and two hydrophobic monounsaturated fatty acids (MUFAs- refer to Section 1.4.2), Oleic acid.

1.4.2: Fatty acid structure and nomenclature

When any lipid undergoes hydrolysis fatty acids are released, where they may undergo enzymatic cleavage back into the cells metabolism, acting as pre-cursors for various functions (see Section 1.3.2). Complex lipids, as already described, all typically comprise of at least two fatty acid components, three in the case of TAG lipids. The fatty acids themselves can vary in terms of carbon chain length and the degree of desaturation. Saturated fatty acids (SATs- those without double bonds) tend to be solids and waxes, whereas unsaturated fatty acids are oils or liquids. The most common saturated fatty acids found within algae are those with hydrocarbon chain lengths of 12, 14, 16 and 18 carbon atoms. Fatty acids containing a single double bond within their structure (regardless of chain length) are referred to as monounsaturated fatty acids (MUFA). Further desaturation of the hydrocarbon chain leads to the classification of polyunsaturated fatty acids (PUFAs), as shown in Figure 1.5. With regard to unsaturated fatty acids, these can range from 16 - 22 carbon atoms, which can contain up to six double bonds (in the *cis*-configuration). Unsaturated fatty acids have greater fluidity, in relation to number of double bonds, becoming less viscous with increasing chain length. Animal fat mainly comprise of saturates whilst plants and fish predominantly contain unsaturated oils (Tapiero *et al.*, 2002). Marine microalgae are renowned for have a greater degree of unsaturation compared to freshwater species, particularly with respect to C20 and C22 fatty acids, and are therefore considered as dominant producers of PUFAs, particularly omega-3 fatty acids (including DHA and EPA) (Behrens and Kyle, 1996).

Systemic nomenclature of fatty acids can be expressed various ways in the literature, however the most accurate way can be expressed as L:B (b_1). Where, L is the length of the hydrocarbon tail; B is the number of double bonds, b_1 = position of the first double bond (with successive bonds b_2, b_3, etc) from the terminal methyl (CH_3) group. Fatty acids fall into three main omega (n-) series (9, 6 and 3), which is often defined within the nomenclature as a suffix. The omega classification is used to reflect the distance (number of carbon atoms) between the last double bond and the terminal methyl carbon in the hydrocarbon tail. For example, the PUFAs ARA, (*20*:4 (5, 8, 11, *14*)) and eicosapentaenoic acid EPA (*20*:5 (5, 8, 11, 14, *17*)) fall into the n-6 and n-3 series, respectively. The position of the last double bond ultimately alters the three-dimensional shape of the molecule affecting it's recognition and binding to cell

receptors and key enzymes (Bryhn, 2001), hence the necessity of the omega series classification. A simplified form of notation (trivial nomenclature) which denotes the omega series as a suffix (n-x, where x = omega series) can also be expressed, without specific location of the double bonds, as L:B (n-x). In this form of nomenclature ARA can be described as 20:4 (*n-6*), and EPA written as 20:5 (*n-3*). Further generalisation can be made with reference to fatty acid chain length (regardless of saturation/ desaturation or position of double bonds) can be expressed as Cn, where C represents the element carbon and n = number of carbon atoms in the chain length (e.g. both ARA and EPA are C20 fatty acids).

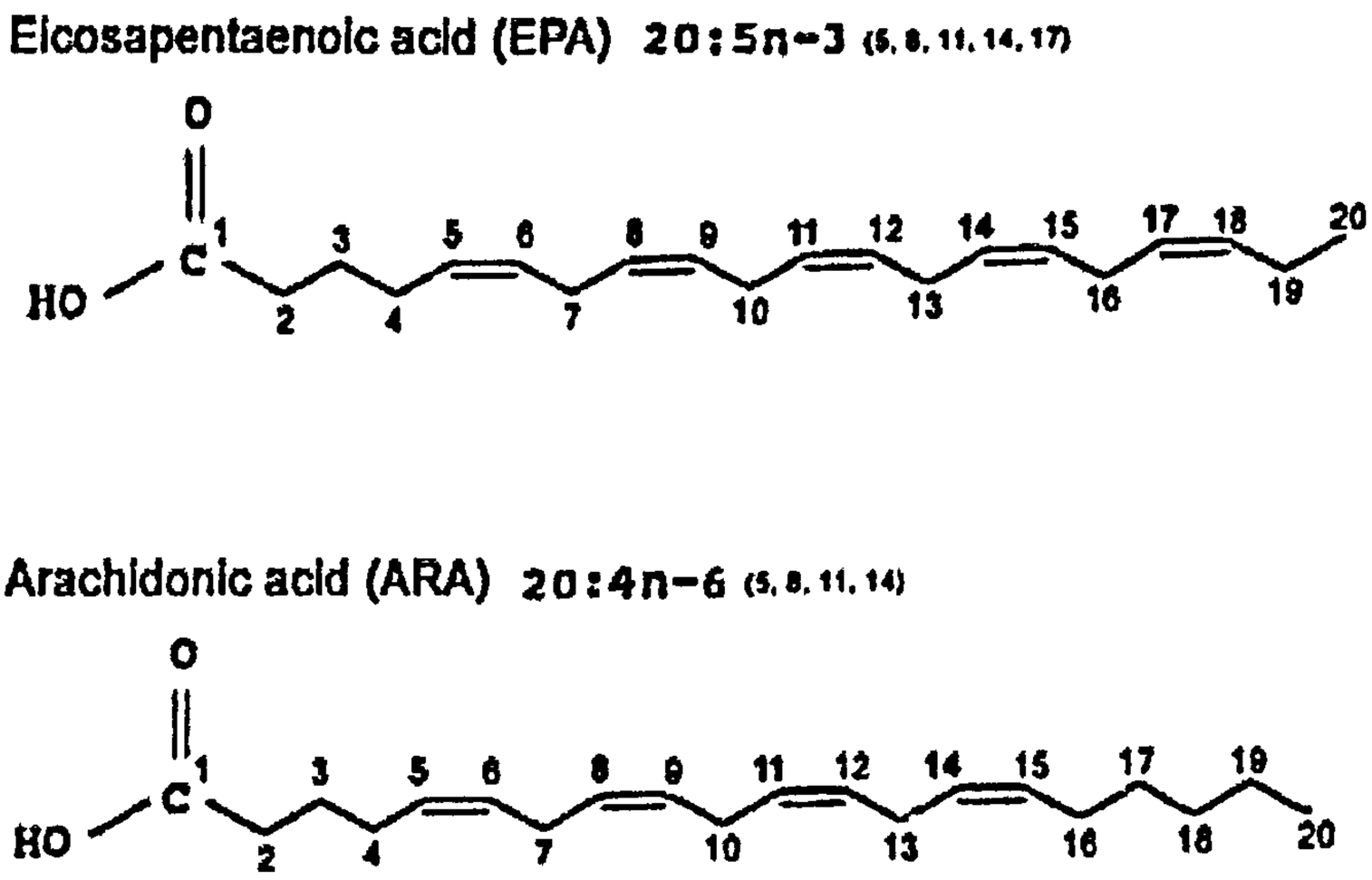

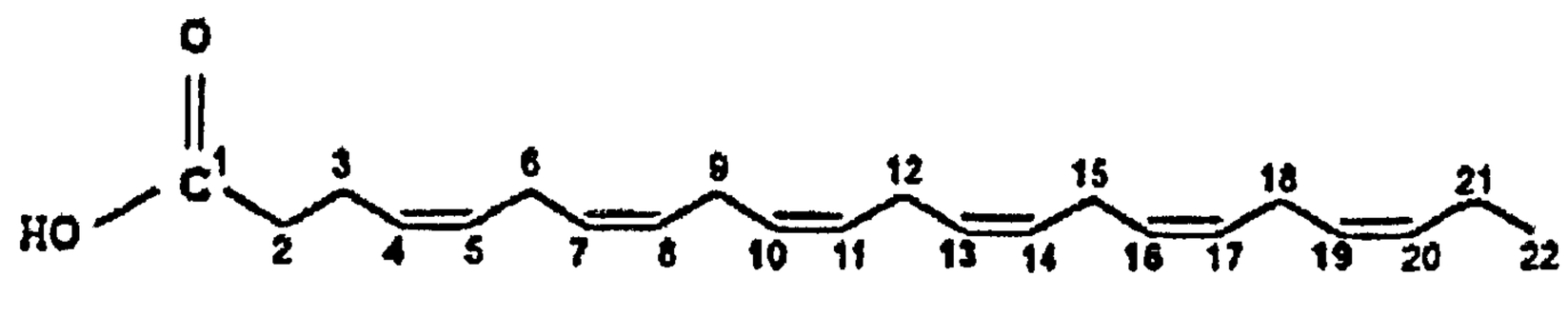

Figure 1.5: Polyunsaturated fatty acids (PUFAs). Basic examples of the hydrocarbon structure which form polyunsaturated fatty acids. Examples include C20 fatty acids: eicosapentaenoic acid (EPA) and arachidonic acid (ARA), as well as the C22 fatty acid docosahexaenoic acid (DHA). Carbon atoms are numbered away from the acyl end group; red numbers signify a double bond. Omega series are also denoted as either n-3 or n-6 depending upon the location of the last double bond from the terminal methyl end group. For further detail, refer to text.

1.4.3: Biosynthesis of polyunsaturated fatty acids (PUFAs)

PUFAs are synthesised using a successive series of enzymes, which elongate and desaturate the hydrocarbon chain (Figure 1.6). Fatty acid synthesis begins with ACCase (a nuclear encoded protein, containing biotin) which induces carboxylation of acetyl CoA to malonyl CoA (NREL, 1996). Acetyl CoA, seen more as a precursor, is found in chloroplasts where it is produced from pyruvate (catalysed by pyruvate dehydrogenase). However, both acetyl CoA and malonyl CoA can be used as carbon donors for chain elongation. The metabolic activity of ACCase can be increased in light and alkaline pH conditions. The absence of ACCase can therefore act as a rate-limiting step responsible for allocation of carbon into lipid pathways (Livne and Sukenik, 1992). The presence of malonyl CoA is the primary substrate for fatty acid synthase and the first step in fatty acid synthesis (Wen and Chen, 2003). The desaturation of bonds within the hydrocarbon tail of stearic acid (a saturate) results in the initial desaturation and successive formation of the n-9, n-6 and n-3 series of PUFAs (see Figure 1.6). Addition of site-specific desaturases, and chain elongation from carbon donors undergo active competition between series. Desaturation occurs at the carboxyl (COOH) end of the hydrocarbon tail (Kyle, 1997). Thus the first double bond is counted from the carboxyl end, with further desaturation continuing towards the terminal methyl end group.

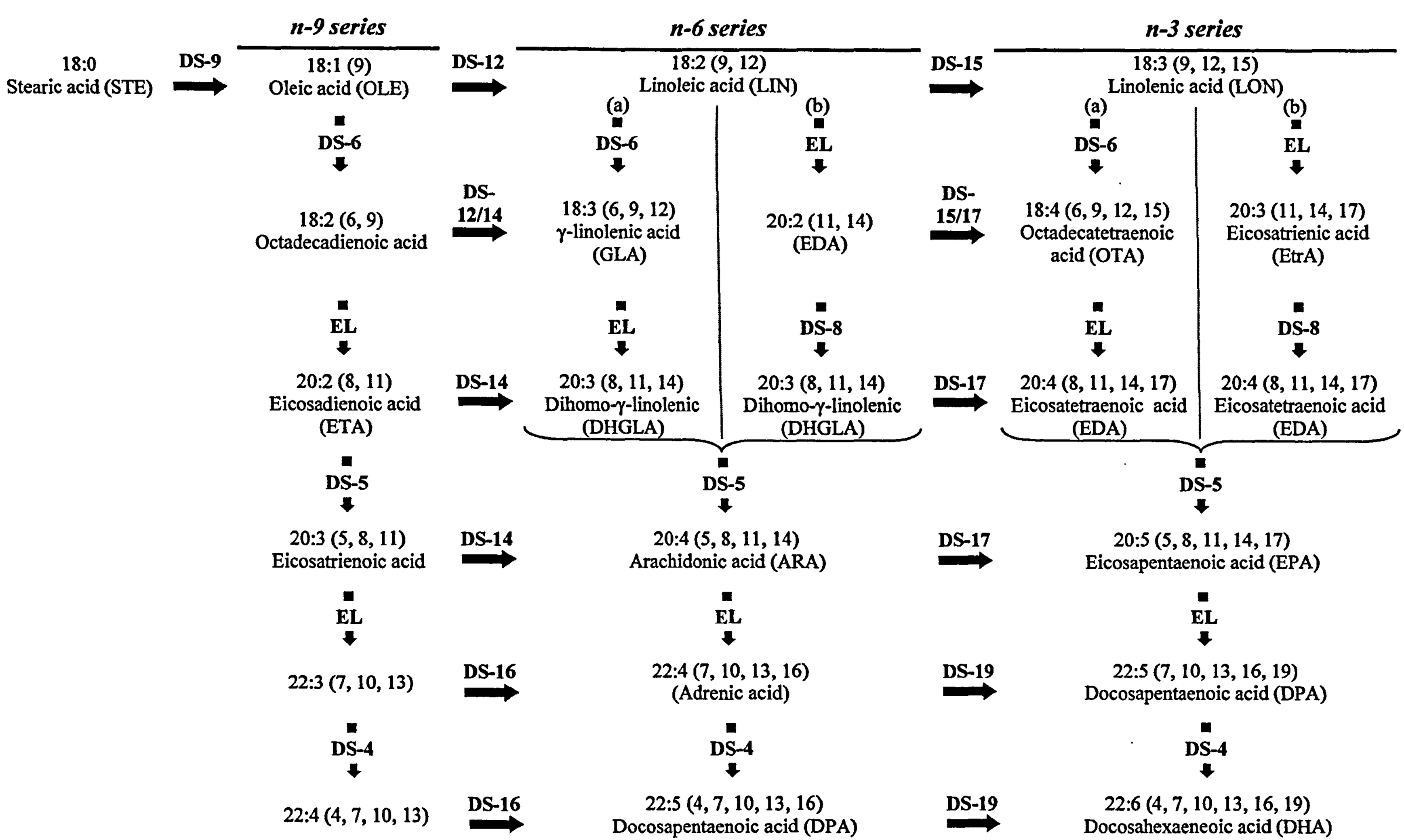

Figure 1.6: Omega 9, 6 and 3 polyunsaturated fatty acid series and there derivatives. Omega (n-) series classification is determined by the difference between position of last double bond and total chain length. Systemic nomenclature (see text) has been used to better explain changes to the hydrocarbon structures as a result of desaturation and elongation. **DS** = desaturase, introducing a double bond (counting from carboxyl end-group) at designated C atom; **EL** = chain elongation, 2 C atoms from a donor (acetyl CoA or malonyl CoA). Two separate pathways: DS-6 (a) and DS-8 (b), are shown for both the n-6 and n-3 series. Trivial names (including shorthand abbreviations) have also given, where possible. (Based upon: Wen and Chen, 2003; Qi *et al.*, 2002; Stuchlík and Zák, 2002; Gill and Valivety, 1997; Kyle, 1997).

1.5: OLEAGINOUS MICROALGAL SPECIES

Since the ASP was launched in 1990 (see Section 1.3), numerous oleaginous (oil producing, i.e. lipid-rich) species of microalgae have been investigated for their commercial potential towards producing PUFAs. In general, marine species are the dominant lipid producers over their freshwater relations. The fatty acid composition of these lipids is however independently varied. On the whole (not accounting for changes to environmental variables), lipid accumulation increases within the TAG lipid fraction as cells age. A review by Behrens and Kyle (1996) summarises the work done by others with regard to the effect of altering specific growth conditions (or parameters), in relation to fatty acid content of various microalgae.

1.5.1: *ISOCHRYSIS GALBANA*

When *I. galbana* was originally isolated by Parke in 1949 it was described physically for phylogeny, as a dinoflagellate with a cell size of 3 – 6 μm. Parke (1949) outlined the morphological changes taking place during the cell cycle. Although no details of its growth conditions or specific biochemical make-up were given, lipid globules described as containing Leucosin (or Chrysolaminarin- an oily carbohydrate) were observed. Later analysis of the 'Parke clone' showed the presence of both DHA and EPA (Fidalgo *et al.*, 1998; Parrish *et al.*, 1998; Perez, 1994; Molina Grima *et al.*, 1992). The 'Tahiti' (T-iso) strain of *Isochrysis* is distinguished from *I. galbana* by some authors as lacking EPA, with a higher optimum growth temperature of 27.5 °C (Liu and Lin, 2001; Molina Grima *et al.*, 1992). Whilst lacking EPA, the T-iso strain generally has higher levels of DHA compared to *I. galbana*. Whilst other authors, claiming to be growing the T-iso variant, report the presence of EPA amongst it's fatty acid profile (Babarro *et al.*, 2001; Renaud *et al.*, 1995; Brown *et al.*, 1993). Even strains of *Isochrysis* containing both EPA and DHA still proved a comparatively higher source of DHA against other oleaginous species of microalgae (Renaud *et al.*, 1999). Table 1.2 compares the various strains of *Isochrysis* used in their studies. This reveals some degree of confusion between authors as to the strain of *Isochrysis* used in their studies, since the presence of EPA or optimal growth temperature (as stated by authors) shows little consistency. Indeed, a high degree of clonal variation (Tzovenis *et al.*, 1997; NREL, 1996) has been noted amongst *Isochrysis* cultures in general.

(Details according to author)			Author (Surname, year)	Growth temp (°C)	EPA detected (yes/ no)
Collection Facility	*Isochrysis* strain	Isolate origin			
ARC	T-iso	Belgium	Tzovenis *et al.*, 2003 Tzovenis *et al.*, 1997	17.5 25	N/A no
CCAP	**I. galbana**	Cambridge, England	Otero *et al.*, 1997a Otero *et al.*, 1997b Fabregas *et al.*, 1985	20 20 15	yes yes N/A
	927/1 (*I. galbana*)	Port Erin, Isle of Man	Poisson and Ergan, 2001 Flynn *et al.*, 1992	20 15	no yes
	927/15 (AL11-4)	Cambridge, England	Sevilla *et al.*, 1998 Molina Grima *et al.*, 1997b Molina Grima *et al.*, 1996 Molina Grima *et al.*, 1994b Molina Grima *et al.*, 1994c	20 20 20 20 20	yes N/A N/A yes yes
	I. galbana (Parke clone, T-iso)	Unknown	Parrish *et al.*, 1998 Fidalgo *et al.*, 1998 Perez, 1994 Molina Grima *et al.*, 1992	25.5 18 20 27.5	yes yes yes yes
CCMP	463	Unknown	Liu and Lin, 2001	25	no
	1324	Unknown	Liu and Lin, 2001 Cho *et al.*, 1999	25 18	no yes
	11324 (*I. aff. galbana*, clone T-iso)	Maine, USA	Valenzuela-Espinoza *et al.*, 2002	20	N/A
	I. galbana	Oban, UK	Sanchez *et al.*, 2000	15	no
CSIC	*I. galbana* (clone T-iso)	Vigo, Spain	Babarro *et al.*, 2001	22	yes
CSIRO	CS117 (T-iso)	Hobart, Tasmania	Renaud *et al.*, 1995 Brown *et al.*, 1993	25-30 25	yes yes
	Isochrysis sp. *(T-iso clone)*	Hobart, Tasmania	Renaud, 2002	25	yes
HIMB	**I. galbana**	Unknown	Kaplan *et al.*, 1986	27	N/A
LKLL	*I. galbana* (Woods hole clone)	Isreal	Herzig and Dubinsky, 1992	22	N/A
PEMBS	*I. galbana* (isolate I)	Isle of Man	Parke, 1949	N/A	***N/A***
SERI	T-iso	Colorado, USA	Livne and Sukenik, 1992	25	no
	S/ISOCH-1	Colorado, USA	Qiang and Richmond, 1994	27	N/A
TML	*I. galbana* TK1	Pingtung, Taiwan	Liu and Lin, 2001 Zhu *et al.*, 1997a Zhu *et al.*, 1997b	25 <35 30	no yes no
UNKNOWN	**I. galbana**	Unknown	Liu and Lin, 2001 Phatarpekar *et al.*, 2000 Whyte, 1987	25 20 20-28	no N/A N/A
	NT13	Darwin harbour, Australia	Renaud *et al.*, 1999	25	yes
	PS11	Port smith, W.Australia	Renaud *et al.*, 1995	20	yes

Table 1.2: Comparison of *Isochrysis* strains used by various authors. Listed based upon origin of strain and type as described by authors. Comparisons of optimal growth temperature used and detection of EPA. Refer to appendices for abbreviations of collection facilities.

1.5.2: *NANNOCHLOROPSIS OCULATA*

N. oculata is a marine microalga, which was first isolated by Droop in 1955. It is perhaps one of the smallest microalga, being a slightly ovoid shape no bigger than between 2 – 4 μm. Because of it's small size (even amongst other microalgae) it is also sometimes referred to as a 'picoplankton' (Hibberd and Leedale, 1972). *N. oculata* is known to tolerate a wide range of temperatures, from 15 to 30 °C (Zittelli *et al.*, 1999). Growth is however phosphate limited (Graham and Wilcox, 2000). *N. oculata* is referred to in aquaculture as 'marine *Chlorella*' it has often been confused with the freshwater species (Fisher *et al.*, 1998). Ultrastructure analysis of the cells organelles later revealed it to be a separate species altogether, despite sharing similar physical characteristics with *Chlorella* (Maruyama *et al.*, 1986). The major difference being the accumulation of lipid globules rich in EPA by *N. oculata* (Maruyama *et al.*, 1997; 1986). *N. oculata* is very delicate with only a thin cell wall, which makes it easy to readily digest by zooplankton and other prey (Kureshy *et al.*, 1999; Duerr *et al.*, 1998).

1.6: 'OPEN' MICROALGAL CULTIVATION SYSTEMS

Microalgae have been grown commercially for over 50 years with varying degrees of success. The major problem is providing an adequate (efficient) lighting regime to maximise photosynthetic potentials of cultures. Whilst heterotrophic growth (using carbon based media to bypass photosynthetic pathways) can eliminate this requirement, media are expensive (Pulz and Scheibenbogen, 1998), can often lead to reduced growth rates (Benemann, 1990) and increase susceptibility to contamination (R. Bowles, pers. com). The methods employed to cultivate microalgae should take into account the physiology of the species being grown (e.g. easily prone to sedimentation and cell damage) and be cost-effective in relation to the value of the end product.

1.6.1: Lakes and ponds

The most common type of open cultures for microalgae are lakes, ponds (either natural or artificial) which are normally no deeper than 20 cm (Pulz and Scheibenbogen, 1998; Qiang and Richmond, 1994; Benemann, 1990). Therefore, large volumes require large plots of land, meaning that productivity in terms of area (areal productivity, $L/m^2/day$) is low. Mixing of these cultures is poor, unless manually managed, since natural tidal currents and winds alone are often insufficient and result in sedimentation. Despite being labour intensive, the technical knowledge needed is basic and therefore open culture systems are sometimes grown in third-world countries where weather conditions are also favourable and the labour costs low. Locations, must also provide a relatively consistent level of irradiance, however cultures can suffer high levels of evaporative loses as a consequence (up to 10 $L/m^2/day$) (Becker, 1994). Yet perhaps the major constraint of such large open ponds and lakes is contamination. Many algal strains are unable to grow successfully in open environments due to predation by zooplankton or competition from other algae and/ or bacteria indigenous to the location (Pulz and Scheibenbogen, 1998). In order to overcome this problem, microalgal strains must ideally be fast growing in order to compete for nutrients or able to grow under highly selective conditions. *D. salina* and *Spirulina* are two such examples for their ability to grow in hyper-haline and alkaline conditions, respectively (Richnomd, 2000). Typical locations for open pond/ lake cultures include: La Paz (Mexico), the Dead Sea (Israel), the Great Salt Lake (Utah)

and the Pink Lake (Western Australia) (Borowitzka, 1999; Pulz and Scheibenbogen, 1998; Benemann, 1990). *Spirulina* is commercially grown in Lake Texcoco (Mexico), which has been modified by pumping water through a series of dykes to resemble a caracol shape ('caracol', the Spanish word for snail) (see Plate 1, below), 3200 m in diameter (Borowitzka, 1999). Aztec Indians are also believed to have harvested *Spirulina* for food from this very lake prior to the arrival of the Spanish explorer, Hernando Cortez in 1513 (Becker, 1994). Meanwhile, one of the largest open lakes for *Dunaliella* cultivation is Hutt lagoon in western Australia (Borowitzka, 1999; Pulz and Scheibenbogen, 1998) which is a highly visible feature of the landscape due to it's accumlation of β-carotene (see Plate 1).

Plate 1: Aerial views of natural microalgal lake cultures. Lake Texcoco, Mexico (top) was originally used by Aztec Indians is now commercially farmed for the production of *Spirulina*. Hutt Lagoon, Western Australia (bottom) is used to produce β-carotene rich *Dunaliella*.

1.6.2: Raceways

During the 1950's microalgal cultivation methods were developed as a means of waste treatment, a result of which was the development of the 'high-rate pond' by Oswald (1963). By essentially using a motorised paddle-wheel, cell productivity was increased as a result of improved nutrient mixing and re-suspension of the culture (Markl and Mather, 1985). This basic principle has lead to the development of elongated ponds featuring a central division from which a paddlewheel extends halfway to re-circulate cultures in a circuit, which coined the term 'raceways' (see Plate 2). Since an area can be devised into separate plots, raceway cultures can also be covered with plastic sheets in order to prevent evaporative loss (Becker, 1994), as commonly suffered with large lake cultures. Alternatively, raceway cultures can also be grown indoors (i.e. greenhouses, which still provide natural light) where temperature can be regulated. Although a relative simple development, this has allowed for better manageability and improved consistency in performance. Such cultures can easily cover an area of 5000 m^2 (0.5 hectare) (Parrish *et al.*, 1998) due to the relative ease with which they can be scaled-up, although a potential size limit of ~5 hectares (given various design considerations) exists due to hydraulic problems, according to Benemann (1990).

Plate 2: Ariel views of microalgal raceway ponds. Cyanotech, Kailua-kona in Hawaii (left). Earthrise farms in Southern California (right) occupies a total area of 100,000 m^2.

1.6.3: 'Poly-bag' cultures

The use of polyethylene bags is seen as the more modern approach for open culturing, allowing cultures to be stored upright (see Plate 3). These consist of vertically draped polyethylene bags filled with culture, capable of holding volumes of up to 500 L each (Fidalgo *et al*., 1998). Wire cages can be used to support larger volumes, or alternatively transparent fibreglass can be used instead for rigidity. Tubes are inserted from top to bottom to provide aeration, using pumps to keep cells in suspension. Air can also be enriched with CO_2 to aid photosynthesis (i.e. preventing photorespiration- refer to Section 1.9.3). Poly-bag cultures, as with raceways, can be grown indoor to allow for more control over environmental variables. A very simple and effective solution, predominantly used by marine hatcheries (Borowitzka, 1997; W. Hartley, pers.com), that requires little or no maintenance. In fact once cultures are harvested; the poly-bags can be easily disposed of, foregoing post-operative cleaning (or 'decommissioning'), being relatively inexpensive to replace (Martinez-Jerónimo and Espinosa-Chávez, 1994). The most significant aspect of the vertical arrangement is that more volume can held per unit area of floor space (i.e. a smaller 'footprint'). However, these cultures still remain largely open and are at risk from contamination (Lin *et al*. 1976).

Plate 3: 'Poly-bag' cultures. Polyethylene bags filled with culture hung from a beam (left). Cultures can be grown indoors although artificial lighting is required (left). A tube is inserted from top to bottom in order to mix and aerate cultures. Larger bags (right) can hold up to 500 L, and are supported using a plastic base and wire mesh.

1.7: 'CLOSED' MICROALGAL CULTIVATION SYSTEMS

The progressive development of open cultures (Section 1.6) helped bring microalgal cultivation into the laboratory (particularly poly-bag cultures), and closer to the microscope of scrutiny. Under which, the susceptibility of cultures to contamination was all too clear. Growing cultures in sealable vessels was the first logical step, however, unlike traditional and well established microbial bioreactor designs; microalgal cultivation must also apply methods to maximise photosynthesis (Benemann, 1990). Having adopted knowledge normally applied to aerobic fermentation systems, microalga growth has improved by controlled manipulation of environmental parameters. This hybrid mix of expertise has led to a variety of closed microalgal systems, to fall under the generically titled umbrella of 'photobioreactors'. Yet whilst algologists may have developed a growing awareness of basic hydrodynamics and mass transfer principles, the solution to fully maximise their vast potential remains largely in the dark. The main draw-back being cost efficiency of such technologically advanced systems, which are comparatively more expensive to run than open cultures. However, the application of photobioreactor cultures can be justified by the production of high-value/ low volume products, such as pharmaceutical health foods. Furthermore, whilst sceptical views may be held by more traditional marine hatcheries (where open cultivation is common practice) a review by Pulz *et al.* (1998) suggests that closed systems can outperform raceways by as much as 300%, in terms of daily productivity.

1.7.1: Conventional stirred tank reactors

Conventional stirred tank reactors (CSTRs) are one of the most common types of reactor used in many areas of microbial fermentation (see Figure 1.7). Their hydrodynamic characteristics are well established, and are a familiar tool within biotechnology laboratories. Sparge lines can be introduced, providing filtered aeration, although these primary serve to oxygenate aerobic cultures and are not themselves a direct means of agitation. Mixing within these systems is strictly mechanical by way of impeller blades within the culture, which are usually propelled by an external motor capable of high speeds (Molina Grima *et al.*, 1996). The geometric arrangement of the impellers can be conFigured in many ways, although the most common type used are referred to as 'Rushton turbines' (Merchuk, 1988). CSTRs are more commonly associated with the growth of yeast or filamentous fungi for production of artificial meat substitutes (e.g, mycoprotein). Certain filamentous strains of algae can be grown in CSTRs (Benemann, 1990), however the majority of microalgae do not generally have the physical tolerance to cope with the pressures (shearing force caused by spatial gradients between two stream of flow) exerted as a consequences of the impeller rotation producing vortices (Acheson, 1990; Merchuk, 1988). Many microalga do not possess a tough outer cell wall, thus causing the cell membrane to rupture as a result of mechanical stress (Benemann, 1990).

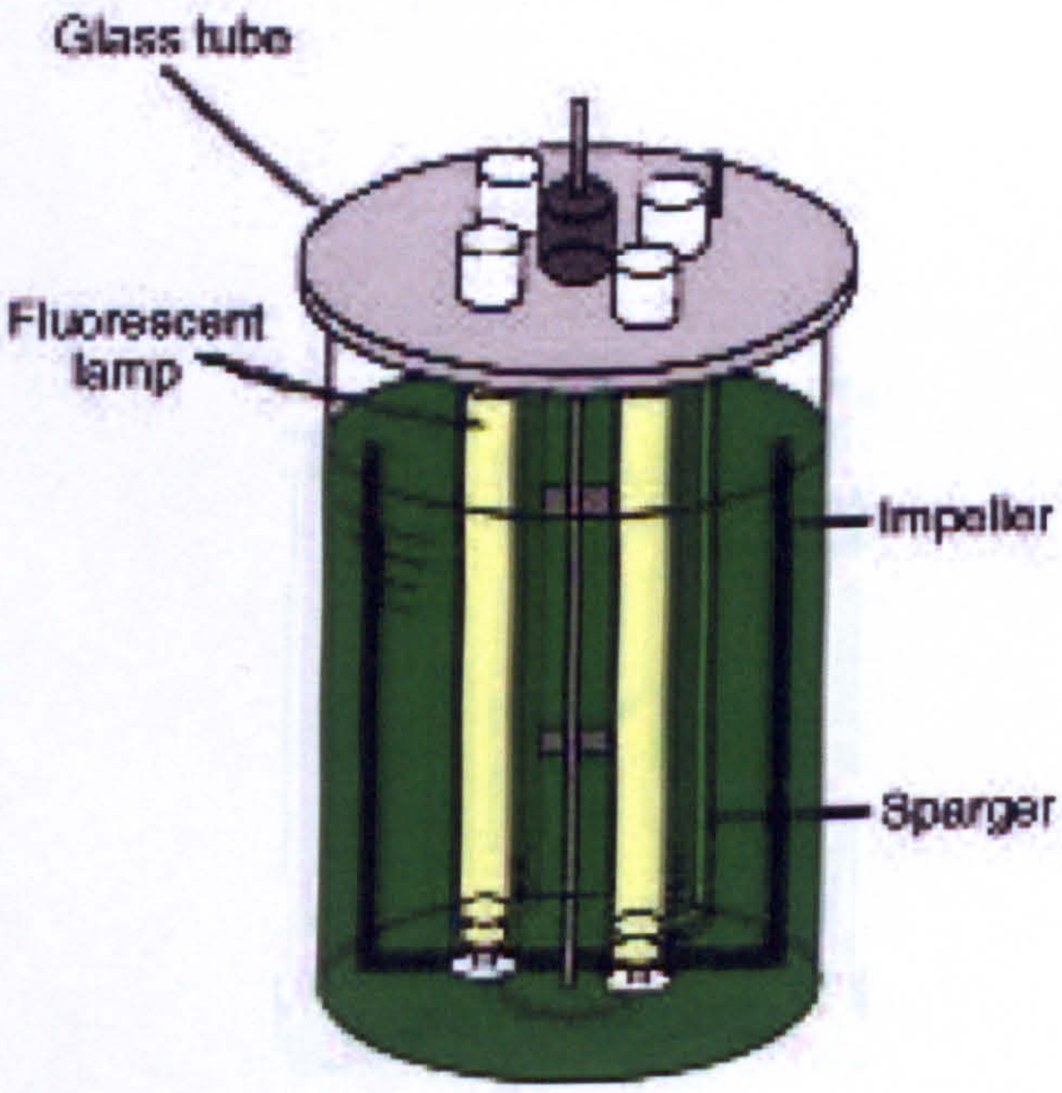

Figure 1.7: Conventional Stirred Tank Reactor with internal illumination

1.7.2: Bubble columns and Air-lift reactors (ALRs)

Bubble columns are similar in principle to open poly-bag cultures (see Section 1.6.3), although this cylindrical photobioreactor is normally constructed of glass, and is fully sealed for increased sterility. The basic design consists of a large aspect ratio (height: diameter) in order to maximise mass transfer time between the gas and liquid phase (Acheson, 1990). This has the advantage of reducing the overall 'footprint area' in which cultures are grown, but also consequently limits scale-up as height increases relative to maintaining aspect ratio. Mixing is provided solely by aeration at the base of the column, which has a lower shearing impact on the cells unlike impeller blades (Hebrard *et al.*, 1996). Bubble size and dispersal is regulated by the use of a sparger (a hollow perforated device) bar or Plate, which can be used to regulate heterogeneous (turbulent) or homogeneous flow regime (refer to Section 4.3.1.ii). Sparger configuration can vary in shape, pores size, pore number, and even fabrication can influence the hydrodynamic properties of a culture (Hebrard, *et al.*, 1996). The main advantage of bubble columns is the lack of moving parts, thus making them easy to construct and maintain in comparison to CSTRs (Otero *et al.*, 1997). Due to a relatively low mass transfer rate, compared to CSTRs, the bubble column has been developed over the years by introduction of baffles (similar in principle to raceway cultures- refer to Section 1.6.2) in order to control re-circulation (an internal-loop) and increase mixing efficiencies (Reitan *et al.*, 1997). Such systems are distinguished from bubble columns as air-lift reactors (ALRs). Sections of directional flow are often referred to as 'risers' and 'downcomers'. The top Section of the photobioreactor is also widened to facilitate gas hold-up within the system. ALRs have essentially evolved in design (see Figure 1.8), with riser Sections wider than the downcomer and the removal of a mid-Section altogether, giving rise to external-loop ALRs.

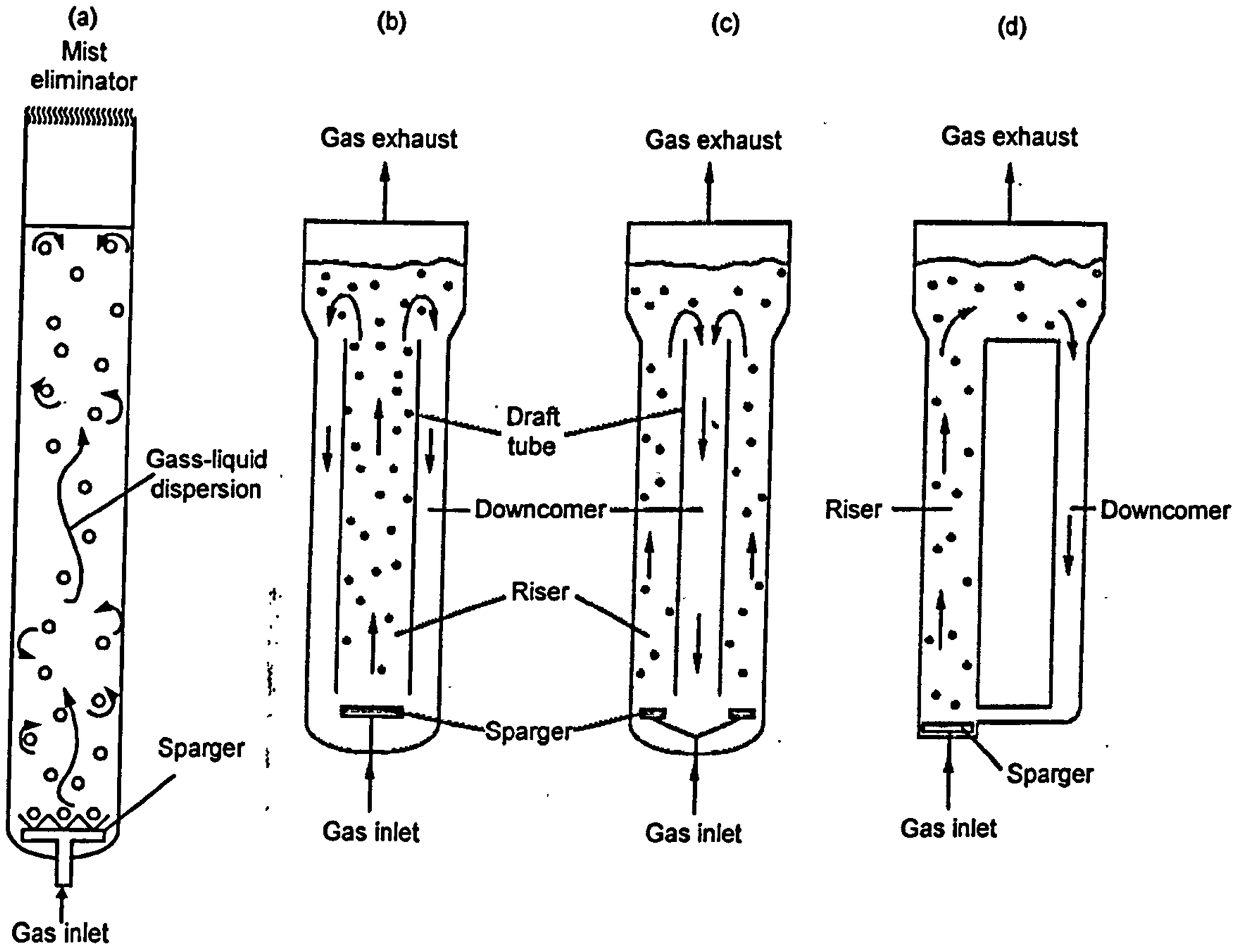

Figure 1.8: Comparative patterns of fluid flow between aerated photobioreactors. Bubble column (a); (b; c) baffled internal-loop air-lift reactors; (d) an external-loop air-lift reactor. Refer to text for details.

1.7.3: Laminar photobioreactors

Laminar photobioreactors are in essence based upon the simple solution evolved by plants over millions of years, that of a flat 'photostage'. Consisting of two parallel pieces of sealed glass or plastic, usually no deeper than 10 cm (Cheng-Wu *et al.*, 2001) in order to reduce the light path (distance needed for light to penetrate through a culture). This helps to maintain 'optically thin' (translucent) cultures, which minimises the effect of self-shading which can be limiting to achieving high cell densities (Richmond *et al.*, 2003). Typically rectangular in shape, they are also referred to as 'Plate-type reactors' (Borowitzka, 1999; Pulz *et al.*, 1995). Outdoor systems can be arranged vertically to hold upto 6000 litres and their orientation automated to track the movement of the sun (Pulz *et al.*, 1995). Whilst, indoor cultures can be illuminated on both sides in order to further minimise effects of self-shading (Plate 4).

Plate 4: Laminar photobioreactor Wageningen university, Netherlands

1.7.4: Tubular photobioreactors

Tubular photobioreactors are based upon external-loop ALRs (see Section 1.7.2), in that the downcomer has become extended, functioning instead as the photostage, serving to increase the surface area to volume ratio available for light absorption (Chrismadha and Borowitzka, 1992) (Figure 1.9). Manifolds at the end of the downcomer can also be used to disperse cultures through separate channels or 'windings' (Plate 5), which is less energetically demanding for the pump and also aids nutrient mixing (N. Clarkson, pers. com). The arrangement of photostage windings can also vary in geometry such as; vertical (Richmond and Zou, 1999), horizontal (Molina Grima *et al.*, 1999), α-type (Zhu *et al.*, 1997), or helical (Perez, 1994) configurations. Tubular photobioreactors have a number of advantages over other closed systems (Renaud *et al.*, 1999), but most importantly is the comparative ease in which these systems can be potentially scaled-up (Borowitzka, 1997; 1994).

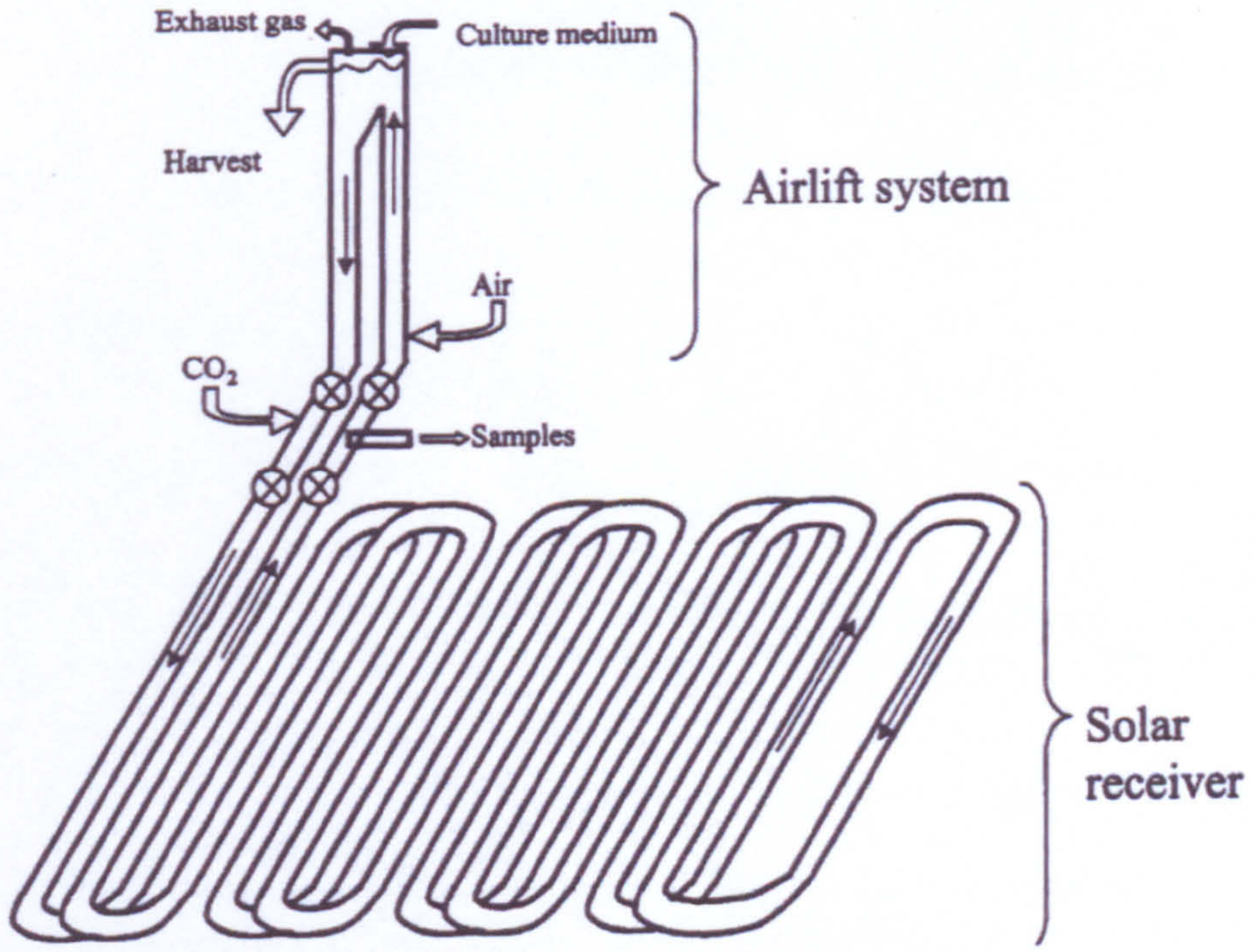

Figure 1.9: Schematic diagram of a horizontal tubular photobioreactor. Downcomer of the air-lift Section leads out into a weaved horizontal photostage (solar receiver), providing a large surface area to volume ratio for light absorption (diagram taken from Molina Grima *et al*., 2001).

Plate 5: A horizontal tubular photobioreactor with manifolds. This system based in Sede Boqer, Israel. Developed by the Jacob Blaustein Institute for Desert Research, the downcomer is devised into parallel rows, which are more energetically efficient for recirculation.

1.8: MICROALGAL PRODUCTION METHODS

Commercial ventures can focus heavily upon production time-scales. Production methods can significantly influence daily harvest volumes, cell density and culture quality. Four main production methods are available:

1.8.1: Batch cultures

A method regularly employed for small-scale experiments or for the step-wise 'scale-up' of cultures into larger volumes. As a production method this approach is more traditionally associated with open microalgal cultures. Harvesting takes place when maximum cell density and/ or product accumulation has been achieved. The entire working volume is extracted and photobioreactor sterilised and re-inoculated. Batch cultures are highly labour intensive and requires adequate timing to ensure the media and inoculum for the next batch is ready in time to replace one which has just been harvested. Several batches can be run in a staggered cycle to each other to ensure continuous harvesting. However, productivity can be compromised as harvesting more often becomes a result of timing rather than ensuring culture optimisation. Monitoring of cell number and quality can become secondary to achieving the time-scales involved in maintaining a set production rota.

1.8.2: Semi-continuous cultures

A known volume is manually harvested, typically no greater than 40 %, and replaced in one bulk amount with fresh medium once every 24 hrs. This provides a high impact in regards to diluting the culture (creating a 'wash-out' effect), but also allows the longest possible period of recovery (cell growth) before the next harvest. As with the batch cultures, this production method is also a labour intensive approach, requiring daily maintenance, although full sterilisation and re-inoculation can potentially be delayed since the daily replenishment of media should prolong operational lifespan. Since there is a daily harvest, unlike batch cultures, maintaining a staggered rotational culture regime is less of a priority. However, if the renewal volume is too great, cell density can be quickly lost and difficult to recover.

1.8.3: Continuous cultures

Continuous cultures feature an outlet or overflow which is level with the cultures working volume. Media is continuously pumped at a fixed rate in order to drip-feed the culture with fresh nutrients. The displacement volume is automatically harvested from the overflow, and thus a constant working volume is maintained. Since media renewal is automated, it is essential that pumps be accurately calibrated. Providing the cultures growth rate is equal to the rate of daily renewal, cell density can reach an equilibrium referred to as 'steady-state growth'. Because the media is supplied continuously, once cultures are running such a production is less labour intensive and can be potentially ran for years before needing to re-inoculate. This allows for more time to monitor culture performance and quality. Continuous cultures were first applied to microalgal cultivation in 1951 (Goldman *et al.*, 1982) as a means of producing increased biomass levels of *Chlorella* as a source of SCP.

1.8.4: Fed-batch cultures

Fed-batch production acts almost as an intermediate between continuous (in that a constant working volume is maintained) and semi-continuous methods (in that media renewal only takes place at a set time of day). Rather than pumping media 24 hrs/ day, timers are used to set a fixed period over which media is added. For example, the same volume, which would otherwise be provided continuously, becomes condensed into a set time-frame (i.e. pumps are set to run for 12 hrs/day). Media renewal rate (L/hr) for that period is increased causing a heightened dilution effect similar to semi-continuous production (which is an instant renewal), but over a longer period. Whilst this means the recovery periods may be comparatively shorter, this can be justified in that the initial impact is less intensive towards cell density than that of a semi-continuous system. Another strategy to increase daily harvest volumes is to increase the dilution rate still further for set periods of media renewal, but allows for longer recovery periods by setting timers to run only every other day as opposed to daily. As with continuous cultures, pumps must be well calibrated.

1.9: LIGHT AND PHOTOSYNTHESIS

1.9.1: The light spectrum and pigments

The electromagnetic spectrum of light is measured in terms of wavelength (λ) expressed as nanometres (nm) with a holistic range of 10^{-5} to 10,000 nm (Ryer, 1997). The pigmentation (colour) of photosynthetic organisms is such that they generally absorb light at a wavelength range between 400 – 700 nm, known as the photosynthetically active region (PAR- as defined by SCOR/ UNESCO (Sakshaug *et al.*, 1997)) of the visible light spectrum (380 – 770 nm). The PAR constitutes the absorption of light by over 600 known individual pigments, primarily consisting of chlorophylls and secondary carotenoids (sub classed carotenes- cyclic derivatives; and xanthophylls- oxygenated derivatives), each with individually specific absorption spectra (Young and Britton, 1993). For example, chlorophyll *a* has absorption peaks within the blue and red light ends of the visible spectrum, which to the human eye appears as a green pigment since this region of the light spectrum (500 – 600 nm) is reflected (Ryer, 1997) (see Figure 1.10). Chlorophyll *a* is the primary pigment of most algae, the presence of which has been used to distinguish cyanobacteria from photosynthetic bacteria (Graham and Wilcox, 2000).

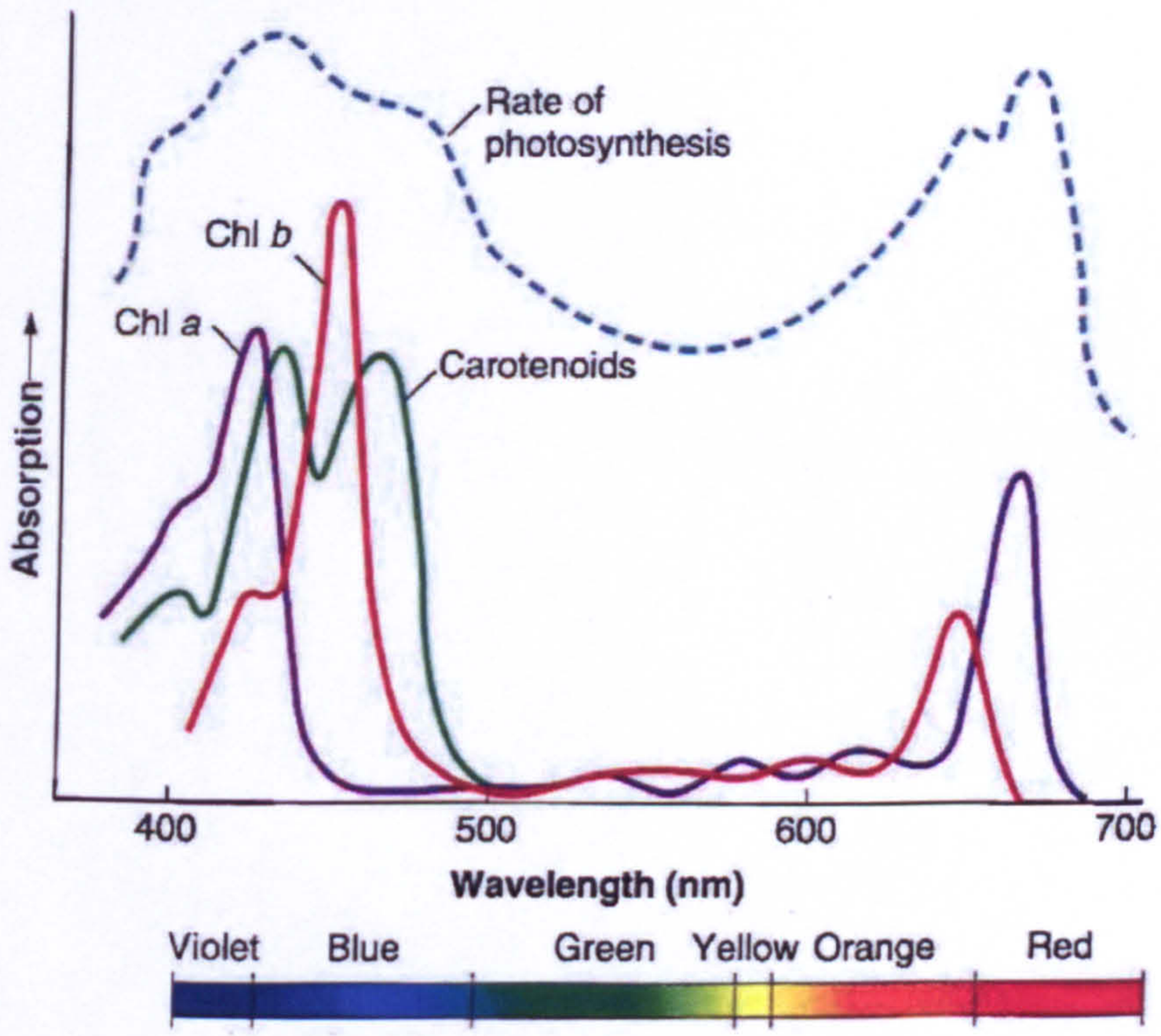

Figure 1.10: An action absorption spectrum. Showing the light absorption ranges across the visible light spectrum of various types pigments used in microalga for photosynthesis.

1.9.2: Cellular light absorption

Any single microalga will contain not just one, but often several pigments with one dominant (primary) and the others (secondary) acting in a supplementary role quenching any excess light energy (along with non-photosynthetic functions). Under adverse (stress) environmental conditions secondary pigments can become more concentrated causing a visible change in colour. Pigments are found within the photosynthetic organelles (collective termed chromoplasts) of a cell, bound by a double membrane (Graham and Wilcox, 2000). The majority of a chromoplast's volume is occupied by an extensive third membrane (the thylakoid membrane) which is folded/ stacked into disc-shaped vesicles called grana, with series of granum connected to each other by irregular Sections of the same membrane (Graham and Wilcox, 2000; Guttman, 1999). The thylakoid divides the chromoplast into an internal (the lumen) and an external space (the stroma). Chromoplasts whose thylakoids comprise primarily of chlorophylls and are specifically referred to as chloroplasts (see Figure 1.11).

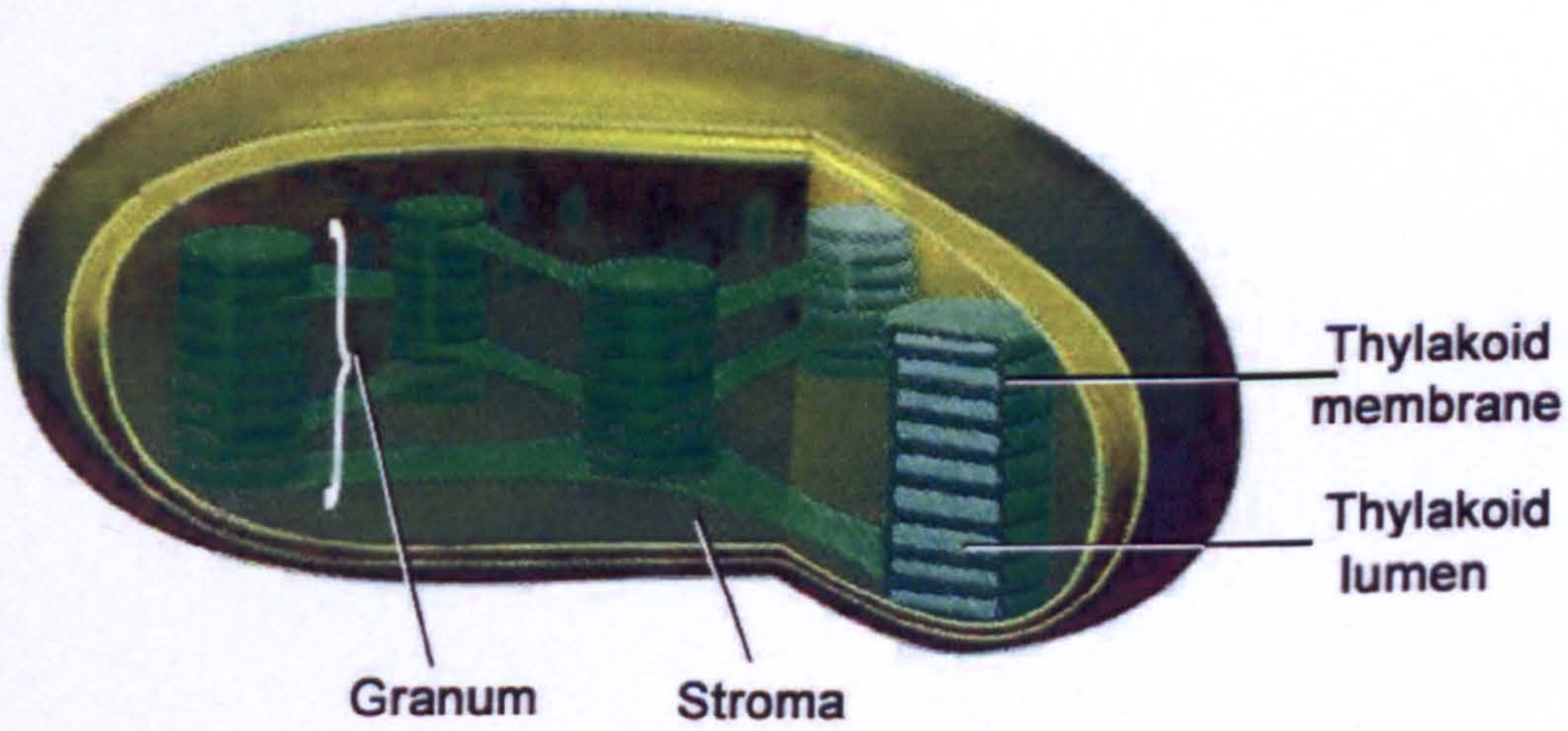

Figure 1.11: Cross-Sectional view of a chloroplast. A chromoplast consisting primarily of chlorophylls. A third internal membrane structure called the thylakoid forms disc-like stacks (granum), creating a partion between the stroma thylakoid lumen. Refer to text for details.

The division of the plastid into thylakoid and stroma is significant in that together they perform two separate phases of photosynthesis termed the light and dark cycles. Light-dependent reactions take place within the thylakoid whilst light-independent (or dark) reactions occur in the stroma. These two phases of photosynthesis are summarised below (see Table 1.3). Photosynthetic pigments contained within the thylakoid membrane bind with proteins to form complexes called photosystems (PS). Chloroplasts feature two photosystems (PS I and PS II). Each photosystem consists of 200 – 300 chlorophyll molecules packed with proteins and act as a light harvesting chlorophyll protein antennae (LHCP) complex, and a reaction centre (Jeffrey *et al.*, 1997; Walker, 1988) (see Figure 1.12). The LHCP is arranged so that any chlorophyll molecule can absorb a photon of light causing excitation of electrons (excitons) and transfer this energy to another, almost like a funnel, until eventually becoming channelled towards the reaction centre (or trap). The electrons excited state is unsTable and eventually returns to it's natural 'ground state', as it loses energy it gives out light as fluorescence. The reaction centres of the two photosystems are identified as P700 in PS I, and P680 in PS II (reflecting their light absorption peaks). Each comprise of a special pair of chlorophyll molecules associated with proteins and electron carriers. Both synthesising chemical energy in the form of adenosine triphosphate (ATP) by a process called photophosphorylation. The LHCP together with the reaction centres of PS I and PS II are collectively referred to a photosynthetic unit (PSU) (Guttman, 1999).

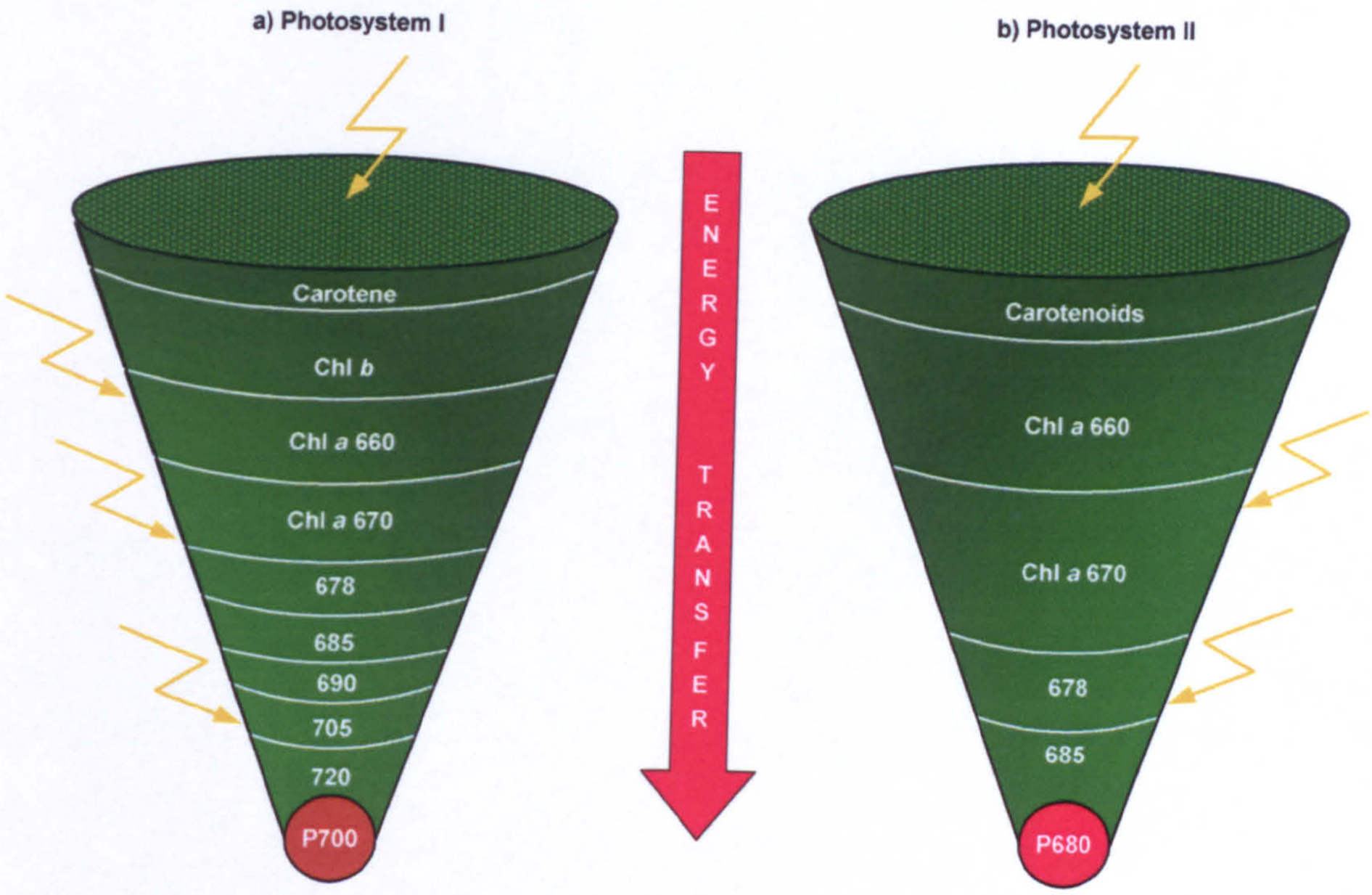

c) Molecular structure of Chlorophyll *a*

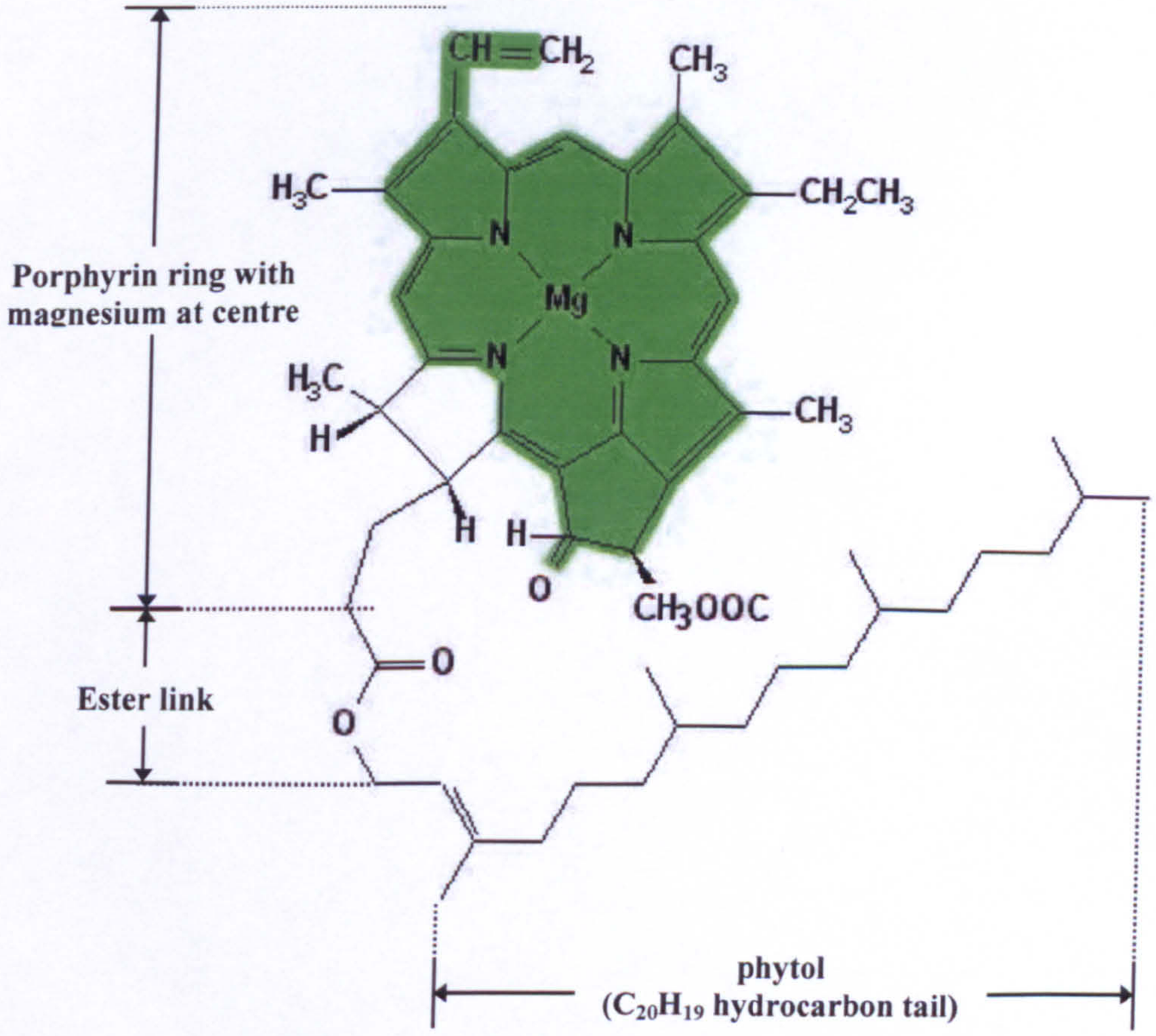

Figure 1.12: Pigments harvesting light. A simplified representation of how light harvesting complexes act as funnels to transfer photon (light) energy, shown by yellow arrows, to the reaction centres of photosystems I (b) and II (b). The molecular structure of chlorophyll *a* (C) consists of porphyrin ring, bound to a phytol (an alcohol) tail. The green region of the porphyrin ring highlights the area where delocalised electrons are formed upon reacting with a photon. Molecular weight = 893.50 (Jeffrey *et al.*, 1997).

1.9.3: Basic photosynthetic pathways

Photosystem I is primarily concerned with generating chemical energy, in the form of adenosine triphosphate (ATP), by a process referred to as cyclic photophosphorylation (Graham and Wilcox, 2000; Guttman, 1999). This begins with the transfer of light energy to the reaction centre of P700 (ground sate) resulting in excitation of an electron to a higher energy level, as the reaction centre becomes oxidised (P700*). A proton gradient is generated along a chain of intermediates within the thylakoid membrane, effectively pumping three protons (H^+) from the chloroplasts stroma into the thylakoid lumen. This results in phosphorylation of adenosine diphosphate (ADP) to ATP which is then transported back into the stroma, whilst PS I returns to it's ground state (Walker, 1988). During oxidation of PS I, an intermediate in the proton gradient, ferredoxin (having been reduced), can either pass along the cyclic path again (as described above) or be used to synthesise NADPH (nicotinamide adenine dinucleotide phosphate hydrogenase) from $NADP^+$. Having taken this secondary route, PS I remains oxidised and temporarily inactive since the cyclic pathway becomes broken. Meanwhile, PS II also oxidised by light energy, donates an electron along a non-cyclic chain of electron carriers (a process called 'the Z scheme'), finally reaching PS I which then reverts back to its ground state. During this electron transport towards PS I, a proton gradient is generated across the thylakoid membrane, which serves to aid ATP synthesis. ATP synthesis via this pathway is referred to as non-cyclic photophosphorylation. However, PS II remains oxidised ($P680^*$) and is reduced back to its ground state as a result of electron released from the splitting of water molecules (photolysis) by an enzyme (Guttman, 1999; Walker, 1988).

Whilst cyclic and non-cyclic photophosporylation, concerned with ATP and NADPH synthesis, both taking place within the chloroplast's thylakoid, carbon fixation occurs in the stroma (see Table 1.3). The pathway of carbon fixation was discovered by Calvin's 'lollipop' experiments (name used to describe the photobioreactor) with *Chlorella*, using the radioisotope carbon-14 (^{14}C) (Guttman, 1999). The cycle begins by using ATP to phosphorylate ribulose 5-phosphate being into ribulose bisphosphate (RuBP) which enters a pathway called 'the Calvin cycle': This 5C sugar becomes carboxylated in the presence of CO_2, to form RuBP carboxylase (a C6 enzyme), which is unsTable and breaks down into two molecules of phosphglyceric acid

(PGA). Additional energy from ATP is used by $NADPH_2$ to eventually reduce PGA into glyceraldehydes 3-phosphate (GTP, a 3C sugar). Six molecules of GTP are produced for every three molecules of CO_2 that enter the cycle. Five molecules of GTP are then used to regenerate RuBP, which re-enters the Calvin cycle, the remainder is used in other metabolic processes (e.g. proteins, lipids and carbohydrates). The metabolic cost of which is nine ATP and six NADPH molecules, produced from both cyclic and non-cyclic photophosphorylation. The integral pathways of photosynthesis are also illustrated in Table 1.3.

It is important to also note that in the presence of oxygen, RuBP can also form RuBP oxygenase (Guttman, 1999). This is thought to be an evolutionary defect, since photosynthesis evolved when oxygen levels on Earth were minimal (Walker, 1988). A by-product of this is the build-up of carbon-rich glycolate. This in turn is broken down by a process called 'photorespiration' in order to recover some carbon. However, this is done at a greater metabolic cost (using $NADPH_2$ and ATP) and CO_2 is also released (Graham and Wilcox, 2000). Ultimately, oxygen is a competitive inhibitor for RuBP and can make photosynthesis energetically inefficient, if concentrations are greater than carbon dioxide.

	LIGHT REACTIONS	DARK REACTIONS
Location in chloroplast	Thylakoid	Stroma
Reactions	<u>Photochemical (light requiring)</u> Light energy causes the flow of electrons from electron 'donors' to electron 'acceptors', along non-cyclic or cyclic pathway. Two photosystems (I and II) are involved. These contain chlorophylls which emit electrons when they absorb light. Water acts as an electron donor to the non-cyclic pathway. Non-cyclic electron flow results in production of ATP and $NADPH_2$	<u>Do not require light (can occur in light)</u> Carbon dioxide is fixed when it is accepted by a 5C compound- Ribulose bisphosphate (RuBP), to form two molecules of a 3C-compound phosphoglyceric acid (PGA), the first product of photosynthesis. A series of reactions (Calvin cycle) occur in which RuBP (the carbon dioxide acceptor) is regenerated and PGA is reduced to sugar
Overall equation	**PS I: Cyclic photophosporylation:** $ADP + Pi \longrightarrow ATP$ (producing ATP for the dark cycle) **or** **PS II: Non-cyclic photophosporylation:** $2H_2O + 2NADP \longrightarrow O_2 + 2NADPH_2$ (photolysis of water producing oxygen)	$CO_2 + H_2O \xrightarrow[2NADPH_2]{3ATP} [CH_2O] + 2H_2O \xrightarrow[2NADP]{3ADP + 3P_i}$
Results	Light energy is converted to chemical energy (ATP and $NADPH_2$). Water is split into hydrogen and oxygen (photolysis). Hydrogen is carried to NADP and oxygen is a waste product	Carbon dioxide is reduced to carbon compounds such as carbohydrates and lipids, using the chemical energy in ATP and hydrogen in $NADPH_2$
Combined equations	Light + Chlorophyll } $2H_2O \rightarrow O_2 + 2H_2$	$[CH_2O]$ $CO_2 + H_2O$
Net equation	$CO_2 + H_2O \xrightarrow[\text{Chlorophyll}]{\text{Light}} [CH_2O] + O_2$	

Table 1.3: A summary of the metabolic pathways involved in photosynthesis. Refer to text for details.

1.10: AIMS

A series flask culture experiments (100 ml working volume) of both *I. galbana* and *N. oculata* were preliminary used in order to assess how various abiotic factors affected performance in terms of cell density and linear growth rates. Oxygen evolution rates were examined as means of assessing photosynthetic efficiency, whilst semi-continuous cultures helped determine cellular yields under a range of dilution rates. Analysis of total lipid and FAME content of cells was also conducted which, coupled with semi-continuous data, was later used to estimate productivity targets for larger volume cultures grown in a tubular photobioreactor.

Having standardised abiotic factors based upon flask culture experiments, *I. galbana* and *N. oculata* were later grown in a 70 L tubular photobioreactor to initially determine maximum cell density when operated in batch mode. Two methods of media renewal (continuous and fed-batch methods) were also tested to compare general growth performance along with estimates of PUFA productivities, derived from previous flask culture results.

Thirdly, the tubular photobioreactor was also physical characterised in order to quantify hydrodynamic attributes associated with mass transfer and lighting regimes, which can influence culture performance. The findings of which are discussed as a potential means of further increasing system productivities and scalability.

CHAPTER 2: GENERAL METHODS

A glossary of terms and abbreviations can be found in Appendix A. Statistical analysis of raw data was conducted to examine if culture conditions had significantly affected results between data sets of known variables, in terms of differences and/ or correlations. Statistical results, referred to in Chapters 4 – 7, were calculated using Minitab® for windows (version 9.2) software. Where significant, *p* values will be referred to in the main text. Full test statistic results are listed in Appendix D to show the test used, degrees of freedom (d.f.) and significance (*p* value).

2.1: CULTURE MAINTENANCE

The micro-algal seed stocks used in this study were originally received from the Culture Collection of Alga and Protozoa (CCAP, Windermere, U.K.). The two marine species selected for use throughout this study were *Isochrysis galbana* (CCAP strain 927/14) and *Nannochloropsis oculata* (CCAP strain 849/1). Strains were obtained from the Port Erin Marine Laboratory, Isle of Man. All cultures were kept in a growth room a Liverpool John Moores university, maintained (unless otherwise stated) at 23 ± 2 °C under continuous illumination, at an irradiance of 80 µmol/m^2/s from fluorescent light banks. Light measurements were always taken using a LI-250A light meter and an LI-190SA quantum probe (LI-COR: Lincoln, Nebraska, USA).

Original seed stocks were provided on agar slopes of f/2 media (see Appendix B), later used to inoculate 150 ml Erlenmeyer flasks (50 ml working volume). In this particular study larger volumes were agitated using an orbital shaker (Lab shaker, Adolf Kurhner A.G: Switzerland) at 110 rpm, to keep cells in suspension. Thus all stocks will be referred to as 250 ml shake flasks (with a 100 ml working volume).

The growth medium used in this study for both algae was sf/2 (see Appendix B), unless otherwise stated, which has been optimised to yield greater biomass productivity for selected marine microalgae (S. Banks. pers. com). This is a modified version of a commonly used marine medium (f/2). Since the algae used in this study were marine species, all medium was formulated using artificial sea-salt ("Coral Reef Red", Red Sea Pharmaceuticals: Israel) dissolved in distilled water at a density of 32 ‰ (unless otherwise stated). This concentration was used to simulate full-strength seawater.

2.1.1: Flask Cultures

Algal stocks were maintained in 250 ml shake flasks. 250 ml Erlenmeyer flasks were filled with 100 ml of media, sealed with non-absorbent cotton wool and foil caps. The flasks were then autoclaved (15 min at 121 °C and 21 psi) using a Midas 55 (Prior Cave: Woolwich, London, England). Inoculation (10 % v/v) was performed aseptically inside an IS CleanAir laminar flow hood (Bassaire: Southampton, England) from the original seed stock cultures. Flask cultures were also used to conduct preliminary experiments, for both *I. galbana* (Chapter 4) and *N. oculata* (Chapter 5), prior to cultivation within aspirators and the tubular photobioreactors.

2.1.2: Aspirator Cultures

Cultures were scaled-up using 5 L rounded flasks (working volume of 4 L) called 'aspirators' (see Figure 2.1). The aspirator was filled with sf/2 media and autoclaved (as above) in two parts- (a) 5 L rounded flask filled with medium and magnetic stirrer (sealed with non-absorbent cotton wool and foil cap) and (b) custom-made (author) rubber bung sealed in an autoclave bag. Inoculation of aspirator cultures was performed under aseptic conditions within a laminar flow cabinet (as above), seeded by 2 × 100 ml flask cultures (200 ml). Pre-autoclaved bungs were then flamed and used to seal the aspirator. These were then maintained by continuous 0.2 μm filtered (PolyVENT 16 filters, Whatman: Stuttgart, Germany) aeration using an air blower (constructed by author- origin of parts, unknown) and illumination (93 $\mu mol/m^2/s$). The magnetic stirrer bar aided mixing. Samples were taken, to monitor culture growth (data not shown), by closing the air outlet tap and opening the sample tap. Sample vials were replaced, with pre-autoclaved vials, by flaming. Aspirators were subsequently used to inoculate the photobioreactors as detailed in Section 3.2.4.

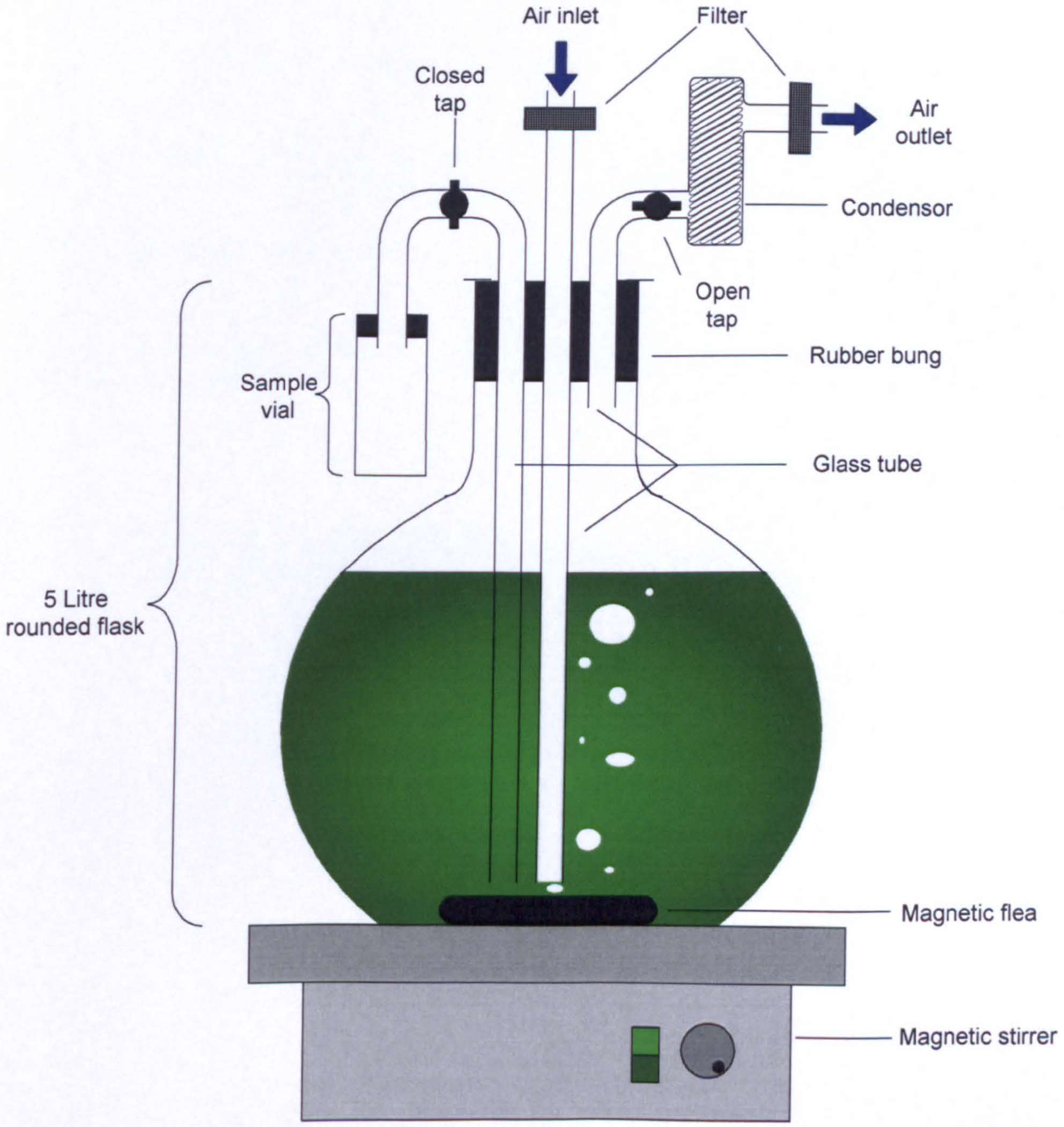

Figure 2.1: Aspirator culture. Cultures were continuously aerated (0.2 μm filtered) and illuminated. A magnetic stirrer and stirrer bar were used to aid mixing. Samples were taken (using aseptic flaming), by controlling tap positions, to monitor growth (data not shown) ready for inoculation of a photobioreactor (Section 3.2.4). Illustration made by the author. NOT TO SCALE.

2.2: GROWTH PERFORMANCE

Cultures were routinely monitored for aspects of growth performance as follows: changes in cell number and size, rate of growth, nutrient absorption, and photosynthetic efficiency of cells. Individual methodologies are detailed below.

2.2.1: Cell count and cell size determination

Cell counts were performed in triplicate to derive a mean and standard error. *I. galbana* was typically diluted to 1 in 100 (0.5 ml in 50 ml) and *N. oculata* to 1 in 500 (0.1 ml in 50 ml). Sodium chloride (6.5 g/L) was filtered under vacuum through a 0.2 µm WCN type filter (Whatman: Stuttgart, Germany) and used as the diluent. Particle counting and sizing was achieved using a Z2 Coulter counter (Beckman Coulter Ltd: Miami, USA). A sample volume of 0.5 ml was drawn through a 70 µm aperture for both algae.

The diameter of *I. galbana* cells was generally measured between 3-6 µm, and *N. oculata* between 2 - 4 µm. Particle size distribution was checked using the signal output to confirm a suitable range for the final cell counts, and adjusted as required. The peak of this distribution was recorded as the mean cell size.

2.2.2: Growth phases and Maximum growth rate calculation

Batch culture growth of micro-algal cultures typically follows four distinct phases (shown in Figure 2.2) were abiotic conditions are favourable to growth:

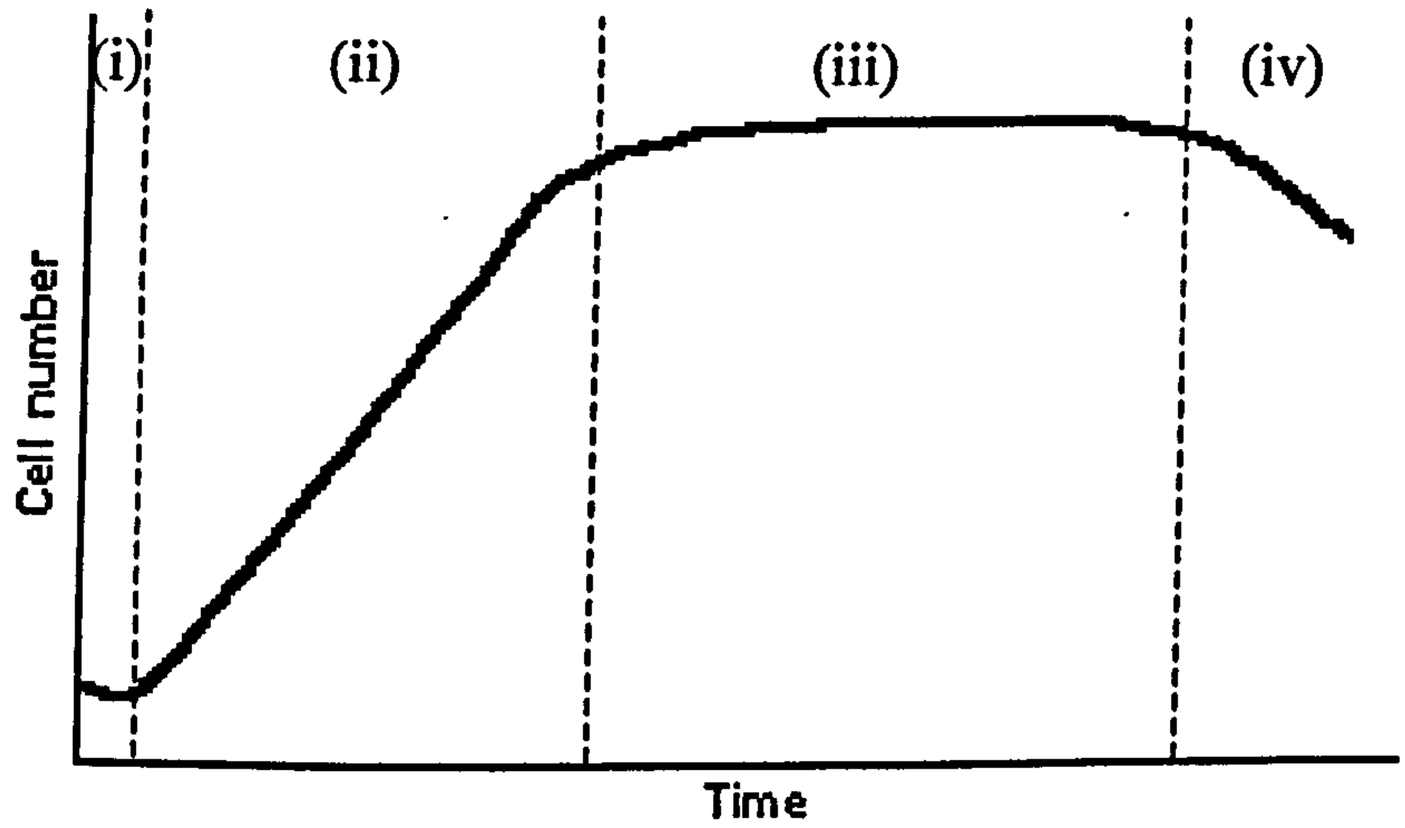

Figure 2.2: Typical microbial growth phases. Microbial growth can normally devised into four main stages: (i) Lag phase; (ii) Linear growth phase; (iii) Stationary phase; (iv) Decline phase. Refer to text for details

(i) Lag phase

Immediately after inoculation of culture into fresh media, there is a short (generally, a few days) acclimation period where cell number remains unchanged.

(ii) Linear growth phase

Once cells have acclimated, nutrient uptake allows for an increase in cell number. Cell population increases as medium nutrients become depleted at a fixed rate, provided other growth variables remain constant, until nutrient levels limit further growth. Linear growth phase was calculated (Equation 1) as a means of measuring cell division. Growth rates (μ) within this phase were calculated as follows:

$$\mu = (N_t / N_0)) / (t_1 - t_0)$$

Equation 1: Linear growth rate calculation. Where N_t = cell count at time t; N_0 = initial cell count at time 0; t = number of days.

(iii) Stationary phase

Eventually growth is said to become nutrient limited, and growth rate decreases until cells enter the third growth phase- stationary phase. During this period cell number remains relatively unchanged as cells breakdown cellular metabolites in the absence of extra-cellular nutrients.

(iv) Decline phase

Having exhausted cellular reserves, the culture then enters the decline phase of the growth curve and cell number decreases as cells breakdown.

2.2.3: Residual nitrate and phosphate levels

Residual (remaining within culture media) nitrate and phosphate levels were measured using a DR/2010 spectral analyser (Hach: Florlffoux, Belgium) and expressed in as mg/L concentration. Samples (50 ml) of culture media were filtered under vacuum, through 0.22 μm filters. Filtrate (2 × 25 ml) was then used to zero the analyser at 500 nm, before adding the contents of the Nitraver5 reagent powder (Permachem reagents, Hach: Florlffoux, Belgium) at room temperature. This was then mixed by shaking capped vials for one minute and left to react for a further 5 min before reading the absorbance to give a value in mg/L. Dilutions were made with artificial seawater (32 ‰).

The same procedure was followed to determine residual phosphate concentrations, with the exception that the filtrate was mixed with PhosVer3 reagent powder (as above) for 15 sec and left to react for 1 min before reading the absorbance at 890 nm.

2.2.4: Chlorophyll extraction and determination

The technique used to extract pigments from algal samples involves two key stages: cellular lysis to release the cell contents; and filtering out of the cellular debris to obtain the pigments. The method adopted for the extraction of chlorophyll *a* from algal samples during this study was based upon that described by Tsavalos (1993).

Aliquot (3 × 3 ml) of culture were centrifuged at 2500 rpm, using a MSE Mistral 1000 (Intergrated Services TCP Inc: Palisades park, New Jersey, USA), for 5 min to separate cells from the supernatant (media and extracellular products), which was subsequently removed. The resulting pellet was then re-suspended in redistilled water and centrifuged, as before, to further purify the sample. The supernatant was again removed, and the remaining pellet of cells re-suspended in redistilled acetone to weaken the tough cell wall of the algae. Samples were then transferred into 5 ml Bijou vials containing glass beads. The vials were then placed in a tissue disintegrator (Mickle Engineering Co. Ltd.: Guildford, England) for 5 min to homogenise the cells and release the cell contents. The homogenate was then filtered with redistilled diethyl-ether to obtain a pigment extract. The extracted pigment samples were then dried using a steady stream of nitrogen (oxygen free) to evaporate off the remaining acetone and ether, and to minimise damage to the pigments.

The extracted pigments were re-suspended in 90 % acetone and analysed with a HP8453 UV/VG spectrophotometer (Agilent: Stockport, England). Absorbance readings were taken at the absorbance peaks of Chlorophyll *a* (664 nm). All data was recorded on PC using the UV-Visible ChemStation software (Rev. A.06.04 (48), Agilent: Stockport, England) supplied. These absorbance values were then used to determine the total chlorophyll content of sample (μg/ml) using the calculation by Humphrey (1979).

2.2.5: Dissolved oxygen evolution

The rate of oxygen evolution from samples was measured using an Oxylab dissolved oxygen meter and an S1 dissolved oxygen electrode disc (Hansatech: King's Lynn, Norfolk, England). Data were recorded onto a PC using the Oxylab (V.1.09) software (Hansatech: King's Lynn, Norfolk, England). Temperature was maintained at 23.4 °C using a RM6 B (Lauda: Osterode am Harz, Germany) waterbath. Lighting was provided by a red (LH11/R) LED probe (Hansetech: King's Lynn, Norfolk, England) with a central wavelength of 610 nm.

Calibration was done using distilled water; aerated for at least 1 hour to achieve 100 % saturation point. A zero calibration point was made by adding sodium dithionite (2 mg), until a stable base-line was seen.

Algal samples (1 ml) were placed in the chamber and the magnetic stirrer set to 100 rpm to keep algal cells in suspension. Dissolved oxygen was initially recorded for 5 min at dark respiration (no light). Photon flux densities (PFD) of 100, 150, 250, 500, 1000, 1500 and 2000 $\mu mol/m^2/s$ were provided, each for a five minute interval of darkness before progressing to the next, with dissolved oxygen being measured at each step (Figure 2.3). This raw data were then used to generate a photosynthetic-irradiance (P-I) curve for a given sample that can be standardised to a cellular or volumetric chlorophyll *a* basis. From this P-I curve, key parameters were measured to characterise algal response increasing PFD (Figure 2.4). Dark respiration (R_d) is defined as the oxygen evolution (negative) in the absence of light. The photosynthetic rate (P) reaches its maximum (P_{max}) as the available light (PFD) reaches saturation. I_k is the PFD at half that required to achieve P_{max}. The initial slope of photosynthesis (α) is a measure of the maximum O_2 production per PFD achieved by the sample.

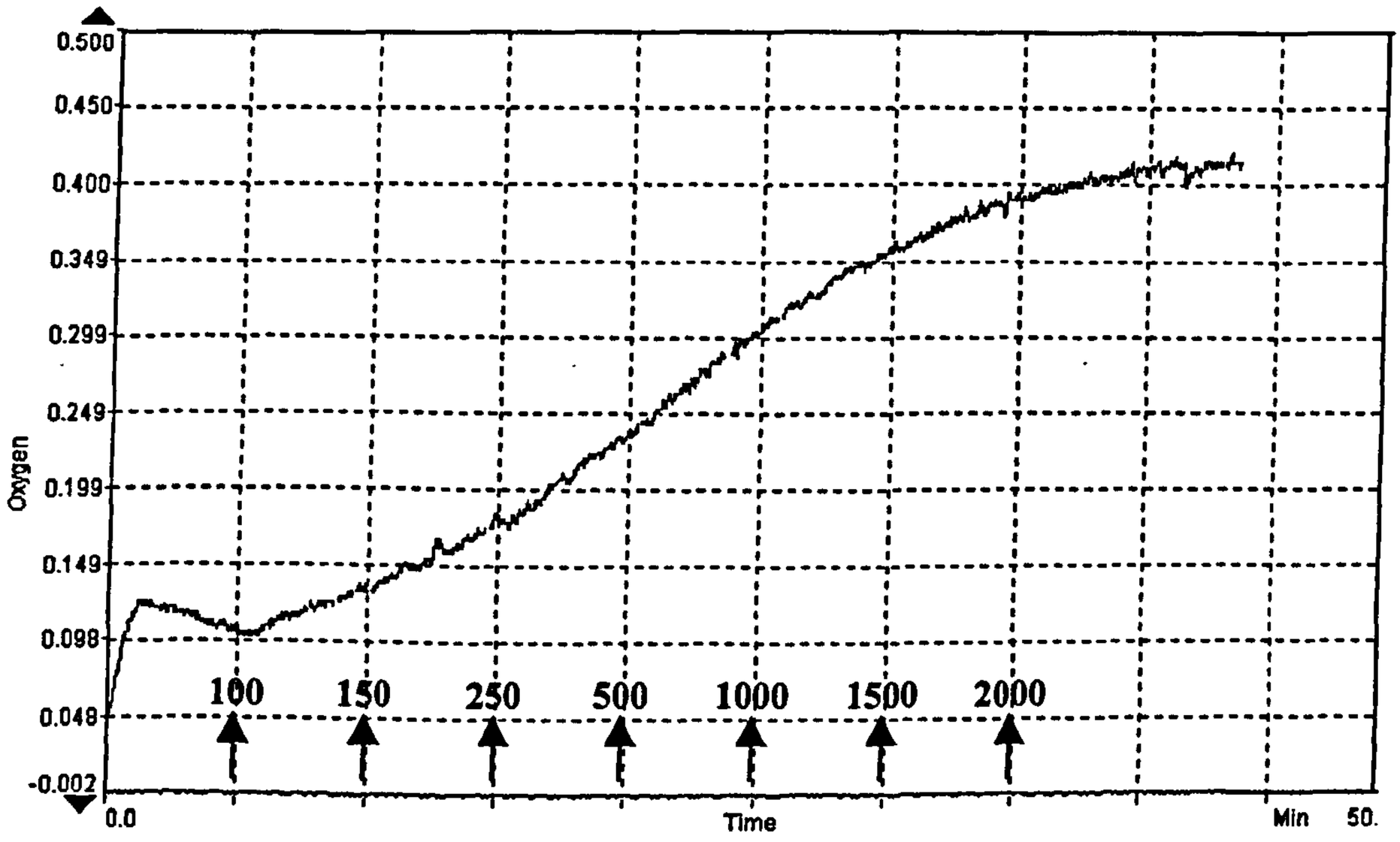

Figure 2.3: Annotated screen-print of realtime oxygen evolution data (an example). Arrows indicate increments in lighting level (Photon Flux Density) every 5 minutes. Sampling ranged from 0 to 2000 µmol/m^2/s after 35 minutes. The photosynthetic rate (P) was measured for each light intensity, before plotting a P-I curve (Figure 2.4).

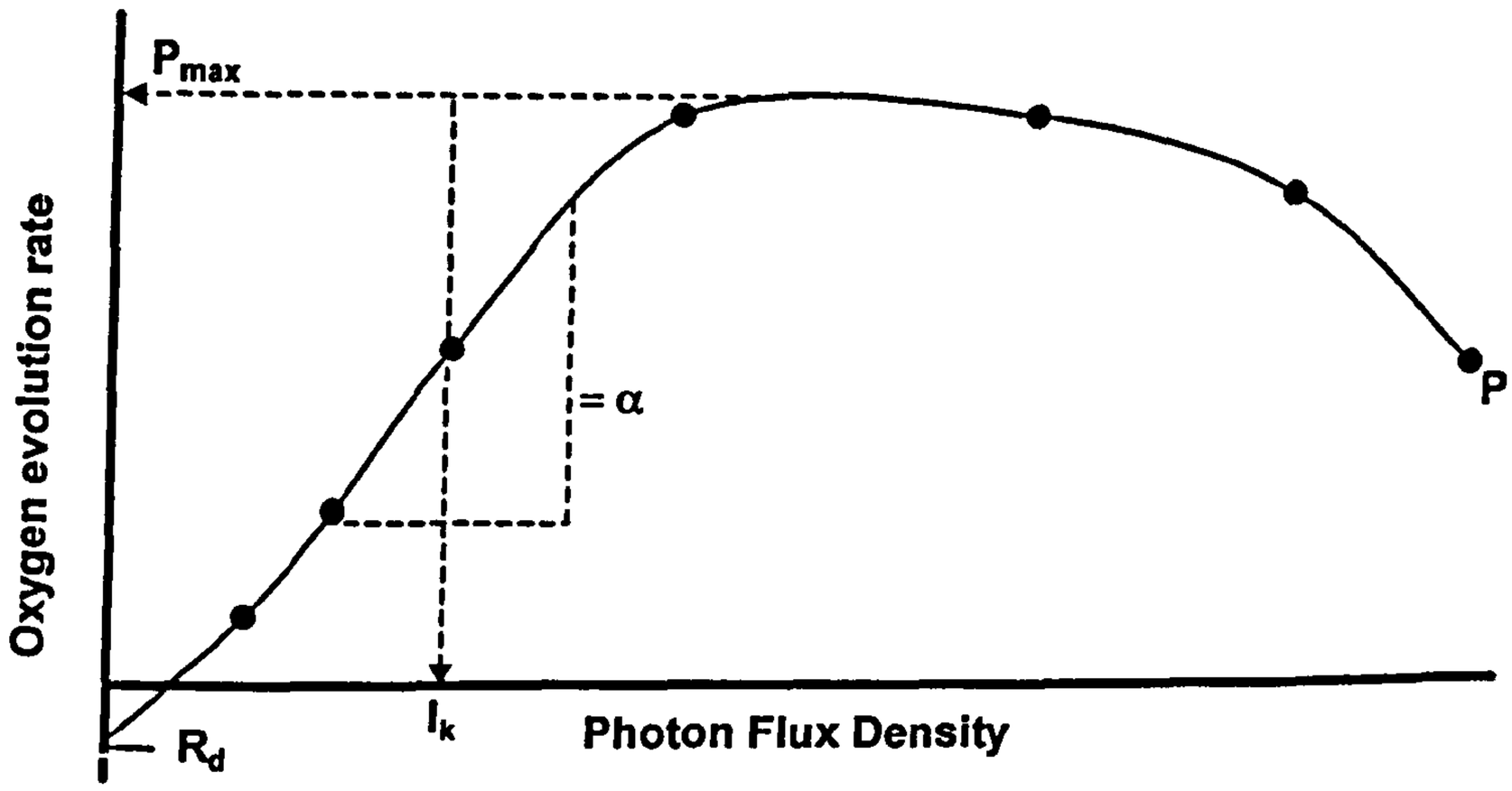

Figure 2.4: Photosynthetic-Irradiance (P-I) curve. Photosynthetic rate (P), where P can be adjusted to cell number or chlorophyll *a* content, is plotted against Photon Flux Density (PFD)/ irradiance. Where R_d = dark respiration rate; α = initial rate of photosynthesis; P_{max} = maximum photosynthetic rate achieved; I_k = light saturation point (PFD at half P_{max}). Photoinhibition is shown at Higher PFDs which results in a reduction in P.

2.3: NUTRITIONAL ANALYSIS

A number of measures relating to the 'nutritional value' of the algal cultures were undertaken as follows:

2.3.1: Dry weights (DW)

A known volume of culture was filtered through pre-dried and weighed GF/F filter paper (Whatmann: Stuttgart, Germany) under vacuum and rinsed through with 25 ml of distilled water. Samples were made in triplicate, and left to dry for 2 days at 95 °C. Filter papers were then subsequently left in a desiccator for at least 1 hour to remove any moisture, before being weighed to within 10^{-5} g using a fine balance (Galaxy 160D from Ohaus: Florham park, Germany) to determine the culture's dry weight (DW).

2.3.2: Ash-free dry weights (AFDW)

To obtain ash-free dry weights, DW samples were dried further at 300 °C for 2 days, before being re-weighed (see above). This weight was then deducted from the DW to give the ash-free content of samples (AFDW).

2.3.3 Total lipid content

Total lipid was extracted and measured using the widely accepted (Scragg *et al.*, 2002; Renaud *et al.*, 1999; Zhu *et al.*, 1997b; Fernandez-Reiriz and Labarta, 1996; Renaud *et al.*, 1995 and Kaplan *et al.*, 1986) method originally used by Bligh and Dyer (1959). Samples (typically 25 ml) were centrifuged for 10 min at 4000 rpm using a Sigma XK15 centrifuge with a swing-out rotor (Oesterode am Harz, Germany). The resulting cell pellets were then re-suspended in 30 ml chloroform: methanol (2 : 1, v/v) (methanol contained 10 ppm butylated hydroxytoluene) and transferred into a 100 ml Schott glass bottle via glass Pasteur pipette. The solution was then homogenised for 30 sec using an Ultra-Turrax-Antriels T25 (ESSLAB: Essex, England) and left to stand for a further 15 sec. The homogenate was funnel filtered (Whatman 1 filter paper) into a 100 ml glass measuring cylinder. The final filtrate volume was then measured and diluted 6 : 1, with potassium chloride (0.88 % w/v).

The filtrate and potassium chloride were mixed in a separating funnel by gentle swirling to allow separation of aqueous and non-aqueous phases. The top layer consisting of the aqueous phase, containing water from the sample. The bottom layer (non-aqueous phase) consisted of the total lipid from the sample in solution with chloroform. This was decanted off and filtered through Whatman (Stuttgart, Germany) phase separating paper (1PS) into a pre-weighed rotary evaporation flask. The lipid–containing solution was then evaporated to dryness using a Büchi (Postfach, Switzerland) rotary evaporator (RE 111 Rotavapour) at 35 °C (Büchi 4611 Water bath). The flask was dried and re-weighed to calculate the total lipid content (mg).

2.3.4 Fatty acid methyl esterification (FAME)

Having determined the total lipid content of a sample, the total lipid was separated into it's component methyl esters as follows, based upon the methods of Lepage and Roy (1984) and Tzovenis *et al.* (1997). A mixture of acetyl-chloride and methanol (3 ml; 5 : 100, v/v) was added to the previously obtained dry lipid (refer to Section 2.3.3), and divided into 3 × 1 ml aliquots. These were placed into brown 2 ml vials, each containing 5 mg Heptadeconoic acid, which acted as an internal standard (that is not associated with any of the algal strains selected in this study). The aliquots were sealed and heated for 1 hour at 100 °C, after which 1 ml of hexane was added to separate the FAME layer (bottom). The FAME layer was transferred to capped vials for analysis by gas chromatography.

2.3.5 Gas chromatography analysis of fatty acid content

All FAME samples were quantitatively analysed using a 30 m × 2.5 mm silicon capillary column (SGE Phenomenex BPX, Agilent: Stockport, UK), with a 0.25 μm thick 70 % cyanopropyl Siloxane matrix as the stationary phase (similar to that used by Tzovenis *et al.*, 1997). The column was heated using in a HP4890A GC (Agilent: Stockport, England). Method was similar to that of Zhu *et al.* (1997a/b). A flame ionisation detector (FID) was used at 260 °C, which was fuelled by a mixture of 300 ml/ min air and 40 ml/ min hydrogen (7.5 : 1). A sample load volume of 1 μl was injected onto the column using a HP6890 auto injector at 250 °C, controlled by a HP G1512A autosampler. Helium was used as the mobile phase carrier gas at a rate of 1 ml/ min. The initial oven temperature was first equilibrated for 5 min at 120 °C, and was then increased at a rate of 4 °C/ min until reaching a final temperature of 240 °C and held for a further 5 min. All data was recorded on PC using ChemStation software (V. 6.01, Agilent: Stockport, England) via a HP35900E interface.

External reference standards previously run under the above conditions were used to qualitatively identify peaks within samples based upon their relative retention times (Figure 2.5 and Table 2.1). All peaks were quantified using the known amount of the internal standard (HDA), which was added to the samples (see Figure 2.5).

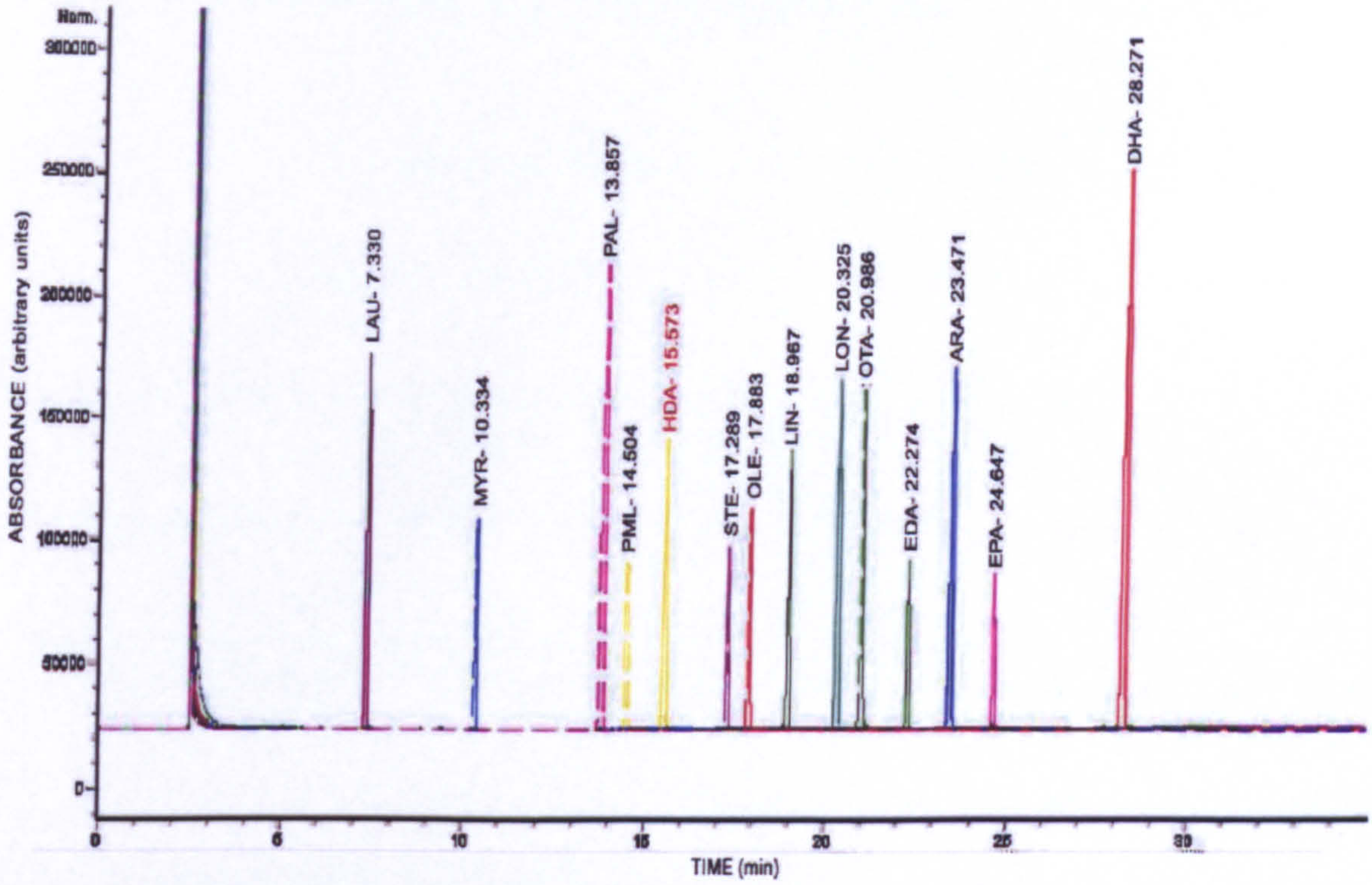

Figure 2.5: Chromatogram of standards. Samples (1 µl) injected (at 250 °C) onto a SGE Phenomenex BPX capillary column. An FID detector (at 260 °C) was used at 300 ml/min air; 40 ml/min hydrogen; 1 ml/min helium as a carrier gas (7.5: 1). The oven temperature was held at 120 °C for 5 min, before increasing at a rate of 4 °C/min for 30 min and held at 240 °C for 5 min. Individual FAME standards overlaid and adjusted to the same baseline, showing their relative retention times- refer to Table 2.1.

FATTY ACID		Formulae	Mr	T_R (min)
(Shorthand)	(Trivial name)			
LAU	Lauric	C12:0	200.3	7.330
MYR	Myristic	C14:0	228.4	10.334
PAL	Palmitic	C16:0	256.4	13.857
PML	Palmitoleic	C16:1	254.4	14.504
HAD	Heptadecanoic	C17:0	270.4	15.573
STE	Stearic	C18:0	284.4	17.289
OLE	Oleic	C18:1 (*n-9*)	282.5	17.883
LIN	Linoleic	C18:2 (*n-6*)	280.4	18.967
LON	Linolenic	C18:3 (*n-3*)	278.4	20.325
OTA	Octadecatetraenoic	C18:4 (*n-3*)	276.4	20.986
EDA	Eicosatetraenoic	C20:4 (*n-3*)	304.5	22.274
ARA	Arachidonic	C20:4 (*n-6*)	304.5	23.471
EPA	Eicosapentaenoic	C20:5 (*n-3*)	302.5	24.647
DHA	Docosahexaenoic	C22:6 (*n-3*)	330.6	28.271

Table 2.1: Known fatty acid reference standards. In order of elution, expressed as retention time (T_R), includes: saturated fatty acids (SAT); mono-unsaturated fatty acids (MUFA); and polyunsaturated fatty acids (PUFA). Unsaturated fatty acids divided into their relative omega series (indicated by *n*-). The external standard (Heptadecanoic acid) is defined as extraneous from the algae in this study. This was added artificially to all FAME samples at 2 µg/ ml and used to calibrate indigenous peaks.

CHAPTER 3: PHOTOBIOREACTOR METHODS

This section will be used to describe the construction; general preparation and maintenance of the tubular photobioreactors used in this study for the cultivation of microalgae, and will also investigate various physical attributes of this system analogous to any commercial biological reactor.

3.1: DESIGN AND CONSTRUCTION

The tubular photobioreactor is a closed system culture vessel, which features a helical photostage with circulation provided by an airlift. The total volume is approximately 87 L, whilst the working volume (defined as the level up to product overflow port) was 70 L. Overall a total height of 2.7 m and a footprint area of 1.13 m^2 was occupied by the photobioreactor (full dimensional details are given in Appendix C).

The photobioreactor was constructed from grey PVC-U (except for the riser and header tank which were made of transparent PVC-U) supported by a stainless steel base, mesh and vertical mast: see Figures 3.1 – 3.7. This can be described better when divided into five main components/ sections:

a) Sparge plate- Located at the base of the riser, this is the point at which air is injected using a pneumatic air pump (Compton compressors: Ashbourne, England) as a means of circulation for the whole system. Filtered air (0.2 µm PolyVent 500) passes through a non-return valve to prevent backflow and draining of the culture volume. The air passes through a flat circular sparge plate (95 mm diameter × 2 mm thick PVC-U), which consists of drilled holes or pores (see Figures 3.5 and 3.7). Both the number and size of the pores can potentially vary. For all cultures grown in this study, a standard plate configuration of 69 holes at a pore diameter of 1 mm was used unless otherwise stated.

b) *Riser*- The riser is the driving force for system re-circulation acting as an airlift. It is the prime area of gas transfer and provides a homogeneous source of gaseous exchange, flowing towards the header tank. Internal diameter of 68 mm.

c) *Header tank-* The inoculum is introduced into the system via the header tank. This is also the site for the addition of nutrients. The tank is well mixed and is the main site for mass transfer in the photobioreactor. An access port at the top of the header tank is used to ensure all inner surfaces of the header tank are cleaned prior to sterilisation (whilst the system is dismantled between runs). Header tanks are also referred to within the literature as phase/ gas-liquid separators (Contreras *et al.*, 1998; Bentrifraouine *et al.*, 1997; Dhauadi *et al.*, 1997; Merchuk and Berzin, 1995), or gas disengagers (Al-Masry and Dukkan, 1997).

d) *Down-comer-* Flow from the header tank to the remainder takes place via the down-comer, assisted by gravity. Diameter is marginally smaller than the riser, at 56 mm.

e) *Manifolds (×2)-* These are located at the inlet and outlet of the photo-stage coil windings, two manifolds are used to divide the fluid flow allowing for more efficient use of the air pump used to aerate the system. The use of a single winding has previously been shown to be much less effective in terms of circulation and mixing (W. Hartley, pers. com). In the 65 L photobioreactor the manifolds split the flow into three separate coil windings, which run parallel to each other (see Figure 3.4).

f) *Photostage-* The photostage the area of the photobioreactor where the algae are directly illuminated. The vertical stack of three parallel coil windings allows for a large volume whilst maintaining a small foot-print area. The narrow tubing allows for a large ratio of surface area : volume, which helps to minimises self-shading in dense algal cultures. Coil windings consisted of 0.25 mm FDA approved food-grade vinyl transparent tubing. The coil windings were bound at regular intervals, with thin plastic wire, onto a stainless steel wire mesh-support (see Figure 3.3).

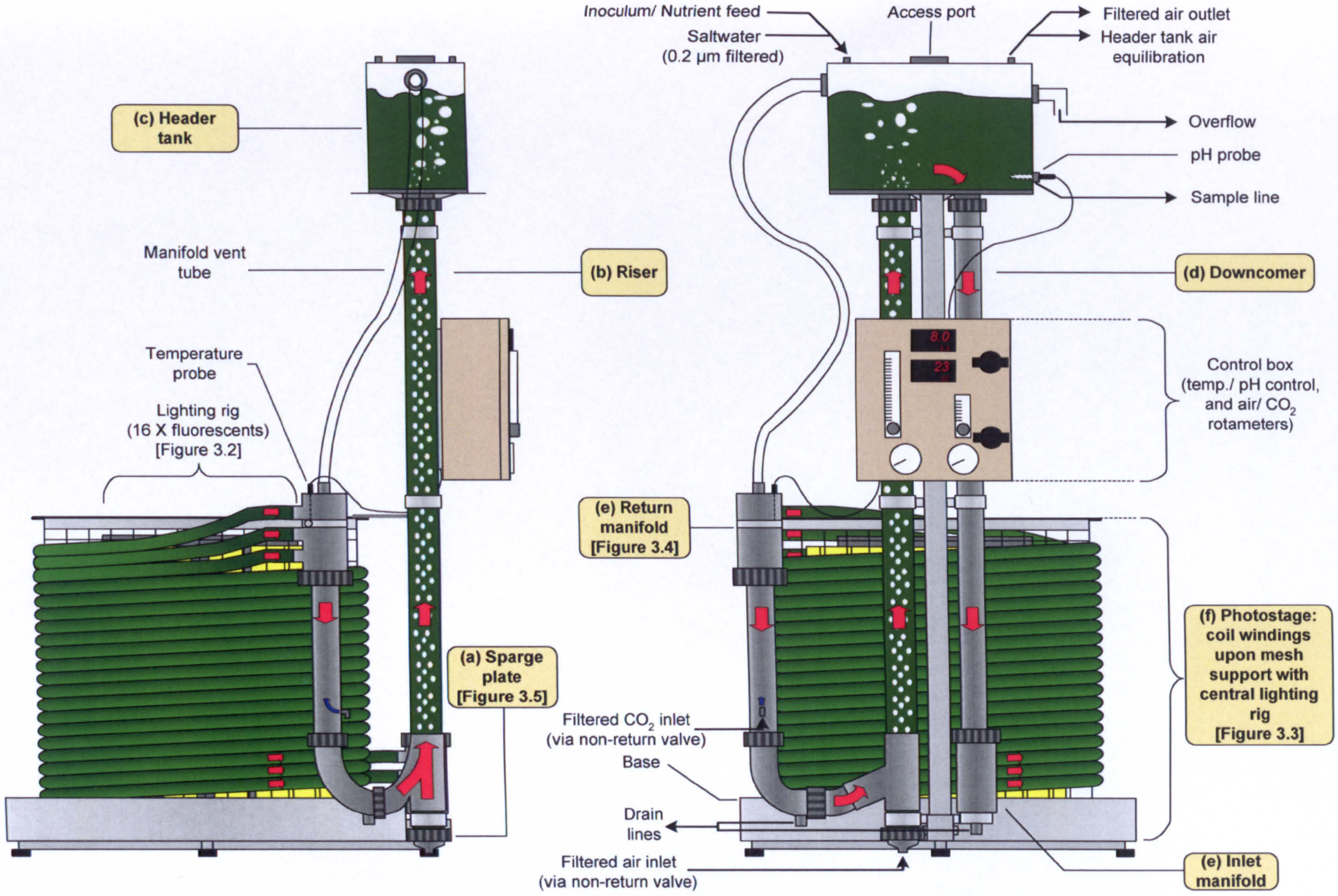

Figure 3.1: Overview of tubular photobioreactor: Side and front views. Red arrows show direction of flow around the system through each of the various components: (a) sparge plate; (b) Riser; (c) Header tank; (d) Downcomer; (e) Manifolds; (f) Photostage. Rubber tubing was attached to drain lines closed using gate-clips. Blue arrows indicate the flow of CO_2. Illustration made by the author. NOT TO SCALE.

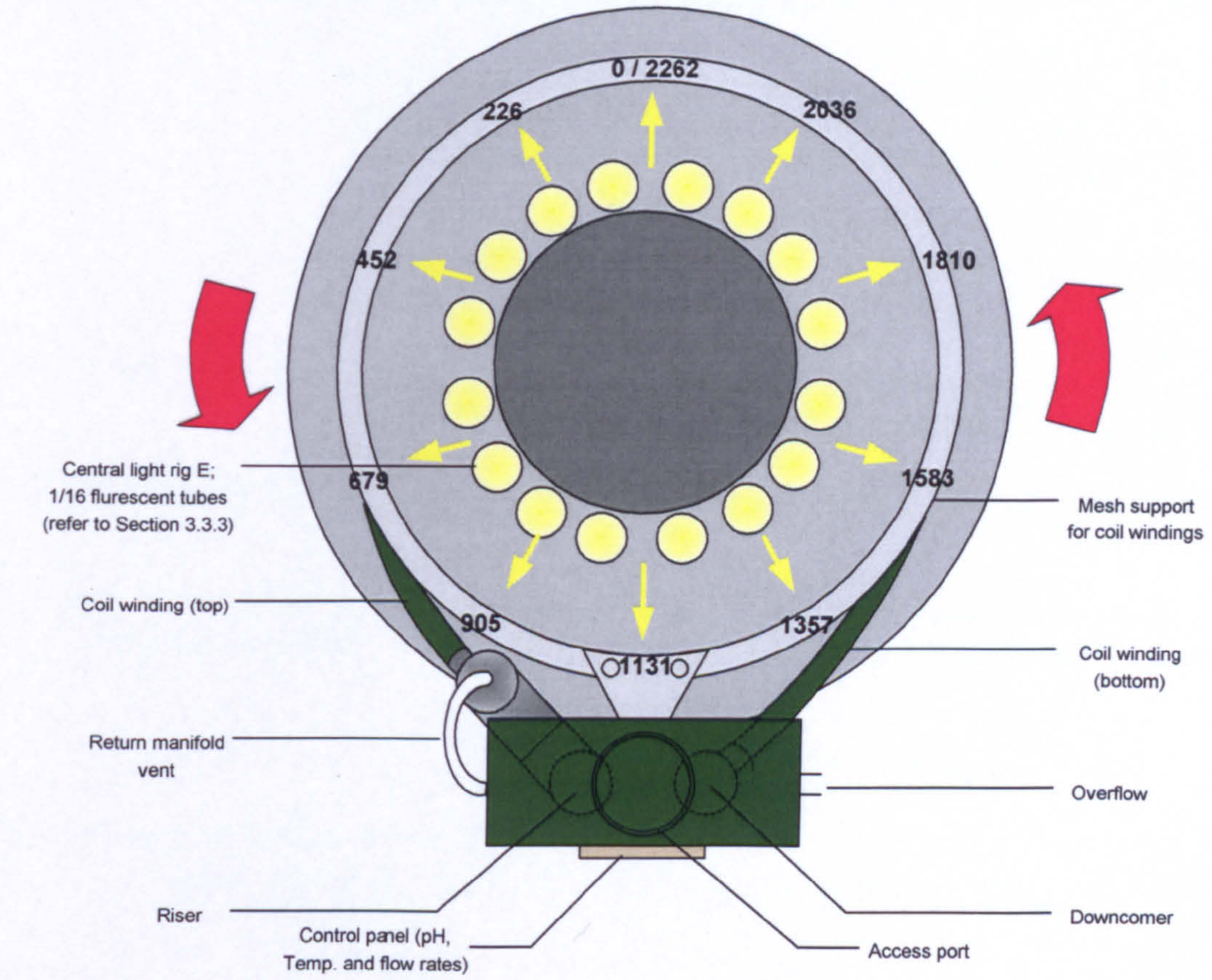

Figure 3.2: Plan view of the tubular photobioreactor. Highlighting the uniform arrangement of the light rig at the centre of the photo-stage, and flow of culture re-circulation (red arrows). Numbers represent equidistant points (yellow arrows) around the circumference of the photostage, used for light measurements (Section 3.3.3). Illustration made by the author. NOT TO SCALE.

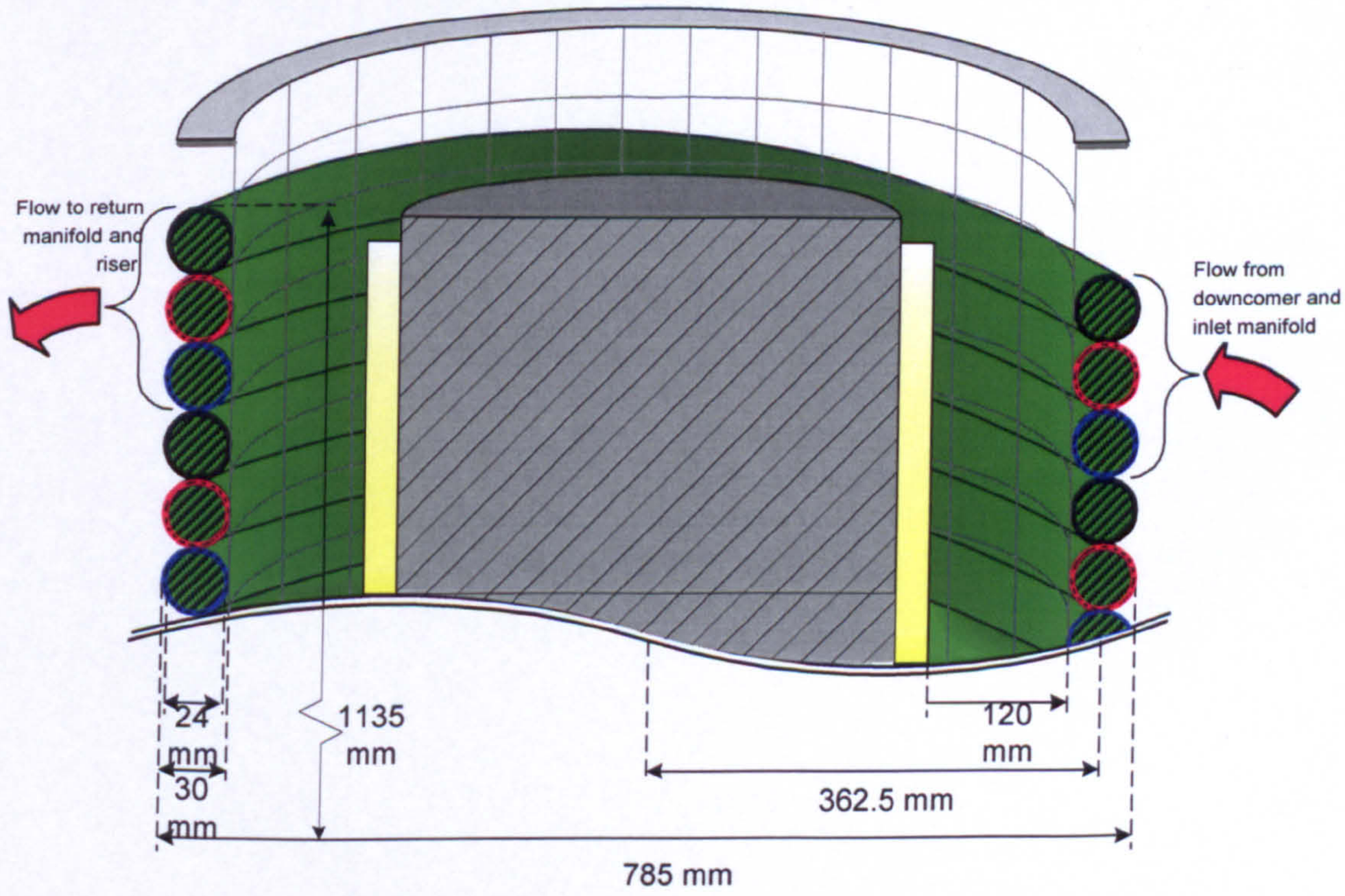

Figure 3.3: Cross-section of the photostage. From outer to inner layer- transparent vinyl tubing of the 3 separate coil-windings; stainless steel wire mesh support (to which the bottom coil-windings are tied to using plastic wire); central lighting rig. Red arrows indicating direction of re-circulation. Illustration made by the author. NOT TO SCALE.

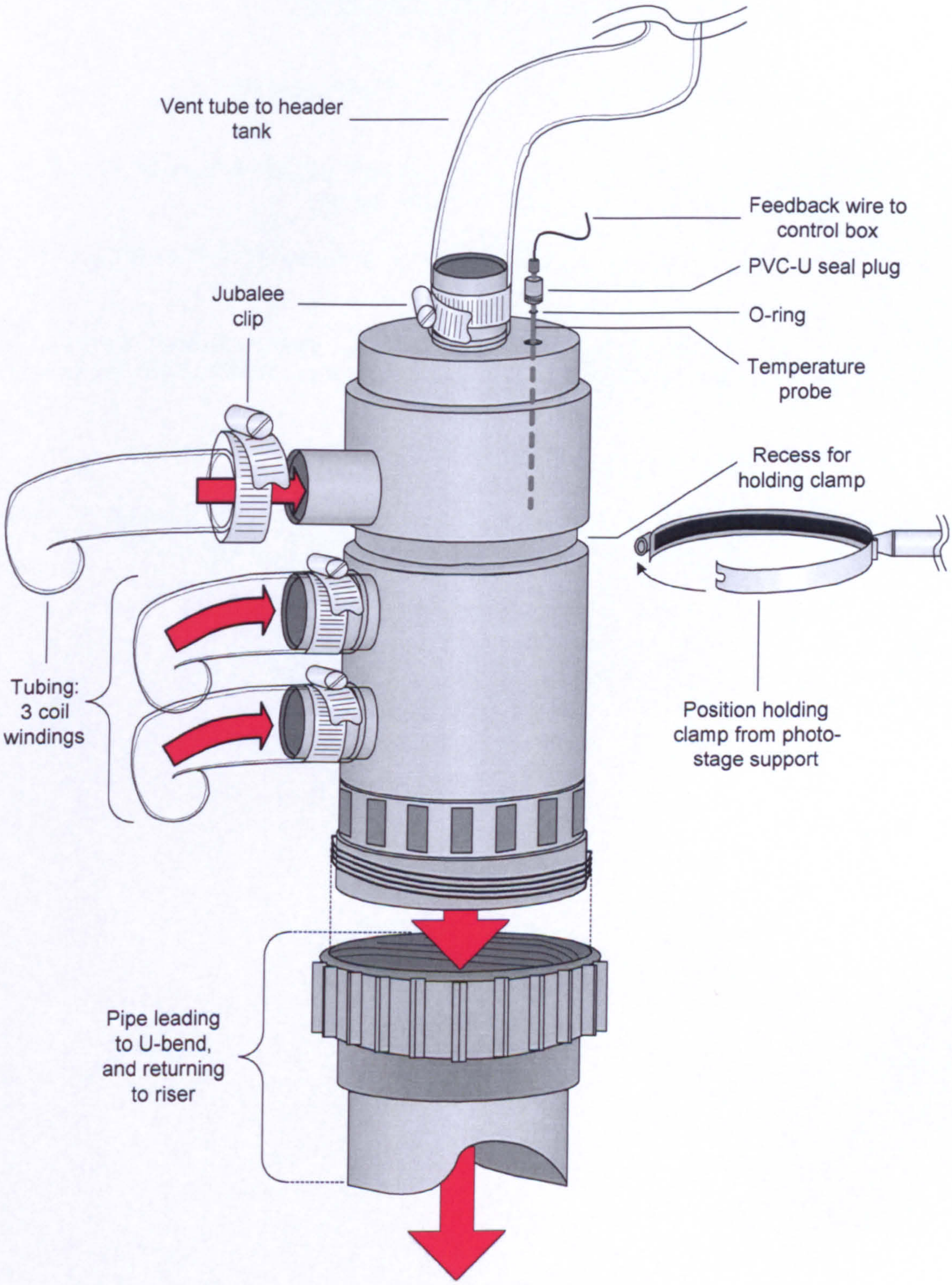

Figure 3.4: Return manifold. Schematic diagram of how coil windings were connected to manifolds, secure with jubilee clips. A clamp extends from the photo-stage support to position and align the manifold, which joins additional piping by a union butt. A temperature probe is located at the top of the return manifold next to the vent. Red arrows indicate direction of fluid flow circulation. Illustration made by the author. NOT TO SCALE.

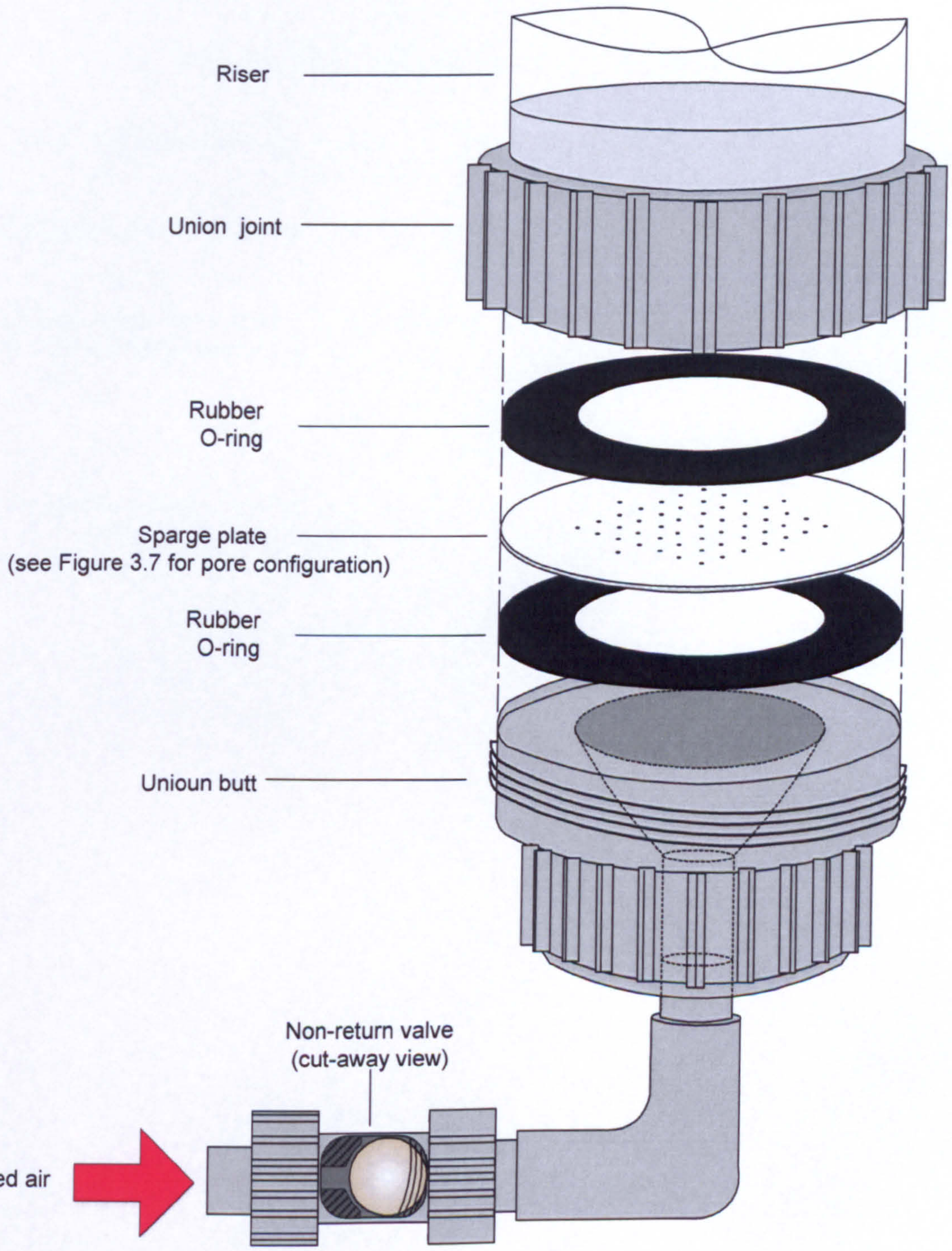

Figure 3.5: Sparge plate arrangement. Pneumatically pumped air was introduced via a rotometer (with L/min calibrations) was filtered prior to entering a non-return valve. This ensured that the culture would not drain when air-flow was interrupted. Air then entered the riser section through a series of pores in the sparge plate. The configuration of which could be changed (as shown in Figure 3.7). Illustration made by the author. NOT TO SCALE.

Plate 6: 70 L indoor tubular photobioreactors. Plates 6a and 6b show various sections of the photobioreactor used in this study for cultivation of *I. galbana* (left) and *N. oculata* (right). See also Figures 3.1 – 3.5 and Appendix C for measurements. The bottom picture shows a close up of photostages of three different caultures: *Tetraselmis sp.* (left- data not shown), *I. galbana* (centre) and *N. oculata* (right).

3.2: MAINTENANCE AND CULTIVATION

3.2.1: Leak testing

Prior to sterilisation of the system, the photobioreactor was leak tested. All ports in and out of the photobioreactor were sealed except the media inlet port of the header tank, which was used to fill the system with tap water. Air was then introduced into the photobioreactor, using a pneumatic pump, via the sparge plate. The photobioreactor was then visually inspected around all joints and seals for signs of leaking. Joints were tightened, and PTFE tape applied where necessary, until leaks were prevented.

3.2.2: Acid wash

Once the system was leak-free, it was then subjected to an acid wash, with the calibrated pH probe sealed *in situ* within the header tank. The purpose of this was to remove any plasticers (used in the moulding of the plastics components of the photobioreactor), since these could potentially inhibit algal growth. This was done by adding 1 M HCl, via the header-tank, to the system until a pH of 2-3 was achieved. The fluid was then allowed to re-circulate for 1 hour before being drained and rinsed three times with tap water. The pH was re-checked to ensure that all traces of acid were removed. Acid washes were generally used on newly constructed photobioreactor, but also used in some post-run sensitisations to effectively remove any 'biofouling' (as seen in Plate 7).

3.2.3: Sterilisation

All tubing connections made during sterilisation of the photobioreactor were swabbed with 75 % (v/v) propan-1-ol (IPA), to prevent microbial contamination. Both air filters (Whatman PolyVENT 40) and the CO_2 filter (Whatman PolyVENT 16) were autoclaved (15 min 121°C, 21 psi) in advance. All input and output lines from the photobioreactor were initially clamped off, except for the header tank air outlet, CO_2 and air inlets. The photobioreactor was then filled with tap water, before adding sodium hyperchlorite (via the open glove port) to give a final concentration of 500 ppm available chlorine. The system was completely filled above it's working volume so as to flush and sterilise the product overflow line when unclamped. Air

and CO_2 inlet non-return valves (NRVs) were back-flushed prior to the addition of the autoclaved filters (as above). An air-line from a pneumatic pump to the photobioreactor air inlet NRV was then established, via the inline filter. A 50 ml syringe was used to remove 25 ml via the sample port, which was then injected back into the header tank via the inoculum line to ensure all entry ports to the header tank were sterile.

A separate filtration system (Fileder Ltd., Maidstone, England) was used to sterilise the growth media. This consisted of three, in-line, Osmonics filter cartridges, containing a 5 µm pre-filter (Purtrex), 0.2 µm (Flowtrex) and a 0.1 µm (Memtrex) filter, respectively. These were sterilised separately from the photobioreactor. This was achieved by filling the cartridge housings with a 250 ppm free chlorine solution (according to manufacturers recommendation). The filter housings were filled, sealed and left for 30 min. The line from the filter system outlet to the media inlet port of the header tank was unclamped. The filter inlet was connected to a water main, and tap water was then used to flush the sodium hyperchlorite solution out of the filters, thereby sterilising the line between the media filters and photobioreactor; used to rinse the photobioreactor. Once refilled with filtered water, the photobioreactor was left to re-circulate for 15 min at a flow rate of 5 L/min. The system was then drained, and refilled twice more with filtered water to remove traces of sodium hyperchlorite. The photobioreactor was then filled with 65 L of filtered pre-mixed sf/2 media.

3.2.4: Inoculation

The photobioreactor was inoculated using 4 L of culture prepared in an aspirator (Section 2.1.2). This was accomplished by connecting the sample line of the aspirator to the inoculation line of the header tank (connection rinsed with 75 %, v/v IPA). The air outlet of the aspirator was clamped off and air pumped into the air outlet. This generated a build-up of positive pressure in the vessel, which forced the culture out of the aspirator and into the photobioreactor.

3.2.5: Culture maintenance

An air flow rate of 15 L/min was used to re-circulate the culture volume. Air was supplemented with CO_2 (vapour withdrawal) at a rate of 1.5 L/min (see Figure 3.6, injection point 1). All nutrient addition was pumped (pre-calibrated) through the filtration system (detailed above) into the header tank. Product overflow/ wash-out was collected, via non-return valve, in 25 L barrels. The standard sparge plate (shown in Figure 3.7) was used for all culture runs.

3.2.6: Post-run decommissioning

The photobioreactor was emptied via the two drain lines (Figure 3.1), and the system dismantled into it's component parts. Each of which was individually hand cleaned (with the exception of the photostage) with warm water. The coil windings of the photostage were 'pigged-out' (an expression derived from a similar process used to clean undersea oil pipes). An adaptor was used to connect the end of each winding to a tap. Water pressure was then used to push three foam bungs around the coil. This process was typically repeated three times for each winding. Having received a preliminary 'wipe-down', the various components were re-assembled and leak tested again before the above methods applied again.

3.3: PHYSICAL CHARACTERISATION

The photobioreactor units used in this study were of a standard configuration. This configuration was physically characterised in terms of gas hold-up, rheology, circulation rates and mass transfer. The above parameters were measured and comparisons made between different rates of aeration, sparge plate configuration and height of the header tank, as a means to optimise the photobioreactor. Water was kept at a salinity of 32 ‰ (1.024 specific gravity) throughout. Aeration was provided by a Rietschle DTE 8 pump (Switzerland).

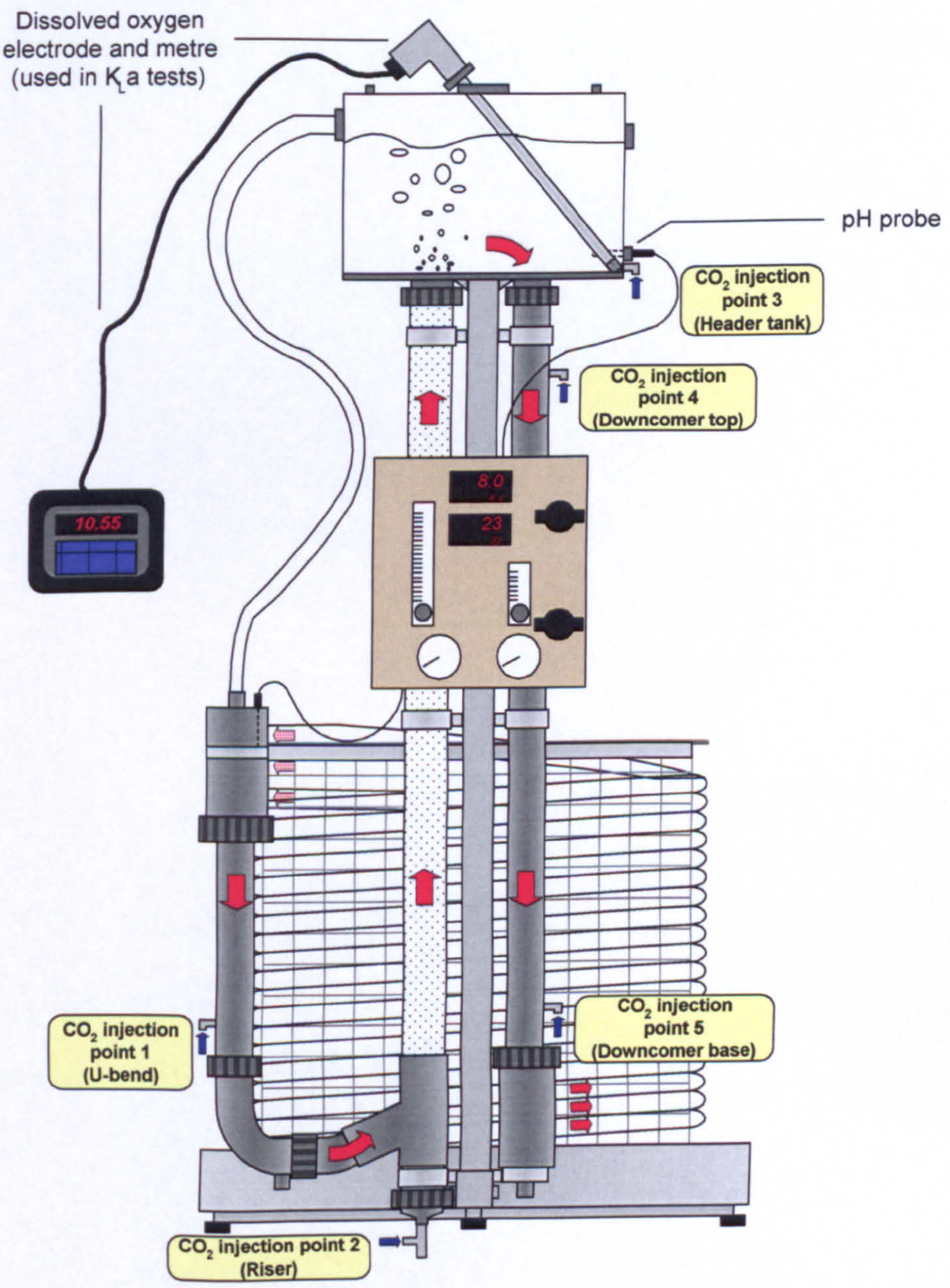

Figure 3.6: Setup of photobioreactor for physical characterisation. Five injection points (blue arrows) were located around the system for addition of 10% CO_2. Gate clips were used to seal tubing fitted to these points when not in use. Refer also to Figure 3.1. Illustration made by the author. NOT TO SCALE.

3.3.1: Measuring sparge plate efficiency

Five sparge plates configurations were examined. All sparge plates used in this study were fabricated from 1.5 mm thick PVC-U, with a total external diameter of 96 mm. However, individual plate configuration differed in terms of pore number and size (see Figure 3.7). Sparge plates of consisting of 25; 46 pores were used at two different pore sizes, 1 (s = small) and 2 mm (L = large). These four sparge-plates were directly compared to the standard sparge plate (69s = 69 × 1 mm pore size), which was later used during cultivation of both *I. galbana* (Section 4.2) and *N. oculata* (Section 5.2). The effects of the sparge plates were determined by the following physical parameters:

i) Re-circulation rate
ii) Riser dynamics
iii) Reynolds number
iv) Gas hold-up
v) Mass transfer

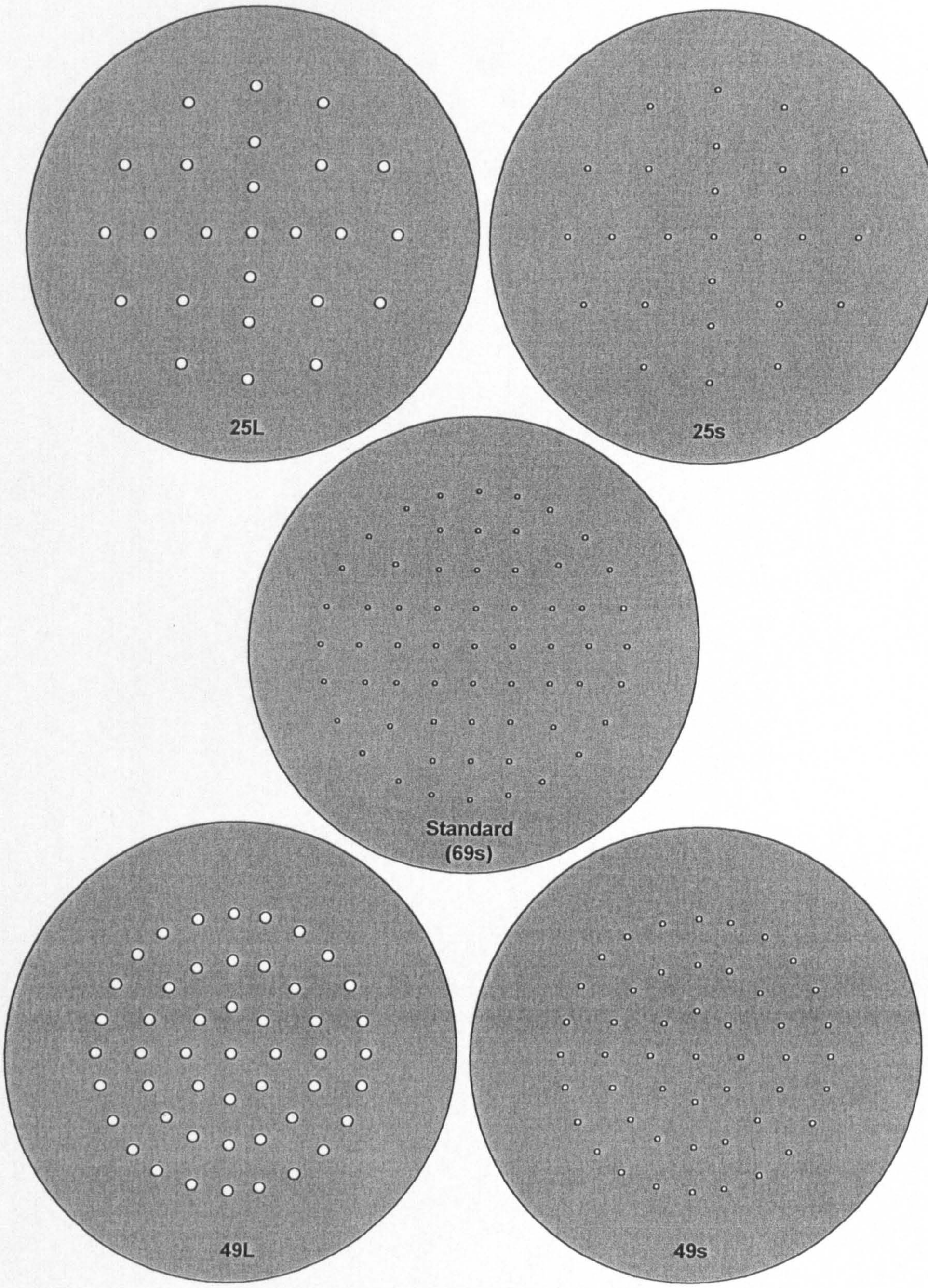

Figure 3.7: Sparge plate configurations. Pore number (25, 49 and 69) and size (L = 2 mm, and s = 1 mm diameter). Scale = 1:1.33 (refer to Figure 3.5). The 'standard' plate configuration (69s) was used during cultivation of *I. galbana* and *N. oculata*.

3.3.1.i: Linear velocity

The aeration rate, used as the sole means of re-circulating the photobioreactor was varied in order to measure the circulation rate around the photostage in terms of linear velocity (m/sec). The effects of aeration were monitored at aeration rates of 5, 10, 15 and 20 L/min. A small piece of foam (acting as a neutrally buoyant particle) was inserted into the down-comer from the header tank. It was then timed as it completed seven windings of the coil. This was repeated three times at each flow rate and an average value calculated for each sparge plate. The length of one winding is 2.26 m.

3.3.1.ii: Riser dynamics

The distribution and formation of bubbles seen within the riser (made from transparent PVC-U) varies with the rate of air-flow at the sparge plate and the actual configuration (in terms of pore size and number) of the sparge plate itself (Figure 3.7). Characterising these riser dynamics is important because heterogeneous bubble formation reduces the efficiency of mass transfer (Hebrard, *et al* 1996) (Figure 3.8).

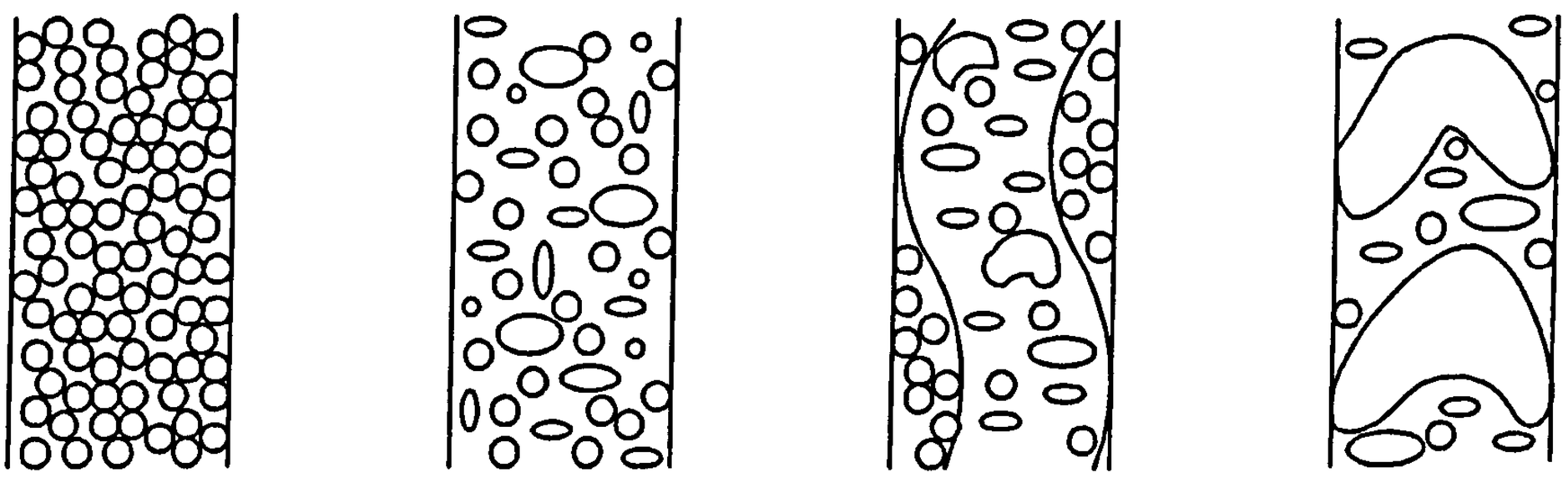

Figure 3.8: Riser dynamics. Typical observed bubble formations under varying rates of aeration

3.3.1.iii: Reynolds number

Reynolds numbers are used to define whether the rheology within a bioreactor is of laminar or turbulent flow. Opinions within the literature vary as to at which point flow changes from being defined as either laminar or turbulent. In this study Reynolds numbers less than 2680 will be defined as representing laminar flow (Carlozzi and Torzillo, 1996), with values greater than 4000 being defined as turbulent. The artificial sea-salts used here to imitate full strength seawater (32 ‰) had a fluid density (p) of 1030 kg/m^3 with a fluid viscosity (μ) of 1.1845 cP (centipoises). Internal diameter of the riser (D) was 68 mm. Reynolds numbers were calculated (equation 2) at air flow rates of 5, 10, 15 and 20 L/min for each sparge plate.

$$\mathrm{Re} \approx D \cdot v \cdot \left[\frac{P}{\mu}\right]$$

Equation 2: Calculating Reynolds number. D = diameter of the tubing, v = linear liquid velocity (m/s), p = fluid density and μ = fluid viscosity.

3.3.1.iv: Gas hold-up

The photobioreactor was filled up to the level of the header tank overflow outlet, without aeration. A tube from the overflow was dropped down to a measuring cylinder. The height from the base of the header tank to the water level was recorded. Aeration was then applied at a rate of 5 L/min until no more water drained into the measuring cylinder and then stopped. The volume collected and the new water level were measured. The same process was repeated at 10, 15 and 20 L/min, successively.

3.3.1.v: Mass transfer

Dissolved oxygen was measured, via the 'gassing out out method', using an Oxyprobe D100 electrode and a 20-03 oxygen transmitter (Broadley-James, San Diego, California, USA). The Oxyprobe was place in the header tank, just above the down-comer (Figure 3.6). The photobioreactor was aerated over-night, with the probe in situ, to determine the oxygen saturation point (C*). The system was then stripped of oxygen by flushing the system with nitrogen (oxygen-free) via the sparge plate. Once stabilised, the nitrogen was then replaced by air. Dissolved oxygen was measured, as detailed by Gavrilescu and Tudose (1996), at 10 sec intervals (in ppm) for 10 min at an aeration rate which gave perfectly bubbly riser dynamics (at a known flow rate). This was performed in triplicate for each sparge plate.

3.3.2: pH control/ CO_2 solubility

CO_2 is used to provide the carbon source for photosynthesis and also used to maintain optimal pH whilst a culture is being grown. In order to make efficient use of CO_2 to regulate pH, the site of CO_2 injection was examined. Injection points included: (1) the u-bend after the return manifold; (2) at the sparge plate; (3) side entry at the header tank; (4) the top of the down-comer and (5) the base of the down-comer (see Figure 3.6). This study was made using the standard sparge plate shown in Figure 3.7. Aeration was provided at a rate of 15 L/min and CO_2 at 1.5 L/min (10 %, v/v). Initial pH was 8.147 ± 0.039. Readings were taken every 10 sec for 10 min, in triplicate.

3.3.3: Lighting regime

Measurements of incident light intensities (I_o) at the inner surface of the photostage (coil windings) were made. The circumference of the photostage was divided into ten equidistant points (228 mm) counter-clockwise along the inner surface of the photostage (Figure 3.2; shown by yellow arrows). Measurement were taken from mid-height of the coils, and measured for 1 complete turn making a total circumference of 2278 mm. A height gain of 90 mm (3 × tubing O.D.) was therefore achieved during 1 turn. Light intensity and distribution regimes upon the inner surface of the photobioreactor's photostage was measured and compared between four lighting setups (Table 3.1):

Light setup	Light Source (fluorescent tube number, manufacturer and type)	Light path (mm)	Fluorescent tubes (N°.)
A	4 × (2 ×) SYLVANIA Grow-Lux F18W (with light diffuser cover)	120	8
B	4 × (2 ×) SYLVANIA Grow-Lux F18W	120	8
C	4 × (2 ×) SYLVANIA Grow-Lux F18W + 4 × OSRAM Fluora L18W	120 + 70	12
D	16 × SYLVANIA Grow-Lux F18W	120	16

Table 3.1: Details of light sources tested for radiation fields. Various types configurations of fluorescent lights used as central light sources for the photostage, as depicted in Figures 3.2 and 3.3. Results shown in Figure 6.6.

CHAPTER 4: *ISOCHRYSIS GALBANA*

4.1: FLASK CULTURES OF *I. GALBANA*

4.1.1: Introduction

Preliminary studies were conducted using 100 ml flask cultures (Section 2.1.1) with the aim of determining optimal growth conditions for *I. galbana*. Two growth media, namely f/2 and sf/2 were compared at half-strength (16 ‰) and full-strength artificial seawater (32 ‰). In addition, the effects of temperature, nitrate concentration, dilution rates and irradiance were studied. Performance was assessed in terms of mean cell density and changes in mean cell size. Where possible algal lipid content and FAME profile were monitored (Section 2.3.3 – 2.3.4).

4.1.2: Media conditions

The performance of the alga, in terms of cell growth and mean cell size, was compared between a commonly used growth medium (f/2) and a modified version of this media (sf/2) (see Appendix B). Both media were prepared at salinities of 16 ‰ and 32 ‰ (half-strength and full strength seawater, respectively). For this study all cultures were grown at under continuous illumination at 80 ± 5 μmol/m^2/s, and a temperature of 23 ± 2 °C.

Cultures of *I. galbana* grown on f/2 (both 16 ‰ and 32 ‰) entered a plateau in growth after day 14 at a mean cell density of 27 × 10^6 cell/ml (Figure 4.1). During the linear growth phase, algae in both f/2 reached a maximum growth rate of 1.60 and 1.71 μ/day (day 1 - 14) for 16 ‰ and 32 ‰ cultures, respectively. However, no significant difference was observed between f/2 cultures at either salinity over the entire culture period ($p = 0.9183$).

The linear growth phase in 16 ‰ s/f2 cultures continued (at a growth rate of 1.49 μ/day) until day 21 before entering stationary phase, at a maximum mean cell density of 40 × 10^6 cell/ml. In contrast, cultures in 32 ‰ sf/2 failed to reach a true stationary phase, and by day 35 had reached the highest mean cell density overall (42 × 10^6 cell/ml) with an average growth rate 1.00 μ/day throughout. However, it must be noted that these cultures also displayed the highest degree of standard error between replicates, and no significant difference was found between the growth of the alga in

the two salinities of sf/2 media tested ($p = 0.473$). Overall, f/2 cultures were the first to enter stationary growth phase and by day 35 a significant difference ($p = 0.032$) was found between the four media conditions tested.

A mean cell size of 4.67 µm was found for all cultures at the start of the experiment (Figure 4.2). Differences in cell size between cultures only became apparent after day 7, where cells grown in both media at 16 ‰ possessed a smaller mean cell size (4.24 - 4.34 µm) compared to those grown in 32 ‰ seawater media (4.45 - 4.69 µm). Changes in cell size for all cultures in this experiment followed a similar trend, with mean cell size increasing gradually until day 21 before sharply peaking on day 24 (where differences between cell size as a result of salinity became more notable). Maximum mean cell sizes of 4.79 and 5.31 µm were recorded for cultures grown in f/2 and sf/2, respectively, although ultimately no statistically significant differences or trends were found for any of the media conditions (formulation or salinity) tested ($p = 0.077$).

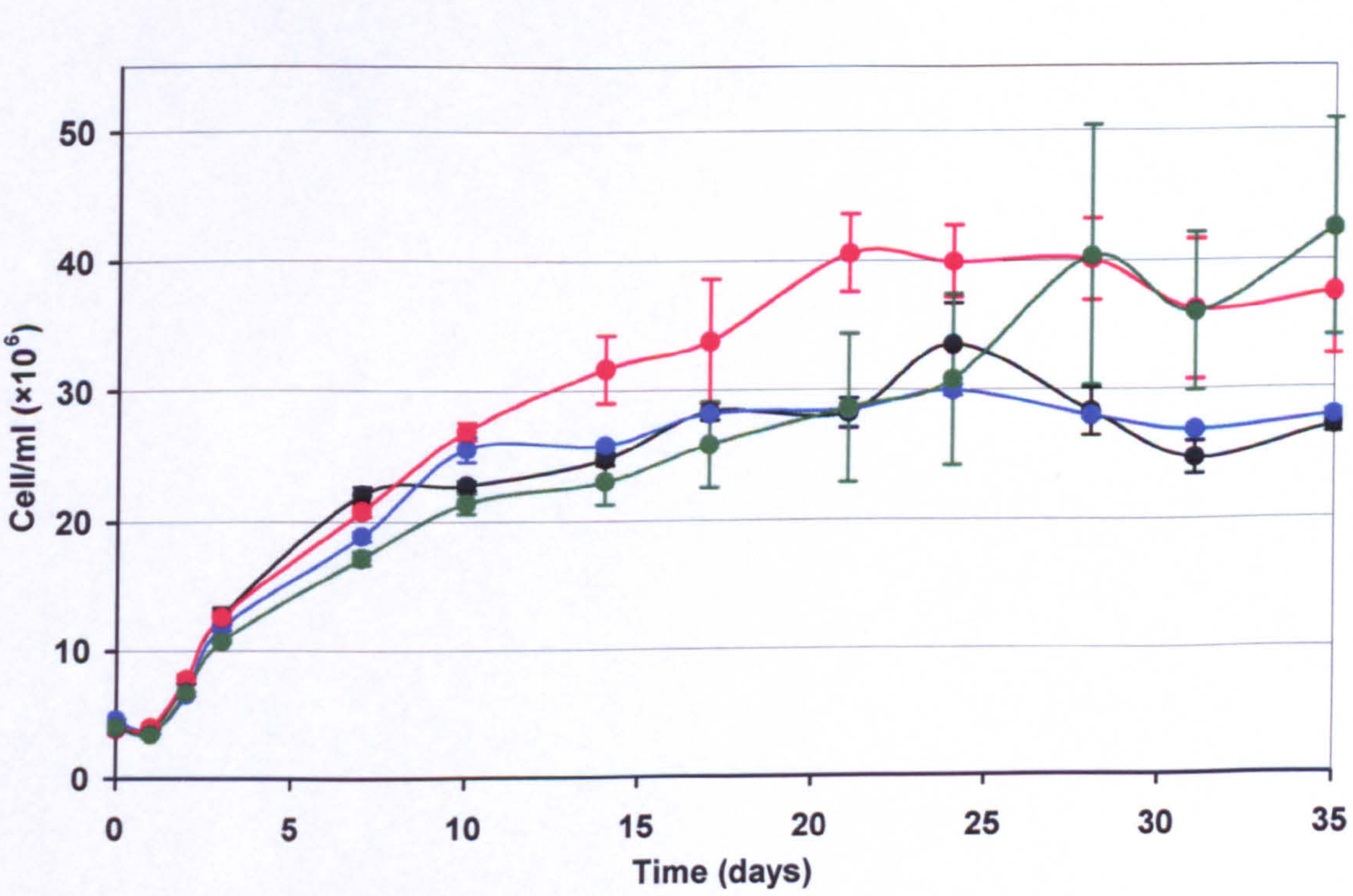

Figure 4.1: Mean cell density of *I. galbana* cultured on two separate media at two salinities (n = 3 ± S.E.). Flasks contained either f/2 at 16 ‰; f/2 at 32 ‰; sf/2 at 16 ‰; sf/2 at 32 ‰ (inoculum cell density at 4.45; 4.63; 3.88 and 4.02 × 10^6 cell/ml, respectively). Refer also to Appendix D for a statistical summary of results.

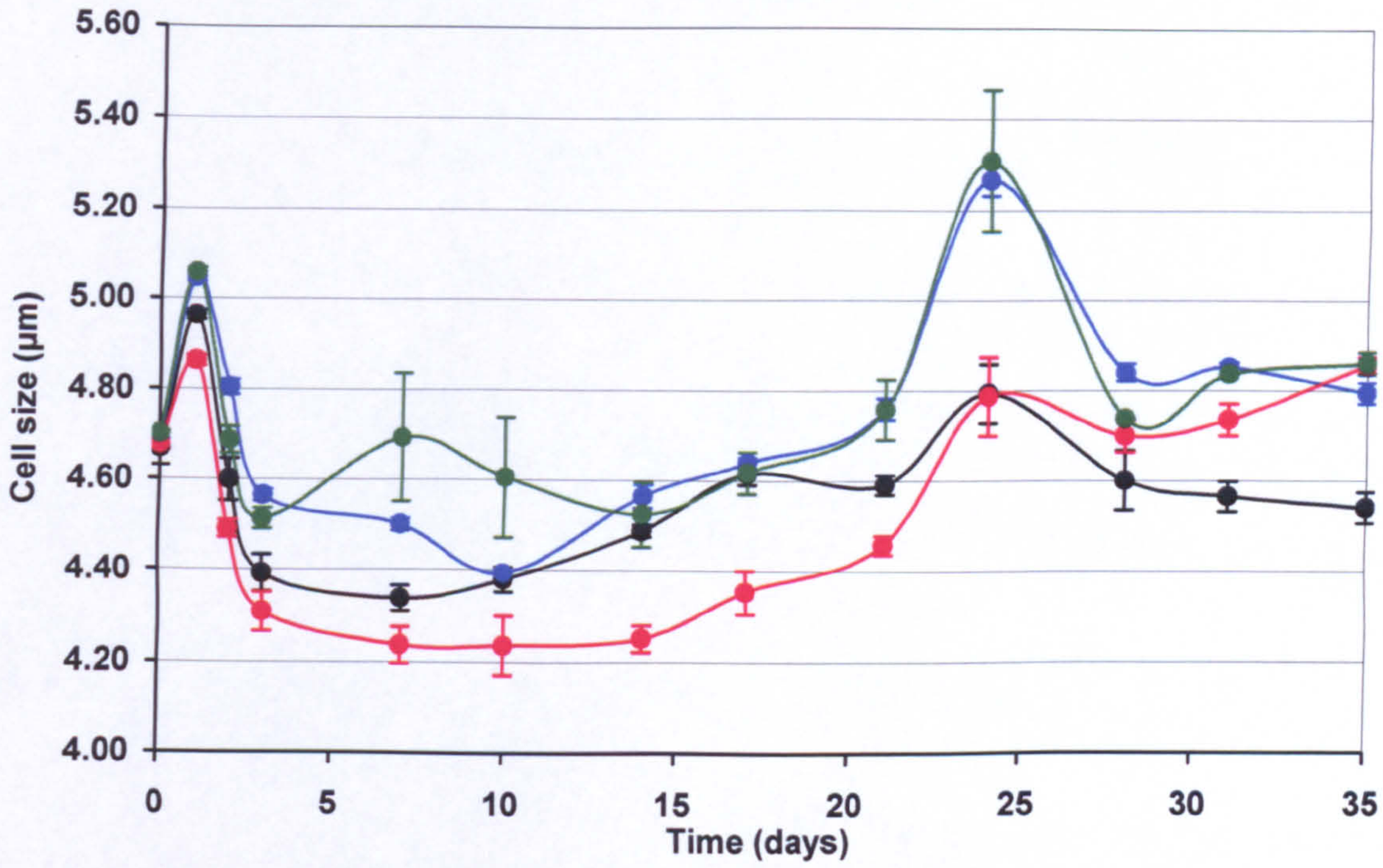

Figure 4.2: Mean cell size of *I. galbana* cultured on two separate media at two salinities (n = 3 ± S.E.). Flasks contained either f/2 at 16 ‰; f/2 at 32 ‰; sf/2 at 16 ‰; sf/2 at 32 ‰. Refer also to Appendix D for a statistical summary of results.

4.1.3: Nitrate limitation

The effect of nitrogen concentration on the growth and cell size of *I. galbana* was examined. Standard sf/2 media at 32 ‰ (see appendix B) was used to compare the effects of varying the concentration of sodium nitrate ($NaNO_3$ at: 3.56, 5.34, 7.12 (control), 8.90 and 10.68 mM were used).

The mean cell density (Figure 4.3) in cultures for all nitrate levels tested was nearly identical up until day 19, each consisting of a three-day lag phase and linear phase growth rates of 2.00 – 3.08 µ/day (for all concentrations). From day 19 onwards, significant differences in cell densities became apparent (*p = 0.002, overall*). *I. galbana* grown at the lowest concentration of $NaNO_3$ (3.56 mM) achieved a maximum mean cell density of 41 × 10^6 cell/ml. At slightly higher nitrate concentrations (5.34 and 7.12 mM) maxima of 48 and 50 × 10^6 cell/ml, respectively were observed with no significant difference between the two (*p = 0.1124*). Whilst cell number in 8.90 mM nitrate reached a maximum of 63 × 10^6 cell/ml, cells maintained in media with 10.68 mM nitrate continued increasing in number towards 70 × 10^6 cell/ml by day 29. Overall a 122 % increase in cell productivity was found by growing *I. galbana* in sf/2 by changing $NaNO_3$ from 3.56 to 10.68 mM.

After initial transfer into fresh media, all cultures increased in mean cell size on day one regardless of nitrate concentration. This was followed by a drop in mean cell size until day five to 4.30 – 4.45 µm before rising again to 4.49 - 4.57 µm on day eight. From day 12 onwards, great variation in mean cell size was observed. Generally, all concentrations with the exception of 3.56 mM $NaNO_3$ decreased mean cell size (remaining within a range of 4.00 – 4.35 µm). At 3.56 mM nitrate, mean cell size was higher at ~4.70 µm and was significantly different compared to the other treatments (*p = <0.008*).

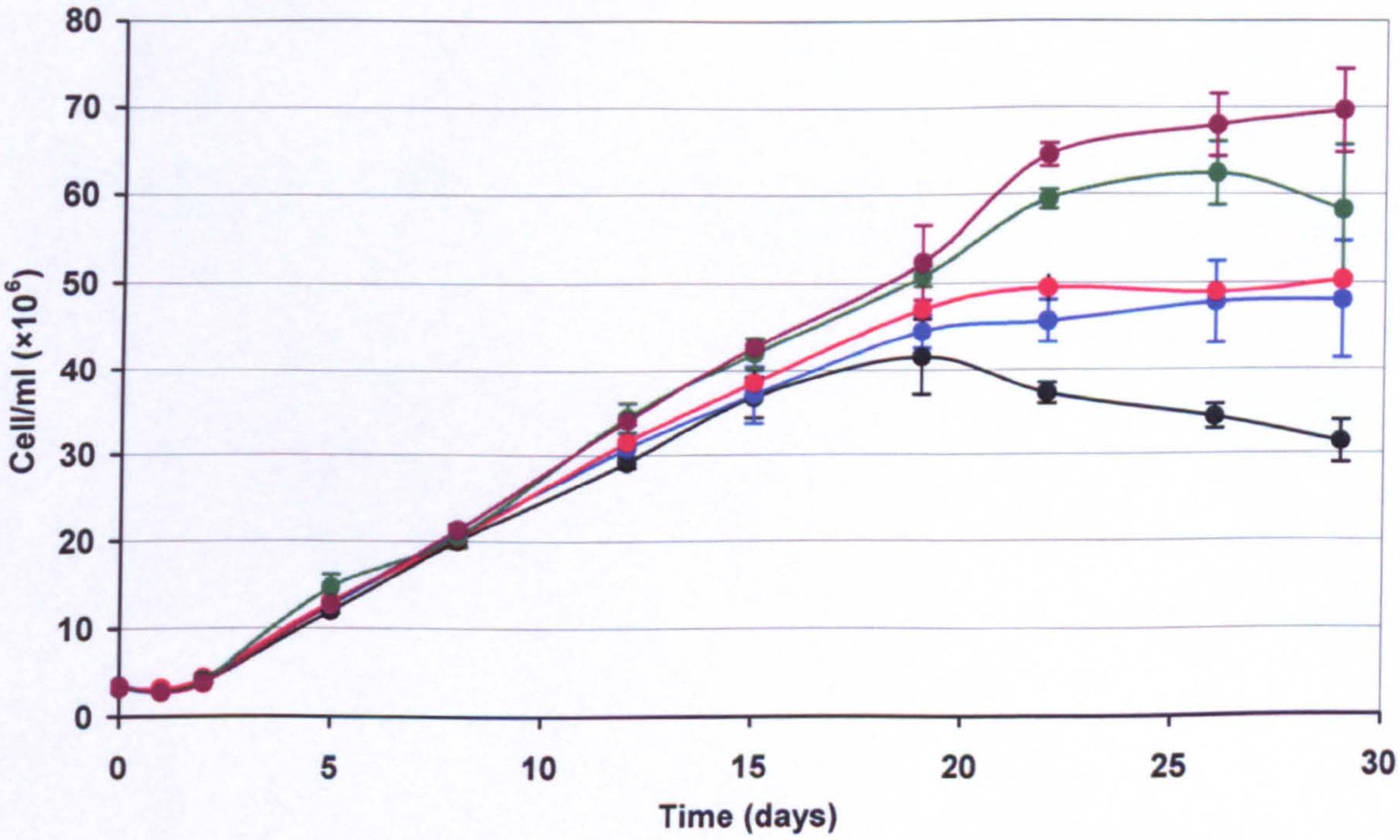

Figure 4.3: Mean cell density of *I. galbana* grown in a range of nitrate concentrations of sf/2 at 32 ‰ (n = 3 ± S.E.). Flasks contained sf/2 at either 3.56 mM; 5.34 mM; 7.12 mM; 8.90 mM; and 10.68 mM nitrate concentration (inoculum cell density at 3.40; 3.53; 3.29; 3.40 and 3.50 × 10^6 cell/ml, respectively). Refer also to Appendix D for a statistical summary of results.

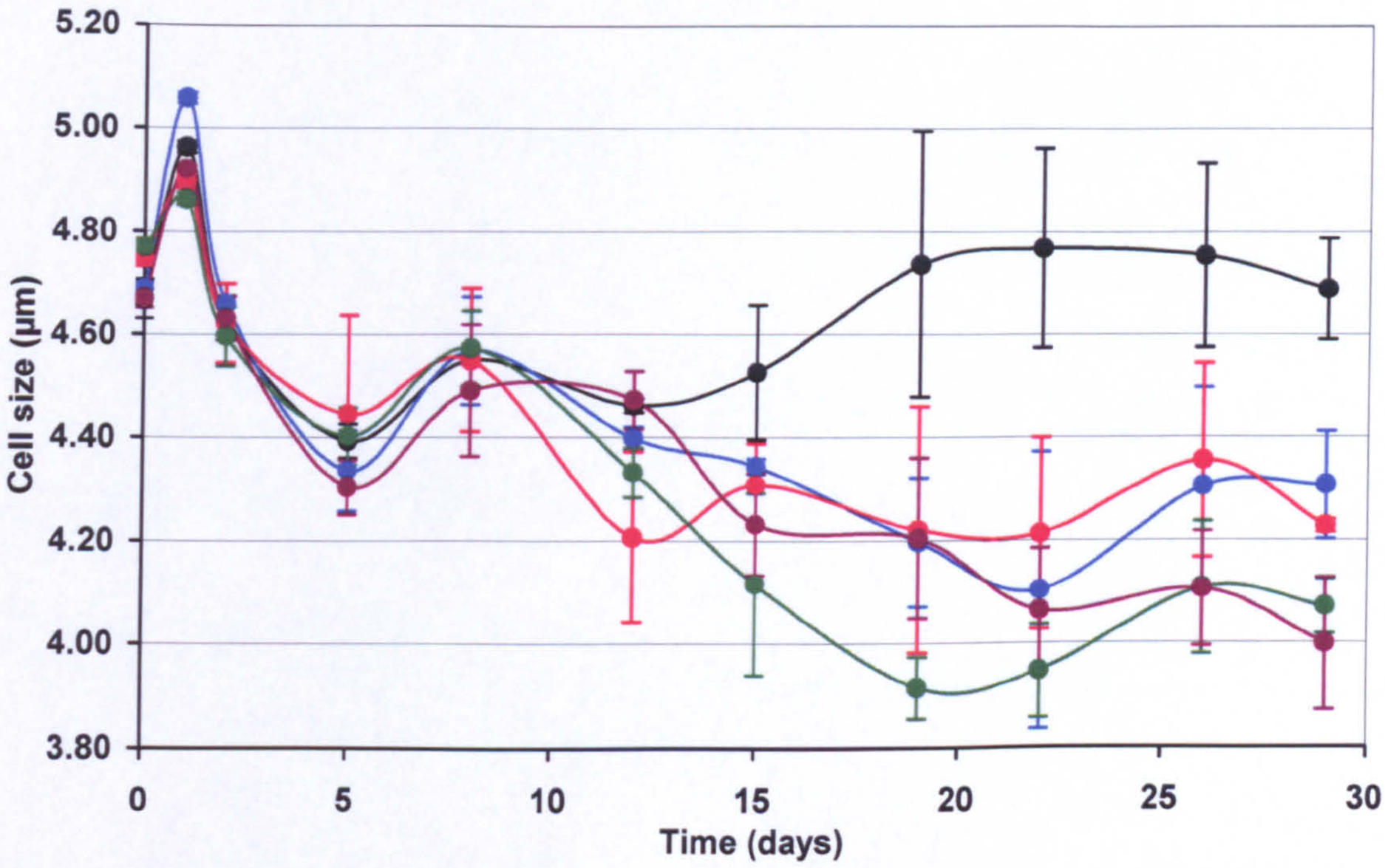

Figure 4.4: Mean cell size of *I. galbana* grown in a range of nitrate concentrations of sf/2 at 32 ‰ (n = 3 ± S.E.). Flasks contained sf/2 at either 3.56 mM; 5.34 mM; 7.12 mM; 8.90 mM; and 10.68 mM nitrate concentration. Refer also to Appendix D for a statistical summary of results.

4.1.4: Temperature

The effect of temperature on the general growth behaviour of *I. galbana* was examined by cultivating the alga at temperatures of 15, 20, 25 and 30 °C. All cultures were seeded from and maintained in sf/2 media at a salinity of 32 ‰. Constant illumination was provided by cool white fluorescent lights, at an irradiance of 122 ± 15 µmol/m^2/s at the surface of the cultures.

At 15 °C, *I. galbana* failed to escape lag phase despite a transient but insignificant rise in population on day 14 (Figure 4.5). Similarly, the response of cells incubated at 30 °C, despite an initial period of linear phase growth (0.71 µ/day), peaked on day 11 (at 10 × 10^6 cell/ml) before cell death became apparent. *I. galbana* responded more favourably to mid-range (20 – 25 °C) temperatures, providing growth rates of 2.34 and 1.81 µ/day at 20 and 25 °C, respectively. A maximum density of 40 × 10^6 cell/ml was achieved by day 21 at 25 °C, whilst incubation at 20 °C increased growth performance by 40 % with a maximum cell density of 56 × 10^6 cell/ml. Overall, a significant relationship was found between growth temperature and mean cell density ($p = <0.002$).

Mean cell size varied at inoculation (4.59 - 5.54 µm) however cells at 15 °C showed an increase in cell size after day two, where cells at higher temperatures all displayed a drop (Figure 4.6), as seen for other cultures in this study. No significant difference was found between cell size of cultures grown at either 20 or 25 °C ($p = 0.1711$). Both reached a relatively stable mean cell size of ~ 4.25 µm (days 11 – 43). The effect of temperature on mean cell size was statistically significant ($p = <0.002$).

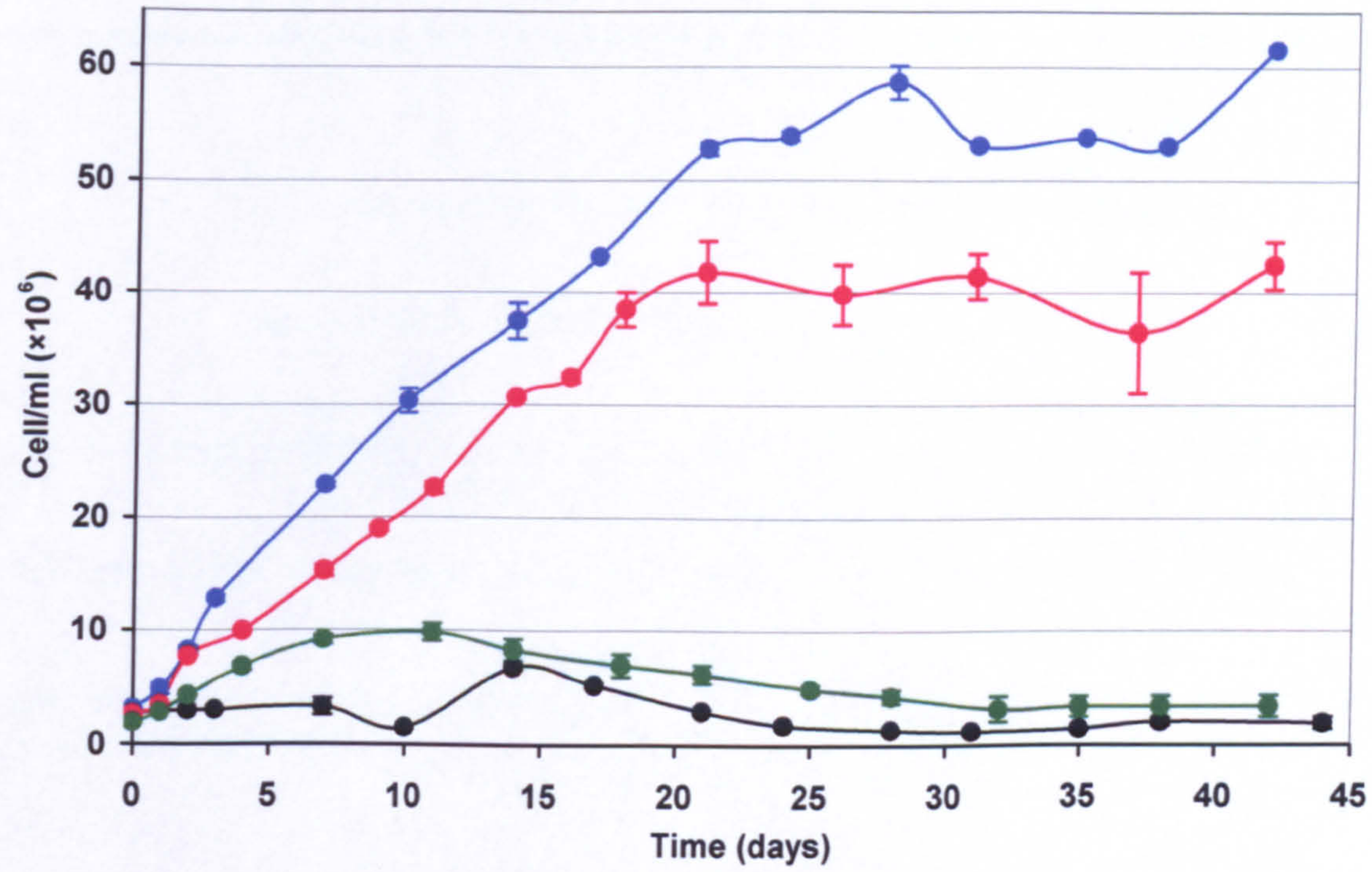

Figure 4.5: Mean cell density of *I. galbana* incubated at a range of growth temperatures (n = 3 ± S.E.). Flasks were incubated at 15 °C; 20 °C; 25 °C and 30 °C (inoculum cell density at 2.74; 3.12; 2.66 and 1.96 × 10^6 cell/ml, respectively). Refer also to Appendix D for a statistical summary of results.

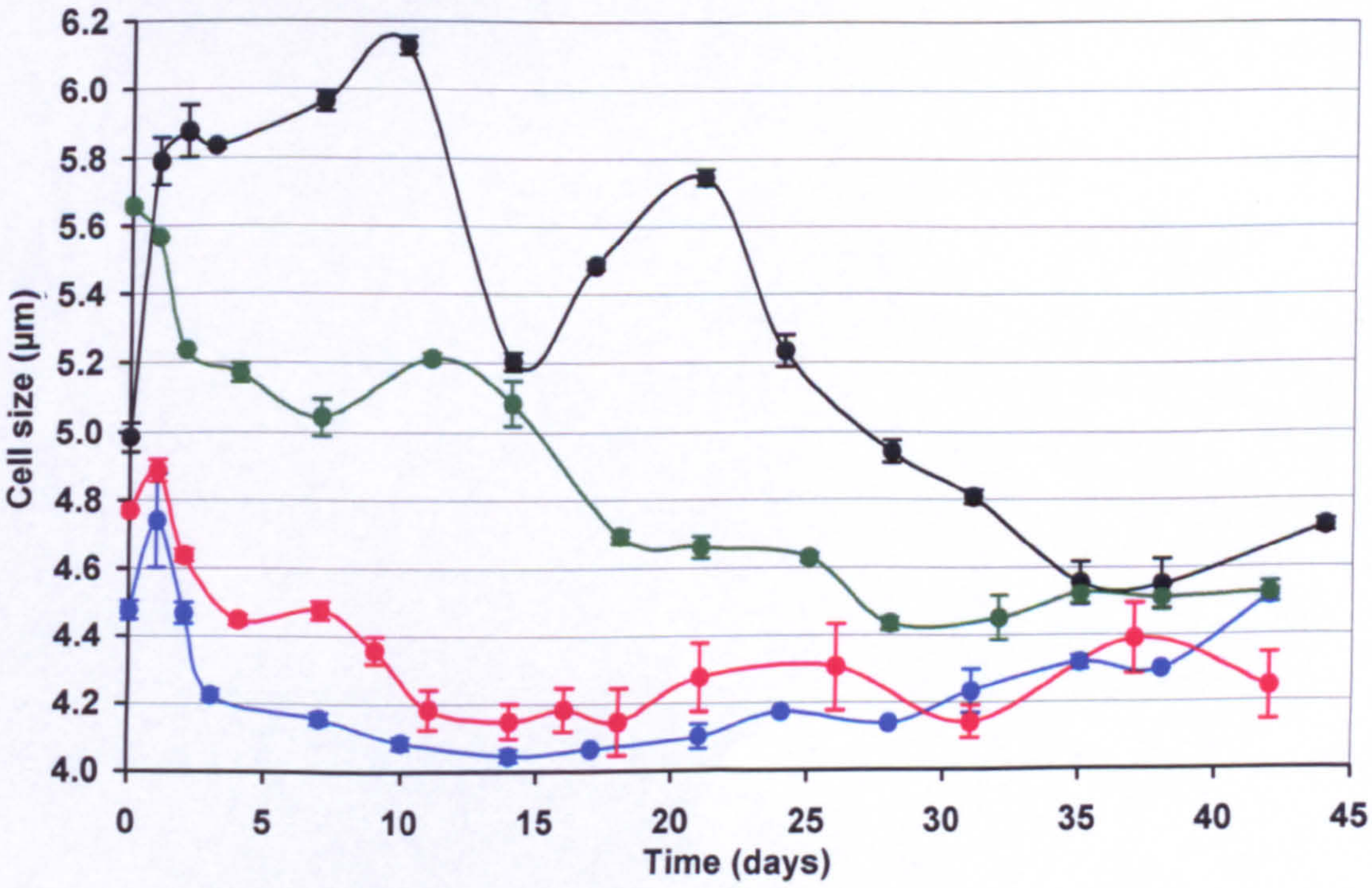

Figure 4.6: Mean cell size of *I. galbana* incubated at a range of growth temperatures (n = 3 ± S.E.). Flasks were incubated at 15 °C; 20 °C; 25 °C and 30 °C. Refer also to Appendix D for a statistical summary of results.

4.1.5: Semi-continuous culture of *I. galbana*

The effect of media renewal with fresh medium, typical of fed-batch/ continuous cultures, was examined using 250 ml shake flask cultures as a model. Each flask contained a total culture volume of 100 ml at inoculation. Cell density was monitored and dilutions began only once cultures were judged to be entering stationary phase. Flasks received either 10, 20, 30 or 40 % media renewal (v/v/day, semi-continuous dilution - refer to Section 1.8.2) with freshly sterilised media (32 ‰ sf/2) using aseptic technique within a laminar flow cabinet. All flasks received the same fresh media from a single stock to avoid any discrepancies in the composition of micro-nutrients given to each flask. All flasks were continuously mixed and maintained at 23 ± 2 °C, with a mean irradiance of 80 µmol/m^2/s.

Despite identical inoculum densities, maximum cell density differed between the four sets of triplicate cultures prior to media renewal, with mean cell counts in the range of 18 - 27 × 10^6 cell/ml (growth rates ranging from 1.10 to 1.76 µ/day) on day 15 (Figure 4.7), although these differences were not statistically significant ($p = 0.952$). At all renewal rates, an immediate reduction in cell density was evident (by 3, 10, 10 and 11 × 10^6 cell/ml for 10, 20, 30 and 40 %, respectively) within the fourth day of media renewal (day 21). Despite this 'wash-out' effect of dilution (Table 4.1), all cultures recovered (in terms of cell density) for this effect by day 21 (after four days of media renewal). Mean cell densities at 10 % renewal showed the most variance between replicates, but generally fell within a steady-state range of 22 – 26 × 10^6 cell/ml. In contrast, cultures of *I. galbana* receiving 40 % media renewal had a steady state range of between 2 and 4 × 10^6 cell/ml. The media renewal rate was inversely proportional to mean cell density, with highly significant differences between each data set ($p = 0.0004$).

At inoculation mean cell size for all flasks in this experiment was ~5.68 µm (Figure 4.8) which was higher than previously observed. Unlike previous experiments this did not alter significantly immediately after inoculation. Mean cell size continued to decrease until day 14, after which application of media renewal rates saw cells responding with a transient increase in mean cell size. Cultures subjected to 10 and 20 % renewal rates displayed very similar changes in mean cell size throughout, and differences in mean cell size as a result of different rates of renewal were generally not significant. The only significant difference observed was between cells receiving 10 and 40 % media renewal ($p = 0.0192$).

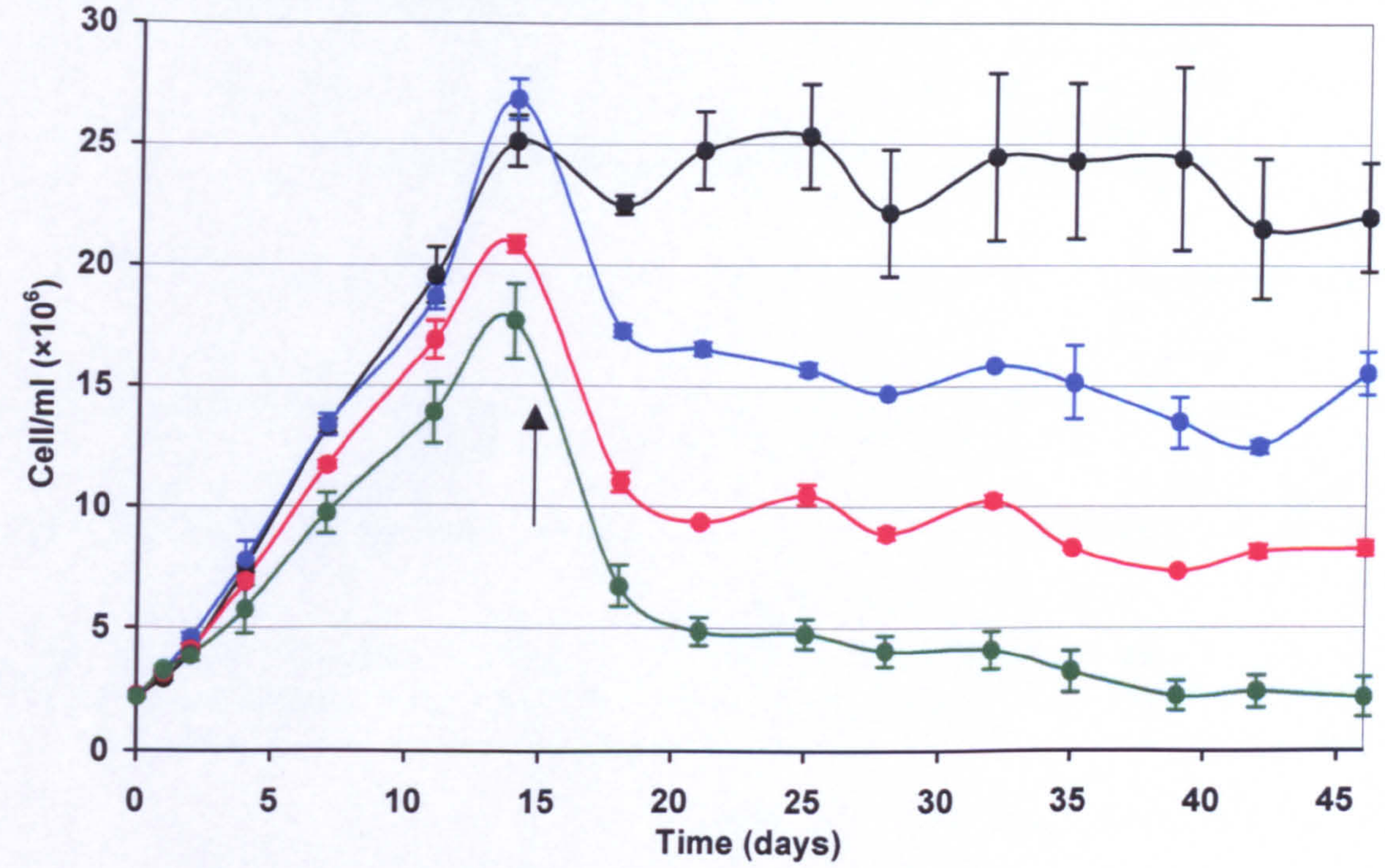

Figure 4.7: Mean cell density of *I. galbana* at a range of semi-continuous media renewal rates (n = 3 ± S.E.). Cultures were diluted with fresh media from day 17 (arrow), at media renewal rates (v/v/day) of 10 %; 20 %; 30 %; and 40 % (inoculum cell density at 2.26; 2.23; 2.24 and 2.20 × 10^6 cell/ml, respectively). Refer also to Appendix D for a statistical summary of results.

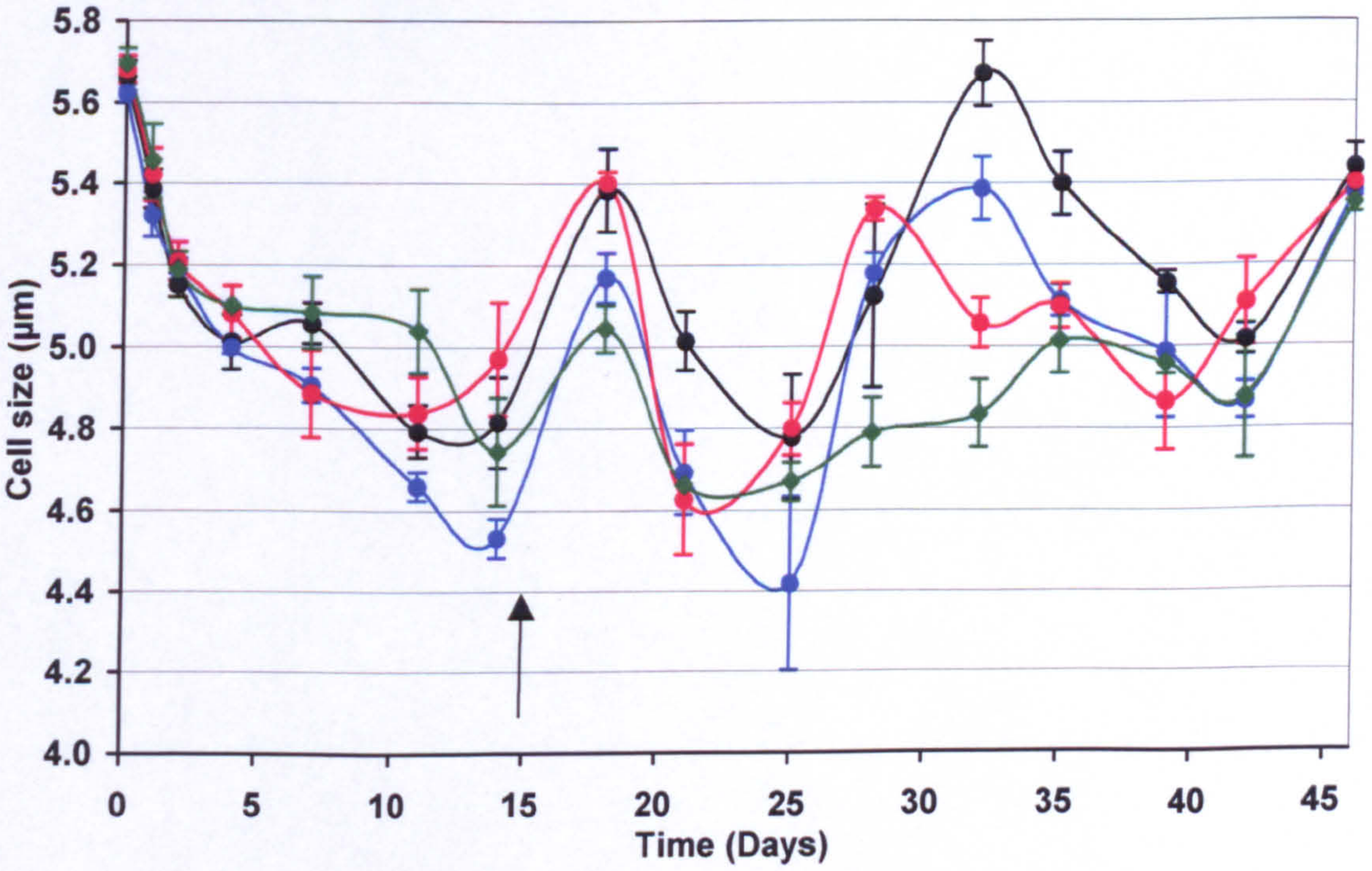

Figure 4.8: Mean cell size of *I. galbana* at a range of semi-continuous media renewal rates (n = 3 ± S.E.). Cultures were diluted with fresh media from day 17 (arrow), at media renewal rates (v/v/day) of 10 %; 20 %; 30 %; and 40 %. Refer also to Appendix D for a statistical summary of results.

Table 4.1 shows cellular response to media renewal rates in terms of initial wash-out and stabilisation (steady state). Average cell density was also scaled up to a 1L culture volume to be used later in projecting FAME productivities (shown in Table 7.1).

Media renewal rate (v/v/day, %)	Dilution response (% cell wash-out)	Steady-state range (cell/ ml × 10^6)	Scaled-up average cell density (cell/ L × 10^{10})
10	10.40	21.50 – 25.50	2.35 ± *0.20*
20	35.59	12.50 – 16.60	1.46 ± *0.21*
30	47.10	7.35 – 10.25	0.88 ± *0.15*
40	61.86	2.20 – 4.10	0.32 ± *0.10*

Table 4.1: Productivity of media renewal rates for *I. galbana* in flask cultures. Working volume maintained at 100 ml.

4.1.6: Oxygen evolution

I. galbana was transferred to fresh sf/2 media (32 ‰), and maintained at 23 °C and 80 µmol/m^2/s continuous irradiance. Cell density and cell size (Figure 4.9) of cultures were monitored throughout, as well as oxygen evolution at a range of irradiances (see Section 2.2.5) during linear-phase growth.

Dark respiration (R_d) was significantly less than P_{max}. Oxygen evolution was highest overall, regardless of irradiance, when sampled on day seven. An irradiance of 500 µmol/m^2/s yielded the highest oxygen output from *I. galbana* at all sample points from cultures maintained at 80 µmol/m^2/s. However, oxygen evolution rates were not consistent during linear-phase growth, dropping off to 0.005 µmol/ min (Table 4.2).

For cells taken at both sample points indicate that I_k (50 – 250 µmol/m^2/s) was higher than the growth conditions provided (80 µmol/m^2/s). Cells grown under this pre-defined light level exhibited a net P_{max} range of 2.66 – 3.94 nmol O_2/ 10^6 cell during linear growth phase.

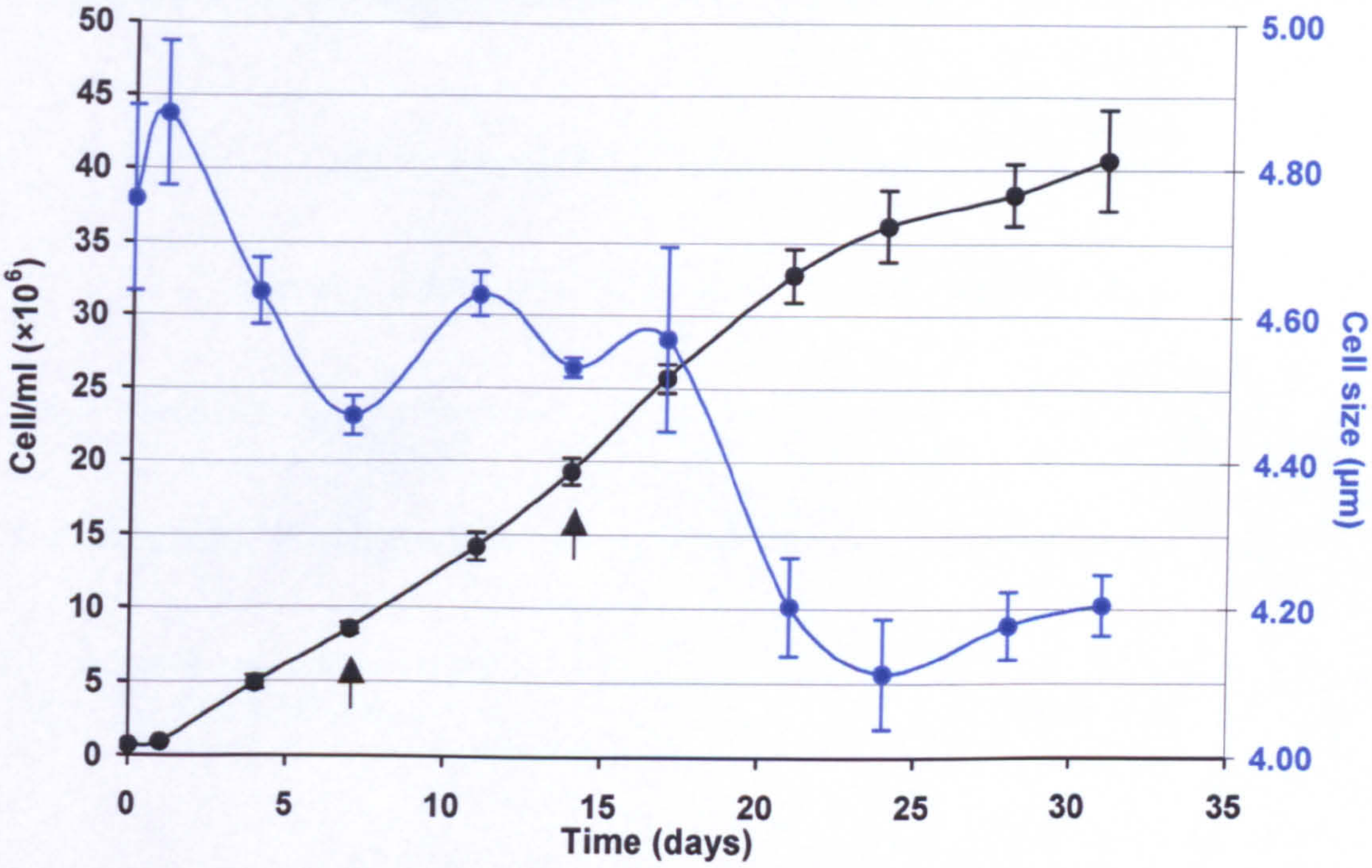

Figure 4.9: Mean cell density and cell size of *I.galabna* in sf/2 at 32 ‰, incubated at 23 °C and under continuous irradiance (80 µmol/m^2/s) (n = 3 ± S.E.). Inoculum cell density at 0.74 × 10^6 cell/ml. Sample points for oxygen evolution analysis taken during linear growth phase, are shown by arrows (see also Table 4.2).

PARAMETER	Time (day)			
	7		14	
	Mean	*S.E.*	Mean	*S.E.*
Cell/ml (× 10^6)	8.54	*0.38*	19.30	*0.94*
R_d (nmol O_2/ 10^6 cell)	-4.02	*0.53*	-1.96	*0.12*
α (pmol O_2/ µmol/m^2/s)	2.79	*0.04*	2.66	*0.08*
Net α (pmol O_2/ µmol/m^2/s)	7.03	*0.09*	4.26	*1.02*
P_{max} (nmol O_2/ 10^6 cell)	-0.08	*0.03*	0.70	*0.03*
Net P_{max} (nmol O_2/ 10^6 cell)	3.94	*0.03*	2.66	*0.03*
I_k (µmol/m^2/s)	250	*0*	50	*0*
µmol/m^2/s/ 10^6 cell At I_k µmol/m^2/s	29.27		2.59	
At 80 µmol/m^2/s	9.37		4.15	

Table 4.2: Cellular-based oxygen P-I curve parameters from flask cultures of *I. galbana* (n = 3). Parameters are described in Section 2.2.5. Net values were derived by subtracting effects of dark respiration (R_d). See Figure 4.9 for culture performance. Refer also to Appendix D for a statistical summary of results.

4.1.7: Total lipid and FAME profile

Comparisons between different media types, as previously highlighted (Figure 4.1), were pooled and their total lipid measured (Table 4.3). Cultures grown in f/2 were found to have a higher total lipid content (by a range of 1.2 - 2.4 times on volumetric scale and 1.5 - 3.8 times on a cellular level) than sf/2 cultures, regardless of salinity.

	Media (formulation and salinity)			
	f/2		sf/2	
	16 ‰	32 ‰	16 ‰	32 ‰
Pooled harvest volume (ml)	269	267	269	266
Pooled cell density ($\times 10^6$ cell/ml)	27.45	28.26	37.89	42.82
Total Lipid (mg)	56	28	24	23
Volumetric lipid (mg/L)	208.18	104.87	89.22	86.47
Cellular lipid (pg/cell)	7.58	3.45	2.35	2.02
FAME (% of Total lipid)	15.87	47.78	46.23	52.75
Volumetric FAME yield (mg/L)	33.05	50.11	41.25	45.61
Cellular FAME yield (fg/cell)	1203.74	1773.22	1088.67	1065.15
DHA (% FAME)	14.04	21.28	19.16	17.47

Table 4.3: Summary comparison of total lipid and FAME profiles for *I. galbana* grown in f/2 and sf/2 at both 16 and 32 ‰. Flasks containing cultures grown on the each media were pooled (n = 3) and the total lipid extracted. Results were standardised in terms of volumetric and cellular yields. Both growth temperature and lighting were standardised for all flasks throughout (see text). All flasks were pooled accordingly after 35 days growth, when all cultures had entered stationary phase (see also Figure 4.1). Individual FAME profiles are shown in Tables 4.4 – 4.7.

From the pooled lipid extracts, FAME profiles were determined for each of the four media (Tables 4.4 – 4.7). Comparisons between the major fatty acid groups based upon percentage total lipid and percentage total FAME, are shown in Figure 4.10. Although cells grown in f/2 at 16 ‰ yielded the highest total lipid their FAME profile, when expressed as a percentage of the total lipid, was the lowest of all four treatments. Furthermore, as a percentage of fatty acids detected, the FAME profile of cells grown in f/2 at 16 ‰ had the lowest proportions of PUFA and the highest content of both SAT and MUFA.

The three most dominant fatty acids found within the FAME profile of *I. galbana* under this study were PAL, OTA and DHA (in descending order). The only exception being for cultures grown in f/2 at 16 ‰ for which results show PAL, OTA and OLE (in descending order) to be their major constituents. Furthermore, the following fatty acids remained undetected irrespective of media conditions (formulation and salinity): LAU, STE, LIN, EDA, ARA and EPA. In addition to which, PML was also absent from cells grown in all sf/2 flasks, whilst LON was only missing from f/2 at 16 ‰. In respect to DHA, levels were highest overall for cells grown in f/2 at 32 ‰, and lowest for the same media formulated in half strength seawater. Increasing salinity significantly increased DHA ($p = <0.05$) independently of other PUFAs ($p = >0.05$) regardless of media formulation when determined on a volumetric basis, as well as percentage fatty acids and of total lipids. However, when calculated on a cellular level changes in salinity provided no significant trends overall to either DHA levels or fatty acids in general ($p = >0.05$). Whilst cultures grown in sf/2 had lower total cellular FAME yields compared to cells maintained in f/2, this was not attributed to any significant differences in PUFAs ($p = 1$) but as a result of lower SATs and MUFAs ($p = 0.0051$ for both).

		Volumetric yield (mg/L)		Cellular yield (fg/cell)		% Fatty Acid		% Total Lipid	
		Mean	S.E.	Mean	S.E.	Mean	S.E.	Mean	S.E.
LAU	(12:0)	-	-	-	-	-	-	-	-
MYR	(14:0)	3.90	*0.32*	141.94	*11.64*	11.82	*1.25*	1.87	*0.15*
PAL	(16:0)	8.01	*0.64*	291.83	*23.24*	24.21	*1.36*	3.85	*0.31*
PML	(16:1)	3.84	*0.23*	140.02	*8.29*	11.62	*0.41*	1.85	*0.11*
STE	(18:0)	-	-	-	-	-	-	-	-
OLE	(18:1 n-9)	5.35	*0.37*	194.72	*13.51*	16.16	*0.74*	2.57	*0.18*
LIN	(18:2 n-6)	-	-	-	-	-	-	-	-
LON	(18:3 n-3)	-	-	-	-	-	-	-	-
OTA	(18:4 n-3)	7.32	*0.46*	266.80	*16.84*	22.14	*0.88*	3.52	*0.22*
EDA	(20:4 n-3)	-	-	-	-	-	-	-	-
ARA	(20:4 n-6)	-	-	-	-	-	-	-	-
EPA	(20:5 n-3)	-	-	-	-	-	-	-	-
DHA	(22:6 n-3)	4.62	*0.60*	168.42	*21.78*	14.04	*2.14*	2.22	*0.29*
TOTAL		**33.05**		**1203.74**		**100.00**		**15.87**	
SAT	(C:0)	11.91		433.77		36.03		5.72	
MUFA	(C:1)	9.19		334.74		27.78		4.41	
PUFA	(C:2>)	11.95		435.23		36.19		5.74	
RATIO	(n-6 : n-3)	*0*		*0*		0		0	

Table 4.4: FAME profile of *I. galbana* grown in f/2 media at 16 ‰ (n = 3 ± S.E.). Cells were harvested on day 35 after incubation at 23 °C under continuous irradiance (80 µmol/m^2/s). Results were derived from a total lipid harvest of 56 mg (208 mg/L or 7.58 pg/cell). Refer to Table 2.1 for full names of each fatty acid. Refer also to Appendix D for a statistical summary of results.

		Volumetric yield (mg/L)		Cellular yield (fg/cell)		% Fatty Acid		% Total Lipid	
		Mean	S.E.	Mean	S.E.	Mean	S.E.	Mean	S.E.
LAU	(12:0)	-	-	-	-	-	-	-	-
MYR	(14:0)	5.06	*0.50*	179.22	*17.69*	10.35	*1.16*	4.83	*0.48*
PAL	(16:0)	7.63	*0.11*	270.07	*3.97*	15.97	*3.55*	7.28	*0.11*
PML	(16:1)	1.99	*0.49*	70.33	*5.13*	3.28	*0.08*	1.89	*0.06*
STE	(18:0)	-	-	-	-	-	-	-	-
OLE	(18:1 n-9)	6.86	*0.46*	242.94	*16.32*	14.12	*2.02*	6.55	*0.44*
LIN	(18:2 n-6)	-	-	-	-	-	-	-	-
LON	(18:3 n-3)	1.79	*0.70*	63.48	*2.43*	2.96	*0.06*	1.71	*0.03*
OTA	(18:4 n-3)	16.04	*3.28*	567.57	*115.93*	32.04	*0.13*	15.29	*3.12*
EDA	(20:4 n-3)	-	-	-	-	-	-	-	-
ARA	(20:4 n-6)	-	-	-	-	-	-	-	-
EPA	(20:5 n-3)	-	-	-	-	-	-	-	-
DHA	(22:6 n-3)	10.73	*2.53*	379.61	*89.50*	21.28	*0.62*	10.23	*2.41*
TOTAL		**50.11**		**1773.22**		**100.00**		**47.78**	
SAT	(C:0)	12.70		449.29		26.32		12.11	
MUFA	(C:1)	8.85		313.27		17.40		8.44	
PUFA	(C:2>)	28.56		1010.66		56.28		27.23	
RATIO	(n-6 : n-3)	0		0		0		0	

Table 4.5: FAME profile of *I. galbana* grown in f/2 media at 32 ‰ (n = 3 ± S.E.). Cells were harvested on day 35 after incubation at 23 °C under continuous irradiance (80 µmol/m^2/s). Results were derived from a total lipid harvest of 28 mg (105 mg/L or 3.45 pg/cell). Refer to Table 2.1 for full names of each fatty acid. Refer also to Appendix D for a statistical summary of results.

		Volumetric yield (mg/L)		Cellular yield (fg/cell)		% Fatty Acid		% Total Lipid	
		Mean	*S.E.*	Mean	*S.E.*	Mean	*S.E.*	Mean	*S.E.*
LAU	(12:0)	-	-	-	-	-	-	-	-
MYR	(14:0)	3.97	*0.07*	104.84	*3.20*	9.63	*2.55*	4.45	*0.12*
PAL	(16:0)	5.51	*0.11*	145.44	*3.40*	13.36	*3.46*	6.18	*0.10*
PML	(16:1)	-	-	-	-	-	-	-	-
STE	(18:0)	-	-	-	-	-	-	-	-
OLE	(18:1 n-9)	4.88	*0.33*	128.85	*4.63*	11.84	*2.15*	5.47	*0.15*
LIN	(18:2 n-6)	-	-	-	-	-	-	-	-
LON	(18:3 n-3)	5.26	*0.33*	138.73	*0.76*	12.74	*1.98*	5.89	*0.62*
OTA	(18:4 n-3)	13.72	*3.79*	362.18	*2.56*	33.27	*4.71*	15.38	*0.21*
EDA	(20:4 n-3)	-	-	-	-	-	-	-	-
ARA	(20:4 n-6)	-	-	-	-	-	-	-	-
EPA	(20:5 n-3)	-	-	-	-	-	-	-	-
DHA	(22:6 n-3)	7.90	*2.79*	208.63	*5.01*	19.16	*3.31*	8.86	*0.22*
TOTAL		**41.25**		**1088.67**		**100.00**		**46.23**	
SAT	(C:0)	9.48		250.28		22.99		10.63	
MUFA	(C:1)	4.88		128.85		11.84		5.47	
PUFA	(C:2>)	26.88		709.54		65.17		30.13	
RATIO	(n-6 : n-3)	0		0		0		0	

Table 4.6: FAME profile of *I. galbana* grown in sf/2 media at 16 ‰ (n = 3 ± S.E.). Cells were harvested on day 35 after incubation at 23 °C under continuous irradiance (80 µmol/m^2/s). Results were derived from a total lipid harvest of 24 mg (89 mg/L or 2.35 pg/cell). Refer to Table 2.1 for full names of each fatty acid. Refer also to Appendix D for a statistical summary of results.

		Volumetric yield (mg/L)		Cellular yield (fg/cell)		% Fatty Acid		% Total Lipid	
		Mean	*S.E.*	Mean	*S.E.*	Mean	*S.E.*	Mean	*S.E.*
LAU	(12:0)	-	-	-	-	-	-	-	-
MYR	(14:0)	5.35	*0.19*	124.93	*2.15*	11.73	*1.25*	6.19	*0.20*
PAL	(16:0)	7.30	*0.38*	170.56	*3.18*	16.01	*0.81*	8.45	*0.08*
PML	(16:1)	-	-	-	-	-	-	-	-
STE	(18:0)	-	-	-	-	-	-	-	-
OLE	(18:1 n-9)	6.40	*0.45*	149.54	*1.33*	14.04	*2.64*	7.41	*0.13*
LIN	(18:2 n-6)	-	-	-	-	-	-	-	-
LON	(18:3 n-3)	3.15	*0.19*	73.57	*3.11*	6.91	*0.57*	3.64	*1.11*
OTA	(18:4 n-3)	15.44	*3.72*	360.47	*5.46*	33.84	*3.88*	17.85	*0.17*
EDA	(20:4 n-3)	-	-	-	-	-	-	-	-
ARA	(20:4 n-6)	-	-	-	-	-	-	-	-
EPA	(20:5 n-3)	-	-	-	-	-	-	-	-
DHA	(22:6 n-3)	7.97	*2.33*	186.09	*5.22*	17.47	*2.95*	9.22	*0.72*
TOTAL		**45.61**		**1065.15**		**100.00**		**52.75**	
SAT	(C:0)	12.65		295.49		27.74		14.64	
MUFA	(C:1)	6.40		149.54		14.04		7.41	
PUFA	(C:2>)	26.56		620.13		58.22		30.71	
RATIO	(n-6 : n-3)	0		0		0		0	

Table 4.7: FAME profile of *I. galbana* grown in sf/2 media at 32 ‰ (n = 3 ± S.E.). Cells were harvested on day 35 after incubation at 23 °C under continuous irradiance (80 µmol/m^2/s). Results were derived from a total lipid harvest of 23 mg (86 mg/L or 2.02 pg/cell). Refer to Table 2.1 for full names of each fatty acid. Refer also to Appendix D for a statistical summary of results.

(a)

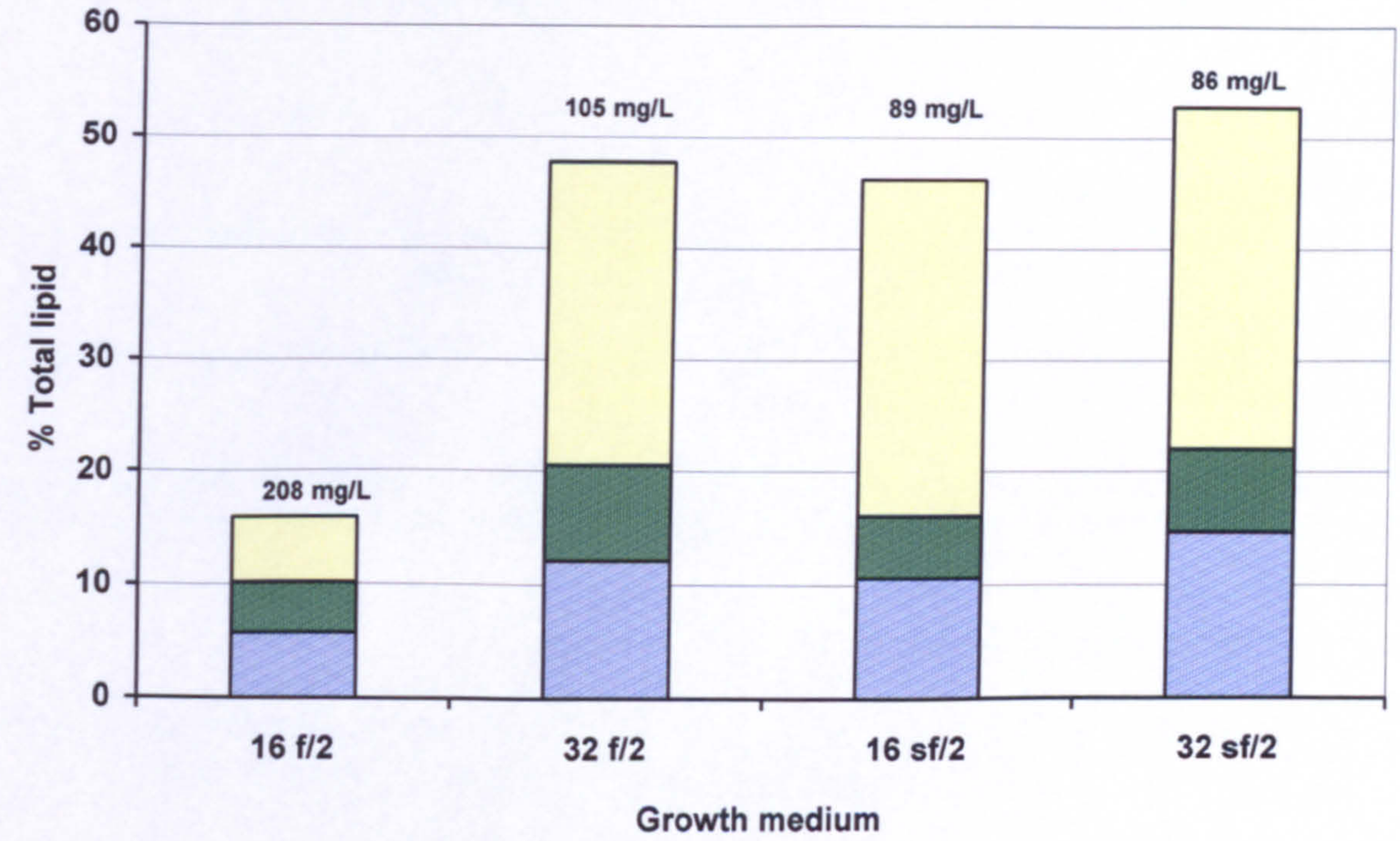

(b)

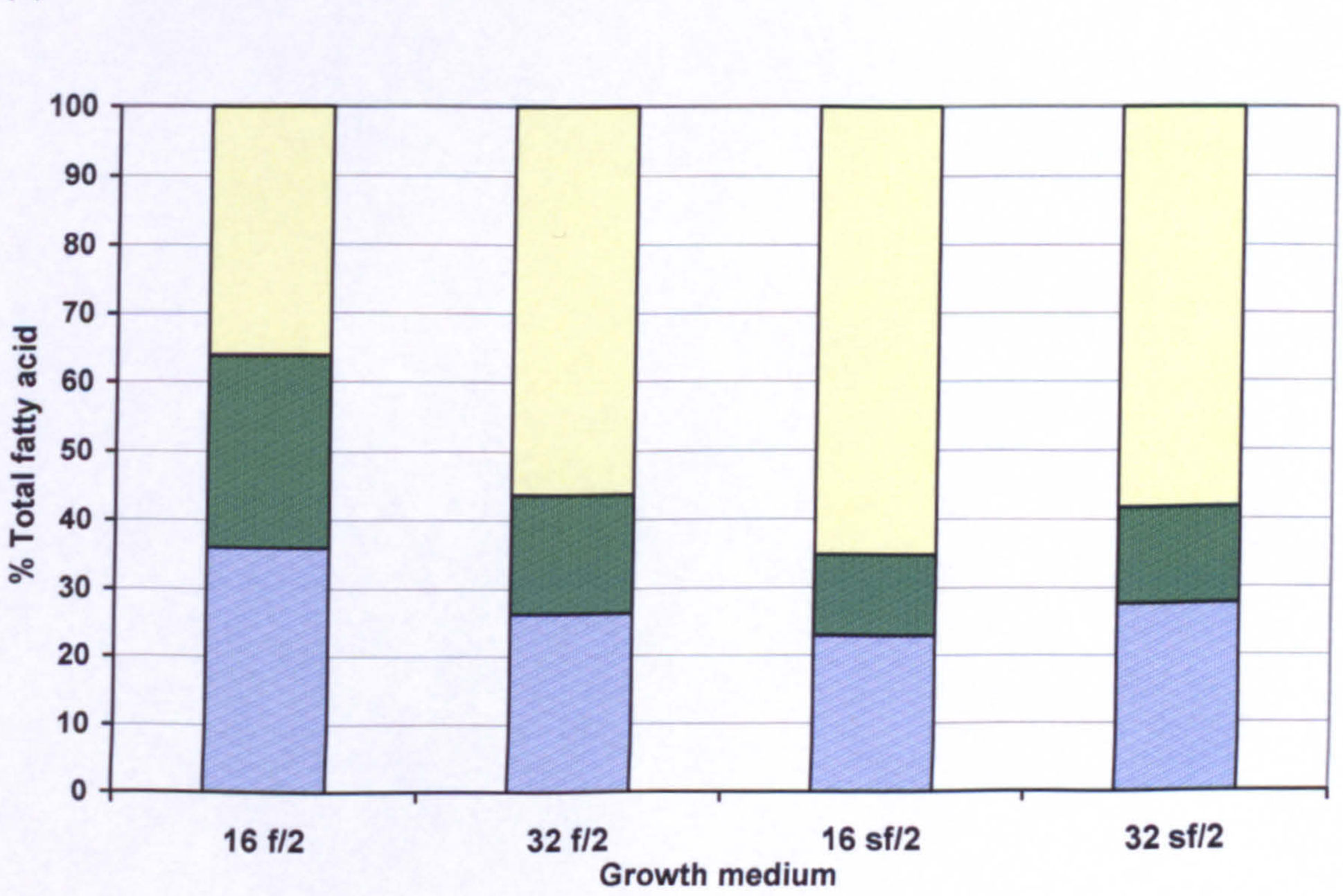

Figure 4.10: Comparison of major fatty acid groups (3 ± S.E.) of *I. galbana* incubated at 23 °C and under continuous irradiance (80 µmol/m²/s). (a) as a percentage of total fatty acid content, and (b) as a percentage of the total lipid: showing Saturated fatty acids; Mono-unsaturated fatty acids and Polyunsaturated fatty acids. Refer also to Appendix D for a statistical summary of results.

4.2: CULTIVATION OF *I. GALBANA* IN A PHOTOBIOREACTOR

Following a range of small-scale (100 ml) experiments, cultures were bulked up into larger (4 L) 'aspirator' cultures (Section 2.1.2). These in turn were used to inoculate the photobioreactor (70 L).

Lighting was provided by continuous (24 hour) illumination provided by a circular light-rig consisting of 16 × F18W fluorescent tubes placed centrally within the coil windings. Initially Sylavania GrowLux (F18W/GRO) tubes were used, as their spectral profile (λ_{max} bandwidths of 400 – 500 and 650 – 700 nm) was similar to the PAR required by these cultures. These were later changed to cool white fluorescents since independent tests on various fluorescent tubes, had later shown no significant difference in culture performance using this light source for *I. galbana* and *N. oculata* (N. Clarkson, pers. comm.). Although these provided an additional spectral range outside PAR (at 500 – 650 nm) which could be seen as wasteful, they were an overall more cost-effective light source being relatively inexpensive.

The photobioreactor was initially operated in batch conditions to simply compare population stability data obtained from earlier flask cultures (Section 4.1). Continuous and fed-batch experiments were later conducted in order to compare productivity of various media renewal regimes. Feb-batch cultures of *I. galbana* were evaluated for changes in FAME profile and oxygen evolution within the photobioreactor.

4.2.1: Batch culture of *I. galbana*

A three-day lag phase was followed by a 21-day linear growth phase at a maximum growth rate of 1.20 μ/day (Figure 4.11). Residual nitrate levels within the growth media decreased steadily until day 24, after which a baseline mean of 3 mg/L remained. Once this baseline was reached cellular growth rate increased to remarkable 5.97 μ/day, giving a maximum mean cell density of 53 × 10^6 cell/ml on day 30 during a brief four-day period of stationary phase. Furthermore, stationary phase growth phase appeared to be short-lived (compared to Figure 4.5).

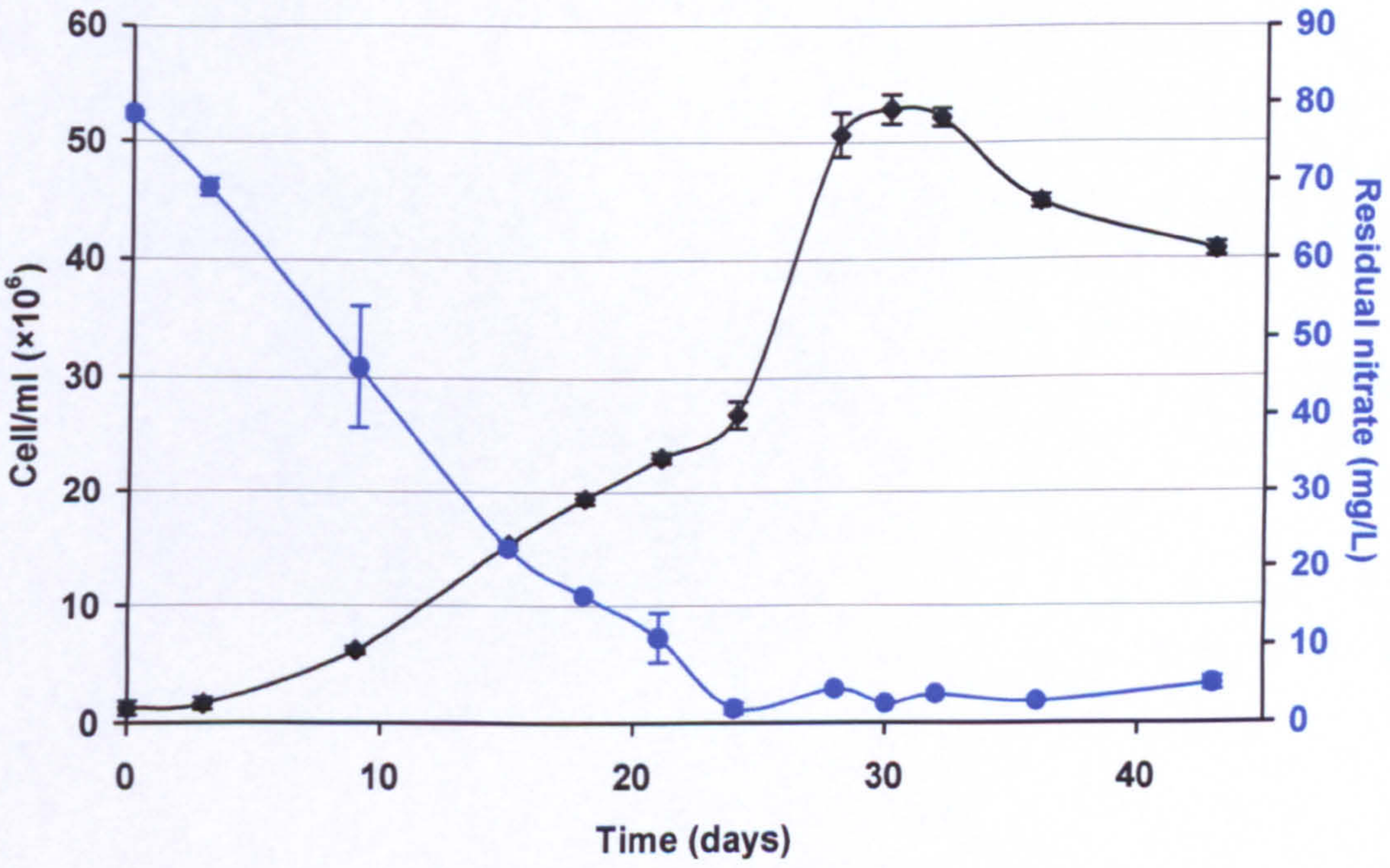

Figure 4.11: Growth of *I. galbana* within a photobioreactor in batch mode operation (n= 3 ± S.E.). Inoculum cell density at 1.27 × 10^6 cell/ml. Continuous irradiance was provided at 107 μmol/m^2/s and temperature maintained at 23 °C throughout. Mean cell density; residual nitrate.

4.2.2: Continuous culture of *I. galbana*

Growth of the alga under initial batch-growth conditions was similar to that shown in Figure 4.11, reaching a maximum cell density of ~50 × 10^6 cell/ml before the culture was switched to continuous mode (Figure 4.12). By day 20, residual nitrate levels had dropped below 40 mg/L, which was higher compared to the previous batch run (Figure 4.11). Although the uptake rate of nitrate was lower in this culture, the growth rate was in fact very much higher (7.07 μ/day) than that showed in Figure 4.11. Since original inoculum cell density was similar for both it is not known what may have caused such a difference. The decision to begin media renewal was based upon the cell density of the culture (see previous maxima) so that media renewal was aimed to begin just prior to onset of stationary phase. Growth during the first thirty-nine days of media renewal was consistent when compared with the thirty days media renewal from flask cultures. Furthermore the steady state range was more than double that of the flask culture model. However, after day 45 residual nitrate levels began to rise (from <10 mg/L, peaking at 40 mg/L). This was sharply followed by a drop in cell density (by ~35 × 10^6 cell/ml) between days 58 and 65. By day 80, cell density had failed to recover (10 × 10^6 cell/ml) and media renewal was stopped. The culture responded favourably as residual nitrate levels again became depleted. Media renewal (as % v/v/day) re-commenced on day 99 following a semi-continuous replenishment of 10 L, and cell density recovered back to a maximum of 60 × 10^6 cell/ml. However, cell density then dropped at a similar rate to ~28 × 10^6 cell/ml. Maximum values of 1.87 and 1.35 g/L were recorded for DW and AFDW, respectively (Figure 4.13) but DW results did not follow same trend as cell density ($p = >0.05$).

Mean cell size (Figure 4.14) remained relatively constant (~4.55 μm) prior to media renewal. This subsequently showed erratic changes, but overall larger cells in continuous mode. A similar trend was noticed by Parrish *et al.* (1998), with N-limited cells becoming larger. Indeed a negative correlation was made between residual nitrate and mean cell size ($p = <0.05$). Overall, residual nitrate levels formed negative relationships towards cell growth in general (DW, AFDW and cell density, $p = <0.02$) under continuous culture conditions, contrary to previous data (Section 4.1.3). Cellular dry weight during the first period of media renewal was on average 30 pg/cell until day 60. As cell numbers decreased, cellular dry weight reached 100

pg/cell towards the end of the first period of media renewal. When media renewal was stopped mean cell size was at a low of 4.20 μm, before continuing to increase (even after media renewal re-started) to 5.90 μm. Cellular dry weight followed a similar trend in the absence of media renewal, but decreased as the second period of media renewal began. Fidalgo *et al.* (1998) reported that cellular dry weight increased with culture age/ nutrient uptake, typically from 47.50 pg/cell in linear growth phase to 76.46 pg/cell in late stationary growth phase from batch cultures of *I. galbana*.

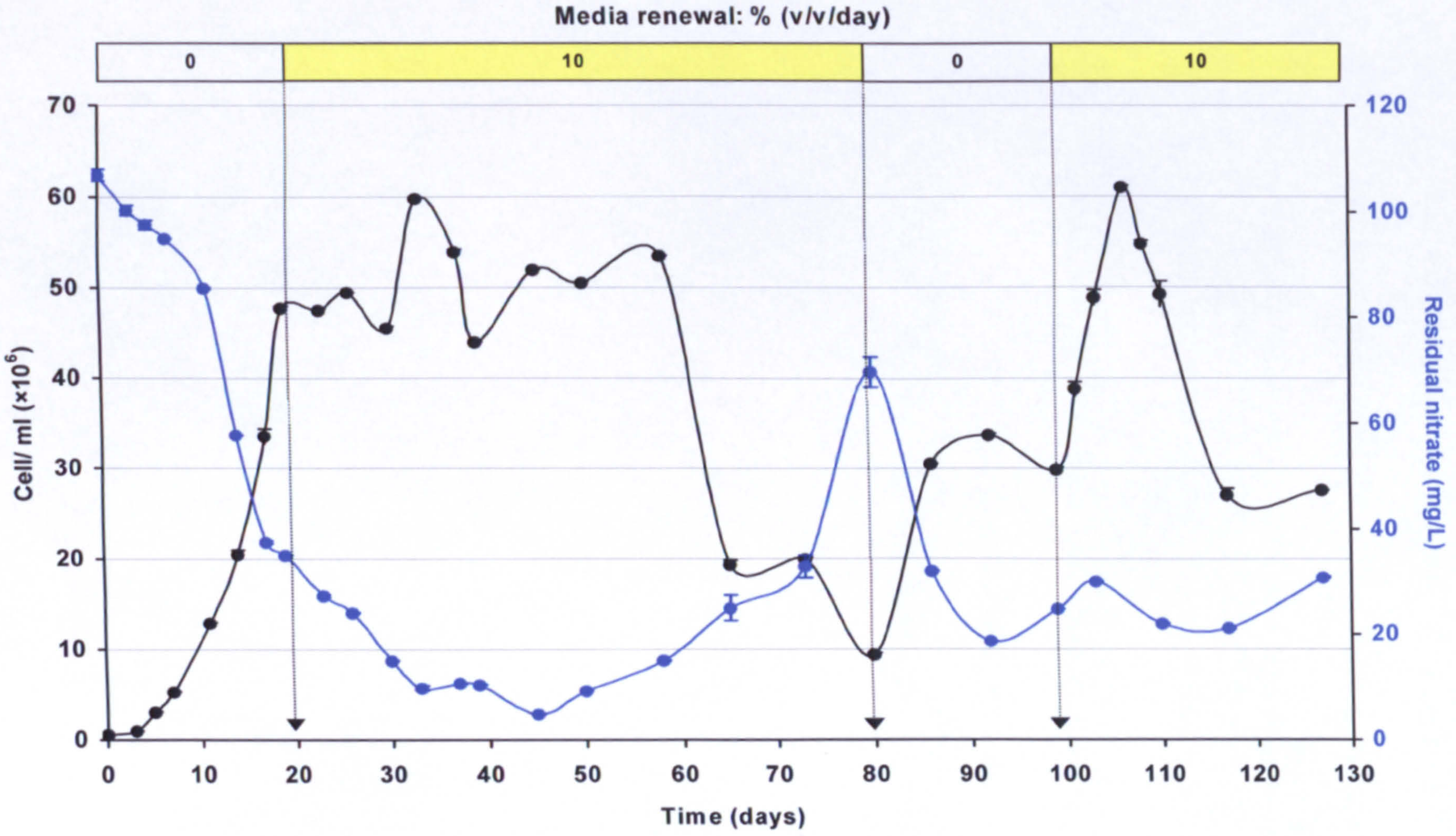

Figure 4.12: Growth of *I. galbana* within a photobioreactor in continuous operation. Inoculum cell density at 0.52×10^6 cell/ml. Continuous irradiance was provided at 107 µmol/m^2/s and temperature maintained at 23 °C throughout. Mean cell density; residual nitrate (n = 3 ± S.E. for all data). Arrows indicate changes in continuous (24:0, on:off) media renewal rate (v/v/day). Refer also to Appendix D for a statistical summary of results.

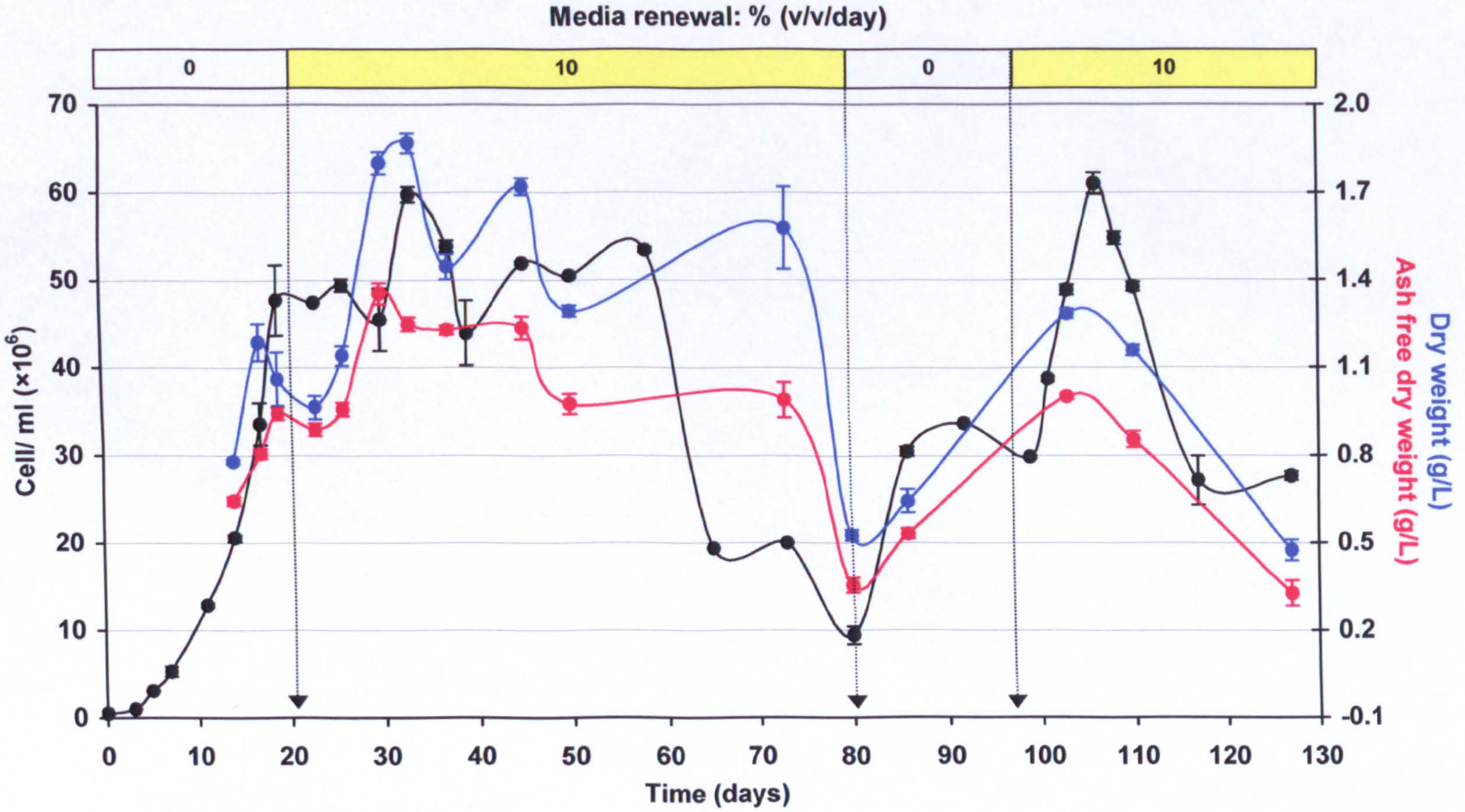

Figure 4.13: Biomass changes of *I. galbana* within a photobioreactor in continuous operation. Inoculum cell density at 0.52×10^6 cell/ml. Continuous irradiance was provided at 107 µmol/m^2/s and temperature maintained at 23 °C throughout. Mean cell density; total dry weight (DW); ash-free dry weight (AFDW) (n = 3 ± S.E. for all data). Arrows indicate changes in continuous (24:0, on:off) media renewal rate (v/v/day). Refer also to Appendix D for a statistical summary of results.

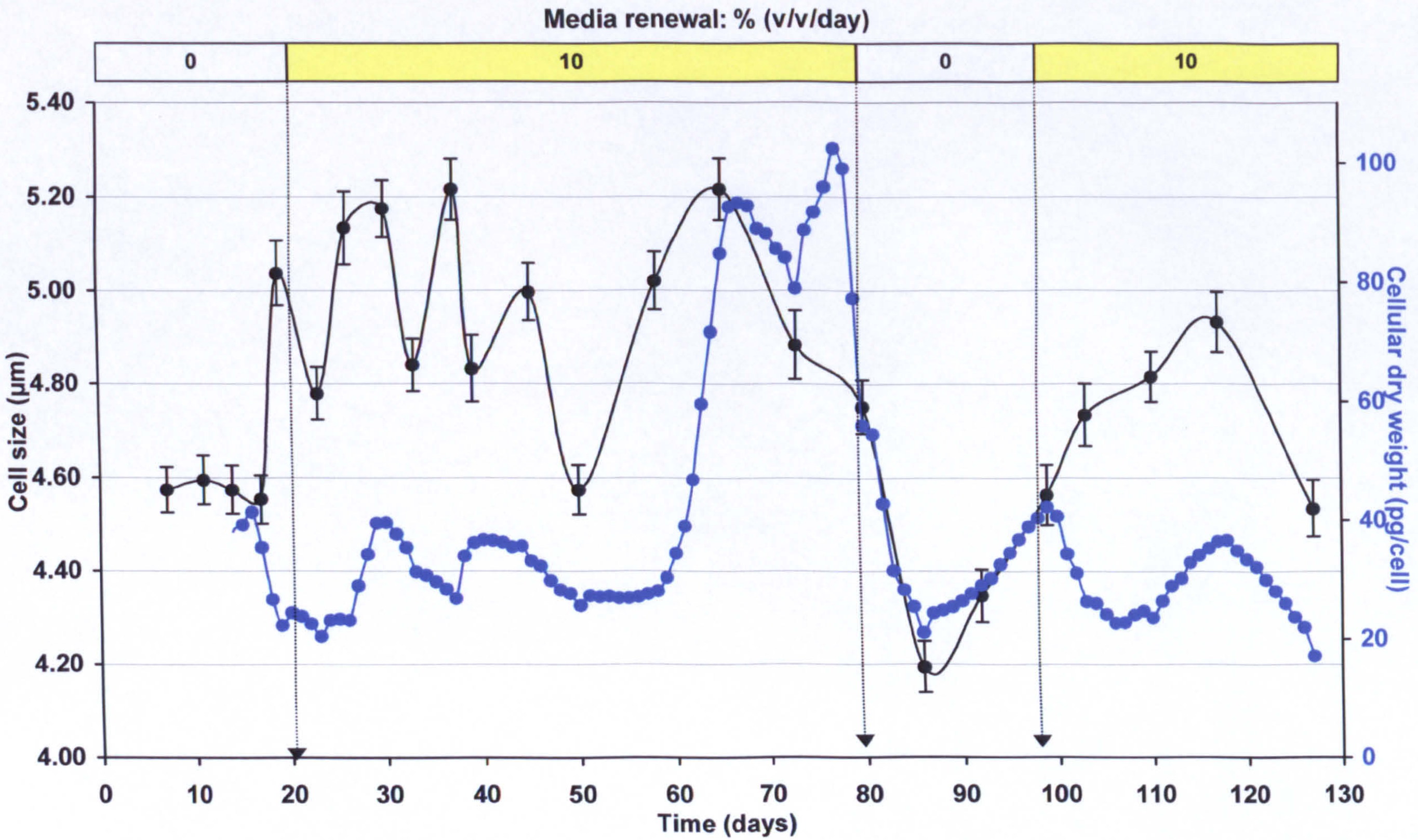

Figure 4.14: Comparison of cell size and cellular dry weight of *I. galbana* within a photobioreactor in continuous operation. Continuous irradiance was provided at 107 µmol/m^2/s and temperature maintained at 23 °C throughout. Mean cell size (µm); cellular dry weight (ng/cell) (n = 3 ± S.E. for all data). Cellular dry weight points have been interpolated. Arrows indicate changes in continuous (24:0, on:off) media renewal rate (v/v/day). Refer also to Appendix D for a statistical summary of results.

4.2.3: Fed-batch culture of *I. galbana*

In the fed-batch culture of *I. galbana*, a maximum cell density of 74 × 10^6 cell/ml (at 7.10 μ/day on day 17) was achieved prior to media renewal on day 19 (Figure 4.15) and was 54 % (26 × 10^6 cell/ml) greater than that of the continuous culture (Section 4.2.2). At this point a fed-batch operation began by replacing 10 % of the working volume over a 4 hr period (at 1.75 L/hr), with a 20 hr recovery period in a daily cycle. Residual phosphate levels displayed a marked response on day 22. On day 32 residual phosphate levels, and later (day 39) nitrate, gradually began to rise. This combined with the continuing decrease in cell number prompted a change in the fed-batch strategy. Despite the drop in cell numbers for this period, dry weight remained around 0.95 g/L from day 19 onwards, whilst ash-free dry weight made up to 93 % of the total dry weight (Figure 4.16). Mean cell size had decreased following inoculation, from 4.70 to 4.20 μm by day 14 (Figure 4.17). At 10 % (v/v/day) media renewal, mean cell size increased to a maximum of 5.70 μm on day 50 as cell density had decreased, showing an inverse relationship between cell number and size ($p = < 0.05$).

On day 56 a second fed-batch strategy was adopted. This comprised of 4 hrs per day media renewal at 20 % (v/v/day) for two days followed by a two-day recovery period, intended to give a similar weekly volumetric harvest (42 L per week compared to 49 L of the fed-batch strategy). This second fed-batch strategy initially saw mean cell size recover from 5.07 to 5.68 μm over ten days. Volumetric levels of Chlorophyll *a* remained between 8 and 12 μg/ml, regardless of media renewal rate/ strategy (Figure 4.18). This was the result of increased cellular levels despite the reduction in cell density ($p = < 0.02$). Chlorophyll *a* was higher than reported by Fabregas *et al.* (1985) for stationary-phase cultures in 30 ‰ seawater (4.5 μg/ml). The accumulation of chlorophyll *a* (on a cellular level) appears to be related to residual levels of both nitrate and phosphate in the culture ($p = < 0.02$). Cellular dry weight (Figure 4.17) increased with the onset of media renewal at a rate of 0.60 ng/cell/day, increasing dramatically (3.89 ng/cell/day) after the second fed-batch strategy was implemented. It was hoped this second strategy would allow sufficient 'recovery time' (48 hrs) for cell number to increase due to uptake of excess nutrients in the absence of any wash-out. However, residual levels of both nitrate and phosphate continued to rise and cell number dropped. Meanwhile, cells were found to increase in size and mass, both coincided with an increased cellular accumulation of chlorophyll *a* ($p = < 0.05$).

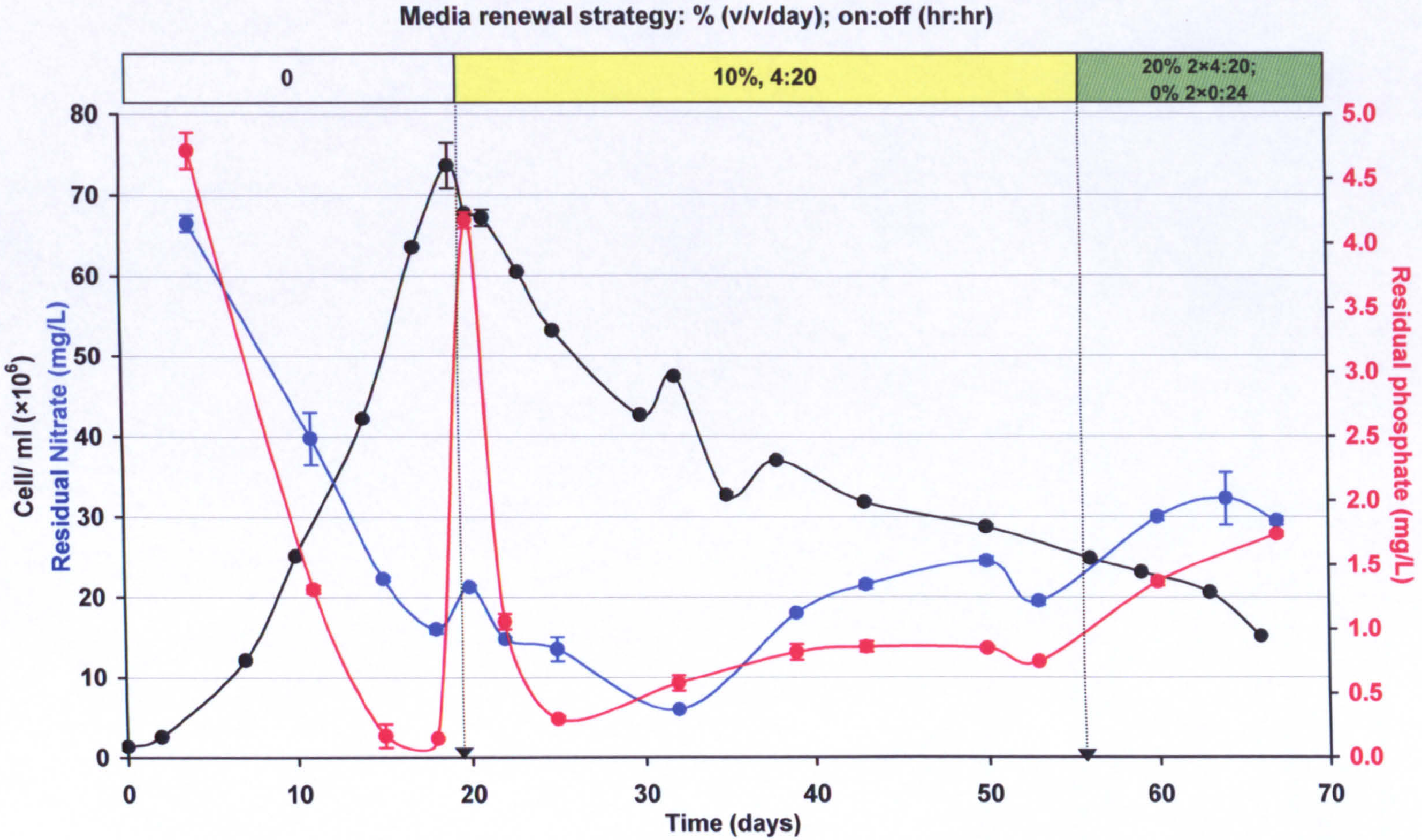

Figure 4.15: Growth of *I. galbana* within a photobioreactor in fed-batch operation. Inoculum cell density at 1.39×10^6 cell/ml. Continuous irradiance was provided at 107 µmol/m^2/s and temperature maintained at 23 °C throughout. Mean cell density; residual nitrate; residual phosphate levels (n = 3 ± S.E. for all data). Arrows indicate change to fed-batch (4:20, on:off) media renewal rate (v/v/day). Refer also to Appendix D for a statistical summary of results.

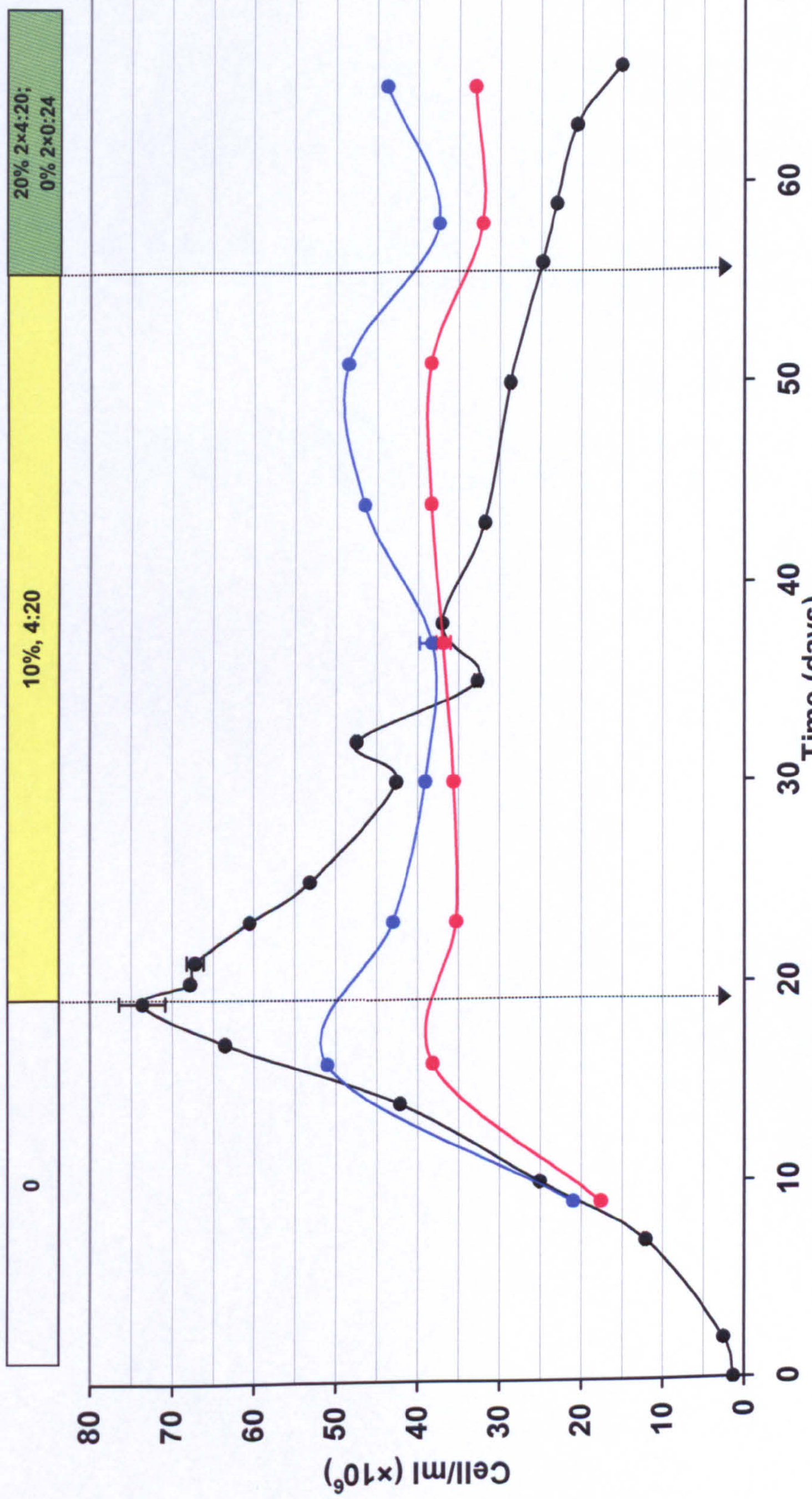

Figure 4.16: Biomass changes of *I. galbana* within a photobioreactor in fed-batch operation. Inoculum cell density at 1.39×10^6 cell/ml. Continuous irradiance was provided at 107 µmol/m^2/s and temperature maintained at 23 °C throughout. Mean cell density; total dry weight (DW); ash-free dry weight (AFDW) ($n = 3 \pm$ S.E. for all data). Arrows indicate change to fed-batch (4:20, on:off) media renewal rate (v/v/day). Refer also to Appendix D for a statistical summary of results.

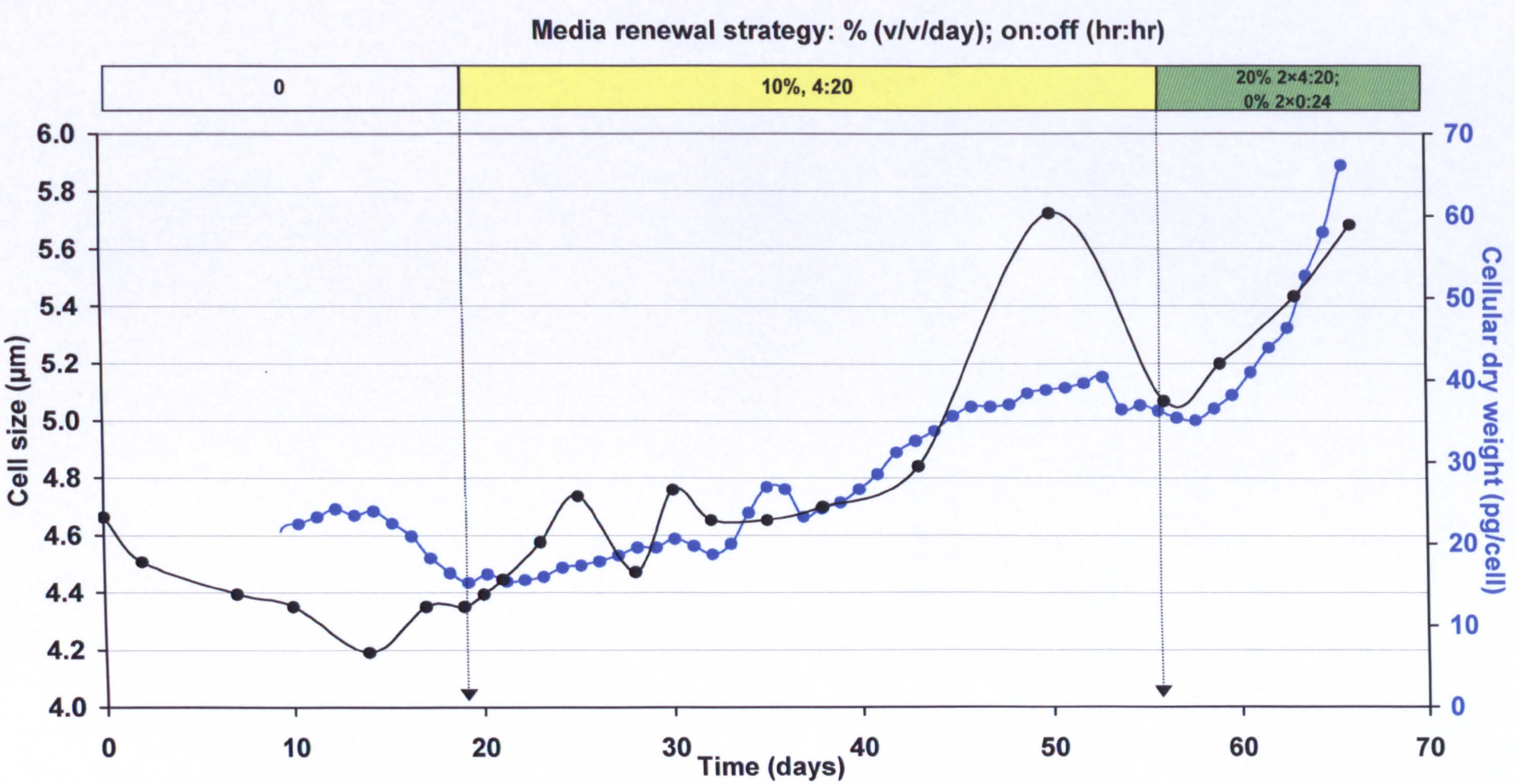

Figure 4.17: Comparison of cell size and cellular dry weight of *I. galbana* within a photobioreactor in fed-batch operation. 24 hour illumination was provided at 107 µmol/m^2/s and temperature maintained at 24 °C throughout. Mean cell size (µm); cellular dry weight (ng/cell) (n = 3 ± S.E. for all data). Cellular dry weight points have been interpolated. Arrows indicate change to fed-batch (4:20, on:off) media renewal rate (v/v/day). Refer also to Appendix D for a statistical summary of results.

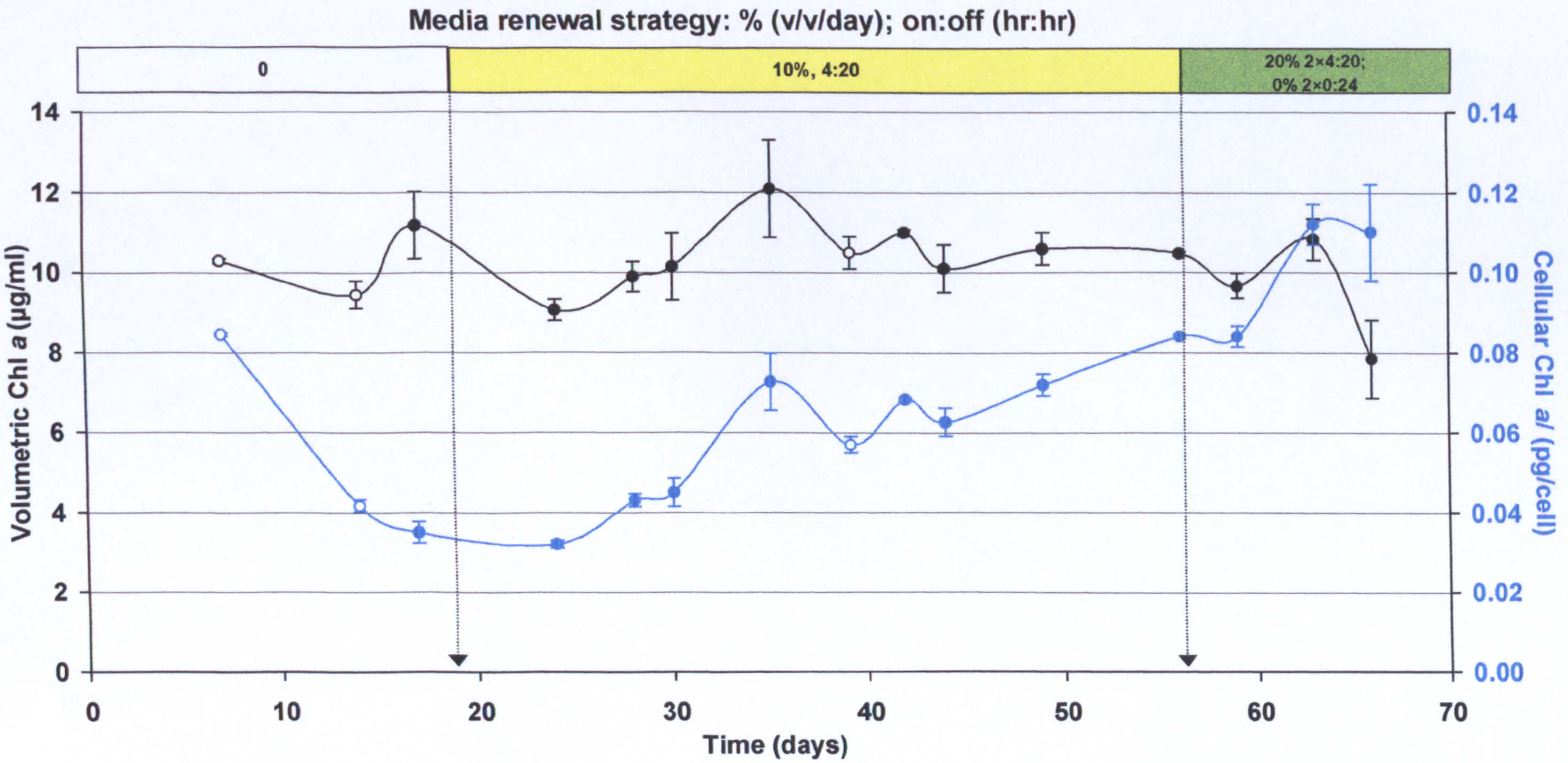

Figure 4.18: Chlorophyll *a* changes in *I. galbana* cultured within a photobioreactor in fed-batch operation. Continuous irradiance was provided at 107 µmol/m^2/s and temperature maintained at 23 °C throughout. Volumetric chlorophyll *a* (µg/ml); cellular chlorophyll *a* (pg/cell) (n = 3 ± S.E. for all data). Cellular dry weight points have been interpolated. Arrows indicate change to fed-batch (4:20, on:off) media renewal rate (v/v/day). Hollowed circles indicate sample points used for oxygen evolution analysis (Tables 4.9 and 4.10). Refer also to Appendix D for a statistical summary of results.

Prior to establishing a media renewal regime (< day 19) oxygen evolution rates were measured during the linear growth phase. These were compared to oxygen evolution readings taken during media renewal strategies 1 (day 39) and 2 (day 66) and standardised according to cellular and volumetric chlorophyll *a* oxygen evolution (Tables 4.8 and 4.9, respectively).

Between days 7 - 14 there was a 30×10^6 cell/ml increase in mean cell density. Net P_{max} during this period ranged from 0.75 - 0.54 nmol O_2/ 10^6 cell, which was lower than previous data from flask experiments (Section 4.1.6). This can be attributed to higher dark respiration rates (more oxygen uptake). The mean cellular α (4.10 pmol O_2/ $\mu mol/m^2/s$; Table 4.8) was also higher indicating more efficient oxygen evolution within the photobioreactor. Optimum oxygen evolution during linear phase growth was found at an I_k irradiance range of between 167 and 208 $\mu mol/m^2/s$ (well above I_o; see also Section 5.5). This I_k range remained the same in both linear phase growth and once a fed-batch regime had commenced, whereas net cellular α more than doubled during the fed-batch periods. Net cellular P_{max} was also comparatively higher during fed-batch periods (0.92 - 2.20 nmol O_2/ 10^6 cell).

PARAMETER	Linear growth phase (batch period)				Fed-batch period			
	Day 7		Day 14		Day 39		Day 66	
	Mean	*S.E.*	Mean	*S.E.*	Mean	*S.E.*	Mean	*S.E.*
Cell/ml ($\times 10^6$)	12.14	*0.20*	42.22	*0.15*	37.04	*0.06*	13.37	*0.01*
R_d (nmol O_2/ 10^6 cell)	-0.34	*0.01*	-0.35	*0.02*	-0.72	*0.09*	-1.07	*0.09*
Cellular α (pmol O_2/ µmol/m^2/s)	4.20	*0.50*	4.00	*0.10*	6.50	*0.10*	10.50	*0.20*
Net cellular α (pmol O_2/ µmol/m^2/s)	6.80	0.65	6.70	*0.21*	12.00	0.28	18.70	*0.22*
P_{max} (nmol O_2/ 10^6 cell)	0.42	*0.07*	0.19	*0.02*	0.20	*0.01*	1.14	0.03
Net P_{max} (nmol O_2/ 10^6 cell)	0.75	*0.05*	0.54	*0.03*	0.92	*0.06*	2.20	*0.09*
I_k (µmol/m^2/s)	166.67	*41.67*	208.33	*41.67*	166.67	*41.67*	208.33	*41.67*
µmol/m^2/s/ 10^6 cell								
At I_k µmol/m^2/s	13.78		4.93		4.50		15.59	
At 107 µmol/m^2/s	8.81		2.53		2.89		8.00	

Table 4.8: Cellular-based oxygen P-I curve parameters from a fed-batch photobioreactor culture of *I. galbana* (n = 3). Net values were derived by subtracting effects of dark respiration (R_d). Cultures were maintained continuously at an irradiance of 107 µmol/m^2/s throughout. Refer also to Appendix D for a statistical summary of results.

Overall, the mean chlorophyll *a* content (volumetric) was fairly consistent (9.97 ± 2.12 µg/ml) throughout the experiment (Figure 4.18) regardless of the growth phase or renewal strategy. However, dark respiration (R_d) increased almost four-fold, on an averaged chlorophyll *a* basis, during linear phase growth (Table 4.9). As a result of which net P_{max} increased to 2.40 nmol O_2/ µg Chl *a*. This was significantly higher than that of Geel *et al.* (1997), who recorded a net P_{max} of 0.13 nmol O_2/ µg Chlorophyll *a* (at 100 µmol/m^2/s continuous irradiance). Net P_{max} continued to increase throughout successive sampling points. A further increase of 0.50 nmol O_2/ µg Chl *a* was found during media renewal, between days 39 - 66. Volumetric chlorophyll *a* content had a statistically negative relationship to I_k (p = *<0.05*), which is consistent with general patterns of photoacclimation (see Section 1.9.2).

PARAMETER	Linear growth phase (batch period)				Fed-batch period			
	Day 7		Day 14		Day 39		Day 66	
	Mean	*S.E.*	Mean	*S.E.*	Mean	*S.E.*	Mean	*S.E.*
Chl *a* (µg/ml)	10.29	*0.06*	9.45	*0.34*	10.49	*0.41*	7.85	*0.91*
R_d (nmol O_2/ µg Chl *a*)	-0.40	*0.07*	-1.54	*0.14*	-2.55	*0.09*	-1.82	*0.15*
α (pmol O_2/ µmol/m^2/s)	4.90	*0.50*	17.90	*0.60*	22.90	*0.70*	17.90	*0.20*
Net α (pmol O_2/ µmol/m^2/s)	7.50	*0.62*	29.80	*0.71*	42.60	*1.02*	31.90	*0.43*
P_{max} (nmol O_2/ µg Chl *a*)	0.49	*0.11*	0.86	*0.14*	0.70	*0.09*	1.94	*0.27*
Net P_{max} (nmol O_2/ µg Chl *a*)	0.88	*0.16*	2.40	*0.44*	3.25	*0.44*	3.75	*0.99*
I_k (µmol/m^2/s)	166.67	*41.67*	208.33	*41.67*	166.67	*41.67*	208.33	*41.67*
µmol/m^2/s/ µg/Chl *a* At I_k µmol/m^2/s	16.20		22.05		15.89		26.54	
At 107 µmol/m^2/s	10.40		11.32		10.20		13.63	

Table 4.9: Chlorophyll *a*-based oxygen P-I curve parameters from a fed-batch photobioreactor culture of *I. galbana* (n = 3). Net values were derived by subtracting effects of dark respiration (R_d). Cultures were maintained continuously at an irradiance of 107 µmol/m^2/s throughout. Refer also to Appendix D for a statistical summary of results.

Total lipid samples were taken on day 16 (77 mg/L), before beginning fed-batch operation of the photobioreactor, and at the end of the experiment on day 66 (63 mg/L) and analysed for their FAME profiles (Table 4.10 and 4.11, respectively).

Cellular DHA levels after 16 days (Table 4.10) were lower than obtained in flask cultures but after a further 40 days cultivation (Table 4.11) were comparatively (with Table 4.7) 13 % higher than previously found, despite its contribution towards the total lipid content being halved. On day 66, 14 L of culture was harvested at a cell density of 15×10^6 cell/ml which, given the FAME profile in Table 4.11, resulted in a harvest of 167.70 mg of PUFA (of which 45.51 mg was DHA).

The fatty acid profile of *I. galbana* on day 66 samples shows the presence of previously undetected fatty acids, namely LAU, STE and LIN. However, overall total volumetric yield had decreased by more than half compared to levels found on day 16 despite cellular yields increasing by over 470 fg/cell in total (Table 4.12). FAME as a percentage of the total lipid halved overall (specifically in relation to DHA). Although DHA, as a percentage of fatty acid content, remained at a similar proportion (13.47 – 13.82 %). Despite the reduced lipid content, there was a minor increase (~7 %) in relative levels of PUFAs and a small reduction in SAT and MUFA content (5 and 2 % of fatty acid, respectively). This increase in PUFA was due to the presence of the n-6 fatty acid LIN (accounting for 12 % of the fatty acids), which was previously undetected.

		Volumetric yield (mg/L)		Cellular yield (fg/cell)		% DW		% AFDW		% Fatty Acid		% Total Lipid	
		Mean	*S.E.*	Mean	*S.E.*	Mean	*S.E.*	Mean	*S.E.*	Mean	*S.E.*	Mean	*S.E.*
LAU	(12:0)	-	-	-	-	-	-	-	-	-	-	-	-
MYR	(14:0)	9.23	*1.27*	167.88	*23.14*	0.80	*0.11*	1.07	*0.15*	15.81	*0.64*	12.04	*1.66*
PAL	(16:0)	9.69	*1.63*	176.25	*29.64*	0.84	*0.14*	1.13	*0.19*	16.51	*0.16*	12.64	*2.13*
PML	(16:1)	6.05	*1.05*	110.05	*19.03*	0.53	*0.09*	0.70	*0.12*	10.30	*0.05*	7.89	*1.37*
STE	(18:0)	-	-	-	-	-	-	-	-	-	-	-	-
OLE	(18:1 n-9)	8.02	*1.45*	145.85	*26.29*	0.70	*0.13*	0.93	*0.17*	13.65	*0.04*	10.46	*1.89*
LIN	(18:2 n-6)	-	-	-	-	-	-	-	-	-	-	-	-
LON	(18:3 n-3)	3.68	*0.65*	66.92	*11.90*	0.32	*0.06*	0.43	*0.08*	6.26	*0.00*	4.80	*0.85*
OTA	(18:4 n-3)	13.92	*2.57*	253.05	*46.76*	1.21	*0.22*	1.62	*0.30*	23.63	*0.18*	18.15	*3.35*
EDA	(20:4 n-3)	-	-	-	-	-	-	-	-	-	-	-	-
ARA	(20:4 n-6)	-	-	-	-	-	-	-	-	-	-	-	-
EPA	(20:5 n-3)	-	-	-	-	-	-	-	-	-	-	-	-
DHA	(22:6 n-3)	8.22	*1.81*	149.49	*32.92*	0.71	*0.16*	0.96	*0.21*	13.87	*0.62*	10.72	*2.36*
TOTAL		**58.82**		**1069.48**		5.11		6.84		**100**		**76.72**	
SAT	(C:0)	**18.93**		**344.13**		1.65		2.20		**32.32**		**24.69**	
MUFA	(C:1)	**14.07**		**255.90**		1.22		1.64		**23.93**		**18.36**	
PUFA	(C:2>)	**25.82**		**469.46**		2.25		3.00		**43.75**		**33.68**	
RATIO	(n-6 : n-3)	**0.00**		**0.00**		0.00		0.00		**0.00**		**0.00**	

Table 4.10: FAME profile of *I. galbana* grown in a tubular photobioreactor prior to media renewal (n = 3 ± S.E.) harvested after 16 days growth under continuous irradiance (107 µmol/m^2/s) in 32 ‰ sf/2 media (Figure 4.15). Results derived from a total lipid harvest of 23 mg (77 mg/L; 1.39 pg/cell; 6.70 % DW). Refer to Table 2.1 for full names of each fatty acid. Refer also to Appendix D for a statistical summary of results.

		Volumetric yield (mg/L)		Cellular yield (fg/cell)		% DW		% AFDW		% Fatty Acid		% Total Lipid	
		Mean	*S.E.*	Mean	*S.E.*	Mean	*S.E.*	Mean	*S.E.*	Mean	*S.E.*	Mean	*S.E.*
LAU	(12:0)	0.27	*0.02*	17.70	*1.19*	0.03	*0.00*	0.04	*0.00*	1.15	*0.01*	0.42	*0.03*
MYR	(14:0)	2.93	*0.16*	193.39	*10.46*	0.30	*0.02*	0.40	*0.02*	12.53	*0.27*	4.62	*0.25*
PAL	(16:0)	2.73	*0.19*	180.26	*12.58*	0.28	*0.02*	0.37	*0.03*	11.66	*0.06*	4.31	*0.30*
PML	(16:1)	1.81	*0.10*	119.85	*6.57*	0.18	*0.01*	0.24	*0.01*	7.76	*0.16*	2.86	*0.16*
STE	(18:0)	0.39	*0.04*	25.88	*2.67*	0.04	*0.00*	0.05	*0.01*	1.67	*0.05*	0.62	*0.06*
OLE	(18:1 n-9)	3.30	*0.26*	217.90	*17.19*	0.33	*0.03*	0.45	*0.04*	14.09	*0.05*	5.21	*0.41*
LIN	(18:2 n-6)	2.98	*0.20*	196.91	*13.06*	0.30	*0.02*	0.40	*0.03*	12.74	*0.11*	4.71	*0.31*
LON	(18:3 n-3)	2.51	*0.16*	165.79	*10.35*	0.25	*0.02*	0.34	*0.02*	10.73	*0.14*	3.96	*0.25*
OTA	(18:4 n-3)	3.24	*0.19*	213.79	*12.27*	0.33	*0.02*	0.44	*0.03*	13.85	*0.25*	5.11	*0.29*
EDA	(20:4 n-3)	-	-	-	-	-	-	-	-	-	-	-	-
ARA	(20:4 n-6)	-	-	-	-	-	-	-	-	-	-	-	-
EPA	(20:5 n-3)	-	-	-	-	-	-	-	-	-	-	-	-
DHA	(22:6 n-3)	3.25	*0.45*	214.70	*29.93*	0.33	*0.05*	0.44	*0.06*	13.82	*0.90*	5.13	*0.72*
TOTAL		**23.40**		**1546.17**		**2.36**		**3.16**		**100**		**36.95**	
SAT	**(C:0)**	**6.31**		**417.23**		**0.64**		**0.85**		**27.01**		**9.97**	
MUFA	**(C:1)**	**5.11**		**337.75**		**0.52**		**0.69**		**21.85**		**8.07**	
PUFA	**(C:2>)**	**11.97**		**791.19**		**1.21**		**1.62**		**51.14**		**18.91**	
RATIO	**(n-6 : n-3)**	**0.33**		**0.33**		**0.33**		**0.33**		**0.33**		**0.33**	

Table 4.11: FAME profile of *I. galbana* grown in a tubular photobioreactor after receiving 4:20Hr cycle of 10 % media renewal (n = 3 ± S.E.) harvested after 66 days growth under continuous irradiance (107 µmol/m^2/s) in 32 ‰ sf/2 media (Figure 4.15). Results derived from a total lipid harvest of 19 mg (63 mg/L; 4.18 pg/cell; 6.29 % DW). Refer to Table 2.1 for full names of each fatty acid. Refer also to Appendix D for a statistical summary of results.

		+/- change in FAME profile					
		mg/L	fg/cell	% DW	% AFDW	% FA	%TL
LAU	(12:0)	+0.27	+17.70	+0.03	+0.04	+1.15	+0.42
MYR	(14:0)	-6.30	+25.51	-0.51	-0.68	-3.28	-7.42
PAL	(16:0)	-6.96	+4.01	-0.57	-0.76	-4.85	-8.33
PML	(16:1)	-4.24	+9.80	-0.34	-0.46	-2.54	-5.03
STE	(18:0)	+0.39	+25.88	+0.04	+0.05	+1.67	+0.62
OLE	(18:1 n-9)	-4.72	+72.05	-0.36	-0.49	+0.44	-5.25
LIN	(18:2 n-6)	+2.98	+196.91	+0.30	+0.40	+12.74	+4.71
LON	(18:3 n-3)	-1.17	+98.87	-0.07	-0.09	+4.47	-0.84
OTA	(18:4 n-3)	-10.68	-39.26	-0.88	-1.18	-9.78	-13.04
EDA	(20:4 n-3)	-	-	-	-	-	-
ARA	(20:4 n-6)	-	-	-	-	-	-
EPA	(20:5 n-3)	-	-	-	-	-	-
DHA	(22:6 n-3)	-4.97	+65.27	-0.39	-0.52	-0.05	-5.59
TOTAL		**-35.42**	**+476.69**	**-2.75**	**-3.68**	**0.00**	**-39.77**
SAT	(C:0)	-12.62	+73.10	-1.01	-1.35	-5.31	-14.72
MUFA	(C:1)	-8.96	+81.85	-0.71	-0.95	-2.08	-10.29
PUFA	(C:2>)	-13.85	+321.73	-1.04	-1.38	+7.39	-14.77
RATIO	(n-6 : n-3)	+0.33	+0.33	+0.03	+0.33	+0.33	+0.33

Table 4.12: Comparative changes in FAME profile of *I. galbana* during growth in a tubular photobioreactor (n = 3 ± S.E.). Differences in FAME profiles over a period of 50 days, between Tables 4.10 (during linear growth phase) and 4.11 (during second fed-batch strategy). Refer to Table 2.1 for full names of each fatty acid. Refer also to Appendix D for a statistical summary of results.

4.3: DISCUSSION

4.3.1: Growth performance

In comparison to *N. oculata* (discussed in Chapter 5), the overall growth performance of *I. galbana* was often variable with substantial differences in cell number/ size between identical culture conditions. This proved to be a central feature of the cultivation of this particular species throughout the study and has been observed by others (N.Clarkson, pers. comm.). Colouration of this alga was also varied, ranging from brown to a dark-green colour. This was perhaps most apparent between triplicates (i.e. all from the same seed flask) used in the media renewal experiment, in which growth rates and maximum cell densities varied by as much as 10 $\times 10^6$ cells/ml between flasks, despite growth conditions being identical for all upto day 17. Further comparison of maximum growth rate under identical 'standard conditions' (32 ‰ sf/2 (containing 7.12 mM $NaNO_3$) at 80 $\mu mol/m^2/s$ irradiance and 23 °C) between flask experiments ranged from 0.71 – 3.08 μ/day. Yet despite this variability, averaged maximum cell densities under these 'standard conditions' were relatively consistent (44 ± 3 $\times 10^6$ cells/ml) between experiments, despite the inconsistency in growth rates. Maximum cell densities reported by other authors are typically lower at <4 (Parrish *et al.*, 1998; Renaud *et al.*, 1995), 21 (Fabregas *et al.*, 1985) and 23 $\times 10^6$ cells/ml (Fidalgo *et al.*, 1998). Kaplan *et al.* (1986) did report a cell density of 50 $\times 10^6$ cells/ml from outdoor paddlewheel cultures, but fails to report detailed growth conditions (other than a maximum irradiance of 2500 $\mu mol/m^2/s$ and overnight temperatures of 18 – 19 °C). Although the effect of irradiance was not thoroughly investigated in this study (data not shown due to poor thermoregulation during 'high-light' experiments), provisional findings revealed that a lower growth temperature (20 °C compared to 25 °C and indeed the control of 23 °C) did increase cell density (60 $\times 10^6$ cells/ml) and growth rate (1.81 μ/day). In comparison, Molina Grima *et al.* (1992) reported achieving a maximum growth rate for *I. galbana* (0.77 μ/day) at 20 °C. The use of sf/2 media was found to be superior to f/2 towards increasing cell density probably due to the significantly higher concentration of $NaNO_3$. Indeed, additional increases of $NaNO_3$ in sf/2 (upto 10.68 mM in this study) obtained the highest cell density observed overall (70 $\times 10^6$ cells/ml). However it should be noted that, Fabregas *et al.* (1985) found concentrations of $NaNO_3$ >16 mM to be inhibitory to *I. galbana*. A lower salinity of 16 ‰ seemed preferable towards higher cell densities, although this was not a significant result. This is consistent with findings of Fabregas *et al.* (1985) and Kaplan *et al.* (1986). Conversely, there is also evidence (Liu and Lin, 2001) to suggest that higher salinities can be used to yield more PUFA (namely n-3).

Compared with flask data, the batch culture grown in the photobioreactor (Section 4.2.1) achieved a higher cell density (53×10^6 cells/ml) with similarities in inoculation density ($< 3 \times 10^6$ cells/ml), media (32 ‰ sf/2) and temperature. This may be attributed to a marginally higher I_o (c.f. 80 and 107 $\mu mol/m^2/s$, respectively) and the addition of 10 % (v/v) CO_2 used primarily to regulate pH. Early experiments (data not shown) revealed growth rate was optimal at pH 8, a result supported by Molina Grima *et al.* (1994c), which may have aided photosynthetic efficiency (in relation to enzyme activation). Subsequent runs in the photobioreactor (Sections 4.2.2 and 4.2.3) provided further increases in linear growth rates (5.13 – 7.10 μ/day) ahead of any media replenishment when compared to the batch run (1.20 μ/day). The mean maximum cell density, again prior to adopting any form of media renewal (i.e. under identical growth conditions), was $58 \pm 8 \times 10^6$ cells/ml between the three photobioreactor runs. This was typically 14×10^6 cells/ml higher than achieved in flask cultures (discussed above).

The batch culture (Section 4.2.1) was viewed as a base model in determining the maximum achievable cell density in the photobioreactor. Media renewal, in the case of the continuous culture (Section 4.2.2), was therefore initiated upon reaching this target. However, having re-examined residual nitrate data from both batch and continuous runs in the photobioreactor, the following evidence suggested that nitrates were not the primary growth-limiting nutrients. Firstly, during the batch run growth had persisted, and at a higher rate, after media nitrates became depleted possibly suggesting an inhibitory affect (contrary to previous results, see Section 4.1.3). Furthermore, prior to any media renewal in the continuous culture, a similar cell density was achieved within a shorter period of time (despite similar inoculum densities and growth conditions) and whilst residual nitrate levels were approximately four-times greater than the previous batch run. As a result of which, it was decided to investigate residual phosphate levels during the third run (fed-batch) in the photobioreactor. The comparison revealed that residual phosphate levels declined faster than nitrates. Between days 17 and 19 when phosphate levels remained constant, linear growth rate had dropped, suggesting the onset of stationary phase growth, which acted as the decisive factor towards beginning media renewal in this instance.

Mean cell size was generally found to increase for the first few days after inoculation, with the exception of the semi-continuous renewal experiment (Section 4.15), which also had the largest mean cell size (5.70 μm), compared to an average inoculum cell size of 4.60 μm used for other experiments (including photobioreactor cultures). Parrish *et al.* (1998) found nitrate-limited continuous cultures of T-iso (Tahitian strain of *I. galbana*) to be larger (4.30 μm) with a slower growth rate (0.15 μ/day) compared to cells maintained in nitrate-replete conditions (4.00 μm, growth rate 0.60 μ/day). This may suggest that the inoculum used in this instance was in late stationary/ early death phase (i.e. severely nitrate limited). Mean cell size was found to be larger during periods of media renewal under continuous conditions, and consistently under fed-batch conditions (from photobioreactor data). This result was contrary to the observations of Otero, *et al.* (1997b) who reported a decrease in cell volume with increasing dilution rate.

During cultivation of *I. galbana* in the photobioreactor, a notable mottling effect, generally referred to as 'biofouling', was seen within the inner surface of the photostage coils (see Plate 7). This phenomenon has been reported to happen with so-called 'Sticky' algal species such as *I. galbana* (Borowitzka, 1999; 1994). Although authors such as Bott (2002) and Youngblood *et al.* (2003) has examined methods of preventing or removing biofilms from glass and polymer surfaces, respectively, the mechanism of cellular adhesion in microalgae is still largely unknown (Callow and Callow, 2002).

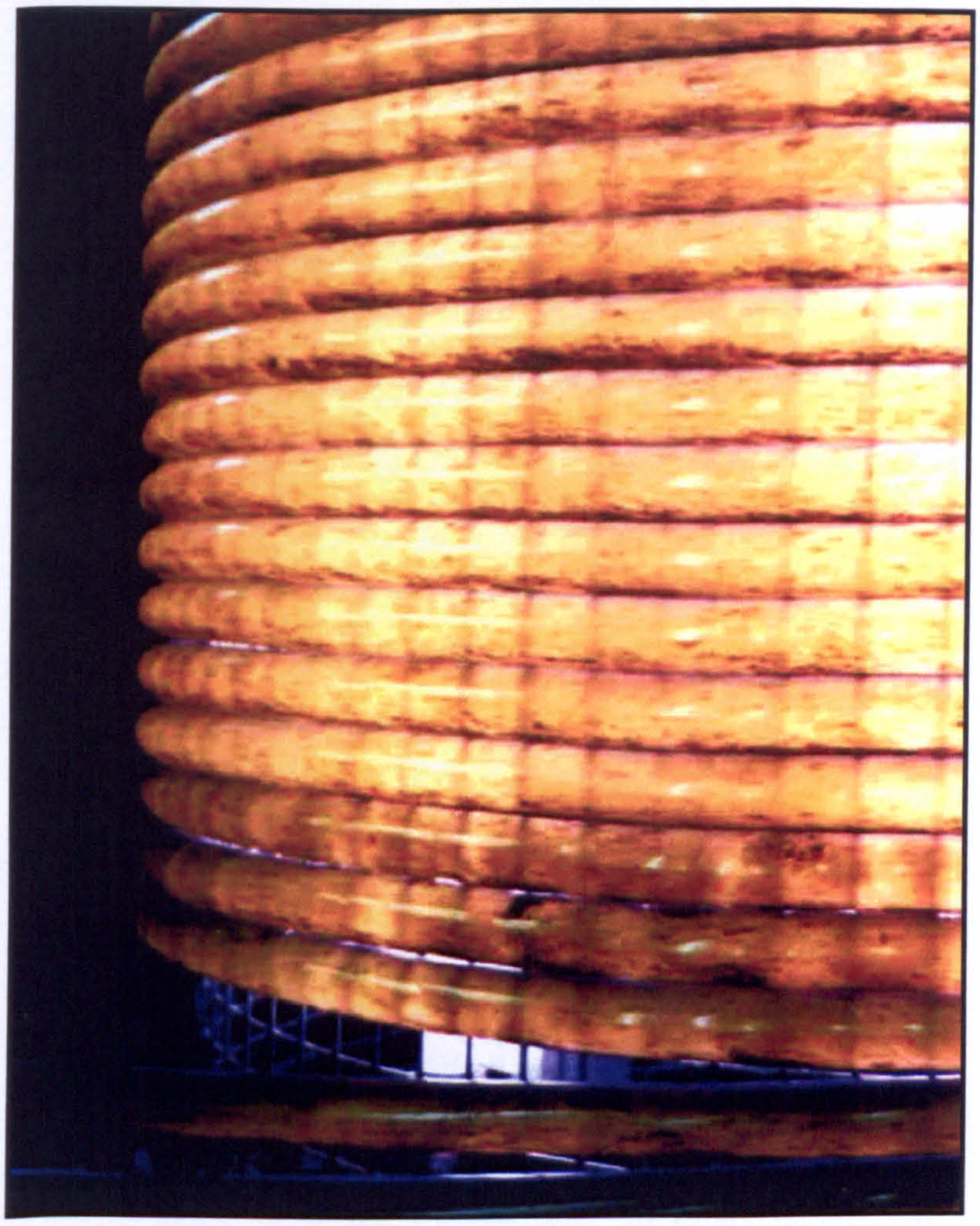

Plate 7: Biofouling of the photostage by *I. galbana*. An adhesive substance produced by this alga results in biofilm becoming visible (mottled effect) on the inner surface of the coil windings.

4.3.2: Media renewal methods

Three different media renewal methods were examined (as detailed in Section 1.8). For the purposes of comparison, a semi-continuous regime was tested during preliminary flask experiments in order to gauge general culture stability within a set range of media renewal rates. However, semi-continuous media renewal of the photobioreactor would be a highly labour intensive process and would defeat the objective of such a system, potentially compromising sterility. Consequently, the photobioreactor was operated to compare continuous and fed-batch methods, having used the semi-continuous results as a model to focus upon a narrower range of renewal rates (10 – 20 %). A full summary can be found in Chapter 7, Tables 7.1 and 7.2.

The results of 30 and 40 % semi-continuous renewal in this study (summarised in Chapter 7; Table 7.1) produced approximately 3 and 1 × 10^8 cells/L/day, respectively. By comparison Otero, *et al.* (1997b) reports a higher cellular productivity in *I. galbana*, during 30 – 40 % semi-continuous media renewal, of 11 × 10^9 cells/L/day. However, productivity of the semi-continuous renewal method within this study was highest at a daily rate of 20 %, resulting in 3 × 10^8 cells/L/day.

The continuous culture of *I. galbana* was productive (i.e. producing harvested biomass) for 90 days (71 % of the total run time), at a 10 % daily media renewal rate giving a harvest volume of 7 L/day (summarised in Chapter 7; Table 7.2). For the first 38 days of media renewal, cell density remained above 45 × 10^6 cells/ml, but nitrate uptake was apparently slower than renewal rate leading to inhibitory levels of residual nitrates. Another alternative is that renewal rate was insufficient to supply enough phosphates (not monitored during this run) to sustain cell density, but were later found to have a higher uptake rate than nitrates (refer to Section 4.3.1; paragraph three). Overall, the total harvest volume was 630 L, which consisted of 25 × 10^{12} cells with a total DW and AFDW of 865 and 652 g, respectively. During the 90 days the photobioreactor was harvestable it typically had a mean cellular and biomass yield of 4 × 10^9 cells/L/day and 137 mg/L/day DW (75 % AFDW), respectively. The daily cellular productivity of the continuous media renewal method in the photobioreactor was a vast improvement upon results from the semi-continuous method employed in the previous flask experiment. Although this remained inferior in comparison to the work of Otero, *et al.* (1997b), who achieved 13 × 10^9 cells/L/day during continuous cultivation of *I. galbana*.

During fed-batch operation, the photobioreactor was 'productive' (harvested), using two different media renewal strategies, for 43 days (65 % of it's operational time) at media renewal rates of between 10 and 20 % (v/v/day). During which the average daily harvest was 8 L. Despite a persistent loss in cell number, a total harvest volume of 343 L was obtained which comprised of 12×10^{12} cells, equating to a DW and AFDW of 332 and 277g, respectively. Ultimately, this resulted in a mean productivity of 4×10^{9} cells/L/day or 111 mg/L/day DW (83 % AFDW) during an average daily harvest over a period of 66 days. Again, cellular productivity was superior compared to the semi-continuous data obtained from flask experiments (c.f. $1 - 2 \times 10^{8}$ cells/L/day at 20 and 10 % media renewal, respectively).

4.3.3: Oxygen evolution

Very little P-I curve data for *Isochrysis* was found within the literature reviewed under this study. Furthermore, in comparison of results one must be mindful of differences in the two main analytical methods used within this field to measure photosynthetic rates (which can be standardised to either a cellular or chlorophyll basis): A fluorescence P-I curve, refers to data obtained using a pulse-amplitude modulation (PAM) method which specifically measures electron flow from PS II (further described by Krause and Weis, 1991). Whereas an oxygen P-I curve (used herein) measures the concentration of gas exchange using a dissolved oxygen electrode. This method produces a lower signal compared to PS II fluorescence (Gilbert *et al.*, 2000) but requires higher chlorophyll concentrations for accuracy, which may be a potential source of experimental error when analysing dilute cultures. Second, there are discrepancies within the literature on how the P-I curve parameters can be taken from a basic curve fit, according to Walker (1988). Several mathematical fits (based on empirical equations or dynamic models) have been used within the literature, as detailed by Henley (1993), making comparison between authors difficult (Gilbert *et al.*, 2000). Different models applied to the same data can therefore yield different parameter values. This may cause inconsistencies in terms of true values. Nonetheless, the patterns and significance of each parameter of the P-I curve remain true to physiological response of the cell, reflecting changes in photosynthetic metabolism. Given differences in methodologies (both in recording and in analysis), parameter *values* will only be *compared where methodology* of the author *closely matches* that of this study. Data on oxygen evolution by authors adopting *different methods* will not be ignored, but will instead only be *reviewed in context of the relationships* observed between P-I curve parameters.

For example, it is known that the photosynthetic rate cannot continually increase proportionally to irradiance. Whilst lower irradiances ($<I_k$) do show a linear relationship with photosynthetic rates, this is because photon absorption is slower than rate of electron transport (Z scheme) from water to CO_2 (Nakajima and Ueda, 1997). This is often referred to as the 'target theory' (Sakshaug *et al.*, 1997). Once irradiance exceeds this capacity (culture becomes light saturated), photosynthetic rate decreases due to exciton spill-over, because carbon fixation (from RuBP) is the rate limiting step. When un-quenched, this excess energy leads to cellular damage by a process of photo-oxidation (Qiang and Richmond, 1994) generally referred to as photo-inhibition. Consequently irradiances above I_k result in pigments becoming increasingly unproductive (serving a non-photochemical, thermal dissipation role instead (Henley, 1993)). Whereas irradiances below I_k may indicate efficient use of photochemical reactions. Therefore I_k could be used to indicate the photoadaptive state of the culture (Sakshaug *et al.*, 1997). Herzig and Dubinsky (1992) and later Geel *et al.* (1997) all maintaining cultures of *I. galbana* under low-light (continuous irradiance, at 100 $\mu mol/m^2/s$) conditions and obtained an I_k of 215 and 200 $\mu mol/m^2/s$ during linear growth phase, respectively. The results of this study (Table 4.2) would seem to indicate a similar photoadaptive state. However, neither Herzig and Dubinsky (1992) nor Geel *et al.* (1997) state cell density or age of the culture sampled, other than to say samples were taken when chlorophyll *a* levels were constant for three days during linear growth. The P-I curve data herein suggests cultures gradually became light-limited since I_k dropped by 80 % as cell density doubled. This could be attributed to both an increase in R_d and P_{max} (Sakshaug *et al.*, 1997). Cellular α also decreased and net P_{max} fell at a rate of 0.40 nmol O_2/ 10^6 cell/ day between days seven and fourteen. Net cellular P_{max} was substantially higher here than that of Herzig and Dubinsky (1992) (0.92 nmol O_2/ 10^6 cell), but this can be explained by differences in R_d (0.18 nmol O_2/ 10^6, compared to -4.02 and -1.96 nmol O_2/ 10^6 cell here). R_d is known to increases with growth rate, as cells pay the metabolic price of accelerated growth, which is typically 20 – 30 % of photosynthesis (Herzig and Dubinsky, 1992). However, the negative R_d values from the results shown would indicate oxygen uptake in the absence of light (typical of photorespiration in the Calvin cycle), yet these cultures were continuously illuminated. Gilbert *et al.* (2000) suggests that oxygen uptake during linear growth phase can also be attributed to increased mitochondrial activity, termed the 'enhanced post-illumination response', in PSII when cultures are light saturated (dilute). Indeed, as cell density increased R_d was also found to increase on day fourteen, which would be indicative of this phenomenon.

4.3.4: Total lipid and FAME profiles

Total lipid extracts from flask cultures of *I. galbana* of ~20 mg (Section 4.1.7) were marginally higher than that achieved by Liu and Lin (2001), with accumulation greatest in f/2 cultures. Most significantly at 16 ‰ (58 mg), yet despite this the total fatty acid content (i.e. lipid quality) only attributed to ~16 % of the total lipid. This result may be due to the presence of high levels of the steroid class of lipids (structurally devoid of a fatty acid component). Meanwhile, increasing salinity had no statistically significant affect towards volumetric MUFA or PUFA levels (with the exception of DHA), however SATs did show a positive correlation ($p = <0.05$). The PUFA fraction of FAMEs (as % total lipid) was highest in sf/2 cultures (Table 4.3). No EPA was found within the FAME profiles of this alga, the absence of which has been used by previous authors to identify the Tahitian (T.iso) strain of *Isochrysis* (Section 1.5.1). However, the other main criteria often used to identify this particular strain is an optimum growth temperature of ~27.5 °C. Results herein show an optimum temperature closer to 20 °C, which contradicts it's 'typical' growth response (as with many authors, compared in Table 1.2). The dominant fatty acid (expressed as a percentage total fatty acids) reported for *Isochrysis* also varies between authors (although both culture conditions and age may contribute to such variability). These are listed in order of increasing chain length and unsaturation as follows: ≤32 % MYR (Renaud, 2002); ≤25 % PML (Fidalgo *et al.*, 1998); ≤34 % OLE (Liu and Lin, 2001); ≤26, ≤25 and 19 % OTA (Brown *et al.*, 1993 and Renaud *et al.*, 1995; 1999, respectively). The results of this study indicate OTA (18:4 n-3) to be the dominant fatty acid (upto 34 %, in 32 ‰ sf/2) during stationary growth phase, with the exception of 16 ‰ f/2 samples (PAL at 24 %). Livne and Sukenik (1992) also detected a high PAL content, specifically amongst the TAG portion of lipids, in association with OLE. Indeed, further comparison between FAME profiles (above) reveals the highest proportion of OLE (16 % of total fatty acids) was also from 16 ‰ f/2 samples. This could therefore be interpreted as evidence of TAG accumulation. DHA content from this study yielded between 14 - 21 % total fatty acids. This was comparatively higher than reported by both Renaud *et al.* (1995) and Fidalgo *et al.* (1998) who found DHA to make-up 11.4 and 8.3 % of the total fatty acid profile, respectively (both using <115 $\mu mol/m^2/s$ 12:12 L:D cycle; 20 and 18 °C; in 25 ‰ f/2 and 36 ‰ 'seawater' enriched with 4 mg/L $NaNO_3$). On a volumetric basis, the DHA content of *I. galbana* ranged from 4.6 – 10.7 mg/L. This was again higher than that reported by Otero *et al.* (1997a,b) or Liu and Lin (2001) (4.3, 1.2 and 4.6 mg/L, respectively) for *Isochrysis*.

The total lipid content of *I. galbana* grown in the photobioreactor (Table 4.10) was comparatively less than that extracted from flask cultures under similar conditions (Table 4.3), accounting for 6.3 and 6.7 % of DW before and after fed-batch production, respectively. This was substantially less than reported by other authors (Renaud, 2002 = 21%; Perez, 1994 = 21 %), and overall the total lipid content was reduced by 18 % during fed-batch media renewal, but on a cellular level had tripled. Additionally, total volumetric FAME had more than halved, yet higher for an average cell during media renewal, aided by the addition of LAU, STE and LIN. Despite which, the proportion of PUFAs had risen 7 % at the expense of SATs and MUFAs, although DHA remained 14 % of the fatty acids. This fed-batch photobioreactor culture of *I. galbana* yielded 15 % more DHA than originally projected from earlier flask experiments for the photobioreactor (Table 7.1). Analysis of *I. galbana*'s FAME profile towards the end of fed-batch growth revealed that total cellular FAME accumulation had increased by 477 fg/cell, predominantly in the form of PUFAs (67 %), when compared with samples taken during linear growth phase (Table 4.12). However, the reduction in cell density yielded a net volumetric loss (total FAME) of 35 mg/L over 40 days. This combination of reduced cell density and increased cellular proportions of polar (unsaturated) fatty acids, is a trend noted by Otero, *et al.* (1997a) as a means to sustain photosynthetic apparatus (in a photo-protective role) when conditions become photo-inhibitory (i.e. to compensate for loss of self-shading). It should be noted that specific lipid fractions (TAG, GL and PL - Section 1.4.2) were not analysed in this study. Nonetheless, the relevance of each class towards PUFA accumulation will be discussed below since differentiating their individual roles is vital to maximising gross productivity.

Total lipid accumulation in *Isochrysis* is generally reported to be inversely proportional to growth rate (Sanchez *et al.*, 2000; Molina Grima *et al.*, 1992) and increases with culture age, with older cells capable of synthesising threefold lipid more than young cells (Molina Grima *et al.*, 1994c). Given that the structural composition of carbohydrates and lipid do not require nitrogen (N), this would suggest carbon flow during N-limiting conditions is diverted away from protein synthesis (which is highest during linear growth phase) (Valenzuela-Espinoza *et al.*, 2002; Livne and Sukenik, 1992). This is supported by the earlier flask culture results of Kaplan *et al.* (1986) who had found N-limited conditions increased total lipid from 24 to 47 % of AFDW in this alga. However, examination of lipid sub-classes by Zhu *et al.* (1997b) would later show that PL decreases while GL levels remain unchanged with culture age. Therefore any total lipid accumulated during stationary growth phase can be specifically

attributed to the TAG fraction (as confirmed by Fidalgo *et al.*, 1998). Indeed, this trend was quantified by Brown and co-workers (1996; 1993) who examined specific lipid fractions to find only trace amounts of TAG during linear growth phase, rising to more than 20 % of the total lipid during stationary phase. Livne and Sukenik (1992) suggest that PUFA synthesis (i.e. overall total lipid quality) is also stimulated during stationary phase in response to nitrogen starvation. A view shared by many authors (Valenzuela-Espinoza *et al.*, 2002; Parrish *et al.*, 1998; Zhu *et al.*, 1997b; Molina Grima *et al.*, 1994c; Brown *et al.*, 1993) is that the majority of total lipid is derived of TAG during stationary growth phase and ultimately the primary source of PUFAs, as cells become starved of nitrogen. As previously highlighted, the major difference between f/2 and sf/2 was the $NaNO_3$ concentration (0.88 and 7.1 mM, respectively), which was positively correlated to increasing cell density (i.e. nitrate concentration of the media is growth limiting). This may explain the higher total lipid content from f/2 cultures, because cells entered stationary growth phase earlier consequently allowing a longer period of time to accumulate TAG. Yet this is contrary to the behaviour of PUFA yields, which were higher in the sf/2 cultures, but is consistent with the work of Molina Grima *et al.* (1992) who found increasing $NaNO_3$ concentrations (by 4 mM) increased PUFA content. Therefore PUFA accumulation may well be attributed to other lipid fractions during nutrient-replete conditions, contrary to the requirement of TAGs.

GL is known to associate with pigment-protein complexes within thylakoid membranes, positively relating to their photosynthetic activity (Zhu *et al.*, 1997b). Compared to the average irradiances used by other authors of >200 $\mu mol/m^2/s$, (Perez, 1994; Qiang and Richmond, 1994; Brown *et al.*, 1993) cultures used here-in could be comparatively classed as low-light adapted (< 150 $\mu mol/m^2/s$). That is to say, conditions reported by other authors to be photo-limited may prove photo-inhibitory if the same conditions applied to low-light adapted cells. Since the GL proportion of total lipid production is associated with pigment complexes, ultimately the photoadaptive state of cells will undoubtedly influence PUFA composition (Brown *et al.*, 1993). Furthermore, GL-PUFA content is reported to increase during cell growth as conditions become increasingly light-limited (Otero, *et al.* 1997b) due to self-shading. Meanwhile, Tzovenis *et al.* (1997) discovered higher cellular DHA levels from comparatively dilute cultures of *Isochrysis* (i.e. in conditions were average irradiance/ cell was higher). This might suggest that DHA has a protective role against photo-oxidation. Yet, high irradiances are known to reduce PSU size (including thylakoids) in *Isochrysis* (see Sections 1.9.2 and 4.3.3), and therefore the DHA response could not be a result of

accumulated within the GL fraction. Indeed, Otero, *et al.* (1997b) concludes that overall DHA (cellular or as % fatty acids) extracted from total lipid, unlike other PUFAs, is "*not clearly* associated with pigments" (i.e. the GL portion of total lipid). This was further supported by Tzovenis and co-workers (1997) who summarised DHA distribution amongst each lipid fraction to vary as follows: PL (30 – 56 %), TAG (26 – 58 %) and GL (12 – 18 %). In other words whilst DHA has been associated with GL (and consequently pigment content) in light-limiting conditions, this role is secondary (relatively unchanged) compared to DHA residing within the non-pigment associated lipid fractions (PL and TAG). The relationship between irradiance level and distribution of DHA may therefore be one of balance, providing photoprotection under both low-light (amongst GL) and high-light levels (amongst TAG), relative to photoadaptive state. The data of Tzovenis *et al.* (1997) also statistically shows that DHA (as % DW, % total FAME and cellular FAME) unlike other PUFAs was synthesised mainly during linear phase growth.

Given that DHA is not *primarily* associated with GL and that TAG is accumulated during stationary phase, the bulk of DHA accumulation during linear phase growth may therefore be attributed to products of active cell division, instead of playing a role in light harvesting. Under natural diurnal conditions Zhu *et al.* (1997a) showed that cell volume increased during the day (photophase), attributed to SAT (STE) and MUFA (OLE) accumulation in response to light intensity, prior to cell division overnight (scotophase), as reflected by increases in both protein and PUFA (both essential components of PL) (Tzovenis *et al.*, 2003). However, outdoor-grown cultures are also subject to drops in overnight temperature, and the results of Renaud *et al.* (1995) indicate that f/2 grown cultures accumulated more total lipid and PUFA (specifically DHA) when the temperature was lowered (to 20 °C). Zhu *et al.* (1997b) found no change in the overall quantity of PL (from cell membranes) at low temperatures from stationary phase cultures of *I. galbana* but examination of FAMEs showed a reduction of SAT, whilst the PUFA proportion (namely LON and DHA) of the PL had increased. Therefore PL quantity increases in relation to cell division, whilst PL quality (as defined by the proportion of PUFA, specifically DHA) is improved by reducing temperatures (within growth tolerance limits), below the growth optimum (Poisson and Ergan, 2001). Low temperatures are known to regulate the genetic expression of n-3 desaturation enzymes (Zhu *et al.*, 1997b), which in-turn increases the ratio of unsaturated to saturated fatty acids (Renaud *et al.*, 1995) within the PL, aiding membrane fluidity.

CHAPTER 5: *NANNOCHLOROPSIS OCULATA*

5.1: FLASK CULTURES OF *N. OCULATA*

5.1.1: Introduction

Preliminary studies were conducted using flask cultures (Section 2.1.1) to determine optimal growth conditions for *N. oculata*. Two growth media (namely, f/2 and sf/2) were compared at salinities of 16 ‰ and 32 ‰. In addition, the effects of temperature, phosphate concentration, dilution rates and irradiance were studied. Performance was assessed in terms of mean cell density and changes in mean cell size. Where possible algal lipid content and FAME profile were monitored (Section 2.3).

5.1.2: Media conditions

The performance of the alga, in terms of cell growth and mean cell size, was compared between a commonly used growth medium (f/2) and a modified version of this media (sf/2). Both media were prepared at salinities of 16 ‰ and 32 ‰ (half-strength and full strength seawater, respectively). All cultures were grown under continuous illumination at 80 ± 5 μmol/m^2/s and a temperature of 23 ± 2 °C.

Cultures showed little sign of lag phase (Figure 5.1), but did undergo fluctuations over the first few days of growth in terms of cell number. By day ten, cultures grown in f/2 at 32 ‰ began to enter a shallow linear phase (compared to the other cultures in this study), at a linear growth rate of 1.49 μ/day (prior to which growth was at 4.46 μ/day). All cultures grown in f/2 reached stationary phase around day 14, regardless of salinity. However, cultures maintained in sf/2 continued in their linear phases (7.16 and 7.07 μ/day for 16 and 32 ‰, respectively) until day 21. The highest cell density was achieved using sf/2 at 16 ‰ on day 21, at 199 ± 15.30 × 10^6 cell/ml. In contrast, cultures grown at 32 ‰ in f/2 remained at approximately 100 × 10^6 cell/ml from day 14 onwards. Overall, there were no statistically significant differences between media of the same salinity or type in terms of the final cell density achieved (Appendix D).

Overall, all cultures displayed a steady increase in their average cell size (from an initial cell size of 2.72 – 2.74 µm) during growth, despite fluctuations within the first two-three days after inoculation (Figure 5.2). Interestingly, both cultures grown at 16 ‰ decreased in their mean cell size whilst those at 32 ‰ increased in size on day one, before all cultures reached near identical cell size again on day two (~2.60 µm). After day 10 all cultures began to steadily increase in cell size. Cultures grown in 32 ‰ f/2 remained the largest throughout, reaching a maximum average cell size of 3.18 µm on day 35. Despite this there was no statistically significant difference between these cells and those grown in sf/2 and/ or at a lower salinity.

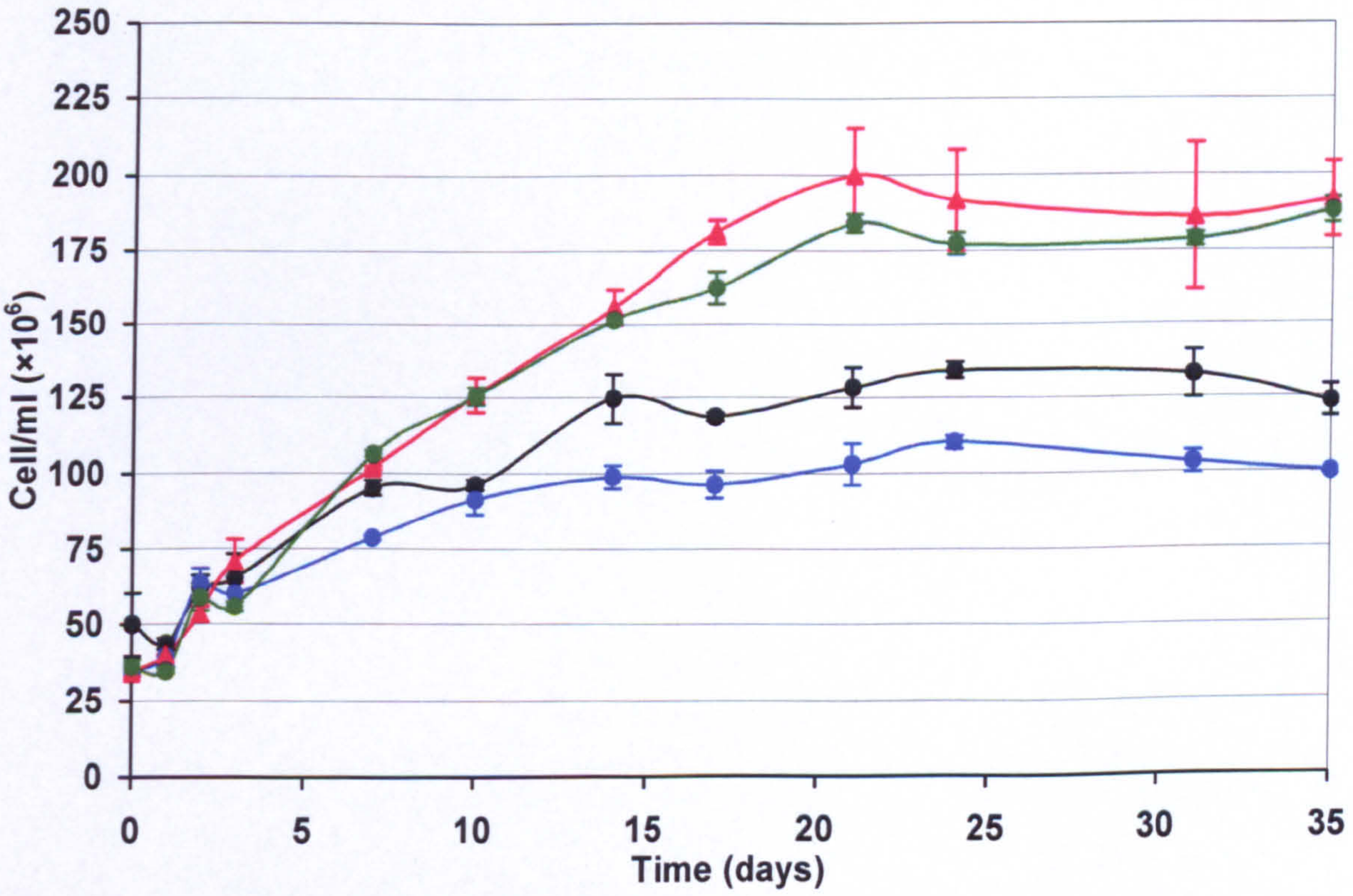

Figure 5.1: Mean cell density of *N. oculata* cultured on two separate media at two salinities (n = 3 ± S.E.). Flasks contained either f/2 at 16 ‰; f/2 at 32 ‰; sf/2 at 16 ‰; sf/2 at 32 ‰ (inoculum cell density at 50.11; 34.70; 34.39 and 36.47 × 10^6 cell/ml, respectively). Refer also to Appendix D for a statistical summary of results.

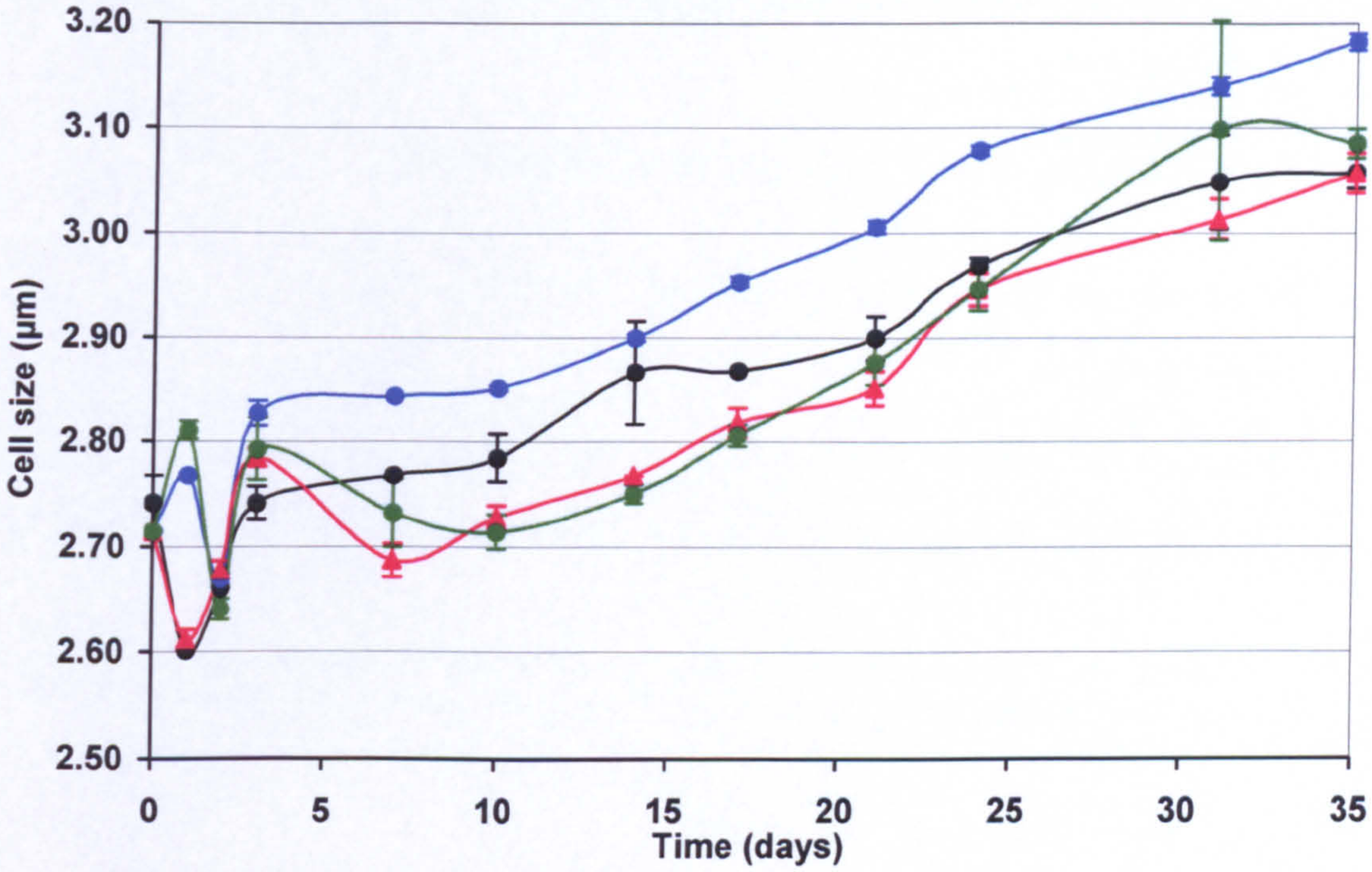

Figure 5.2: Mean cell size of *N. oculata* cultured on two separate media at two salinities (n = 3 ± S.E.). Flasks contained either f/2 at 16 ‰; f/2 at 32 ‰; sf/2 at 16 ‰; sf/2 at 32 ‰. Refer also to Appendix D for a statistical summary of results.

5.1.3: Phosphate limitation

The effects of nutrient limitation were examined in relation to the phosphate content of sf/2 media at 32 ‰. Standard sf/2 media (see Appendix B) was used to compare the effect of varying the levels sodium di-hydrogen phosphate ($NaH_2PO_4.H_2O$) at concentrations of 0.05; 0.10 (control standard); 0.14; 0.17 and 0.19 mM. All were formulated in full-strength artificial sea-salt water.

All cultures showed growth rates of 8.21, 9.42, 9.88, 8.72, 9.16 µ/day upto day seven at phosphate concentrations of 0.05, 0.10, 0.14, 0.17, and 0.19 mM, respectively. After this period, growth of cells at 0.05 mM phosphate began levelling off by day 17 to approximately 105 × 10^6 cell/ml (Figure 5.3). Cultures grown using 0.10 mM phosphate achieved a maximum density of around 140 × 10^6 cell/ml from day 14 onwards. Growth under higher levels of phosphate was improved. At 0.19 mM phosphate a cell density of 282 × 10^6 cell/ml was achieved. The only significant difference in cell density between cultures grown in sf/2 was between those inoculated in media containing 0.05 and 0.19 mM phosphate ($p = 0.0421$). In addition to which there was a significantly positive relationship between phosphate concentration and cell density ($p = <0.05$).

As in the previous study, the cell size of all the cultures was variable in the first few days following inoculation. After this cells grown at 0.10; 0.14; 0.17 and 0.19 mM phosphate displayed a near-identical trend in cell size, with no significant difference between them. Overall during the growth phase (days 7 – 17), mean cell size increased throughout the experiment to day 42, for all cultures. In contrast, cells maintained in sf/2 media at 0.05 mM phosphate displayed a different trend. The mean cell size of these cultures was already larger by day seven (2.95 μm) than those kept under other concentrations, and continued increasing until day 28 when it reached a maximum mean cell size of ~3.33 μm. There were significant differences found in mean cell sizes of cultures with regard to phosphate concentrations deviating from the standard level (0.10 mM) typically used in sf/2 ($p = 0.007 - 0.031$). After 42 days growth, the lowest mean cell size was (3.23 μm) at 0.17 mM, whilst the largest cell size reached (3.48 μm) was at 0.10 mM phosphate. Overall, a significantly negative correlation was found in relation to mean cell size and the phosphate concentration of sf/2 at 32 ‰ ($p = < 0.02$).

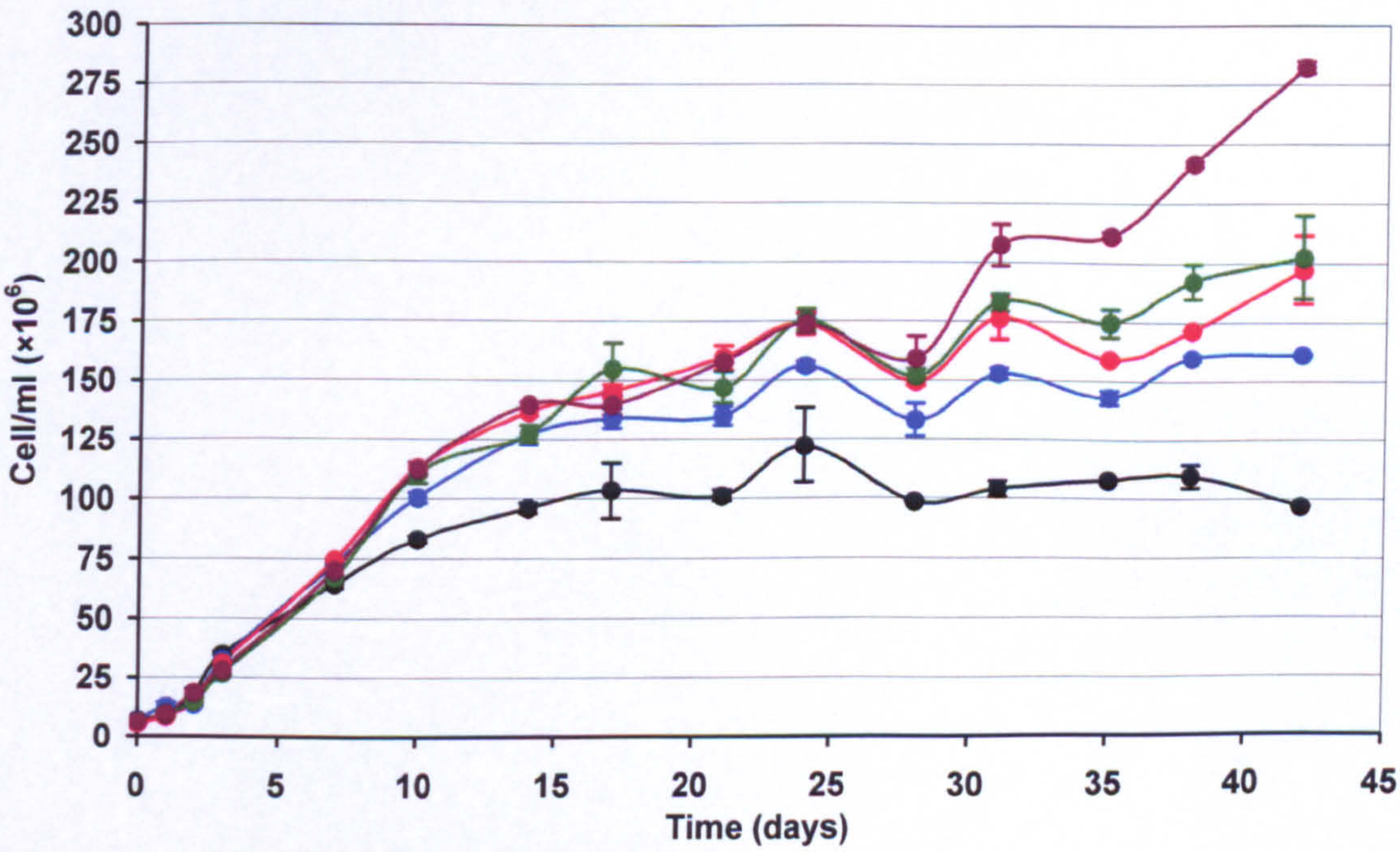

Figure 5.3: Mean cell density of *N. oculata* grown in a range of phosphate concentrations of sf/2 at 32 ‰ (n = 3 ± S.E.). Flasks contained sf/2 at either 0.05 mM; 0.10 mM; 0.14 mM; 0.17 mM or 0.19 mM phosphate concentration (inoculum cell density at 6.82; 6.86; 5.67; 6.26 and 6.44 × 10^6 cell/ml, respectively). Refer also to Appendix D for a statistical summary of results.

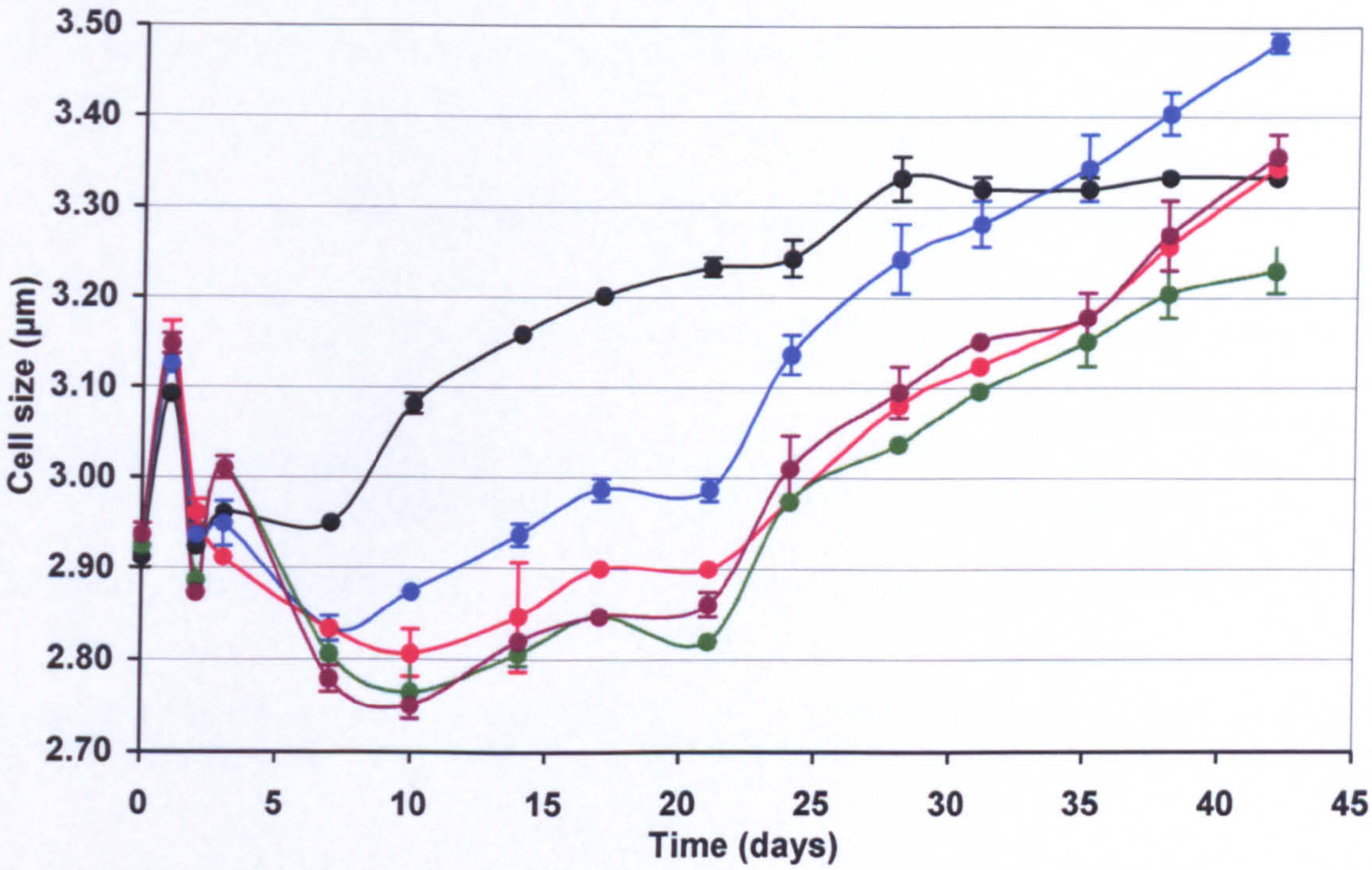

Figure 5.4: Mean cell size of *N. oculata* grown in a range of phosphate concentrations of sf/2 at 32 ‰ (n = 3 ± S.E.). Flasks contained sf/2 at either 0.05 mM; 0.10 mM; 0.14 mM; 0.17 mM or 0.19 mM phosphate concentration. Refer also to Appendix D for a statistical summary of results.

5.1.4: Temperature

The effect of temperature on the growth of *N. oculata* was examined at 15, 20, 25 and 30 °C. All cultures were seeded from and maintained in sf/2 media at a salinity of 32 ‰. Illumination (24 Hr) was provided by cool white fluorescent lights, giving an irradiance of 122 ± 15 μmol/m^2/s at the surface of the cultures.

Cultures of *N. oculata* were able to grow within a temperature range of 15 – 25 °C (Figure 5.5), with cells incubated at 30 °C rapidly becoming bleached and failing to grow. Surviving cultures showed only a one day lag-phase. Linear-phase growth rate was highest (14.19 μ/day) at 20 °C between days 1 - 7. Although cultures did not appear to enter a true stationary phase, growth rates fell sharply on days 7, 9 and 14 at 20 °C, 25 °C and 15 °C, respectively. At both 20 and 25 °C a maximum of 180 × 10^6 cell/ml was achieved on day 42. There was no significant difference between cell densities achieved at 20 °C and 25 °C. By far the most sustained growth was displayed at 15 °C, which achieved the highest cell density of all incubations, at 369 × 10^6 cell/ml, with a maximum growth rate of 8.18 μ/day. This cell density was approximately twice that of those obtained at 20 and 25 °C. Cultures incubated at 15 °C were pooled for total lipid extraction and analysis of FAME profile (Table 5.8). This will be discussed later within this Chapter (see Section 5.1.7).

Cultures, at all temperatures, displayed an increase in cell size of between 0.25 μm (20 °C) to 0.48 μm (30 °C) immediately following inoculation (Figure 5.6). Subsequently, cells grown at 20 °C showed a continuous increase in mean cell size from day 7 - 42 reaching an overall maximum of 3.50 μm. Cultures maintained at 15 °C displayed a similar trend of increase from day 14 at a slower rate, achieving a mean cell size of 3.11 μm by day 44. In contrast, a temperature of 25 °C promoted a stable cell size of 3.10 μm from day 16 onwards, whilst the highest temperature in this study (30 °C) resulted in the smallest overall cell size on day 42 (2.76 μm).

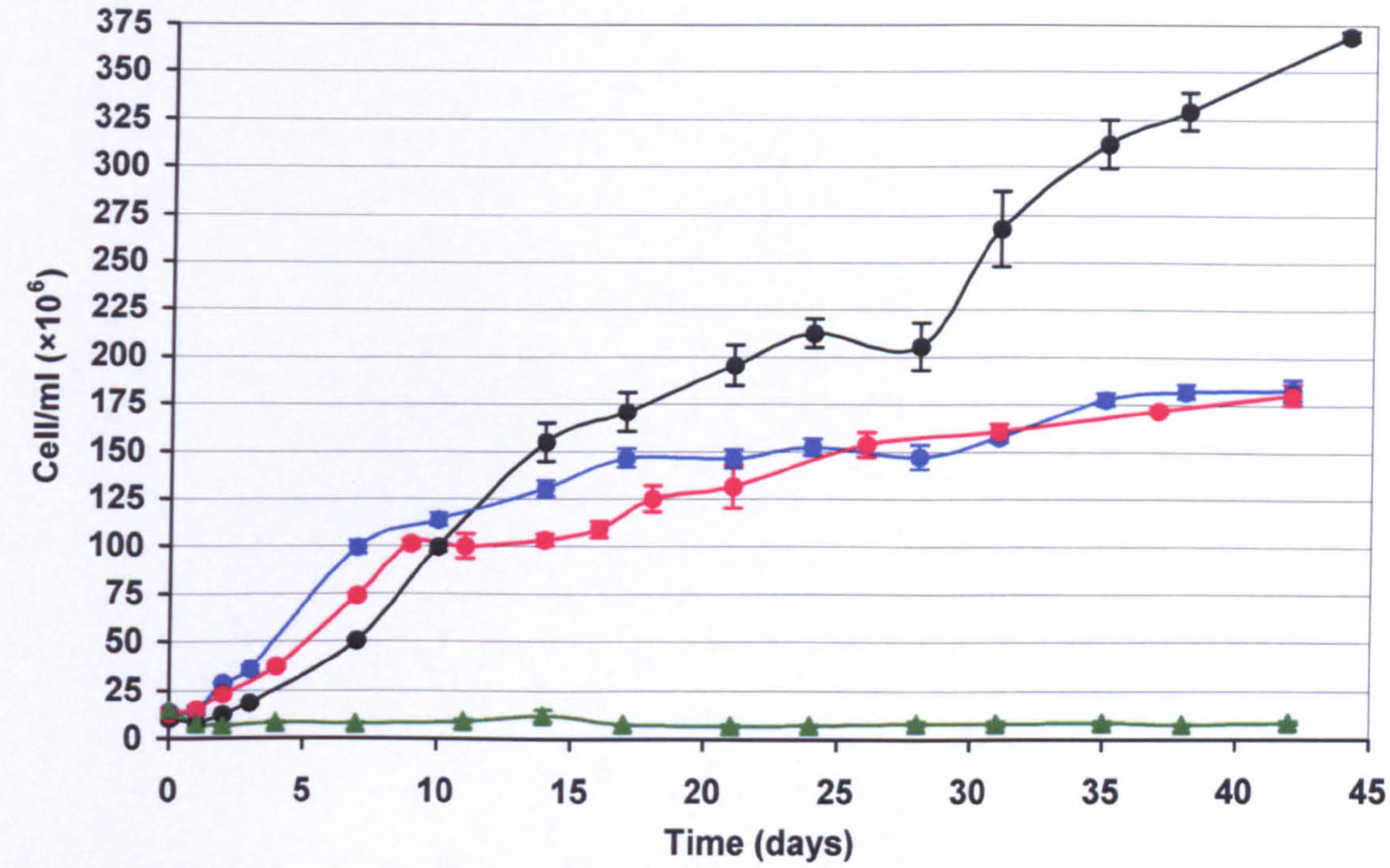

Figure 5.5: Mean cell density of *N. oculata* incubated at a range of growth temperatures (n = 3 ± S.E.). Flasks were incubated at 15 °C; 20 °C; 25 °C and 30 °C (inoculum cell density at 10.16; 14.97; 13.03 and 14.96 × 10^6 cell/ml, respectively). Refer also to Appendix D for a statistical summary of results.

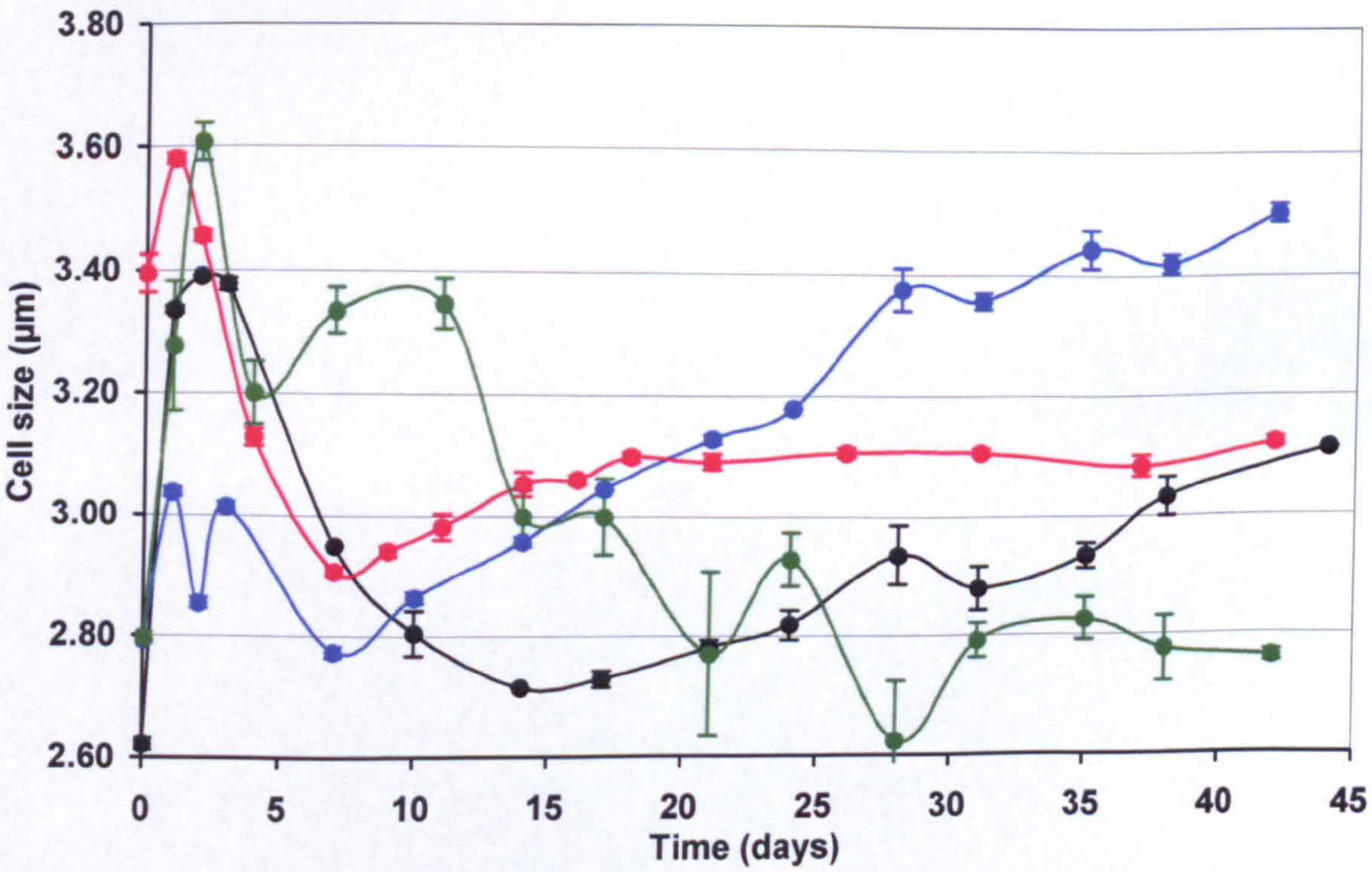

Figure 5.6: Mean cell size of *N. oculata* incubated at a range of growth temperatures (n = 3 ± S.E.). Flasks were incubated at 15 °C; 20 °C; 25 °C and 30 °C. Refer also to Appendix D for a statistical summary of results.

5.1.5: Semi-continuous culture of *N. oculata*

The effect of media renewal with fresh medium, typical of fed-batch and/ or continuous cultures, was examined using shake flask cultures (100 ml) as a model. Cell density was monitored throughout and media dilution began only once cultures were judged to have started to enter stationary phase. Flasks received 10; 20; 30 or 40 % media renewal (v/v/day semi-continuous dilution- refer to Section 1.9.3) with freshly sterilised media (32 ‰ sf/2) using aseptic technique within a laminar flow cabinet. All flasks received the same fresh media from a single stock to avoid any discrepancies in the composition of micro-nutrients given to each flask. All flasks were continuously mixed and maintained at 23 ± 2 °C, with an average irradiance of 80 μmol/m^2/s.

All cultures were initially maintained in batch growth under identical conditions up until day 17. They displayed near-identical growth patterns (Figure 5.7) and although growth rate varied from 13.75 to 16.38 μ/day (media renewal rates of 40 and 30 % being the lowest and highest, respectively), there was no significant difference between them in terms of mean cell density. Dilutions (media renewal of media) began directly after sampling on day 17 and immediately revealed signs of reduced growth rates (all subsequent sampling was done directly prior to media renewal). Differences in growth between renewal rates became immediately apparent within four days of media replenishment, with a 9; 37; 57 and 74 % decrease (or 'wash-out') in cell numbers for flasks receiving media renewal rates of 10; 20; 30 and 40 %, respectively. Although flasks receiving 40 % media renewal appeared to suffer the greatest loss overall, they were the first to apparently reach a quasi-steady state (approx. 16 - 20 × 10^6 cell/ml) by day 28. Cultures receiving 30 % renewal appeared to adjust more gradually to the dilution effect, levelling-off after day 31 to approximately 26 × 10^6 cell/ml. A significant difference was found between the cell densities of 30 and 40 % renewal rates from day 21 - 45 ($p = 0.0136$), cells receiving 10 % media renewal showing the greatest variation ($p = <0.003$). At 20 % media renewal, cell number stabilised at ~36 - 40 × 10^6 cell/ml. Perhaps the most marked response was at 10 % where cultures (day 28 – 42) displayed cell densities oscillating between 90 – 130 × 10^6 cell/ml (line of best fit at 112 × 10^6 cell/ml).

From an initial mean cell size of 2.60 μm for all flask cultures, a range of sizes from 3.08 – 3.22 μm had developed by day three (Figure 5.8). Mean cell size underwent a rapid increase in all treatments during the first few days of culture. Over the full duration of this experiment, mean cell size of all cultures did not increase significantly, in contrast to previous batch experiments, perhaps reflecting a 'wash-out' of older cells and some replacement by younger, smaller cells in the population as a whole. However, the overall response (from day 21 onwards) to increasing media renewal (dilution) rates was found to result in significantly larger cells ($p = <0.02$), upto day 35. Overall, in semi-continuous mode the cell size was variable, with the cells grown at a 10 % dilution rate being the smallest.

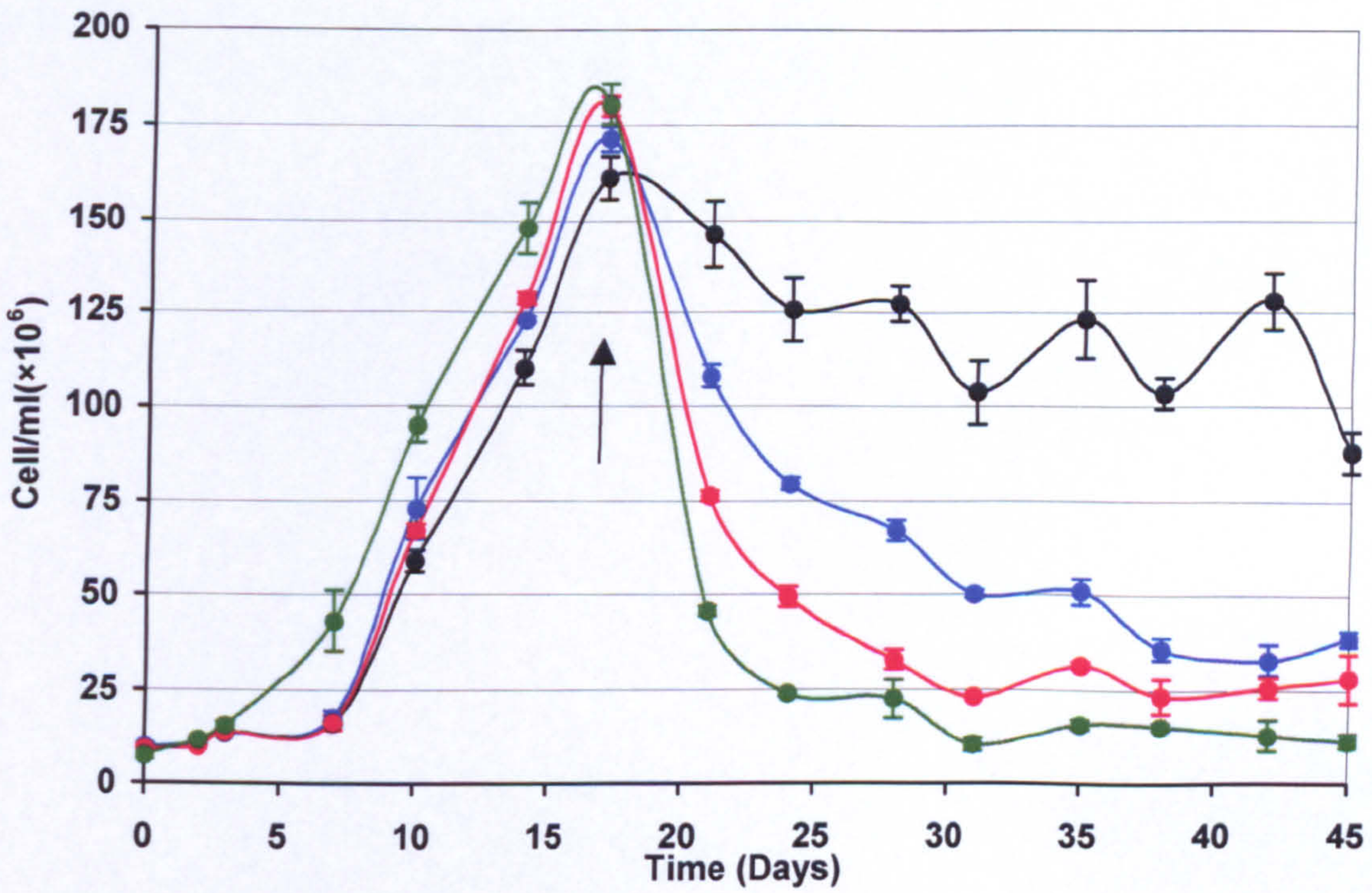

Figure 5.7: Mean cell density of *N. oculata* at a range of semi-continuous media renewal rates (n = 3 ± S.E.). Cultures were diluted with fresh media from day 17 (arrow), at media renewal rates (v/v/day) of 10 %; 20 %; 30 %; and 40 % (inoculum cell density at 9.65; 9.85; 9.32 and 7.46 × 10^6 cell/ml, respectively). Refer also to Appendix D for a statistical summary of results.

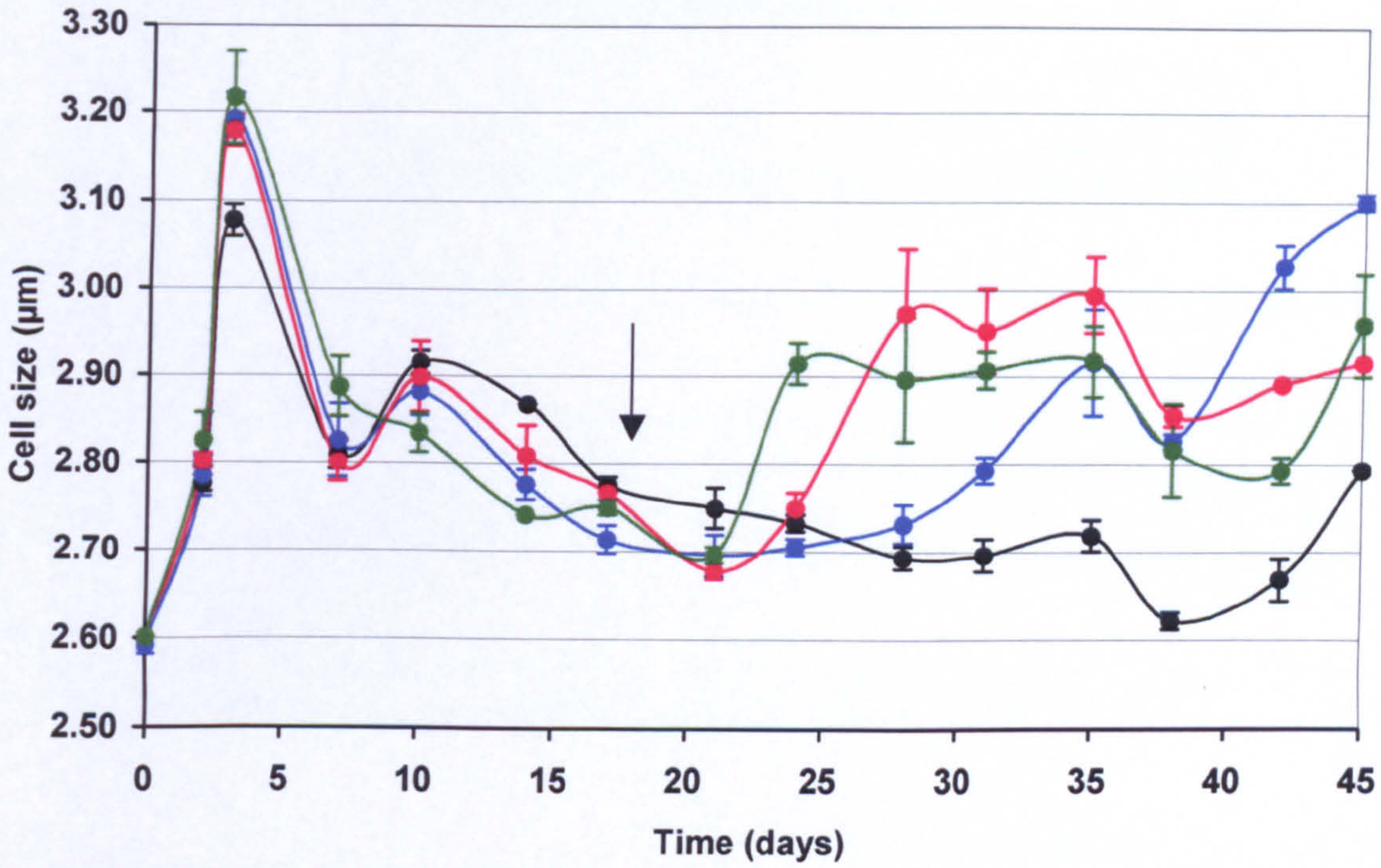

Figure 5.8: Mean cell size of *N. oculata* at a range of semi-continuous media renewal rates (n = 3 ± S.E.). Cultures were diluted with fresh media from day 17 (arrow), at media renewal rates (v/v/day) of 10 %; 20 %; 30 %; and 40 %. Refer also to Appendix D for a statistical summary of results.

Table 5.1 shows the response of the alga to media renewal rates in terms of initial 'wash-out' and stabilisation (steady state). Average cell density was also scaled up to a 1L culture volume to be used later in projecting FAME productivities (Section 7.1.2).

Media renewal rate (v/v/day, %)	Dilution response (% cell wash-out)	Steady-state range (cell/ ml × 10^6)	Scaled-up average cell density (cell/ L × 10^{10})
10	9.37	90 – 130	11.00 ± *1.50*
20	37.08	36 – 40	3.80 ± *0.20*
30	57.68	23 – 32	2.75 ± *0.45*
40	74.60	16 - 20	1.80 ± *0.20*

Table 5.1: Productivity of media renewal rates for *N. oculata* in flask cultures. Working volume maintained at 100 ml.

5.1.6: Oxygen evolution

N. oculata was transferred to fresh sf/2 media at 32 ‰, and maintained at 23 °C and 80 µmol/m^2/s irradiance (24 Hr). Cell density and cell size (Figure 5.9) of cultures were monitored throughout, in addition to which 1 ml samples were taken (shown by arrows) to monitor changes in oxygen evolution at increasing PFDs as detailed in Section 2.2.5.

Oxygen evolution was highest overall, regardless of PFD, when sampled on day 8. A PFD of 500 µmol/m^2/s yielded the highest oxygen output from samples at all sample points from cultures maintained at 80 µmol/m^2/s. However, oxygen evolution rates were not consistent, dropping off to 0.005 µmol/min (Table 5.2).

Both sample points highlight that I_k (183 – 208 µmol/m^2/s) was higher than the growth conditions provided (80 µmol/m^2/s). Cells grown under this pre-defined light level exhibited a net P_{max} range of 0.06 – 0.20 nmol O_2/ 10^6 cell during linear growth phase.

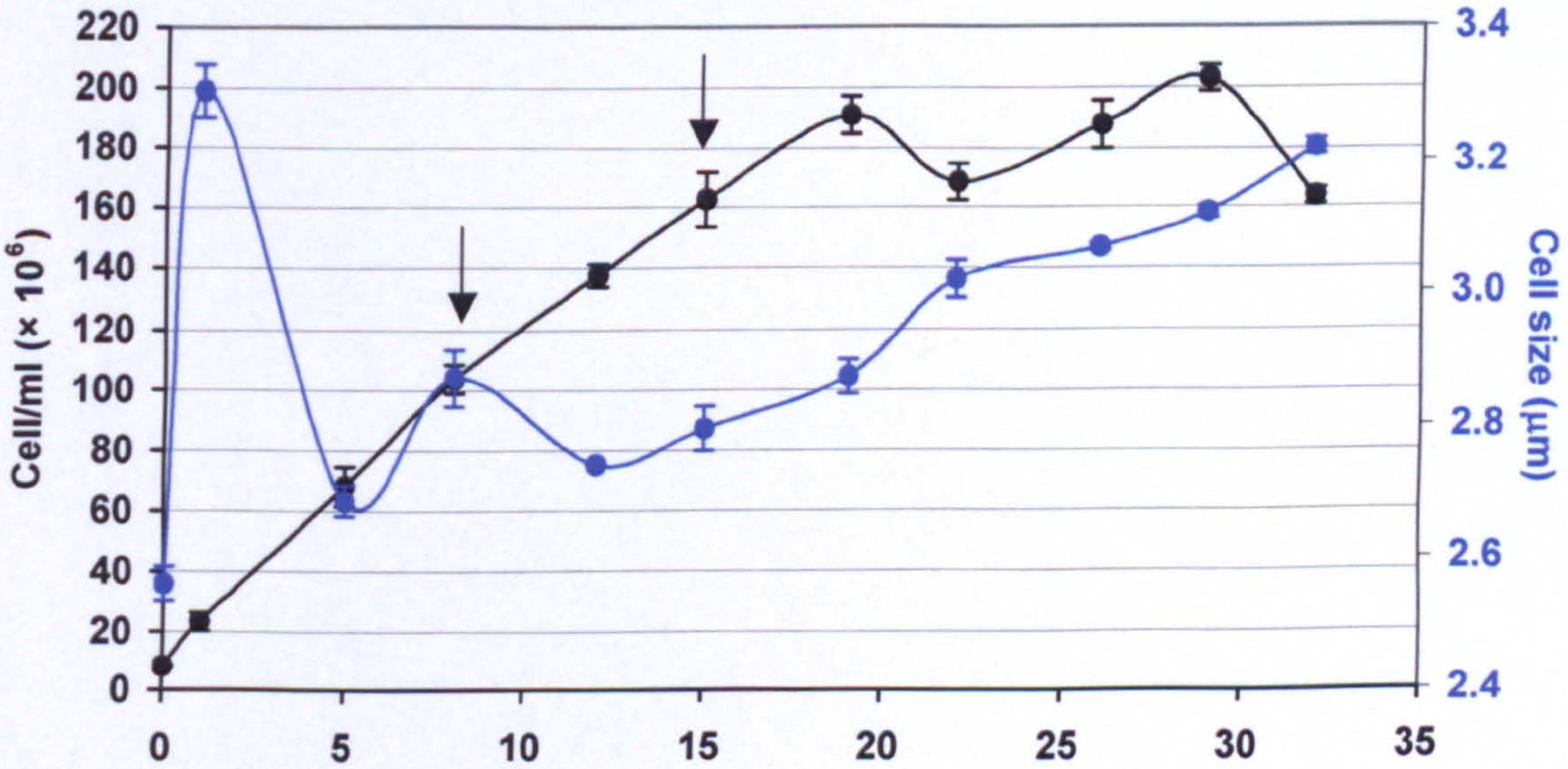

Figure 5.9: Mean cell density and cell size of *N. oculata* in sf/2 at 32 ‰, incubated at 23 °C and under continuous irradiance (80 µmol/m^2/s) (n = 3 ± S.E.). Inoculum cell density at 7.97 × 10^6 cell/ml. Sample points for oxygen evolution analysis taken during linear growth phase, are shown by arrows (see also Table 5.2).

PARAMETER	Time (day)			
	8		15	
	Mean	*S.E.*	Mean	*S.E.*
Cell/ml ($\times 10^6$)	103.91	*4.92*	162.53	*8.96*
R_d (nmol $O_2/10^6$ cell)	-0.08	*0.00*	-0.02	*0.00*
α (pmol O_2/ µmol/m^2/s)	1.10	*0.10*	0.30	*0.10*
Net α (pmolO_2/ µmol/m^2/s)	1.80	*0.11*	0.50	*0.10*
P_{max} (nmol $O_2/10^6$ cell)	0.12	*0.01*	0.04	*0.01*
Net P_{max} (nmol $O_2/10^6$ cell)	0.20	*0.01*	0.06	*0.01*
I_k (µmol/m^2/s)	183.33	*66.67*	208.33	*41.67*
µmol/m^2/s /10^6 cell At I_k µmol/m^2/s	1.76		1.28	
At 80 µmol/m^2/s	0.77		0.49	

Table 5.2: Cellular-based oxygen P-I curve parameters from flask cultures of *N. oculata* (n = 3). Parameters are described in Section 2.2.5. Net values were derived by subtracting effects of dark respiration (R_d). See Figure 5.9 for culture performance. Refer also to Appendix D for a statistical summary of results.

5.1.7: Total lipid and FAME profiles

In order to determine both the lipid content and FAME profile of *N. oculata* grown in different media conditions, replicates from each treatment were first pooled and their total lipid measured (Table 5.3). Cultures grown in f/2 were found to have a larger total lipid content which, when determined on a per cell basis, was over twice the amount of that found within sf/2 cultures, regardless of salinity. From the pooled lipid extracts, FAME profiles were determined for each of the four media conditions (Tables 5.4 – 5.7). Comparisons between the major fatty acid groups (based upon percentage total lipid and percentage total FAME) are shown in Figure 5.10.

	Media (formulation and salinity)			
	f/2		sf/2	
	16 ‰	32 ‰	16 ‰	32 ‰
Pooled harvest volume (ml)	283	279	278	284
Pooled cell density (Cell/ ml × 10^6)	125.63	105.23	196.50	189.33
Total Lipid yield (mg)	58	49	26	37
Volumetric lipid (mg/L)	204.95	175.63	93.53	130.28
Cellular lipid (pg/cell)	1.63	1.67	0.48	0.69
FAME (% of Total lipid)	43.51	25.52	40.82	50.05
Volumetric FAME yield (mg/L)	89.16	44.82	38.18	65.20
Cellular FAME yield (fg/cell)	709.71	425.95	194.29	344.42
EPA (% FAME)	25.31	30.35	55.26	35.44

Table 5.3: Summary comparison of total lipid and FAME profiles for *N. oculata* grown in f/2 and sf/2 at both 16 and 32 ‰. Flasks containing cultures grown on the each media were pooled (n = 3) and the total lipid extracted. Results were standardised in terms of volumetric and cellular yields. Both growth temperature and lighting were standardised for all flasks throughout (see text). All flasks were pooled accordingly after 35 days growth, when all cultures had entered stationary phase (see also Figure 5.1). Individual FAME profiles are shown in Tables 5.4 – 5.7.

All media tested (both in terms of formulation and salinity) showed an absence (i.e. below detectable limits) of the following fatty acids: LAU; STE; LIN; LON; OTA; EDA; DHA. In addition to which, cells cultured at 16 ‰ (both f/2 and sf/2) also lacked detectable levels of both MYR and ARA, whilst OLE was not detected from cultures grown at 16 ‰ in sf/2 (refer to Table 2.1 for full nomenclatures). Although f/2 cultures generally yielded the most total lipid, the PUFA content of sf/2 cultures, when expressed as a percentage of the total lipid, was comparatively double that of f/2 grown cultures (Figure 5.10). In terms of total FAME (volumetric, mg/L), f/2 grown cultures overall resulted in the highest proportions of MUFA (up to 51 % of fatty acids- see Figure 5.10), the majority of which was PML (shown in Tables 5.4 and 5.5).

SAT levels were also the highest in cells maintained in 16 ‰ f/2 (comprising solely of PAL). Despite the relatively high total lipid yield of cultures grown in 16 ‰ f/2 (of which 44 % of the total lipid contained FAMEs), EPA concentration was in fact the lowest proportion found overall (25 % total fatty acids). In comparison, sf/2 cultures at the same salinity (Table 5.6) consisted of over twice the amount of PUFA comparatively (Figure 5.10), comprised solely of EPA. In terms of PUFAs, neither f/2 or sf/2 cultures synthesised any of the n-6 PUFAs tested for in this study at 16 ‰. At 32 ‰ the only measurable n-6 PUFA was ARA, which was found at equal concentrations in cultures grown in f/2 and sf/2 alike. However, in terms of both volumetric and percentage total lipid these cultures were divided with 32 ‰ sf/2 producing the most and 32 ‰ f/2 the least PUFA (i.e. EPA).

Overall, the difference in SATs was statistically found to result from changing salinity, but only when standardised as a percentage of the total FAME ($p = 0.0306$). Differences in FAME profiles, with the exception of the volumetric based results, appear to be more pronounced in sf/2 grown cultures regardless of salinity. Cell growth in f/2 media produced more total lipid from fewer cells with a mean value of 1.65 pg/cell compared with 0.59 pg/cell from cultures grown in sf/2). However, as a proportion of the total lipid, cultures in sf/2 consisted 22 % PUFA, compared with a 9 % fraction in f/2.

		Volumetric yield (mg/L)		Cellular yield (fg/cell)		% Fatty Acid		% Total Lipid	
		Mean	*S.E.*	Mean	*S.E.*	Mean	*S.E.*	Mean	*S.E.*
LAU	(12:0)	-	-	-	-	-	-	-	-
MYR	(14:0)	-	-	-	-	-	-	-	-
PAL	(16:0)	21.43	*4.33*	170.58	*34.45*	24.06	*0.11*	10.46	*2.11*
PML	(16:1)	27.03	*5.76*	215.16	*45.83*	30.27	*0.21*	13.19	*2.81*
STE	(18:0)	-	-	-	-	-	-	-	-
OLE	(18:1 n-9)	18.74	*6.61*	149.19	*52.61*	20.36	*3.21*	9.15	*3.22*
LIN	(18:2 n-6)	-	-	-	-	-	-	-	-
LON	(18:3 n-3)	-	-	-	-	-	-	-	-
OTA	(18:4 n-3)	-	-	-	-	-	-	-	-
EDA	(20:4 n-3)	-	-	-	-	-	-	-	-
ARA	(20:4 n-6)	-	-	-	-	-	-	-	-
EPA	(20:5 n-3)	21.96	*1.70*	174.78	*13.57*	25.31	*3.31*	10.71	*0.83*
DHA	(22:6 n-3)	-	-	-	-	-	-	-	-
TOTAL		**89.16**		**709.71**		**100.00**		**43.51**	
SAT	(C:0)	21.43		170.58		24.06		8.31	
MUFA	(C:1)	45.77		364.35		50.63		17.75	
PUFA	(C:2>)	21.96		174.78		25.31		8.51	
RATIO (n-6 : n-3)		0.00		0.00		0.00		0.00	

Table 5.4: FAME profile of *N. oculata* grown in f/2 media at 16 ‰ (n = 3 ± S.E.). Cells were harvested on day 35 after incubation at 23 °C under continuous irradiance (80 µmol/m^2/s). Results were derived from a total lipid harvest of 58 mg (205 mg/L or 1.63 pg/cell). Refer to Table 2.1 for full names of each fatty acid. Refer also to Appendix D for a statistical summary of results.

		Volumetric yield (mg/L)		Cellular yield (fg/cell)		% Fatty Acid		% Total Lipid	
		Mean	*S.E.*	Mean	*S.E.*	Mean	*S.E.*	Mean	*S.E.*
LAU	(12:0)	-	-	-	-	-	-	-	-
MYR	(14:0)	2.73	*0.15*	25.97	*1.39*	6.11	*0.13*	1.56	*0.08*
PAL	(16:0)	9.39	*2.05*	89.24	*19.43*	20.73	*3.03*	5.35	*1.16*
PML	(16:1)	10.42	*3.73*	98.97	*35.42*	22.74	*6.63*	5.93	*2.12*
STE	(18:0)	-	-	-	-	-	-	-	-
OLE	(18:1 n-9)	6.23	*0.50*	59.16	*4.77*	13.88	*0.09*	3.54	*0.29*
LIN	(18:2 n-6)	-	-	-	-	-	-	-	-
LON	(18:3 n-3)	-	-	-	-	-	-	-	-
OTA	(18:4 n-3)	-	-	-	-	-	-	-	-
EDA	(20:4 n-3)	-	-	-	-	-	-	-	-
ARA	(20:4 n-6)	2.74	*0.27*	26.04	*2.61*	6.19	*1.07*	1.56	*0.16*
EPA	(20:5 n-3)	13.32	*2.83*	126.57	*26.86*	30.35	*8.55*	7.58	*1.61*
DHA	(22:6 n-3)	-	-	-	-	-	-	-	-
TOTAL		**44.82**		**425.95**		**100.00**		**25.52**	
SAT	(C:0)	12.12		115.21		26.84		6.90	
MUFA	(C:1)	16.65		158.13		36.62		9.48	
PUFA	(C:2>)	16.06		152.61		36.54		9.14	
RATIO (n-6 : n-3)		0.21		0.21		0.20		0.21	

Table 5.5: FAME profile of *N. oculata* grown in f/2 media at 32 ‰ (n = 3 ± S.E.). Cells were harvested on day 35 after incubation at 23 °C under continuous irradiance (80 µmol/m^2/s). Results were derived from a total lipid harvest of 49mg (176 mg/L or 1.67 pg/cell). Refer to Table 2.1 for full names of each fatty acid. Refer also to Appendix D for a statistical summary of results.

		Volumetric yield (mg/L)		Cellular yield (fg/cell)		% Fatty Acid		% Total Lipid	
		Mean	*S.E.*	Mean	*S.E.*	Mean	*S.E.*	Mean	*S.E.*
LAU	(12:0)	-	-	-	-	-	-	-	-
MYR	(14:0)	-	-	-	-	-	-	-	-
PAL	(16:0)	8.66	0.05	*44.07*	*2.55*	22.68	*3.88*	9.26	*0.89*
PML	(16:1)	8.42	0.04	*42.85*	*3.54*	22.05	*2.64*	9.00	*0.16*
STE	(18:0)	-	-	-	-	-	-	-	-
OLE	(18:1 n-9)	-	-	-	-	-	-	-	-
LIN	(18:2 n-6)	-	-	-	-	-	-	-	-
LON	(18:3 n-3)	-	-	-	-	-	-	-	-
OTA	(18:4 n-3)	-	-	-	-	-	-	-	-
EDA	(20:4 n-3)	-	-	-	-	-	-	-	-
ARA	(20:4 n-6)	-	-	-	-	-	-	-	-
EPA	(20:5 n-3)	21.10	0.17	107.37	*5.13*	55.26	*4.73*	22.56	*0.48*
DHA	(22:6 n-3)	-	-	-	-	-	-	-	-
TOTAL		**38.18**		**194.29**		**100.00**		**40.82**	
SAT	(C:0)	8.66		44.07		22.68		9.26	
MUFA	(C:1)	8.42		42.85		22.05		9.00	
PUFA	(C:2>)	21.10		107.37		55.26		22.56	
RATIO (n-6 : n-3)		0		0		0		0	

Table 5.6: FAME profile of *N. oculata* grown in sf/2 media at 16 ‰ (n = 3 ± S.E.). Cells were harvested on day 35 after incubation at 23 °C under continuous irradiance (80 µmol/m^2/s). Results were derived from a total lipid harvest of 26 mg (94 mg/L or 0.48 pg/cell). Refer to Table 2.1 for full names of each fatty acid. Refer also to Appendix D for a statistical summary of results.

		Volumetric yield (mg/L)		Cellular yield (fg/cell)		% Fatty Acid		% Total Lipid	
		Mean	*S.E.*	Mean	*S.E.*	Mean	*S.E.*	Mean	*S.E.*
LAU	(12:0)	-	-	-	-	-	-	-	-
MYR	(14:0)	4.02	*0.09*	21.25	*0.45*	6.17	*0.06*	3.09	*0.07*
PAL	(16:0)	14.47	*0.76*	*76.44*	*4.02*	22.21	*1.43*	11.11	*0.58*
PML	(16:1)	14.14	*0.07*	*74.71*	*0.35*	21.70	*0.36*	10.86	*0.05*
STE	(18:0)	-	-	-	-	-	-	-	-
OLE	(18:1 n-9)	5.33	*0.10*	28.16	*0.51*	8.18	*0.25*	4.09	*0.07*
LIN	(18:2 n-6)	-	-	-	-	-	-	-	-
LON	(18:3 n-3)	-	-	-	-	-	-	-	-
OTA	(18:4 n-3)	-	-	-	-	-	-	-	-
EDA	(20:4 n-3)	-	-	-	-	-	-	-	-
ARA	(20:4 n-6)	4.11	*0.14*	21.71	*0.76*	6.30	*0.15*	3.16	*0.11*
EPA	(20:5 n-3)	23.13	*1.47*	122.15	*7.78*	35.44	*1.84*	17.75	*1.13*
DHA	(22:6 n-3)	-	-	-	-	-	-	-	-
TOTAL		**65.20**		**344.42**		**100.00**		**50.05**	
SAT	(C:0)	18.49		97.69		28.38		14.20	
MUFA	(C:1)	19.47		102.87		29.88		14.95	
PUFA	(C:2>)	27.24		143.86		41.74		20.91	
RATIO (n-6 : n-3)		0.18		0.18		0.18		0.18	

Table 5.7: FAME profile of *N. oculata* grown in sf/2 media at 32 ‰ (n = 3 ± S.E.). Cells were harvested on day 35 after incubation at 23 °C under continuous irradiance (80 µmol/m^2/s). Results were derived from a total lipid harvest of 37 mg (130 mg/L or 0.69 pg/cell). Refer to Table 2.1 for full names of each fatty acid. Refer also to Appendix D for a statistical summary of results.

(a)

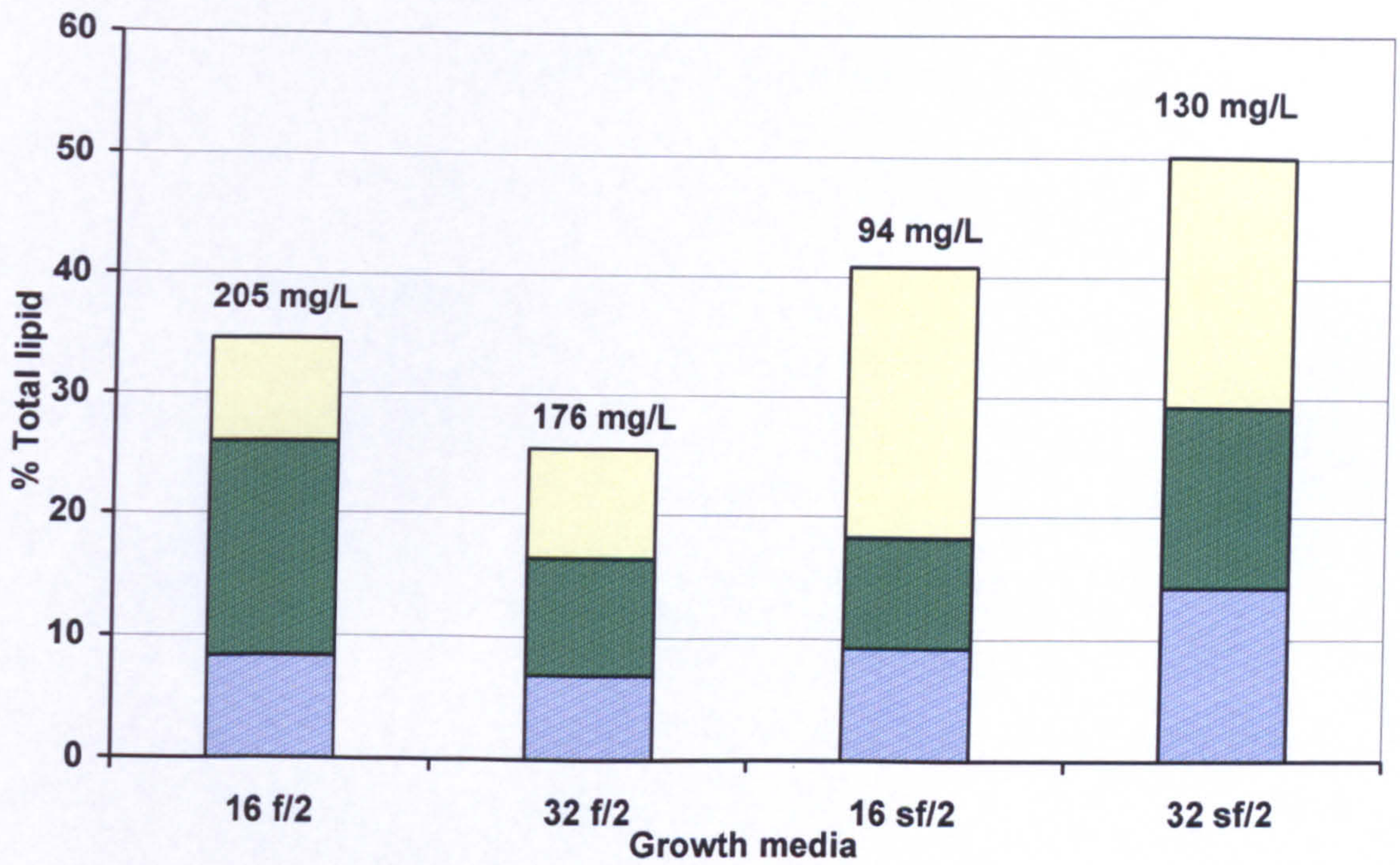

(b)

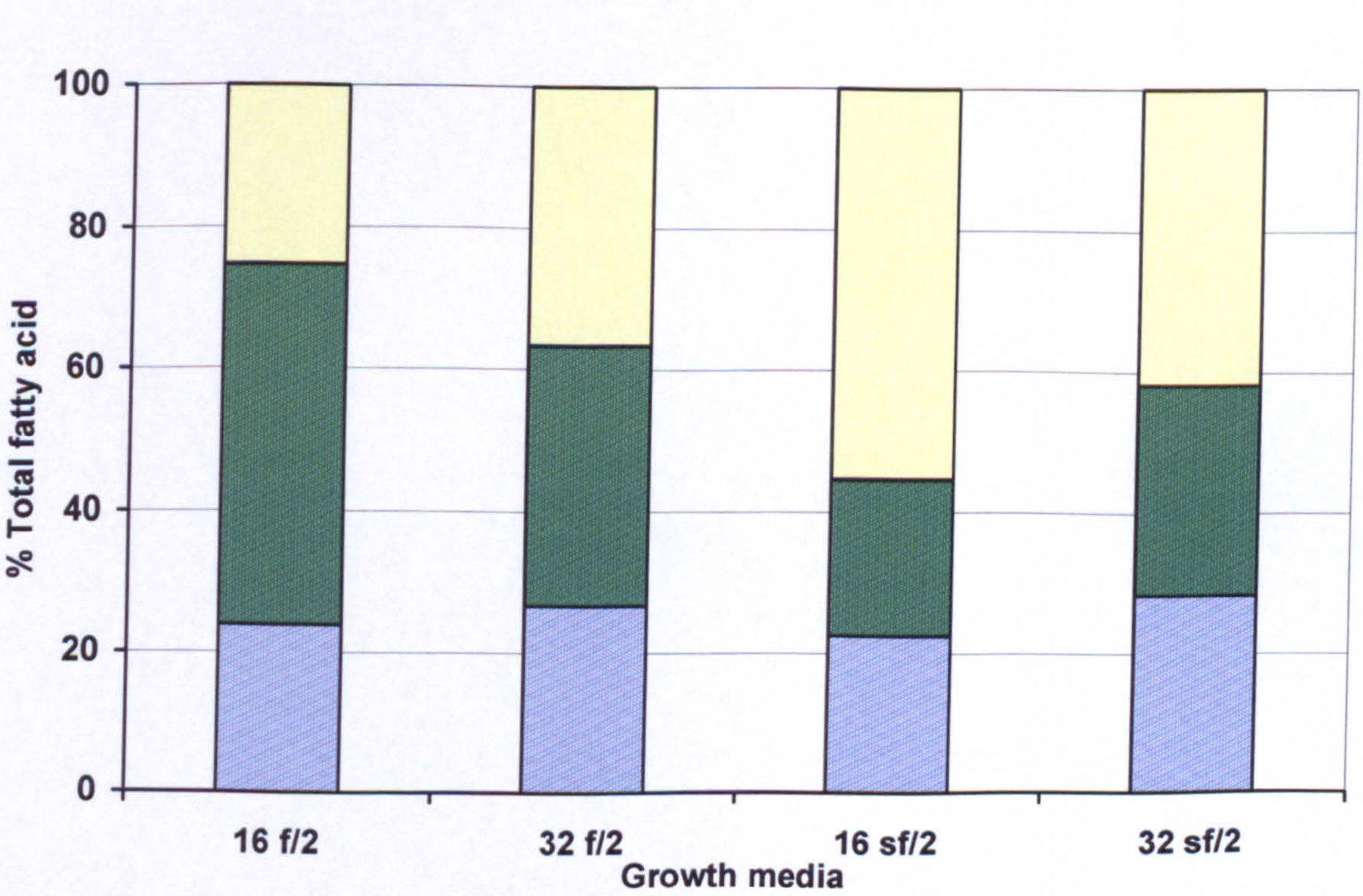

Figure 5.10: Comparison of major fatty acid groups (3 ± S.E.) of *N. oculata* incubated at 23 °C and under continuous irradiance (80 µmol/m^2/s). (a) as a percentage of total fatty acid content (total lipid value labelled above each bar), and (b) as a percentage of the total lipid: showing Saturated fatty acids; Mono-unsaturated fatty acids and Polyunsaturated fatty acids. Refer also to Appendix D for a statistical summary of results.

Further to changes in media compositions, cells previously maintained at 32 ‰ sf/2 incubated at 15 °C (Section 5.1.4) had been harvested, and were of interest due to their continued cell growth to 369 × 10^6 cell/ml. Which yielded a total lipid volume of 140 mg/L or 0.38 ng/cell. The FAME profile was determined, and direct comparison for the effect of temperature upon FAME profile is shown in Tables 5.7 (from a total lipid harvest of 130 mg/L or 0.20 ng/ cell) and 6.8 for *N. oculata* grown at 23 and 15 °C, respectively.

LIN, which was absent for all media conditions tested at 23 °C, was detected when *N. oculata* was cultured at 15 °C. The total volumetric FAME yield was also increased by reducing the growth temperature but only as a result of the higher cell density achieved, rather than cellular accumulation (which was lower than previously recorded, at 0.58 pg/cell). This was also true for the elevated volumetric yields of PML and EPA seen in cultures grown at 15 °C. As a percentage of total lipid, the overall FAME content was lower at 15 °C. Within the FAME profile, PUFA content remained similar (as a percentage of total fatty acids), whereas SAT levels decreased and MUFA increased compared to cultures previously grown at 23 °C, although not significantly.

		Volumetric yield (mg/L)		Cellular yield (fg/cell)		% Fatty Acid		% Total Lipid	
		Mean	*S.E.*	Mean	*S.E.*	Mean	*S.E.*	Mean	*S.E.*
LAU	(12:0)	-	-	-	-	-	-	-	-
MYR	(14:0)	5.94	*0.03*	16.04	*0.15*	6.49	*0.08*	2.75	*0.02*
PAL	(16:0)	14.48	*0.13*	39.09	*0.20*	15.82	*0.05*	6.70	*0.06*
PML	(16:1)	21.94	*0.07*	59.22	*0.03*	23.97	*0.07*	10.15	*0.03*
STE	(18:0)	-	-	-	-	-	-	-	-
OLE	(18:1 n-9)	10.54	*0.12*	28.44	*0.20*	11.52	*0.06*	4.88	*0.05*
LIN	(18:2 n-6)	4.55	*0.03*	12.28	*0.03*	4.97	*0.00*	2.11	*0.01*
LON	(18:3 n-3)	-	-	-	-	-	-	-	-
OTA	(18:4 n-3)	-	-	-	-	-	-	-	-
EDA	(20:4 n-3)	-	-	-	-	-	-	-	-
ARA	(20:4 n-6)	4.29	*0.06*	11.58	*0.13*	4.69	*0.04*	1.98	*0.03*
EPA	(20:5 n-3)	29.77	*0.17*	80.35	*0.16*	32.53	*0.01*	13.77	*0.08*
DHA	(22:6 n-3)	-	-	-	-	-	-	-	-
TOTAL		91.53		246.99		100		42.33	
SAT	(C:0)	20.43		55.13		22.32		9.45	
MUFA	(C:1)	32.48		87.66		35.49		15.02	
PUFA	(C:2>)	38.62		104.21		42.19		17.86	
RATIO	(n-6 : n-3)	0.30		0.30		0.30		0.30	

Table 5.8: FAME of *N. oculata* grown at 15 °C (n = 3 ± S.E.). Cells were harvested after 44 days growth under continuous irradiance (80 µmol/m^2/s) in sf/2 media at 32 ‰ (Figure 5.5). Results were derived from a total lipid harvest of 40 mg (140 mg/L or 0.58 pg/cell). Refer to Table 2.1 for full names of each fatty acid.

5.2: CULTIVATION OF *N. OCULATA* IN A PHOTOBIOREACTOR

5.2.1: Batch culture of *N. oculata*

During batch mode in the photobioreactor, a lag phase in the growth of *N. oculata* was seen to last until day eight, after which cell number began to rise and increased to a rate of 16.49 μ/day from day 11 – 20 (Figure 5.11). After which, cells entered a relatively brief stationary phase. The decline phase followed immediately thereafter. Residual phosphate levels in the growth medium decreased in line with growth of the culture, decreasing at a rate of 0.57 mg/L/day between days 8 – 20 before stabilising at about 0.6 mg/L having. In comparison, residual nitrate levels declined fairly steadily throughout the culture period at a rate of 2.33 mg/L/day. Overall, a maximal cell density of 176 × 10^6 cell/ml was achieved after 24 days, despite a lag phase of eight days.

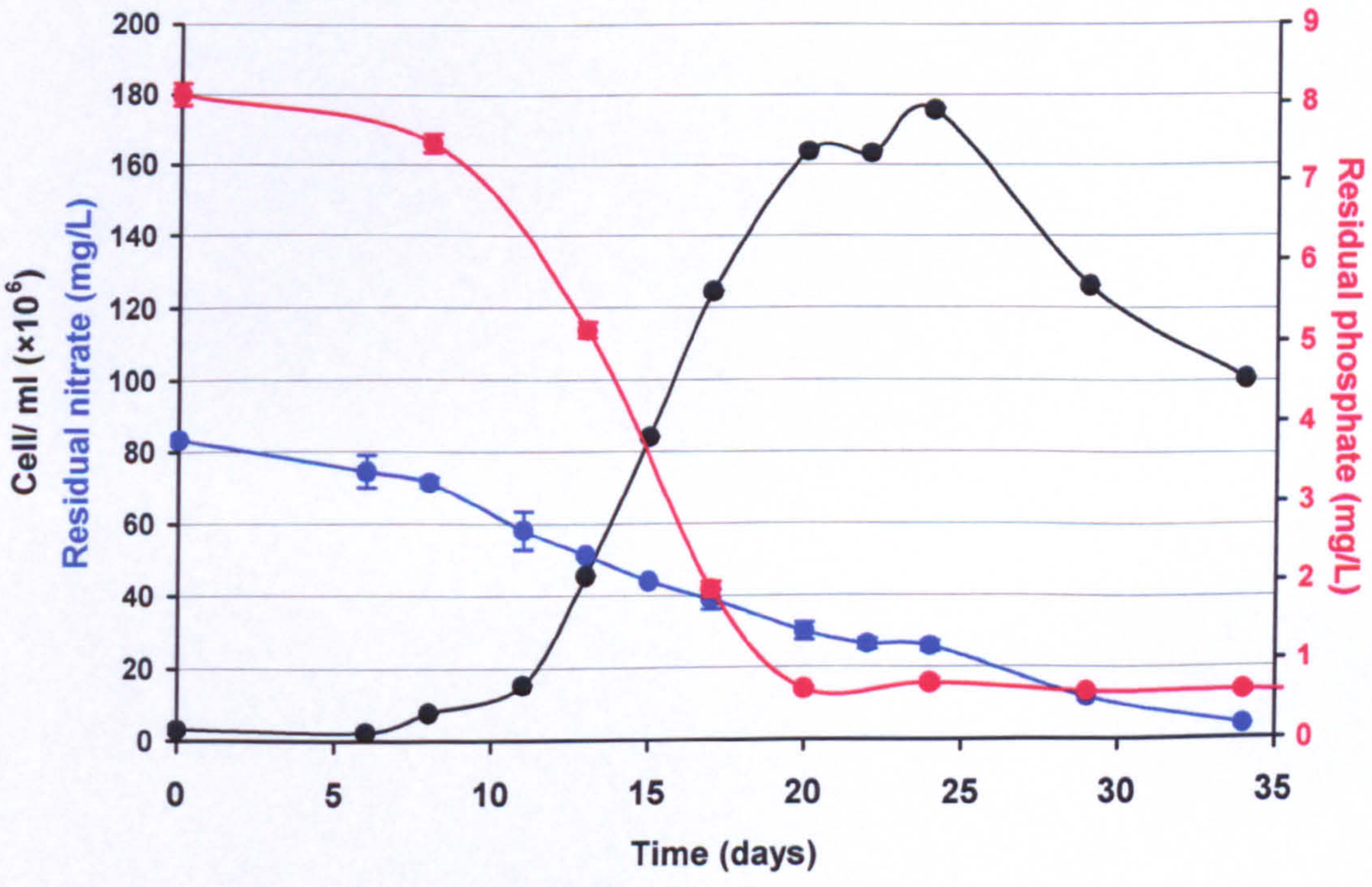

Figure 5.11: Growth of *N. oculata* within a photobioreactor in batch mode operation (n= 3 ± S.E.). Inoculum cell density at 3.20 × 10^6 cell/ml. Continuous irradiance was provided at 107 μmol/m^2/s and temperature was maintained at 23 °C throughout. Mean cell density; residual nitrate; residual phosphate.

5.2.2: Continuous culture of *N. oculata*

In contrast to the batch mode growth of *N. oculata* in the photobioreactor (Section 5.2.1), a lag phase was not apparent in this culture, having been inoculated at a higher cell density. A maximum growth rate of 14.03 μ/day was achieved during the linear growth-phase (days 2 – 14) reaching a maximum cell density, prior to media renewal, of 180 × 10^6 cell/ml (Figure 5.12). At this point media renewal was started at 10 % (v/v/day). Following this, cell number continued to increase and the levels of residual nitrate and phosphate still declined. As a result the media renewal rate was doubled to 20 % (v/v/day) (day 28) with the aim of increasing productivity. However, levels of residual nitrate and phosphate increased whilst cell number dropped from 200 to 38 × 10^6 cell/ml in just 19 days. This regime was maintained, as it was initially believed this was a result of 'wash-out' and that cell numbers may stabilise. Stopping media renewal on day 47 resulted in signs of revival in cell number as residual levels of nitrate and phosphate dropped. After a period of recovery, media renewal at 10 % (v/v/day) was resumed (day 63), as this rate was earlier seen to be sufficient to maintain cell growth without increasing residual nutrient levels. However, this regime failed to have the desired effect and so media renewal was stopped again on day 68. A further attempt at media renewal was introduced on day 75 before stopping after just four days, cell numbers failed to increase despite monitoring for a further 31 days. Statistically, although levels of residual nitrate and phosphate appeared to be paired in their rate of change ($p = <0.02$), neither was significantly correlated with changes in media renewal rate. The media renewal rate proved to have a highly significant influence over both cell density and cell size ($p = <0.02$ for both), and cell size was also found to correlate well with total dry weight ($p = <0.05$) (see below).

In terms of biomass, both total and ash-free dry weight followed the trend of cell number (Figure 5.13). Overall, ash accounted for 65 to 90% of the total dry weight. Total dry weight reached a maximum of 1.34 g/L (day 21) whilst receiving 10 % (v/v/day) media renewal. Ash-free dry weight at this time was 1.11 g/L (83 % of total dry weight). Cell dry weight (Figure 5.14) was 6 ng/cell up until day 40 (during 20% media renewal rate). This value doubled within seven days to 11.7 ng/cell (coinciding with changes in cell size). The termination of media renewal (day 47) resulted in a decrease in cell dry weight (a trend inversely mirrored by mean cell size). From day 56 cellular dry weight increased to reach a maximum of 20.5 ng/cell.

Mean cell size (Figure 5.14) increased from inoculation up to 3.07 μm on day 28. Following a period of 20 % (v/v/day) media renewal mean cell size then dropped to 2.98 μm. Despite brief fluctuations the overall cell size then continued increased from day 47 towards a maximum of 3.14 μm (day 110).

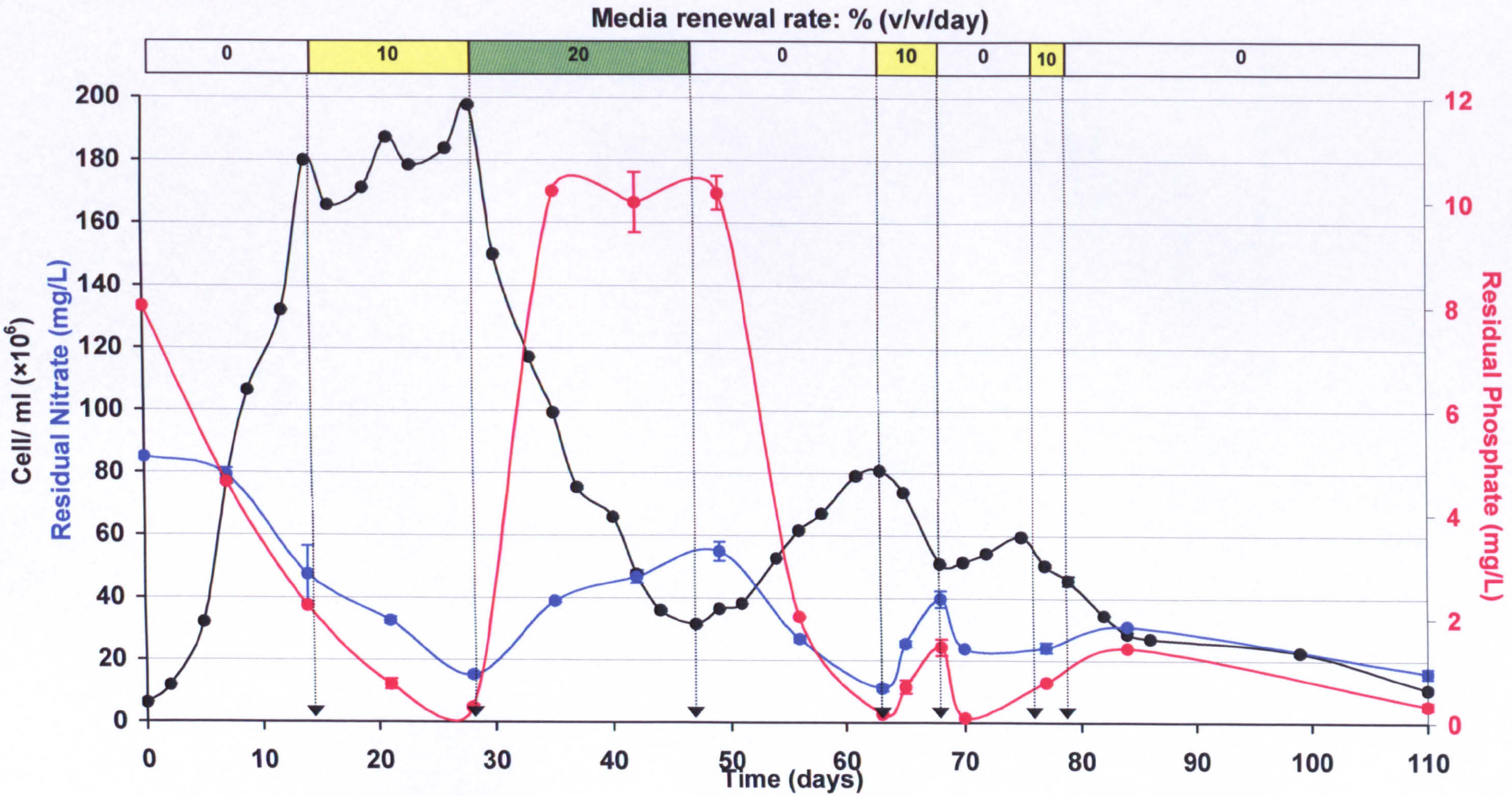

Figure 5.12: Growth of *N. oculata* within a photobioreactor in continuous operation. Inoculum cell density at 6.20×10^6 cell/ml. Continuous irradiance was maintained at 107 µmol/m^2/s and temperature maintained at 23 °C throughout. Mean cell density; residual nitrate; residual phosphate levels (n = 3 ± S.E. for all data). Arrows indicate changes in continuous (24:0, on:off) media renewal rate (v/v/day). Refer also to Appendix D for a statistical summary of results.

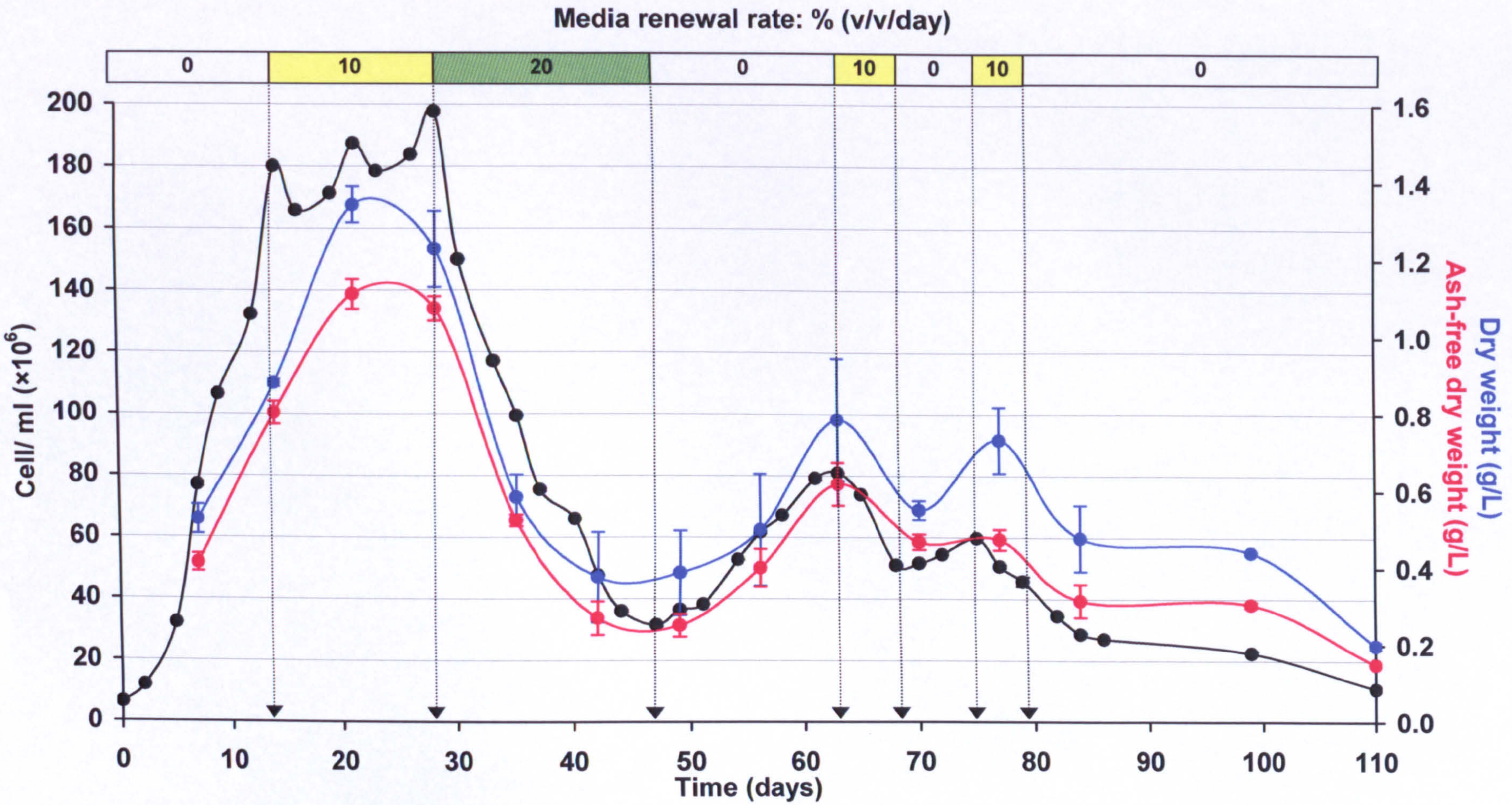

Figure 5.13: Biomass changes of *N. oculata* within a photobioreactor in continuous operation. Inoculum cell density at 6.20×10^6 cell/ml. Continuous irradiance was maintained at 107 µmol/m^2/s and temperature maintained at 23 °C throughout. Mean cell density (shown for convienance); total dry weight (DW); ash-free dry weight (AFDW) (n = 3 ± S.E. for all data). Arrows indicate changes in continuous (24:0, on:off) media renewal rate (v/v/day). Refer also to Appendix D for a statistical summary of results.

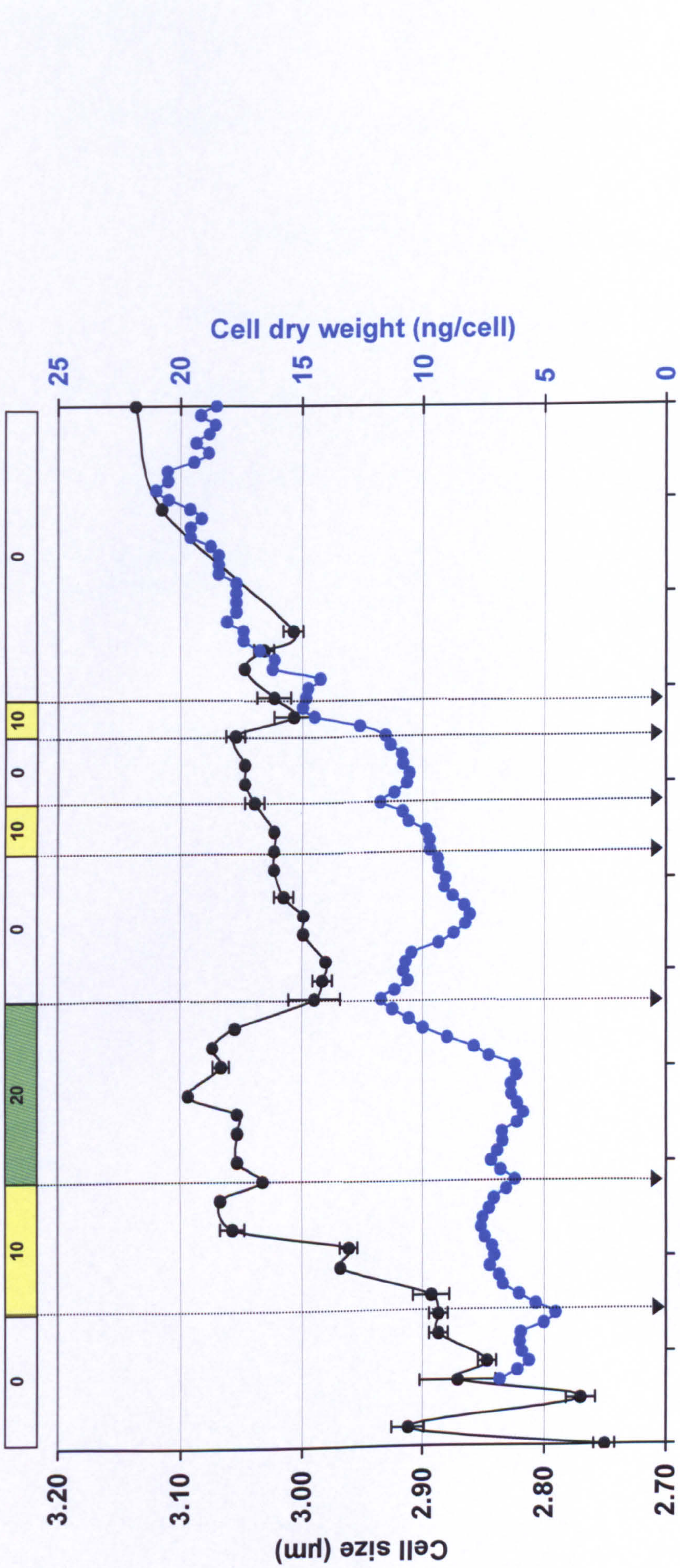

Figure 5.14: Comparison of cell size and cell dry weight of *N. oculata* within a photobioreactor in continuous operation. Continuous irradiance was maintained at 107 µmol/m^2/s and temperature maintained at 24 °C throughout. Mean cell size (µm); cellular dry weight (ng/cell) (n = 3 ± S.E. for all data). Arrows indicate changes in continuous (24:0, on:off) media renewal rate (v/v/day). Refer also to Appendix D for a statistical summary of results.

5.2.3: Fed-batch culture of *N. oculata*

In the initial stages of this fed-batch culture of *N. oculata*, lag phase was again short-lived (c.f. Sections 5.2.1 and 5.2.2) and by day three the cell density had already doubled. Growth continued (at 7.31 μ/day between days 1 - 16), reaching a maximum cell density, prior to media renewal, of 146×10^6 cell/ml on day 21 (Figure 5.15). At this point the culture was thought to be entering into stationary phase (later and at a lower cell density than the run described in Section 5.2.2) and was switched to a daily media renewal of 10% (v/v/day) from day 22 onwards. Media pumps were operated on a fed-batch ratio of 4 : 20 hours (on : off) in order to minimise possible dilution or 'wash-out' effect on the culture, during which an overall maximum cell density of 165×10^6 cell/ml was achieved (day 34). Overall, changes in DW and AFDW followed a similar trend to that of mean cell density (Figure 5.16) reaching a maximum DW of 1.4 g/L (days 22 – 35; 1.3 g/L AFDW) following initiation of the fed-batch regime. AFDW accounted for 63 - 93 % of DW during the course of this run. Despite a period of relatively steady-state growth (days 35 – 50), both DW and AFDW dropped. Residual nitrate levels (Figure 5.15) within the media had began to decrease, in line with growth of the culture, after day 3 at a rate of 3.55 mg/L/day to 20 mg/L (phosphate; 1 mg/L). Once the fed-batch regime was begun, levels of residual nitrate and phosphate remained below 40 and 1.5 mg/L, respectively.

A brief rise in mean cell size immediately followed inoculation (Figure 5.17), shortly followed by a sharp increase until day eight, reaching a mean cell size of 3.15 μm. Subsequent changes to cell size were relatively minor and gradual. A maximum mean cell size of 3.34 μm was achieved by day 25, before steadily decreasing to 3.00 μm by day 49. Cell dry weight showed a maximum value of 10.87 ng/cell on day 14 (prior to the use of the fed-batch regime). Once media renewal had commenced, cell dry weight fell from 10.0 – 7.5 ng/cell.

Chlorophyll *a* levels (Figure 5.18) initially peaked on day eight (11.16 μg/ml; 0.024 pg/cell), before declining between days 13 - 16. Recovery was apparent on day 20 (11.16 μg/ml; 0.024 pg/cell) until the onset of media renewal, which had a more profound effect on chlorophyll *a* levels. During fed-batch operation, cellular chlorophyll *a* fell within a range of 0.007 - 0.014 pg/cell (or 5.43 – 10.25 μg/ml).

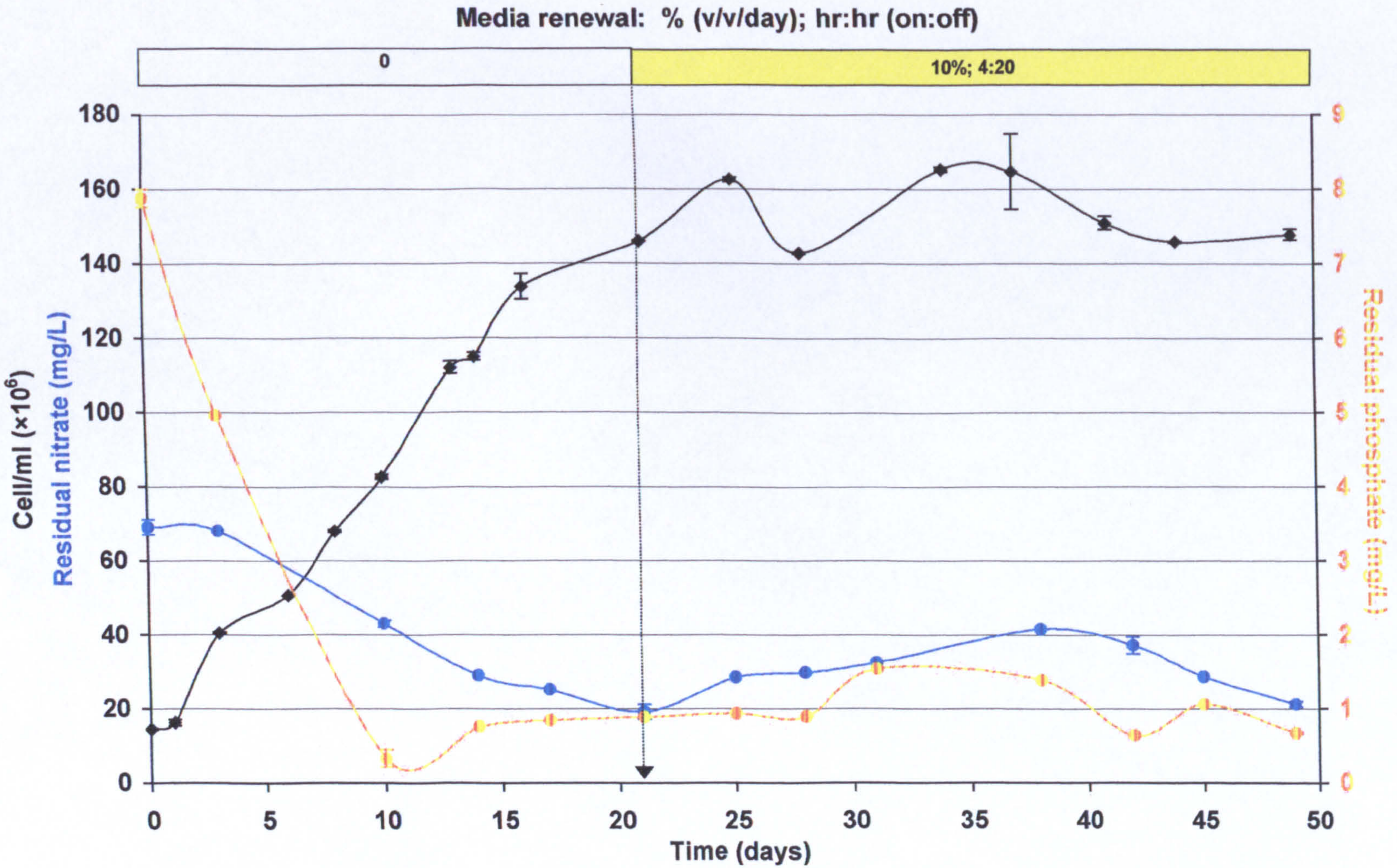

Figure 5.15: Growth of *N. oculata* within a photobioreactor in fed-batch operation. Inoculum cell density at 14.52×10^6 cell/ml. Continuous irradiance was provided at 107 µmol/m^2/s and temperature maintained at 23 °C throughout. Mean cell density; residual nitrate; residual phosphate levels (n = 3 ± S.E. for all data). Arrows indicate change to fed-batch (4:20, on:off) media renewal rate (v/v/day). Refer also to Appendix D for a statistical summary of results.

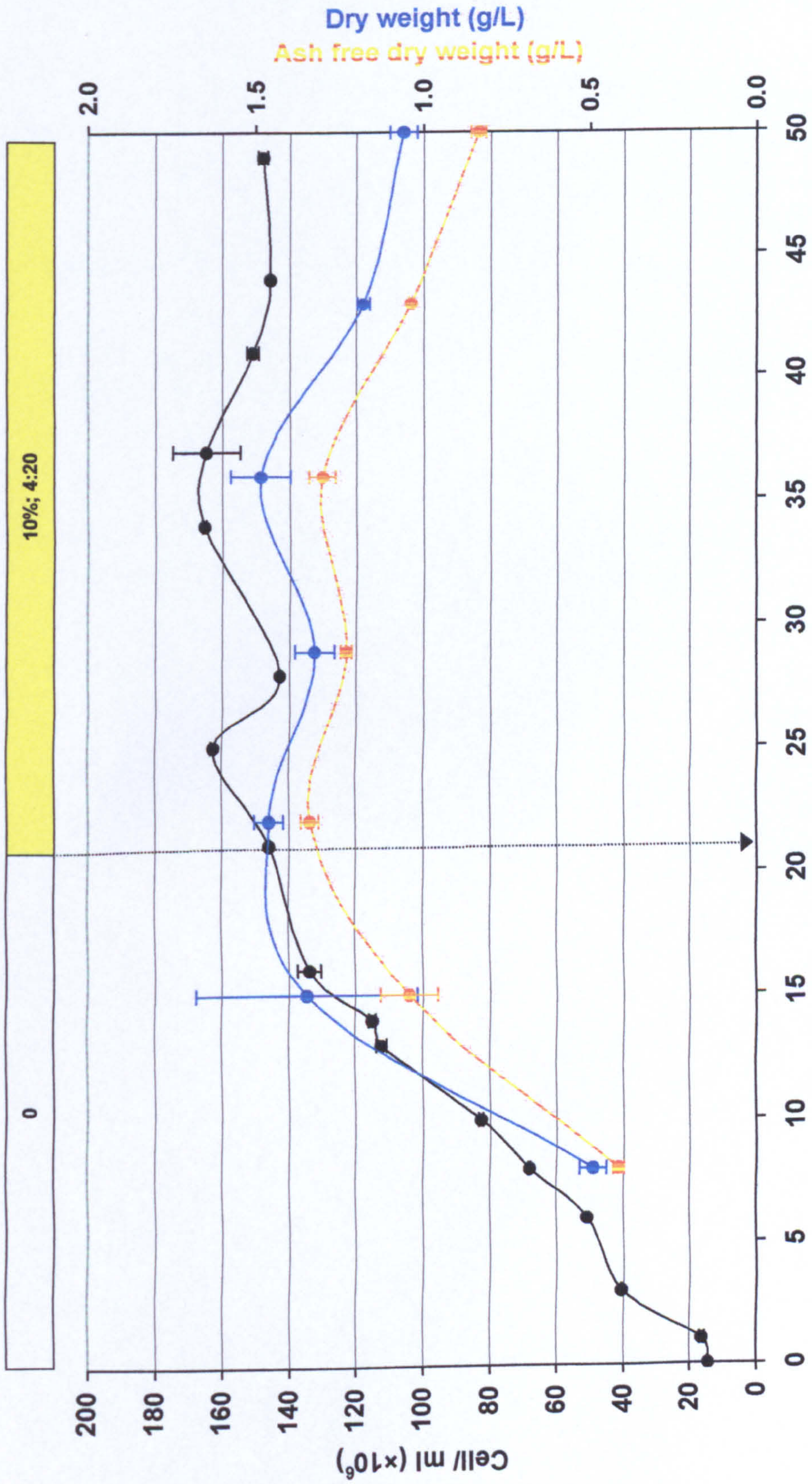

Figure 5.16: Biomass changes of *N. oculata* within a photobioreactor in fed-batch operation. Inoculum cell density at 14.52×10^6 cell/ml. Continuous irradiance was provided at 107 µmol/m^2/s and temperature maintained at 23 °C throughout. Mean cell density; total dry weight (DW); ash-free dry weight (AFDW) ($n = 3 \pm$ S.E. for all data). Arrows indicate change to fed-batch (4:20, on:off) media renewal rate (v/v/day). Refer also to Appendix D for a statistical summary of results.

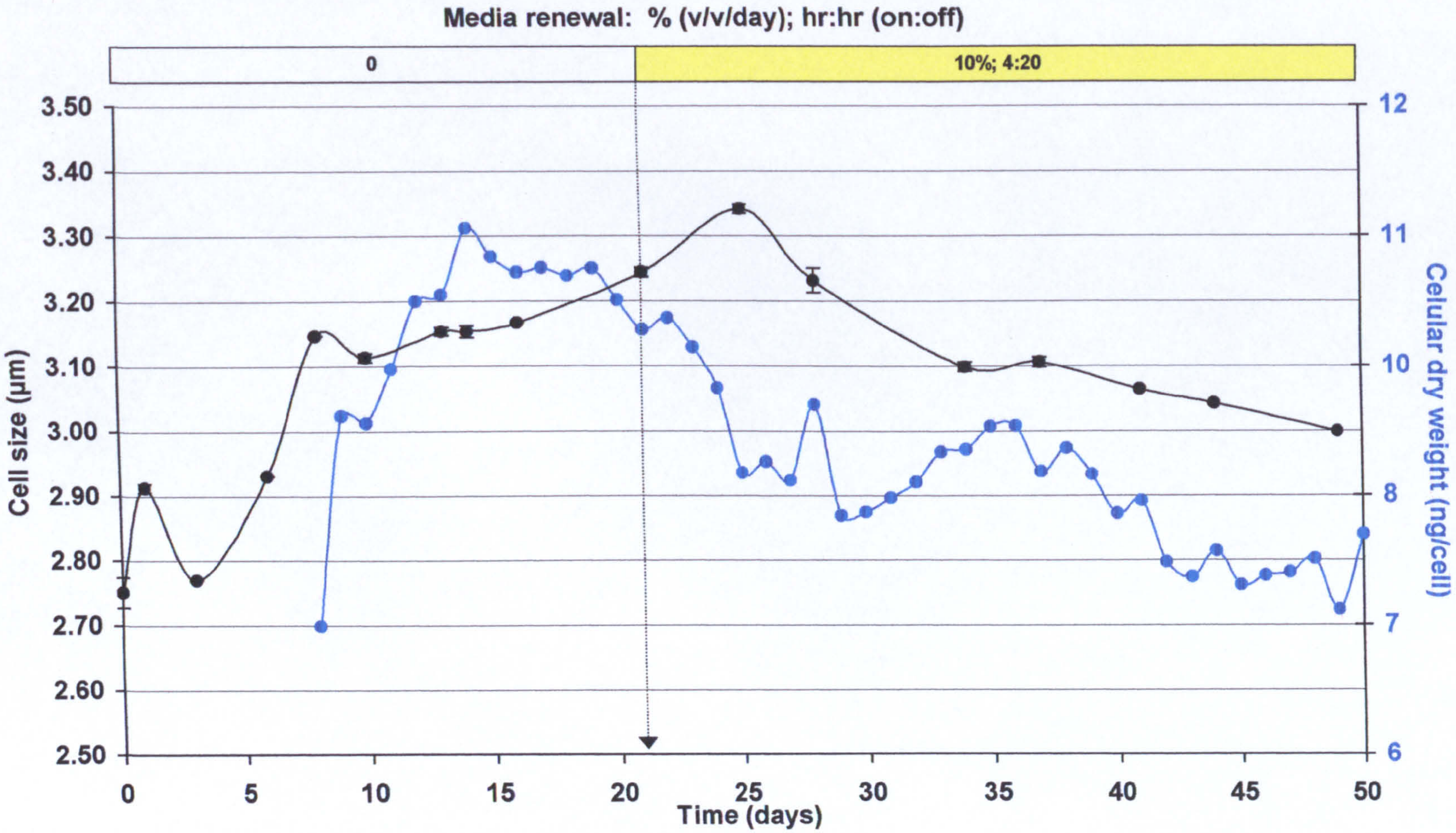

Figure 5.17: Comparison of cell size and cellular dry weight of *N. oculata* within a photobioreactor in fed-batch operation. Continuous irradiance was provided at 107 µmol/m^2/s and temperature maintained at 23 °C throughout. Mean cell size (µm); cellular dry weight (ng/cell) (n = 3 ± S.E. for all data). Cellular dry weight points have been interpolated. Arrows indicate change to fed-batch (4:22, on:off) media renewal rate (v/v/day). Refer also to Appendix D for a statistical summary of results.

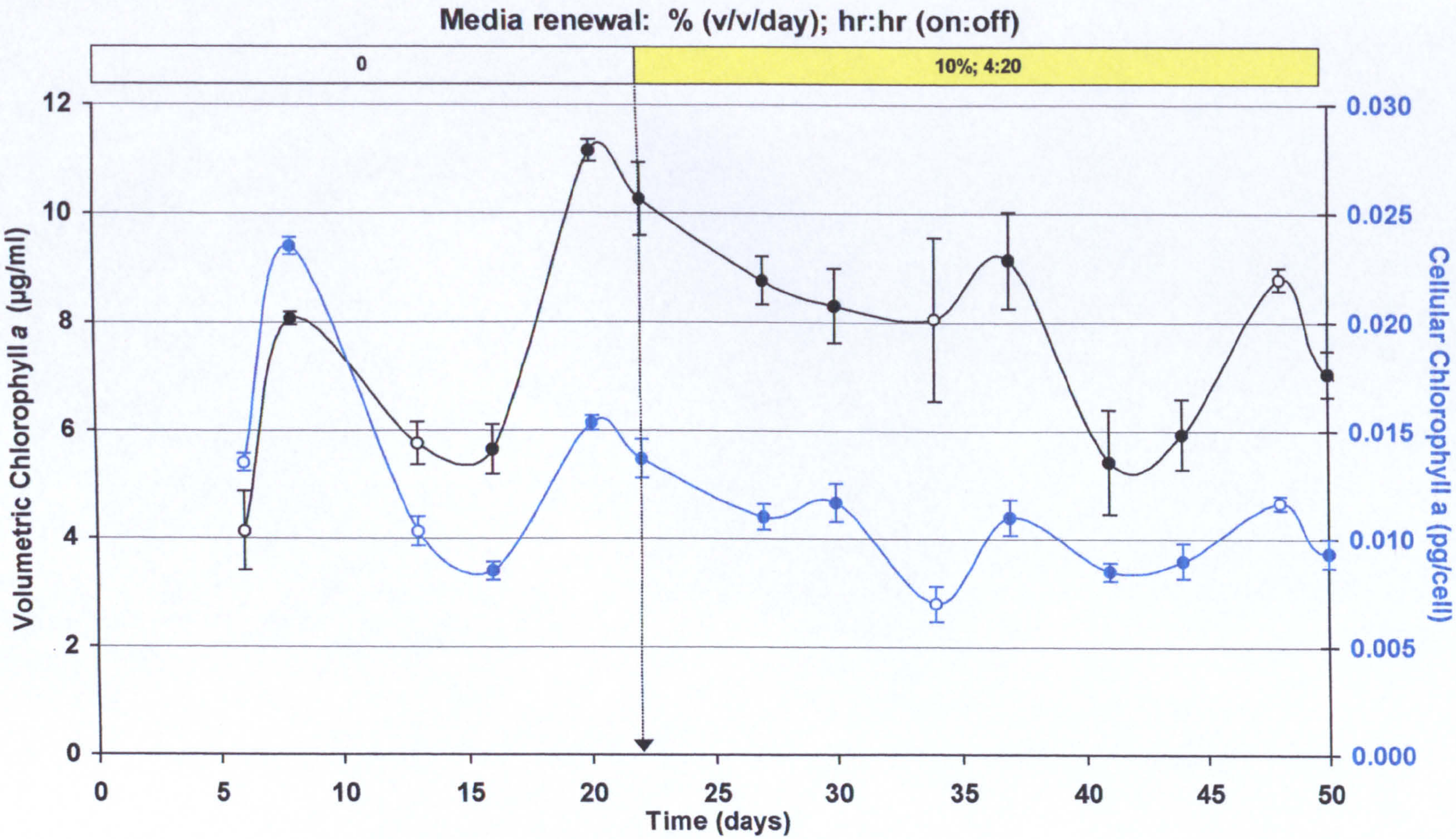

Figure 5.18: Chlorophyll *a* changes in *N. oculata* cultured within a photobioreactor in fed-batch operation. Continuous irradiance was provided at 107 µmol/m^2/s and temperature maintained at 23 °C throughout. Volumetric chlorophyll *a* (µg/ml); cellular chlorophyll *a* (pg/cell) (n = 3 ± S.E. for all data). Arrows indicate change to fed-batch (4:20, on:off) media renewal rate (v/v/day). Open circles indicate sample points used for oxygen evolution analysis (see Tables 5.9 and 5.10). Refer also to Appendix D for a statistical summary of results.

Oxygen evolution of *N. oculata* in the photobioreactor was measured on days six and 13 (during linear growth phase, prior to a media renewal regime), and on days 34 and 48 (during fed-batch mode at 10 % (v/v/day)). Oxygen evolution was standardised to both a cellular (Table 5.9) and volumetric (Table 5.10) chlorophyll *a* basis.

During linear phase growth (days 6 - 13) net P_{max} ranged from 0.31 - 1.33 nmol O_2/ 10^6 cell with a mean α of 0.0075 (Table 5.9), whilst cell density increased by 71.37 × 10^6 cell/ml. Optimum oxygen evolution during linear phase growth was found at an I_k PFD range of 208 - 333 µmol/m^2/s. In fed-batch mode (at a mean cell density of 165 × 10^6 cell/ml) I_k increased to 417 µmol/m^2/s, which gave a mean net P_{max} of 0.40 nmol O_2/ 10^6 cell.

PARAMETER	Linear growth phase (batch period)				Fed-batch period			
	Day 6		Day 13		Day 34		Day 48	
	Mean	*S.E.*	Mean	*S.E.*	Mean	*S.E.*	Mean	*S.E.*
Cell/ml (× 10^6)	50.76	*0.64*	112.12	*1.60*	165.37	*0.58*	147.86	*1.44*
R_d (nmol O_2/10^6 cell)	-0.75	*0.41*	-0.09	*0.06*	-0.13	*0.03*	-0.27	*0.02*
Cellular α (pmol O_2/ µmol/m^2/s)	6.90	*0.07*	1.50	*0.17*	1.30	*0.19*	2.40	*0.09*
Net cellular α (pmol O_2/ µmol/m^2/s)	12.70	*0.10*	2.03	*0.20*	2.30	*0.20*	4.50	*0.10*
P_{max} (nmol O_2/10^6 cell)	0.58	*0.01*	0.22	*0.05*	0.15	*0.04*	0.24	*0.01*
Net P_{max} (nmol O_2/10^6 cell)	1.33	*0.40*	0.31	*0.11*	0.28	*0.02*	0.51	*0.01*
I_k (µmol/m^2/s)	208.33	*41.67*	333.33	*83.33*	416.67	*83.33*	416.67	*83.33*
µmol/m^2/s/10^6 cell At I_k µmol/m^2/s	4.10		2.97		2.52		2.83	
At 107 µmol/m^2/s	2.11		0.95		0.65		0.72	

Table 5.9: Cellular-based oxygen P-I curve parameters from a fed-batch photobioreactor culture of *N. oculata* (n = 3). Net values were derived by subtracting the effects of dark respiration (R_d). Cultures were maintained continuously at a PFD of 107 µmol/m^2/s throughout. Refer also to Appendix D for a statistical summary of results. Refer also to Appendix D for a statistical summary of results.

The Chlorophyll *a* content of *N. oculata* whilst receiving media renewal was on average 3.48 µg/ml higher than during earlier linear growth phase (days 6 – 13), yet net P_{max} was typically more efficient during the earlier phase by 8.05 nmol O_2/ µg Chl *a* (Chl *a* α of 0.06 in linear growth phase samples compared to 0.03 in fed-batch mode). The optimum irradiance in relation to chlorophyll *a* content (as given by the P-I curve parameter, I_k) remained within a range of 47.40 – 57.97 PFD/ µg Chl *a*. In reality, given that irradiance at the surface of the photostage was 107 µmol/m^2/s, this varied from 11.38 – 24.15 PFD/ µg Chl *a*.

PARAMETER	Linear growth phase (batch period)				Fed-batch period			
	Day 6		Day 13		Day 34		Day 48	
	Mean	*S.E.*	Mean	*S.E.*	Mean	*S.E.*	Mean	*S.E.*
Chl *a* (µg/ml)	4.14	*0.73*	5.75	*1.00*	8.06	*1.43*	8.79	*0.21*
R_d (nmol O_2/µg Chl *a*)	-9.26	*5.01*	-2.23	*0.83*	-2.46	*0.53*	-4.47	*0.30*
α (pmol O_2/ µmol/m^2/s)	84.60	*1.80*	35.20	*1.60*	24.5	*0.70*	40.50	*0.70*
Net α (pmol O_2/ µmol/m^2/s)	155.80	*5.13*	52.40	*1.82*	43.50	*1.20*	74.90	*1.27*
P_{max} (nmol O_2/µg Chl *a*)	7.07	*0.11*	4.54	*0.58*	2.80	*0.77*	4.11	*0.15*
Net P_{max} (nmol O_2/µg Chl *a*)	16.33	*4.90*	6.77	*1.41*	5.26	*0.77*	8.58	*0.16*
I_k (µmol/m^2/s)	208.33	*41.67*	333.33	*83.33*	416.67	*83.33*	416.67	*83.33*
µmol/m^2/s/µg Chl *a* At I_k µmol/m^2/s	50.32		57.97		51.70		47.40	
At 107 µmol/m^2/s	25.85		18.61		13.28		12.17	

Table 5.10: Chlorophyll *a*-based oxygen P-I curve parameters from a fed-batch photobioreactor culture of *N. oculata* (n = 3). Net values were derived by subtracting the effects of dark respiration (R_d). Cultures were maintained continuously at a PFD of 107 µmol/m^2/s throughout. Refer also to Appendix D for a statistical summary of results.

The total lipid content of *N. oculata* was determined towards the end of the linear growth phase (day 22, yielding 103 mg/L) and finally at the end of the experiment (day 50, yielding 297 mg/L). The FAME profiles of which are shown in Tables 5.11 and 5.12, respectively. When expressed as a percentage of DW, total lipid represented 7 and 28 % for the two sampling points.

At the end of the run (day 50) 14 L of culture was harvested (at 148 × 10^6 cell/ml) which given the FAME profile in Table 5.12, resulted in an overall harvest of 328 mg of PUFA (of which 248 mg was EPA). This result yielded 62 % more EPA than originally projected for the tubular photobioreactor, based on earlier flask experiments (refer to Table 7.1).

In fed-batch mode, *N. oculata* yielded almost three-times more total lipid than samples taken before the addition of fresh media (c.f. day 50 with day 22). A doubling in total volumetric and cellular yields of FAMEs was also observed from cells harvested during fed-batch mode, with the additional of previously undetected LAU, STE and LIN (reflected by increases in SAT and MUFA content). Whilst volumetric levels of EPA marginally increased, the ratio of n-6 : n-3 PUFA was found to have doubled. Despite increases in both volumetric and cellular yields between days 22 and 50, the PUFA content of *N. oculata* had dropped by ~8 % of a proportion of the total fatty acids and had almost halved when expressed as a percentage of total lipid.

		Volumetric yield (mg/L)		Cellular yield (fg/cell)		% DW		% AFDW		% Fatty Acid		% Total Lipid	
		Mean	*S.E.*	Mean	*S.E.*	Mean	*S.E.*	Mean	*S.E.*	Mean	*S.E.*	Mean	*S.E.*
LAU	(12:0)	-	-	-	-	-	-	-	-	-	-	-	-
MYR	(14:0)	3.85	*0.51*	26.40	*3.48*	0.26	*0.03*	0.29	*0.04*	8.90	*0.84*	3.73	*0.49*
PAL	(16:0)	8.47	*0.28*	58.01	*1.95*	0.58	*0.02*	0.63	*0.02*	19.56	*0.99*	8.19	*0.27*
PML	(16:1)	11.47	*0.43*	78.61	*2.95*	0.79	*0.03*	0.86	*0.03*	26.51	*0.96*	11.10	*0.42*
STE	(18:0)	-	-	-	-	-	-	-	-	-	-	-	-
OLE	(18:1 n-9)	3.72	*0.08*	25.48	*0.54*	0.25	*0.01*	0.28	*0.01*	8.59	*0.42*	3.60	*0.08*
LIN	(18:2 n-6)	-	-	-	-	-	-	-	-	-	-	-	-
LON	(18:3 n-3)	-	-	-	-	-	-	-	-	-	-	-	-
OTA	(18:4 n-3)	-	-	-	-	-	-	-	-	-	-	-	-
EDA	(20:4 n-3)	-	-	-	-	-	-	-	-	-	-	-	-
ARA	(20:4 n-6)	3.29	*0.24*	22.52	*1.62*	0.23	*0.02*	0.25	*0.02*	7.59	*0.18*	3.18	*0.23*
EPA	(20:5 n-3)	12.49	*0.73*	85.54	*4.98*	0.86	*0.05*	0.93	*0.05*	28.84	*0.99*	12.08	*0.70*
DHA	(22:6 n-3)	-	-	-	-	-	-	-	-	-	-	-	-
TOTAL		**43.29**		**296.57**		**2.96**		**3.23**		**100**		**41.89**	
SAT	(C:0)	12.32		84.41		0.84		0.92		28.46		11.92	
MUFA	(C:1)	15.19		104.09		1.04		1.13		35.10		14.70	
PUFA	(C:2>)	15.77		108.06		1.08		1.18		36.44		15.26	
RATIO (n-6 : n-3)		0.26		0.26		0.29		0.27		0.26		0.26	

Table 5.11: FAME profile of *N. oculata* grown in a photobioreactor prior to receiving 4:20Hr cycle of 10 % media renewal (n = 3 ± S.E.) harvested after 22 days growth under continuous irradiance (107 µmol/m²/s) in 32 ‰ sf/2 media (Figure 5.15). Results derived from a total lipid harvest of 31 mg (103 mg/L; 0.71 pg/cell; 7.05 % DW). Refer to Table 2.1 for full names of each fatty acid. Refer also to Appendix D for a statistical summary of results.

		Volumetric yield (mg/L)		Cellular yield (fg/cell)		% DW		% AFDW		% Fatty Acid		% Total Lipid	
		Mean	*S.E.*	Mean	*S.E.*	Mean	*S.E.*	Mean	*S.E.*	Mean	*S.E.*	Mean	*S.E.*
LAU	(12:0)	1.66	*0.43*	11.25	*2.89*	0.16	*0.04*	0.20	*0.05*	1.70	*0.05*	0.56	*0.14*
MYR	(14:0)	4.81	*1.09*	32.50	*7.37*	0.45	*0.10*	0.58	*0.13*	4.91	*0.01*	1.62	*0.37*
PAL	(16:0)	25.94	*4.53*	175.46	*30.63*	2.45	*0.43*	3.11	*0.54*	26.52	*1.57*	8.74	*1.53*
PML	(16:1)	24.87	*5.46*	168.18	*36.94*	2.35	*0.52*	2.98	*0.65*	25.42	*0.26*	8.38	*1.84*
STE	(18:0)	2.18	*0.45*	14.75	*3.05*	0.21	*0.04*	0.26	*0.05*	2.23	*1.05*	0.74	*0.15*
OLE	(18:1 n-9)	11.02	*1.72*	74.54	*11.61*	1.04	*0.16*	1.32	*0.21*	11.27	*0.90*	3.72	*0.58*
LIN	(18:2 n-6)	3.97	*0.86*	26.82	*5.81*	0.37	*0.08*	0.47	*0.10*	4.05	*0.05*	1.34	*0.29*
LON	(18:3 n-3)	-	-	-	-	-	-	-	-	-	-	-	-
OTA	(18:4 n-3)	-	-	-	-	-	-	-	-	-	-	-	-
EDA	(20:4 n-3)	-	-	-	-	-	-	-	-	-	-	-	-
ARA	(20:4 n-6)	5.66	*1.36*	38.25	*9.20*	0.53	*0.13*	0.68	*0.16*	5.78	*0.07*	1.91	*0.46*
EPA	(20:5 n-3)	17.73	*4.38*	119.88	*29.64*	1.67	*0.41*	2.12	*0.52*	18.12	*0.35*	5.97	*1.48*
DHA	(22:6 n-3)	-	-	-	-	-	-	-	-	-	-	-	-
TOTAL		97.83		661.63		9.24		11.72		100		32.98	
SAT	(C:0)	34.59		233.96		3.27		4.14		35.36		11.66	
MUFA	(C:1)	35.89		242.72		3.39		4.30		36.69		12.10	
PUFA	(C:2>)	27.35		184.95		2.58		3.27		27.95		9.22	
RATIO (n-6 : n-3)		0.54		0.54		0.54		0.54		0.54		0.54	

Table 5.12: FAME profile of *N. oculata* grown in a photobioreactor during media renewal (n = 3 ± S.E.) harvested after 50 days growth under continuous irradiance (107 µmol/m^2/s) in 32 ‰ sf/2 media (Figure 5.15). Results derived from a total lipid harvest of 89 mg (297 mg/L; 2.01 pg/cell; 28.05 % DW). Refer to Table 2.1 for full names of each fatty acid. Refer also to Appendix D for a statistical summary of results.

		+/- change in FAME profile					
		mg/L	fg/cell	% DW	% AFDW	% FA	% TL
LAU	(12:0)	+1.66	+11.25	+0.16	+0.20	+1.70	+0.56
MYR	(14:0)	+0.95	+6.10	+0.19	+0.29	-3.99	-2.11
PAL	(16:0)	+17.48	+117.44	+1.87	+2.48	+6.96	+0.55
PML	(16:1)	+13.39	+89.57	+1.56	+2.12	-1.09	-2.72
STE	(18:0)	+2.18	+14.75	+0.21	+0.26	+2.23	+0.74
OLE	(18:1 n-9)	+7.30	+49.06	+0.79	+1.04	+2.67	+0.12
LIN	(18:2 n-6)	+3.97	+26.82	+0.37	+0.47	+4.05	+1.34
LON	(18:3 n-3)	-	-	-	-	-	-
OTA	(18:4 n-3)	-	-	-	-	-	-
EDA	(20:4 n-3)	-	-	-	-	-	-
ARA	(20:4 n-6)	+2.37	+15.72	+0.30	+0.43	-1.81	-1.28
EPA	(20:5 n-3)	+5.24	+34.34	+0.81	+1.19	-10.72	-6.11
DHA	(22:6 n-3)	-	-	-	-	-	-
TOTAL		**+54.54**	**+365.06**	**+6.28**	**+8.49**	**0.00**	**-8.91**
SAT	(C:0)	+22.27	+149.54	+2.43	+3.22	+6.90	-0.26
MUFA	(C:1)	+20.69	+138.63	+2.35	+3.17	+1.59	-2.61
PUFA	(C:2>)	+11.57	+76.89	+1.50	+2.09	-8.48	-6.05
RATIO	(n-6 : n-3)	+0.28	+0.28	+0.28	+0.28	+0.28	+0.28

Table 5.13: Comparative changes in FAME profile of *N. oculata* during growth in a tubular photobioreactor. Differences in FAME profiles over a period of 28 days, between Tables 5.11 and 5.12 (throughout fed-batch production). Refer to Table 2.1 for full names of each fatty acid. Refer also to Appendix D for a statistical summary of results.

5.3: Discussion

Areas of discussion follow those previously highlighted for *I. galbana* (Section 4.3) and therefore some terminology, which has already been described, may also apply herein. However, only analysis and review of data specific to *N. oculata* will be given here.

5.3.1: Growth performance

Inoculation densities between flask experiments varied from 6 to 35 × 10^6 cells/ml. During batch growth, under standard growth conditions (32 ‰ sf/2 (containing 0.10 mM $NaH_2PO_4.H_2O$) at 80 µmol/m^2/s irradiance and 23 °C), flask cultures of *N. oculata* on average achieved a maximum cell density of 182 ± 7 × 10^6 cells/ml. Batch culture growth of *N. oculata* in the photobioreactor (under similar conditions), obtained a maximum cell density of 176 × 10^6 cells/ml, which was consistent with flask experiments despite a lower inoculation density (3 × 10^6 cells/ml). Conversely, the fed-batch culture, prior to media renewal, had the lowest maximum cell density (146 × 10^6 cells/ml) and growth rate (7.31 µ/day) of the three photobioreactor runs, despite receiving the highest inoculation density (~15 × 10^6 cells/ml). By comparison, during identical conditions in the continuous culture run of the photobioreactor (again prior to media renewal), a maximum cell density of 180 × 10^6 cells/ml was reached in only 14 days (14.03 µ/day). Given that flask-grown cultures under similar conditions showed remarkably little difference with respect to their maximum cell densities (discussed above), this might suggest a degree of instability of *N. oculata* when cultivated in the photobioreactor. However, in terms of the maximum linear growth rates (i.e. time taken to reach said densities) both flask and photobioreactor cultures, under 'standard conditions', showed similar ranges (7.07 to 16.38 µ/day and 7.31 to 16.49 µ/day, respectively). The inconsistent inoculation densities (shown in Figure legends) used both within and between the flask and photobioreactor cultures may explain this variability in range, as a source of experimental error to be considered. That said, it is perhaps noteworthy to highlight that regardless of inoculation density used, linear growth rates still higher than levels reported between authors (Sukenik *et al*, 1989; Maruyama *et al*, 1986) of 0.40 – 0.90 µ/day, although both authors fail to define their growth rate calculations. In general, the cell densities achieved within this

study also compared favourably against other authors (Tonon *et al*, 2002; Sukenik 1999a; Sukenik *et al*, 1989) who typically reported cell densities below 100 × 10^6 cells/ml. Furthermore, the data herein also provides evidence that even higher cell densities can be achieved by increasing media phosphate levels (282 × 10^6 cells/ml achieved in 0.19 mM phosphate; Section 5.1.3) or by reducing growth temperature to 15 °C (369 × 10^6 cells/ml; Section 5.1.4). Yet, authors such as Cheng-Wu *et al.* (2001) and Zou *et al.* (2000) have reported "ultrahigh" cell densities of upto 1050 and 14000 × 10^6 cells/ml, respectively for *N. oculata*. The work of Zou *et al.* (2000) allows the reader to make numerous assumptions within the method, but generally refers to regularly removing cell debris and re-suspending cells into fresh media. Whilst this approach is seemingly labour intensive, there is growing evidence (Richmond *et al.*, 2003; Rodolfi *et al.*, 2003) to suggest this acts to remove "auto-inhibitory particulates of active cell division" (Richmond, 2000) thus allowing further cell growth. Time and costs of such an approach may be worth consideration for commercial-scale operations, possibly addressing potential automation of such a process to reduce labour.

In terms of mean cell size, inoculate ranged from 2.59 to 2.93 µm. All experiments showed fluctuations within the first few days of growth after which mean cell size continually increased (towards the end of the sample period reaching a maximum mean cell size in the range of between 3.10 and 3.50 µm). The only two exceptions being the results from the temperature and semi-continuous renewal experiments. By comparing growth temperatures (Section 5.1.4), from day 15 onwards, *N. oculata* grown at 30 °C decreased in mean cell size staying below 3.00 µm, whilst 25 °C cells consistently remained at ~3.10 µm. Only cultures grown at 15 and 20 °C continued to increase in cell size from day 15 onwards, reaching 3.11 and 3.50 µm, respectively. This shows that growth temperatures of between 15 to 23 °C (the 'standard' growth temperature) encourage cell growth in terms of mean cell size. Although conditions prior to media renewal (day 17) were 'standard', failed to show any increase in cell size, increases to cell size were subsequently found to be significantly proportional to dilution rate ($p = <0.02$).

5.3.2: Media renewal methods

Whilst steady-state cell densities of semi-continuous flask cultures decreased with increasing renewal rates, as a result of 'wash-out', mean cell harvest remained within $50 - 58 \times 10^9$ cells/day and PUFA harvest of 7 – 8 mg/day when maintained at 20 – 40 % (Table 7.1). However cellular harvest was highest under a media renewal regime of 10 %, at 77×10^9 cells/day, which when translated in terms yield per unit working volume of the photobioreactor (having assumed a similar 'steady-state' cell density could be maintained) would be equivalent to 11×10^8 cells/L/day.

The continuous culture of *N. oculata* grown in the photobioreactor was productive (i.e. producing harvested biomass) for 46 days (42 % of the total run time) due to problems managing population stability. At 10 - 20 % media renewal harvest volumes of 7 to 14 L per day were collected, respectively which averaged to ~9.89 L/day over periods of productivity. The total harvest volume was 455 L and consisted of 48×10^{12} cells (105×10^9 cells/L). The total DW and AFDW of the harvested cells was 348 and 287 g, respectively. Overall, the harvested volume had a mean cell density of 15 $\times 10^9$ cells/L/day or 107 mg/L/day DW (83 % AFDW) over the 110 days the photobioreactor was operated (refer to Table 7.2).

During fed-batch operation, the photobioreactor was productive (harvested) for 28 days (56 % of it's operational time) at 10 % (v/v/day) media renewal equivalent to an average daily harvest of 7 L. A total harvest volume of 196 L was produced which comprised of 31×10^{12} cells, with a DW and AFDW of 266 and 216 g, respectively. Ultimately, this resulted in a mean cell density of 16×10^9 cells/L/day and a mean biomass (DW) yield of 136 mg/L/day (81 % AFDW) from an average daily harvest (refer to Table 7.2).

5.3.3: Oxygen evolution

Comparative data for *N. oculata* in terms of oxygen evolution and photosynthetic performance is limited. The data of Fisher *et al.* (1996) was found to provide the closest comparison, although the model used to fit the P-I curve parameters varies from the method used in this study. Fisher *et al.* (1996) obtained a net P_{max} of 0.50 and 0.15 nmol $O_2/10^6$ cell for 'low-light' (30 µmol/m^2/s) and 'high-light' (650 µmol/m^2/s) adapted cells of *N. oculata*, respectively. Preliminary flask work within this study (maintained at 80 µmol/m^2/s) found net P_{max} levels to be 0.20 nmol $O_2/10^6$ cell (day 8), before falling to 0.06 nmol $O_2/10^6$ cell towards the end of the linear growth phase (day 15). Within the context of this study net P_{max} can generally be seen to decrease with increasing cell density (see Tables 5.2 and 5.9) perhaps as a result of self-shading. This can be correlated (p = *<0.02*) to an increase in I_k as cell density increases (i.e. more light required to compensate for self-shading). Yet by comparison, it can be shown that Fisher *et al.* (1996) in addition to differences in irradiance levels, also kept relatively dilute cultures (6 × 10^6 cells/ml). Therefore, it is reasonable to assume that if cell densities were adjusted accordingly, cultures of *N. oculata* from this study would be comparatively more productive in terms of net oxygen evolution. Yet I_k, when standardised per 10^6 cells, varied considerably between the results of flask and fed-batch samples, perhaps due to a difference in irradiance levels (~27 µmol/m^2/s higher for photobioreactor cultures). Since PSU numbers (associated with chlorophyll content) are known to adjust to changes in light intensity (Zou and Richmond, 2002; Fisher *et al.*, 1998) it would be more accurate to standardise I_k to chlorophyll *a* content. As shown from fed-batch samples (Table 5.10), this would suggest maintaining cultures at an irradiance of 52 ± 2 µmol/m^2/s per µg Chl *a* to maintain optimum oxygen evolution rate (α).

As cell number increases, volumetric chlorophyll *a* levels increase to compensate for the effects of self-shading. A fixed light level can therefore potentially inhibit cell division (as a function of α), as equilibrium is reached between irradiance distribution (I_{av}) and the volumetric pigment content (primarily chlorophyll *a*) of the culture. Various authors have derived mathematical models to determine light absorption efficiency by way of general 'biomass extinction co-efficients' (Gilbert, 2000; Molina Grima, 1997a; Ogbonna *et al*, 1995a; 1995b; Molina Grima, 1994a; Perez, 1994) and 'Chlorophyll *a* specific absorption coefficients' (Fisher, 1996) catalysed by the pioneering works of Bannister (1974).

5.3.4: Total lipid and FAME profile

The total lipid content of *N. oculata* was highest in cultures grown in f/2. However, in terms of lipid quality, sf/2 cultures were found to have consisted of a statistically higher proportion of PUFAs (percentage of the FAME profiles). The work of previous authors on *Nannochloropsis* has shown either PAL (26 – 38 %) (Sukenik *et al.*, 1989; Tonon *et al.*, 2002) or PML (25 – 33 %) (Hodgson *et al.*, 1991; Ben-Amotz *et al.*, 1987; Suen *et al.*, 1987; Maruyama *et al.*, 1986) to be the dominant fatty acid (when expressed as percentage total fatty acids) present in stationary growth-phase cultures. This compares favourably with the results of *N. oculata* grown in 16 ‰ f/2, which produced 30 % PML (as the dominant fatty acid). However, when *N. oculata* was cultivated in other media formulations, used in this study, EPA was found to be the dominant fatty acid during stationary growth phase (30 – 55 %). This compared best to the results of Sukenik *et al.* (1989) who found that a "growth-limiting light intensity" (35 μmol/m^2/s) resulted in 38 % EPA, whilst yields of 37 and 26 % PAL (as the dominant fatty acid) were recorded at higher irradiances of 290 and 550 μmol/m^2/s, respectively (samples were taken during late linear/ early stationary growth phase). Although no mention is given to the photoadaptive state of the inoculum used in the study of Sukenik *et al.* (1989), it can be assumed that cultures were maintained at 290 μmol/m^2/s. Indeed Hodgson *et al.* later (1991) noted that 'over illumination' resulted in photosynthetically fixed carbon being allocated towards PAL and PML synthesis. By lowering growth temperature (from 23 to 15 °C, c.f. Tables 5.7 and 5.8), in 32 ‰ sf/2 cultures of *N. oculata*, total cellular FAME accumulation was reduced but as a result of increased cell density, volumetric FAME accumulation at 15 °C was higher. Lowering temperature caused unsaturation, increasing the proportion of MUFAs. In the photobioreactor, during fed-batch growth of *N. oculata*, total lipid quadrupled (from 7 to 28 % DW) and the overall volumetric FAME more than doubled (increasing by ~55 mg/L). However, this volumetric increase was not a result of PUFA accumulation (content of which dropped by ~9 % of the total fatty acids), but instead due to increased SAT and MUFA levels (namely PAL, PML and OLE) over 30 days of fed-batch renewal. Despite this, EPA levels managed a net increase on a cellular level of ~34 fg/cell. However, on the whole EPA was found to account for only 18 % of the total fatty acids (day 50), in contrast to 29 % prior to media renewal (day 22) and the 35 % achieved in stationary-phase flask

cultures (32 ‰ sf/2) of *N. oculata*. Whilst specific lipid fractions (GL, PL and TAG - Section 1.4.1) were not analysed in this study, having re-viewed the work of other authors (see also, Section 5.3.4) with *N. oculata*, each will be discussed below to better understand their separate roles towards PUFA accumulation.

Unlike the other n-3 fatty acids found in *N. oculata*, EPA (and ARA) is known to accumulate during dark periods (Sukenik, 1991a) and is associated with cellular chlorophyll (Zou and Richmond, 2002; Zittelli *et al.*, 1999; Hodgson *et al.*, 1991; Sukenik 1991a; Sukenik *et al.*, 1989), as the main component of GL in the thylakoid (EPA alone can account for 70 % of GL, according to Hodgson *et al.* (1991). Furthermore, increasing light intensity is known to reduce PSU number (thylakoid) (Fisher *et al.*, 1998; 1996), associated GL content and ultimately cellular EPA levels during linear growth phase. Given that the results of the oxygen evolution data reveal I_o to be persistently less than I_k, it can be concluded that irradiance levels within this study were sub-optimal. This may have restricted growth in terms of cell density, yet low-light adapted cells (80 $\mu mol/m^2/s$, as cultured here) could be likely to contain more PSUs and consequently thylakoid associated GL, consisting predominantly of EPA.

PLs are integral components of cell membranes and are responsive (i.e. in FAME profile), for example, to changes in temperature with respect to maintaining membrane fluidity (Section 5.3.4). The data from this study (Tables 5.7 and 5.8, for comparison of percentage fatty acids) suggests that such changes (increasing FAME chain length), seen when the temperature was dropped by 7 °C, was primarily accomplished by synthesising LIN (12 %) from the desaturation and elongation of PAL (6 % less). Hodgson *et al.* (1991) comments that PL is predominantly composed of C18 fatty acids. Thus, the emergence of LIN coupled with higher levels of OLE (both C18 fatty acids), when *N. oculata* was grown at 15 °C, may therefore provide some evidence of PL accumulation. Although ultimately, lowering the temperature succeeded in reducing SAT concentrations within the total lipid, but failed to trigger PUFA enrichment.

Accumulation of both GL and PL (polar lipids) is known to take place during linear growth phase (Tonon *et al.*, 2002), yet the FAME profiles for the present study were derived from stationary growth phase cultures. The balance between polar and neutral lipids (TAG) has also been linked to the growth rate of *N. oculata* (Hodgson *et al.*, 1991). A slower growth rate can be attributed to nutrient limitation inhibiting cell division (due to a lack of protein synthesis), instead favouring the storage of energy into carbohydrates and lipids rather than proteins (Sukenik, 1991a) (i.e. TAG, reported to account for upto 79 % of the total lipid in *Nannochloropsis*; Suen *et al.*, 1987). Although TAGs mainly consist of C16 SATs (e.g. PAL) and MUFAs (e.g. PML) (Hodgson *et al.*, 1991), during early stationary phase, fatty acid chain length does increase over time. Indeed, Tonon *et al.* (2002) report finding 68 % (120 fg/cell) of total EPA was allocated within the TAG fraction after ~17 days of stationary phase growth. By comparison cellular EPA yields within this study ranged from 127 – 175 fg/cell after 15 days in stationary growth phase (in sf/2), perhaps indicating a similar trend. EPA is believed to build up within TAG as a result of re-directed carbon flow towards carbohydrate and lipid, under nitrate-limiting conditions and "*in the presence of light* over time" (Sukenik, 1991a). Although Tonon *et al.* (2002) recorded total fatty acid concentrations of 2000 fg/cell (more than double the maximum achieved here), EPA only contributed 9 % of the total fatty acids, compared to a minimum of 18 % within this study.

CHAPTER 6: PHOTOBIOREACTOR CHARACTERISATION

The photobioreactor used in this study was examined in order to characterise some of it's key physio-chemical parameters. The main objective was to optimise key abiotic parameters that may ultimately result in greater algal productivities. All tests were done using full strength (32 ‰) unfiltered artificial sea-water at room temperature. Details of the photobioreactor are given in Chapter 3.

Linear fluid velocity, gas-hold up, Reynolds number and mass transfer can all be collectively used to measure mixing efficiency. Characterisation of the riser dynamic is a highly subjective method of assessing bubble formations/ swarming, but does help to visualise riser behaviour, whilst Reynolds number is a means of quantifying whether flow in the riser is turbulent or laminar. Gas hold-up represents the interfacial area of gas available for mass transfer to occur.

6.1: LINEAR FLUID VELOCITY AND RISER DYNAMICS

A range of sparge plates (see Figure 3.3 for details) were compared for providing fluid flow around the photobioreactor. In addition to the effect of different configurations on linear fluid velocity, changes in riser dynamics were also recorded (Figure 6.1). It should be noted that characterisation of riser dynamics is not fully quantifiable, but is more subjective in nature.

At an air-flow rate of 5 L/min there was no significant difference in linear fluid velocity between any of the sparge plates. However, with increasing air-flow rate significant differences were observed (Figure 6.1). Ultimately, the air-flow rate was the single most statistically important factor in increasing linear fluid velocity ($p = 0.02$). Decreasing the pore size resulted in a positive correlation with linear fluid velocity independent of the number of pores ($p = <0.05$). However, altering pore density alone failed to produce a significant difference regardless of the air-flow rate employed.

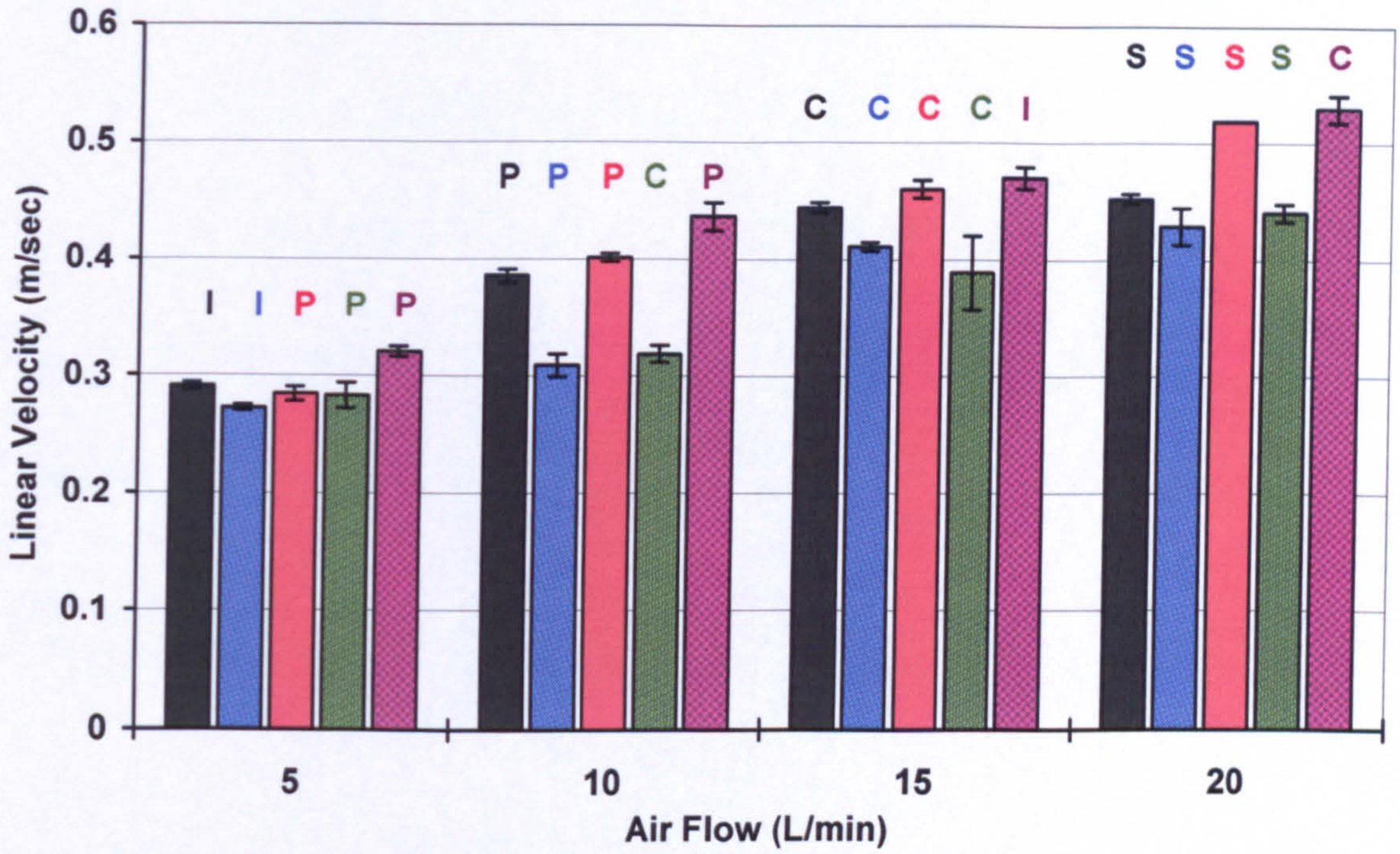

Figure 6.1: Linear fluid velocity and riser dynamics as a function of sparge plate configuration (n = 3 ± S.E.). Sparge plates of varied pore size and number (Figure 3.7); 25s; 25L; 49s; 49L; 69s were used within the photobioreactor at air-flow rates of 5, 10, 15 and 20 L/min to measure linear velocities around the coil windings. Riser dynamics (Figure 3.8) are also shown for each sparge plate and air-flow rate as I= imperfect; P= perfect, S= slug, C= churn flow. All measurements were performed using 32 ‰ artificial sea-water at room temperature.

In terms of riser dynamics, flow rates of ≥15 L/min produced either churn-turbulent or slug-flow behaviour. Plate 49L was the only sparge plate to exhibit churn-turbulent behaviour at 10 L/min, whilst all others displayed perfect-bubbly flow (Figure 6.1). Although no direct correlation could be made between riser dynamics as a result of altering pore size, overall a significant difference in riser dynamics did exist between the two pore sizes used ($p = 0.0057$). Air-flow rate was found to produce the major differences in riser dynamics, giving a highly significant relationship ($p = <0.02$). Photography of bubble formation and swarming within the riser proved difficult and instead, photographs of the header tank (Plates 8 to 11 were taken to better illustrate the effect of changing the air-flow rate. A pulsing effect was seen in the header tank as riser dynamics displayed churn-turbulent or slug-flow characteristics (see also Figure 3.8).

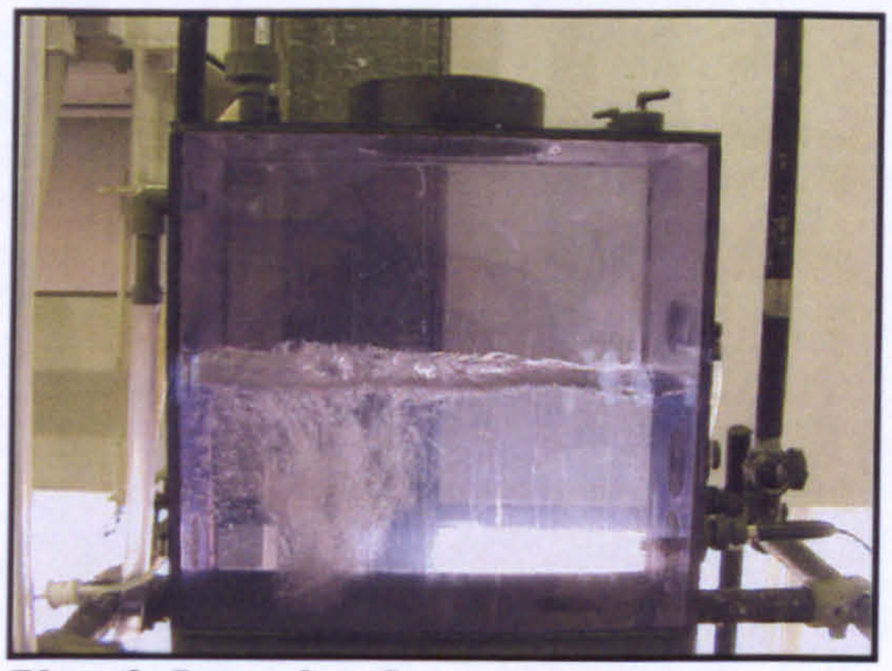

Plate 8: Imperfect flow

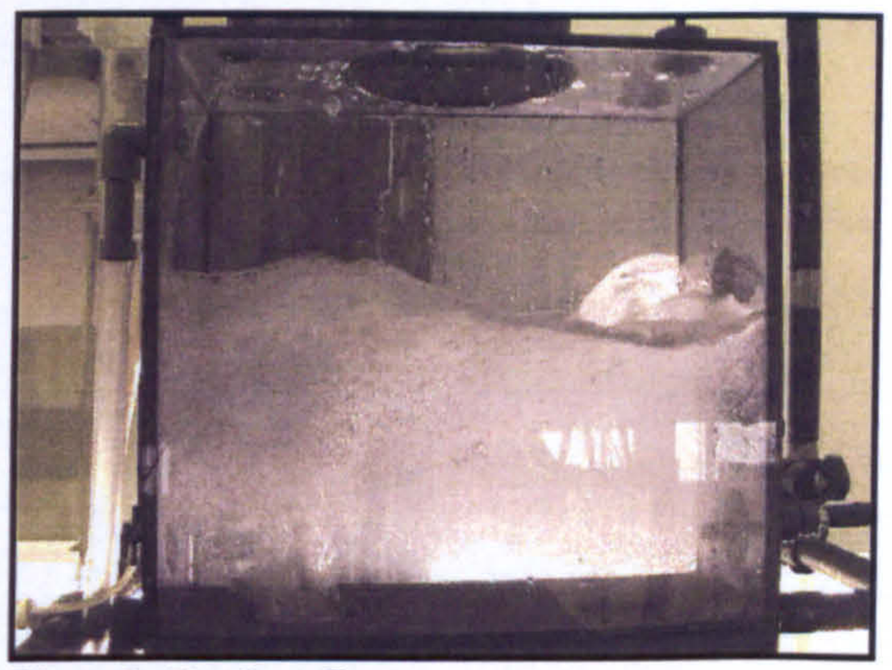

Plate 9: Perfect flow

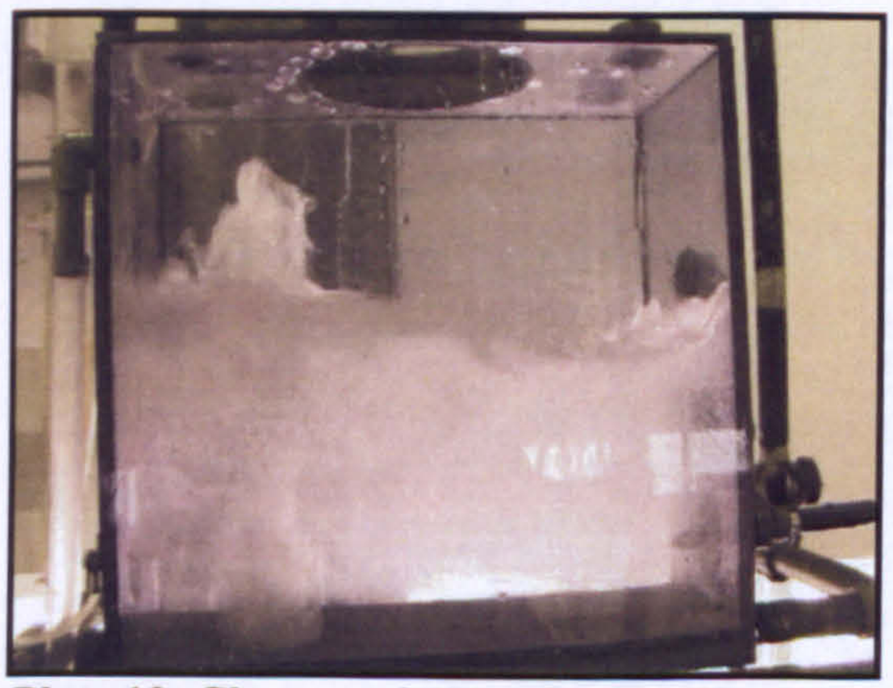

Plate 10: Churn-turbulent flow

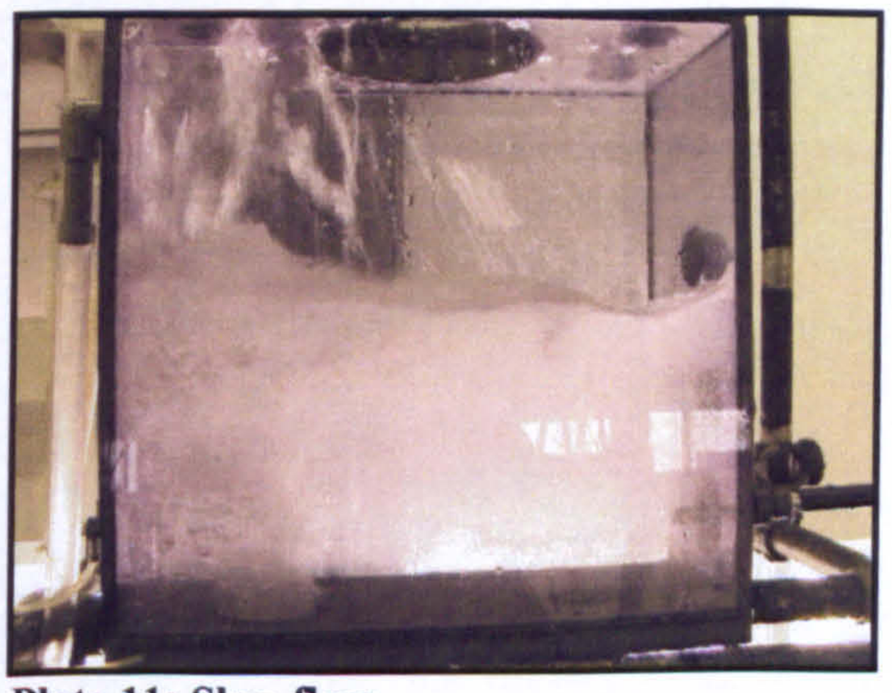

Plate 11: Slug-flow

Plates 8 – 11: Changes in fluid dynamics of header tank. Increasing air-flow rate increases fluid mixing in the header tank, becoming turbulent and pulsing. See also Figure 3.8.

Various sections of the photobioreactor can be divided into light (transparent) and dark (opaque) zones (illustrated in Table 6.1). The ratio of light to dark zones, or more specifically the time spent, accounting for distance travelled, within each can be an important with regards to light distribution (see Section 6.6.2.ii) with implications towards the photosynthetic efficiency of a culture (see Section 6.6.2.iv). Light zones included the translucent sections of the riser and header tank (accounting for ambient light), as well as the photostage. The photostage alone, accounting for 61 % of the photobioreactor's working volume (refer to Appendix C), is calculated to occupy 90 % of the cultures residence time whilst re-circulating around the system. The header tank and riser accounting for an additional 4 % due to ambient light.

Air-flow rate (L/ min)		5	10	15	20
Mean linear fluid velocity (m/ sec)		0.32	0.44	0.47	0.53
SECTION	DISTANCE (m)	MEAN RESIDENCE/ RE-CIRCULATION TIME (sec)			
(1) Riser	2.12	6.61	4.81	4.50	3.99
(2) Header tank	0.35	1.09	0.80	0.74	0.66
(3) Photostage	57.68	180.25	131.09	122.72	108.83
(4) × 2 Manifold	0.25	1.54	1.12	1.04	0.92
(5) U-bend	1.44	4.51	3.28	3.07	2.72
(6) Downcomer	1.75	5.48	3.98	3.73	3.31
Total re-circulation time:		199.48	145.08	135.80	120.43
Light zones (sections: 1, 2, 3):		187.95	136.70	127.96	113.48
Dark zones (sections: 4, 5, 6):		11.53	8.38	7.84	6.95

Table 6.1: Mean residence times around the photobioreactor (n = 3). Given the known dimensions of the photobioreactor (refer to Appendix C) and linear velocities is possible to estimate the residence time of cells within each section (defined in Section 3.1). The photobioreactor can be further divided into light and dark zones. Light zones are those sections composed of transparent materials where cultures are subjected to direct and ambient irradiance.

6.2: GAS HOLD-UP AND REYNOLDS NUMBERS

Although gas hold-up did vary between sparge plates at identical air-flow rates, differences were found to be statistically insignificant. Instead, gas hold-up in the photobioreactor was directly related to air-flow rate ($p = <0.02$).

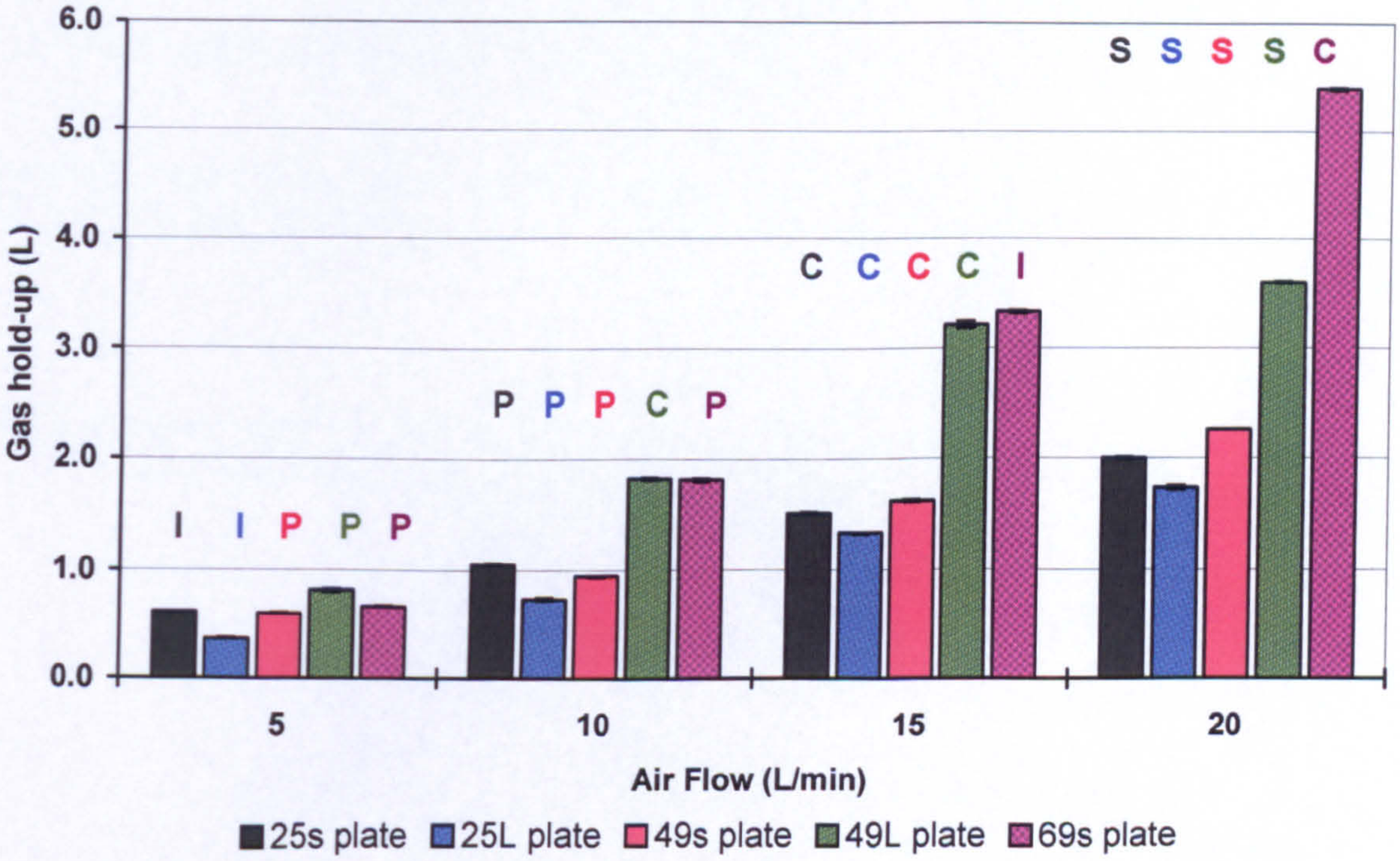

Figure 6.2: Effect of sparge plate configuration on gas hold-up (n = 3 ± S.E.). Gas hold-up was measured at air-flow rates of 5, 10, 15 and 20 L/min through each sparge plates (25s; 25L; 49s; 49L; 69s) shown in Figure 3.7. All measurements were performed using 32 ‰ artificial sea-water at room temperature. I= imperfect; P= perfect, S= slug, C= churn flow.

Flow based on the Reynolds number was defined as turbulent (i.e. >4000) regardless of each air-flow rate examined (Figure 6.3). However, differences were apparent between each sparge plate and a smaller pore size was statistically proven to increase Reynolds number ($p = <0.05$). In contrast, pore density did not alter Reynolds number significantly. Overall, the air-flow rate was found to have the greatest influence over Reynolds number ($p = <0.02$).

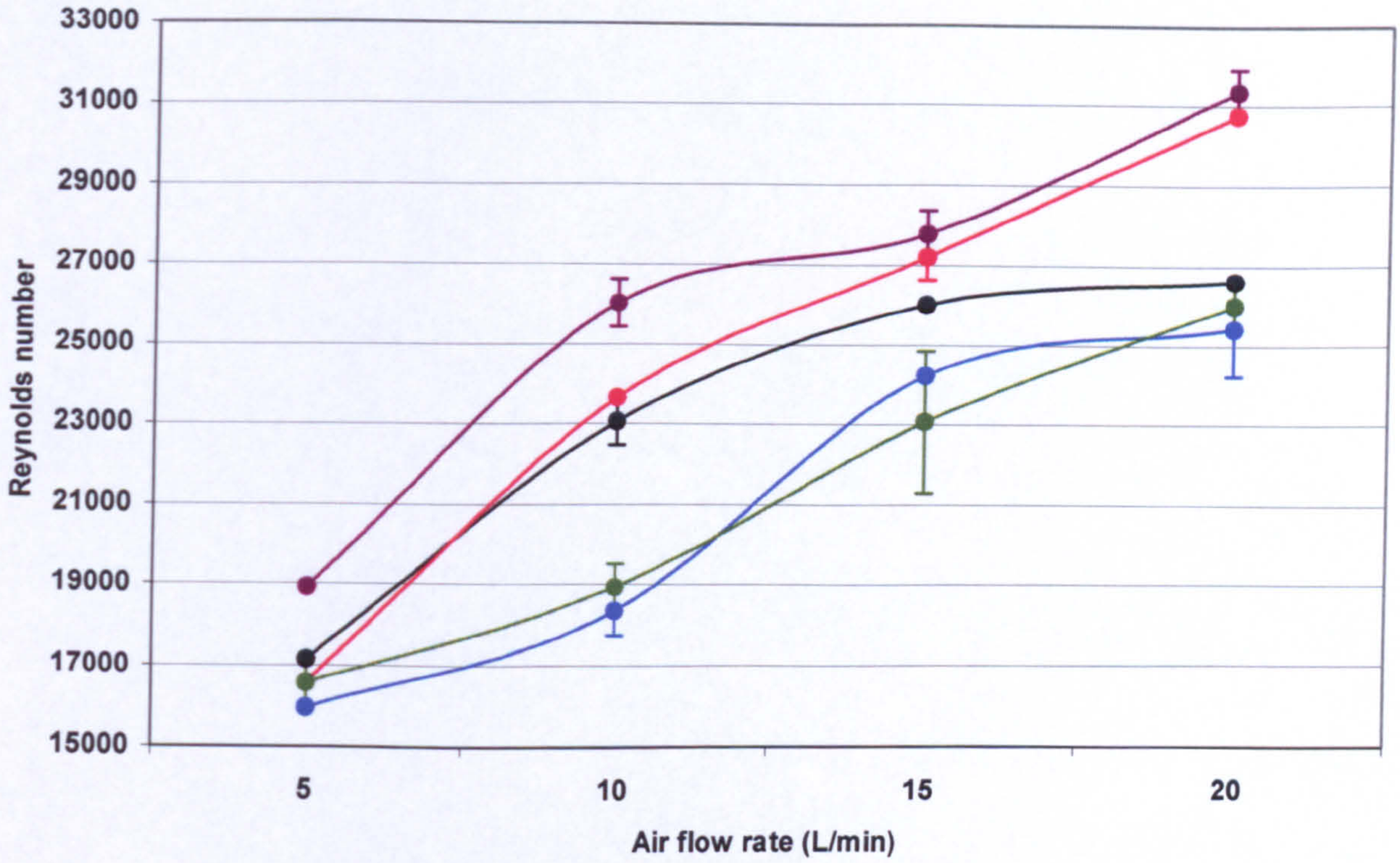

Figure 6.3: Reynolds numbers for the photobioreactor containing 32 ‰ artificial sea-water (n = 3 ± S.E.). This was determined at air-flow rates of 5, 10, 15 and 20 L/min through each sparge plate (25s; 25L; 49s; 49L; 69s) shown in Figure 3.7.

6.3: MASS TRANSFER

Mass transfer was measured in the photobioreactor for all sparge plates at air-flow rates which gave perfect riser dynamics. Perfect riser dynamics were found at an air-flow rate of 10 L/min for all sparge plates, with the exception of 49L for which this was seen at 5 L/min (Figure 6.4); this provided the lowest K_La (9.68 h^{-1}). The highest K_La values were achieved in plates with a small pore size ($p = 0.011$), reaching 19 h^{-1} (sparge plates 49s and 69s), whereas changes to pore density failed to significantly influence mass transfer. Comparison between fresh water and artificial sea-water (data not shown) was not statistically significant.

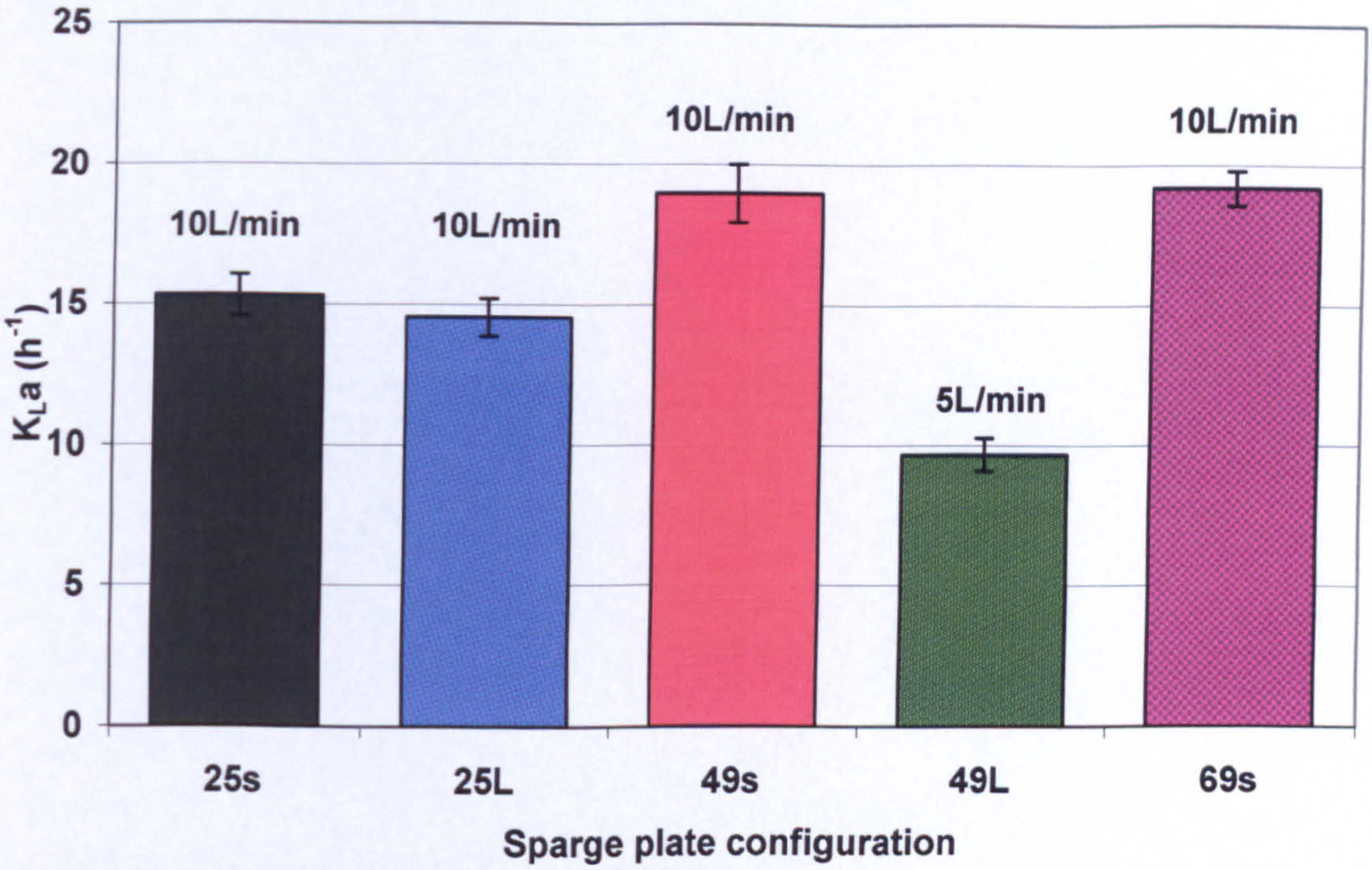

Figure 6.4: Effect of sparge plate configuration on mass transfer rate, with perfect riser dynamics (n = 3 ± S.E.). K_la was measured at an air-flow rate which gave perfect riser dynamics (labelled above each plate). Sparge plate configurations (25s; 25L; 49s; 49L; 69s) as detailed in Figure 3.7. All measurements were performed using 32 ‰ artificial sea-water at room temperature.

6.4: pH CONTROL/ CO_2 SOLUBILITY

For photosynthetic organisms CO_2 is essential for conversion of light into chemical energy. A lack of CO_2 will ultimately affect photosynthetic efficiency of the organism, in terms of producing commercially viable photochemical by-products. CO_2 is often introduced into an air feed as a supplement to aid growth of microalgae (Olaizola, 2003; Clayton, 2002; Contreras *et al.*, 1998; Watanabe and Hall, 1996; Goldman *et al.*, 1982; Markl, 1977). However, if CO_2 becomes stripped from the system before entering solution (gas-liquid transfer), the process is economically inefficient and wasteful. With this in mind, pre-selected injection points located throughout the photobioreactor (see Figure 3.6) were monitored via changes to pH in order to estimate CO_2 solubility and to determine where in the photobioreactor is the most effective site for CO_2 injection.

CO_2 injection at the sparge plate was the quickest to take effect in terms of solubility, with only a 20 sec lag (i.e. delay before a response was elicited). Yet results from this injection point were highly variable (Figure 6.5). Injection of CO_2 into the header

tank was the slowest to produce a reaction towards pH, with a lag of 90 sec (Table 6.2). This also resulted in the slowest rate of absorption. In terms of overall pH drop, CO_2 injection at the U-bend was the least effective (with an overall pH change of 0.56), despite a comparative short lag (30 sec). Injection at the base of the downcomer however resulted in a pH change of –1.68. Despite changes in pH having the second longest lag, the rate of change (reflecting CO_2 solubility) was the highest when injected at this point (-0.018/ sec), and was second in terms of reaching saturation point (no further drop on pH). Furthermore, this injection site produced the largest difference between pre and post (after 600 sec) CO_2 injection.

CO_2 injection point at: (refer to Figure 3.6)	**Mean lag (sec)**	**Max rate (pH/ sec)**	**Saturation time (sec)**	**pH difference after 600 sec**
(1) U-bend	30	-0.006	90	-0.56
(2) Sparge plate	20	-0.005	180	-1.01
(3) Header tank	90	-0.002	560	-0.90
(4) Top of downcomer	60	-0.008	210	-1.54
(5) Base of downcomer	70	-0.018	150	-1.68

Table 6.2: Summary of pH response to CO_2 injection source (n = 3). Refer to text for details. See also Figure 6.5

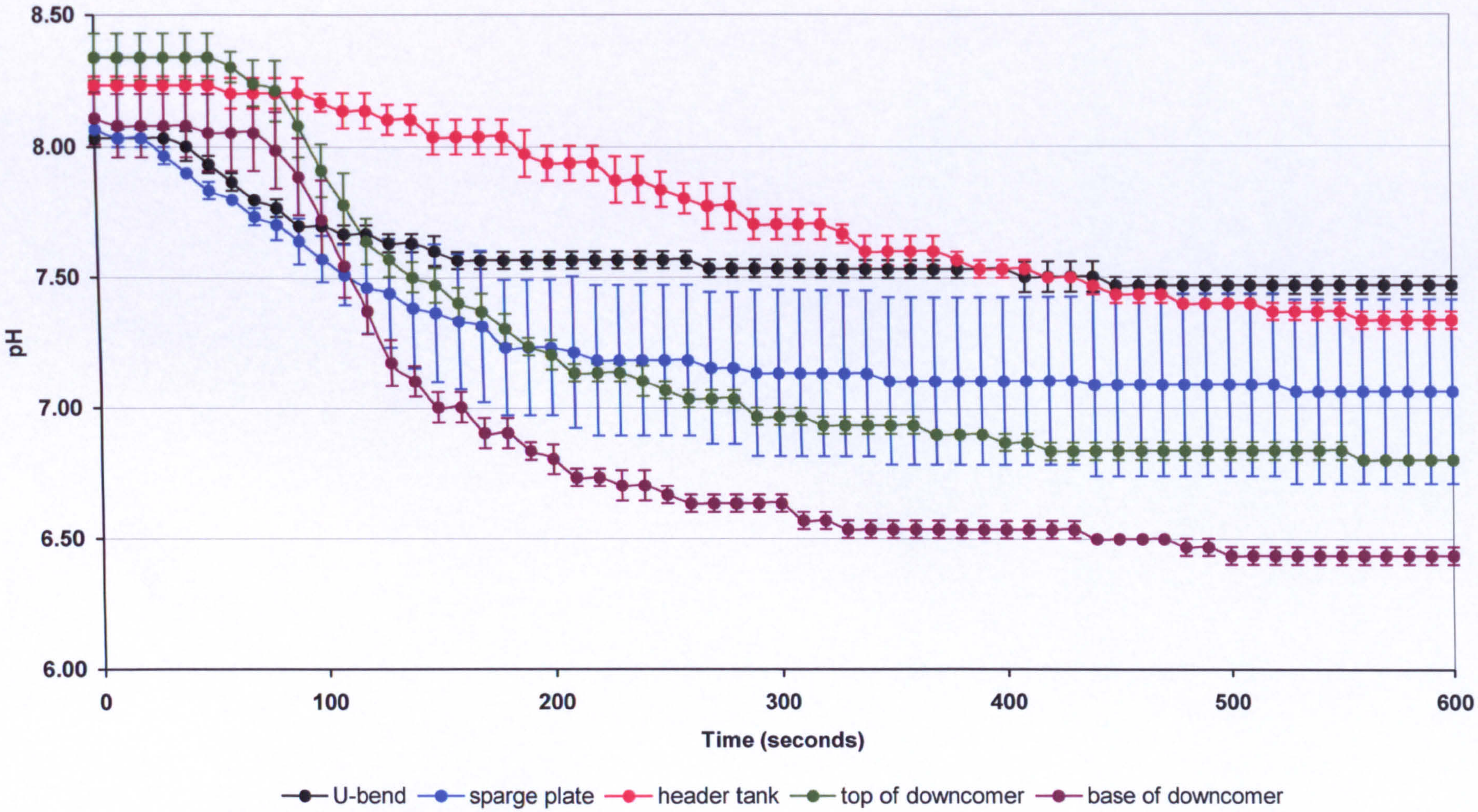

Figure 6.5: Comparison of CO_2 solubility in the photobioreactor from a range of injection points. An air-flow through the standard sparge (69s) plate was set at 15 L/min to re-circulate full strength sea-water around the photobioreactor. CO_2 was injected at a rate of 1.5 L/min at various locations (see Figure 3.6). Changes in pH were recorded every 10 seconds for 600 seconds at room temperature (n = 3 ± S.E.).

6.5: LIGHT.REGIME

Four different lighting arrangements were placed centrally within the photostage (Figure 3.2) in order to compare lighting regime in terms of the distribution of light and the overall level of irradiance provided. Light distribution became more uniform with the addition of more fluorescent tubes, which also improved the overall mean irradiance level around the photostage. The removal of light diffusing covers (B) failed to provide a significant increase to irradiance (Table 6.3) or to light distribution at the photostage (Figure 6.6). Both mean irradiance and distribution (mean deviation) improved by increasing the number of fluorescent tubes in the centre of the photostage.

Light setup	N°. Fluorescent tubes	Irradiance (µmol/m²/sec)		Mean deviation (% ±)
		Mean	Std err.	
A	8	50.13	5.24	10.45
B	8	51.48	6.49	12.61
C	12	72.17	3.58	4.96
D	16	107.33	4.25	3.96

Table 6.3: Comparison of light irradiance levels between light setups. A summary of light intensity and distribution of radiation fields shown in Figure 6.6.

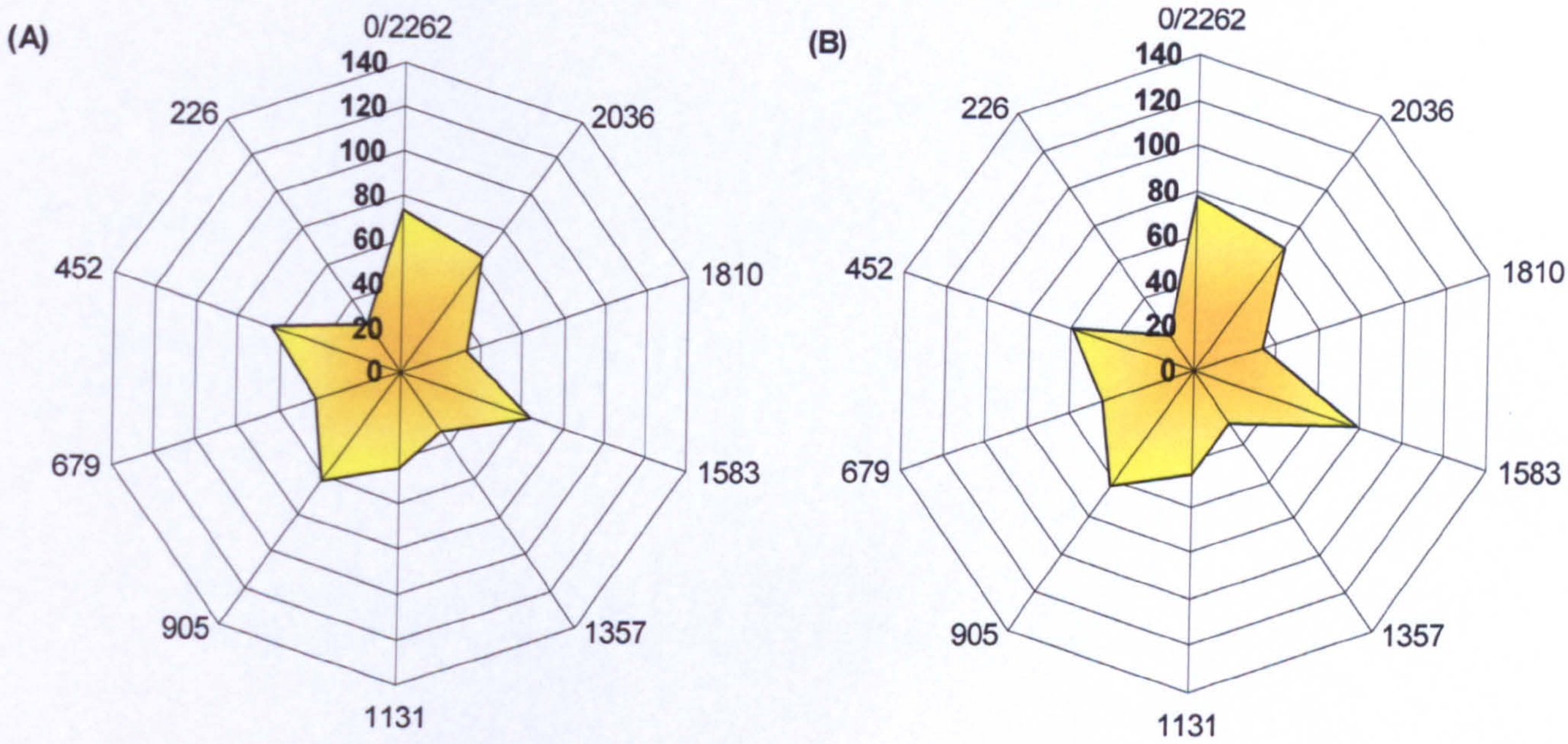

Figure 6.6: Lighting distribution graphs. A comparison of light irradiance and distribution (measurements taken from the inner circumference of the photobioreactor photostage, see Figure 3.2). (A) 8 × SYLVANIA Grow-Lux F18W (with light diffusing cover); (B) 8 × SYLVANIA Grow-Lux F18W (without light diffusing cover); (C) 8 × SYLVANIA Grow-Lux F18W (without light diffusing cover) plus 4 × OSRAM Fluora L18W; (D) 16 × SYLVANIA Grow-Lux F18W. Irradiance levels shown in **bold**.

6.6: DISCUSSION

6.6.1: Mixing efficiency

Provided the air-flow rate was ≥10 L/min, linear fluid velocity in the photobioreactor photostage was over 30 m/sec which is sufficient to prevent sedimentation in microalgal cultures (Hall *et al.*, 2002; Hebrard *et al.*, 1996; Fredrickson and Tsuchiya, 1970). Although air-flow rate was the primary factor, reducing the pore size statistically increased linear fluid velocity ($p = <0.05$, Figure 6.1). Based upon the riser dynamics, it was found that air-flow rates >10 L/min (regardless of the sparge plate used) caused fluid flow to become highly erratic (Plates 10 and 11). Reynolds numbers (Figure 6.3) showed turbulent flow behaviour in the riser regardless of air-flow rate or riser dynamics, although sparge plates with smaller pore size were seen to be advantageous. Slug flow led to pulsing within the riser, and a volatile behaviour (energy dissipation) became evident in the header tank. Overall, gas-hold up was directly related to air-flow rate, with changes to sparge plate configuration yielding no statistical differences or trends. Gas hold-up within the header tank is a cumulative result of mean bubble size, a parameter not measured in this study.

For photosynthetic cultures, once growth reaches a light saturated point, further growth becomes limited by CO_2 (Rorrer and Mullikin, 1999). Since it is known that a linear relationship exists between productivity and K_La in microalgal cultures (Fregapane *et al.*, 1999), maximising mass transfer is of commercial interest. Although mass transfer was measured here using dissolved O_2 levels, these results are easily converted to dissolved CO_2 by multiplying K_La by 0.98 (Contreras *et al.*, 1998). Rorrer and Mullikin (1999) define a K_La of 2.5 Hr to be growth limiting for photosynthetic cultures. Results herein gave mean K_La values of 9-18 Hr under 'perfectly bubbly' riser dynamic conditions. Furthermore, mass transfer rates were higher than reported by Hall *et al.* (2002) who adopted a similar design (14.4 Hr). The main geometric factor affecting mass transfer in airlift systems is thought to be the cross sectional area ratio of the downcomer to the riser column, Ad:Ar (Fraser *et al.*, 1994). A high ratio would typically indicate poor gas hold-up and K_La, because the flow rate in riser would be too fast to allow sufficient time for gaseous transfer (Bello *et al.*, 1985). Whilst a small Ad:Ar results in a low liquid velocity, thus increasing

bubble residence time in riser (Fraser *et al.*, 1994; Merchuk, 1990; Chisti *et al.*, 1988). The ratio of Ad:Ar in the photobioreactor used in this study (0.82) is higher than those reported for other external loop ALRs (0.00; 0.00; 0.11; 0.43 and 0.54 for Fernandez *et al.*, 2001; Benyahia and Jones, 1997; Bello *et al.*, 1985; Fraser *et al.*, 1994 and Dhauadi *et al.*, 1997, respectively), which all achieved higher mass transfer rates. It should also be noted that values vary depending upon the location of the dissolved oxygen probe (Benyahia and Jones, 1997). The probe used in this study was located at the top of the downcomer to prevent bubble adhesion from the riser. This also gave a closer representation of oxygen (and consequently CO_2) flowing towards the photostage, and not stripped or vented from the header tank as a result of bubble breakage.

Ultimately, mass transfer is largely dependent upon the convective mechanisms of hydrodynamic flow, associated with turbulent eddy flow. This implies the existence of adjacent parallel flow patterns at different velocities (Acheson, 1990). The spatial gradient of velocities between two streams of flow is called the shear rate. Whilst shear rate contributes towards convective mixing of the culture volume, it can however, physically inhibit growth due to cellular damage (Merchuk, 1988). This may become apparent by signs of foaming in the header tank (Eriksen *et al.*, 1998). Thus an optimum shear limit, and consequently mass transfer rate, for a given vessel, must exist for a given culture dependent upon the resistance of the cell, mechanical forces and the extent of deformation (morphology) cells can withstand without inhibiting productivity. Shear forces within bubble columns or airlift reactors are attributed to both (a) hydrodynamic forces generated at the sparger and within the riser, and (b) the interfacial area (bubble-cell interaction) as a result of bubble breakage and coalescence along the riser and at air-medium interfaces (hydrostatic pressure gradients within the header tank) (Contreras *et al.*, 1998). Although the difference between the two pore sizes used in the construction of sparge plates for this study was only 1 mm, this did provide significant differences in the physical performance of the photobioreactor as a result of changes in bubble formation. Within the literature there is some divide as to the definition of 'small' and 'large' bubbles (Merchuk and Berzin, 1995). 'Small bubbles' have greater surface tension and will exert more force upon breakup, making them potentially damaging to fragile cells (i.e. lacking cell walls) resulting in foaming. Yet, they have a smaller surface

area and will therefore collect fewer cells than 'large bubbles' and also have a lower probability of coalescing within the riser (Michaels *et al.*, 1996). Eriksen *et al.* (1998) concluded that 'small bubbles' (<1 mm) are more efficient than 'large bubbles' (5 - 15 mm) for mass transfer because a larger surface area to volume ratio aids diffusion.

With regards to additional CO_2 enrichment to regulate pH, the site of injection in the photobioreactor showed considerable variation in terms of effect. CO_2 injection at the U-bend, as featured in growth of both *I. galbana* (Section 4.2) and *N. oculata* (Section 5.2), despite having a short lag period in terms of response time, overall failed to significantly reduce pH when compared to other injection sites. Since pH drift is known to occur (becoming more alkaline) with increased cell densities, this can eventually inhibit cell division (Liu and Lin, 2001; Sanchez *et al.*, 2000; Molina Grima *et al.*, 1994c; Perez, 1994; Molina Grima *et al.*, 1992) and therefore counteractive measures (increasing acidity) may extend cell growth. Injection at the base of the downcomer was found to be the most efficient location for CO_2 injection and it is recommended that this may help further improve cell densities of future cultures grown in the photobioreactor.

6.6.2: Lighting regime

The provision of incident irradiance, it's cellular absorption and subsequent metabolic conversion has been reported by countless researchers over the past century and quantified by numerous hypothetical, theoretical and mathematical equations and models. Analysis of a photobioreactor's lighting regime should focus upon four key areas:

(i) Light source (artificial or natural)
(ii) Light distribution/ radiation field
(iii) Light absorption
(iv) Photosynthetic efficiency

6.6.2.i: Artificial light sources

The economical optimisation of efficient lighting is perhaps the most inhibiting factor preventing commercial scale-up of photobioreactors. This is mainly due to the energy requirements of using artificial lighting alone. Other critical, culture specific, factors such as light quality, quantity and latent heat production must also be considered and are all dependent upon the method of lighting (i.e. natural and externally or internally artificial).

Fluorescent tubes are the common light source of choice amongst algologists when designing indoor photobioreactors. Indeed, not only have fluorescent lights proved themselves economically they are also available in a range of spectral quality combined with relatively low heat production. Unfortunately fluorescent lighting is limited in terms of the level of light quantity (irradiance) they can provide individually and despite a potential lifespan of years, the spectral quality of fluorescents can become substantially diminished after only six months, and should ideally be replaced regularly (an added cost). A range of fluorescents were initially examined and two were used during the course of this study (floura and grow-lux) based upon both spectral quality (as given by suppliers catalogues) and the actual growth response of cultures (data not shown). It has been established, during the course of this study (refer to Sections 4.3.3 and 5.3.3), that cultures may have become 'low-light adapted' (photo-adaptation) as a result of low irradiance levels reaching the

culture surface, indicating that cultures are not maximising potential photosynthetic efficiencies, with growth (cell density) becoming light-limited. Therefore adjusting light levels to suit cell density or more specifically chlorophyll *a* levels, may generate further cell growth. Whilst a range of 'high-powered light sources' (such as metal halides and tungsten halogen lamps) do exist and have been used to overcome problems of self-shading in dense micro-algal cultures, such light sources typically require more energy (Wattage). Furthermore, they generate high levels of convective heat, which can cause cultures to overheat, requiring additional thermostats or cooling systems to maintain optimum growth temperatures. The introduction of fibre-optic technology has allowed for in-direct use of high-powered light sources, since a larger surface area : volume ratio means heat can dissipate along the length of the fibre. Indeed, this technology has been used by some researchers (Duerr, *et al.* 1998; Pulz, and Scheibenbogen 1998; McStay, *et al.* 1995; Pulz, *et al.* 1995; Mori, 1986), albeit with limited success since the irradiance from fibre-optics has an extremely directional and narrow radiation field, coupled with a degree of light diffusion and refraction (loss) along the length of the fibre. More recently however, there has been growing interest in the use of light emitting diodes (LEDs), specifically by algologists over the last decade, since LEDs are relatively cheap, have low energy requirements and produce little heat. LEDs are fabricated from layers of compounds, which can be varied to an extent to alter light quality, quantity and efficiency. Although early LEDs have been used to achieve irradiance levels of 900 $\mu mol/m^2/sec$ (Lee and Palsson, 1994a), these only provided an optimum wavelength of 680 nm, with a 30 nm bandwidth (red part of the visible spectrum- refer to Figure 1.10). More recent advances in LED fabrication have resulted in white light-emitting diodes with spectral wavelengths near identical to PAR, as required by photosynthetic organisms (Mazzeo *et al.*, 2002; Ho *et al.*, 2001; Schlotter *et al.*, 1999; Nakamura, 1997). The major attraction is the energetic saving made from using LEDs, and Kim *et al.* (1996) report illuminating a plate-type photobioreactor with 352 LEDs, at an energetic cost of only 6.6 Watts. Such efficiency would be a major commercial benefit in reducing overhead costs of maintaining artificially illuminated photobioreactors.

6.6.2.ii: Light distribution/ radiation field

Secondary factors such as light absorption (see Section 6.6.2.iii), reflection, and refraction (leading to loss of photon energy) as a result of the geometry between the light source and the photostage surface, must also be considered in the photobioreactor design. By centralising the light source within a coiled photostage, the geometry of the photostage featured here was aimed primarily to reduce reflection/ refraction, although the transverse curvature of the tubing used may account for refraction to a degree. However, the main barrier to light distribution at the photostage was the stainless steel mesh used to support the coil windings of the photostage. When calculated (data not shown) this was found to occupy ~12 % of the photostage's surface area, and did affect measurements (blocking light path) when taken at equidistant points around the inner circumference of the photostage. Whilst internally illuminated photobioreactors may overcome such issues, they remain hindered by design limitations in terms of overheating cultures (although some designs also incorporate cooling jackets for lighting inserts) and reducing culture volume (Ogbonna, *et al.* 1999). Biofouling (as shown in Plate 7), which applies to both internally and externally illuminated photobioreactors, is another factor preventing light distribution to cultures, although this may be species specific (so-called 'sticky algae', as discussed in Section 4.3.1). Indeed, biofiouling was evident during this study in *I. galbana* but not *N. oculata.*

In addition to considering the physical attributes of a photobioreactor (to maximise I_o at the culture surface), light distribution should also be considered within the culture volume itself. Aside from direct measurements (from internal light probes), many researchers have attempted to mathematically model the effects of cell density or biomass on light distribution. A majority of mathematical models account for the effects of Lambert-Beer's law to describe light distribution/ radiation fields, which assumes that: (1) the direction of incident radiation remains unchanged as it crosses through the culture; (2) the radiation is monochromatic; (3) scattering effect due to solid particles is negligible compared to absorption. As predicted by Lambert-Beer's law, light attenuation by cells generates gradients of light at any given point (I_p) within a culture. In a homogenously mixed culture the average irradiance (I_{av}) is a mean of the I_p found in every element of the culture volume (Molina Grima *et al.*, 1994a and Perez, 1994). However, Fernandez *et al.* (1997) comments that whilst this

may fit experimental data at low cell concentrations, deviations at higher cell densities may be the result of differential absorption and/ or scattering. *Mono-dimensional* model, such as that used by Fernandez *et al.* (1997) assumes the light field remains isotropic throughout the whole culture and that light absorption (E_a) and light scattering (E_s) are independent. Bi-dimensional models of light distribution (*2-D radiation field*) based upon Lambert-Beer's law have also been proposed (Molina Grima *et al.*, 1996; 1994a), and assume the photobioreactor is cylindrical and evenly illuminated from all sides. From this Molina Grima *et al.* (1996) also went on to derived equations to express *3-D radiation fields* use radial and axial co-ordinates, to define the angular influx of photons emitted by a light source to a specific point within the photobioreactor. Such 3-D models are commonly used to predict culture behaviour in outdoor environments to account for the effects of the Earth's rotation in relation to the sun (Molina Grima *et al.*, 2001). However such equations become limited when the emitting radiation field is on the culture surface, or ambient if measuring light (no defined light source to measure distance). Meanwhile, Ogbonna and co-workers theory (1995b) for light distribution (the light supply coefficient, Kiv) is based upon the critical light intensity (I_c) required for cell growth. This being the irradiance at which respiration breaks even, inhibiting cell growth (on a P-I curve this would be the irradiance at which oxygen evolution is 0- see Figure 2.3). By taking into account the biomass extinction coefficient (Ogbonna *et al.*, 1995a), cell density and photostage geometry, Kiv acts as an index to measure the point at which self-shading results in half the illuminated culture volume reaches I_c,.

6.6.2.iii: Light absorption

Subsequent analysis of the tubing used in the coil windings (data not shown) also revealed that 32 % (n = 12) of irradiance (I_o) was absorbed across the cross-section of the photostage windings (difference between irradiances measured at I_o and externally opposing wall- 30 mm), when the system was filled with filtered water. Thus approximately a third of irradiance (~36 μmol/m^2/sec) was lost to absorption by the material (foodgrade PVC-U). Therefore, for commercial scale operations such detail regarding photostage fabrication (in addition to geometry, discussed above) would be a prudent consideration in terms of further maximising the efficiency of a chosen light source. This appears to be an area that has been neglected by algologists in general, focusing primarily upon light absorption within the culture volume.

Bannister and Weidemann (1984 and Bannister, 1974) first determined that the incident irradiation (I_o) at a cultures surface becomes absorbed/ extinguished by particulate matter (K_w, abiotic absorption coefficient) and organic matter (K_c, biotic extinction coefficient otherwise termed the phytoplankton extinction coefficient). K_c was described as chlorophyll-specific/ dependent, yet this was non-species specific and was erroneously assumed to be constant, until it was recognised that a more dynamic theory was needed. This later became termed the biomass absorption coefficient (K_a), which considers both pigment and non-pigment absorption of light by cells with values for *I. galbana* being reported between 0.18 and 1.76 g/m^2 (Molina Grima *et al.*, 1997a; 1994a; Perez, 1994). Particular focus has been drawn towards the chlorophyll content of cells, from which Fisher *et al.* (1996) derived the chlorophyll *a* specific *in vivo* absorption coefficient (a^*). This accounts for the size and geometry of the cell as well as it's chlorophyll content, with an increase in cellular chlorophyll typically resulting in a decrease of a^*.

6.6.2.iv: Photosynthetic efficiency

Ultimately, once a cell has absorbed light energy it must then undergo photosynthesis, from which chemical energy is used to drive the cells metabolism. It is estimated that 1 nmol of chlorophyll can produce 50 - 400 nmol of oxygen per hour (Lee and Palsson, 1994a). The rate at which carbon is photosynthetically fixed and oxygen produced (α) is reflected by changes to cell growth and division (Henley, 1993; Herzig and Dubinsky, 1992).

The volumetric efficiency of this process is dependent upon the photoadaptive state of cells (a^*), cell density (K_a), average irradiance per cell (I_{av}) and dissolved CO_2 (K_La) within the medium. Furthermore, sufficient time should be allowed to excite the reaction centres of PSI and PSII and allow them to return their ground states, to prevent cellular damage. This principle can also be applied as a valuable consideration to be made in designing a photobioreactor. Although lighting within this study was supplied continuously, cultures within the photobioreactor would have been subjected to a 'flashing light effect' whilst re-circulating between light and dark zones (refer to Figure 6.1). The frequency of which, is referred to as the light intermittency period (Fredrickson and Tsuchiya, 1970) and can significantly influence a culture's photosynthetic efficiency (Richmond *et al.*, 2003; Clayton, 2002), ultimately affecting chemical energy availability for active cell division. Even individual cells within the photostage will still experience a degree of light intermittency (on the scale of milli-seconds) due to the effects of self-shading. Therefore it can be argued that changing the ratio of light to dark zones (by both time and/ or frequency) experienced by cells, can affect photosynthetic efficiency in terms of excitation and recovery times of chlorophyll *a* reaction centres. Degen *et al.* (2001) claimed that volumetric productivity could be enhanced if culture cycled between light to dark zones at a ratio of 1:10. Further investigation into such minor alterations may therefore prove extremely cost effective.

CHAPTER 7: DISCUSSION AND CONCLUSIONS

7.1: CULTURE COMPARISONS BETWEEN *I. GALBANA* AND *N. OCULATA*

7.1.1: Growth performance

The performance of *I. galbana* proved to be generally unpredictable, in terms of growth rates and cell densities achieved during identical growth conditions between experiments. Furthermore, the *Isochrysis sp.* used within this study when compared with previous authors cannot be clearly defined as either *I. galbana* or 'T.iso' (see Section 1.5.1). However, it has also been noted that such discrepancies may be due to a high degree of clonal variation within the species (Tzovenis *et al.*, 1997), which may prove to be advantageous towards possible mutagenesis research in future studies (Qi *et al.*, 2003; 2002). When *I. galbana* was grown within the photobioreactor, 'biofouling' was often seen to accumulate in the coil windings (refer to Section 4.3.1). While this did not appear to be the case for *N. oculata*, it is reportedly said to be prone to "excessive exudation and cell aggregation" under high irradiances (Zittelli *et al.*, 1999). However, relatively low light levels were used here. *N. oculata* is also reported by other authors as secreting auto-inhibitory particles into the media as a by-product of active cell division (Richmond *et al.*, 2003; Rodolfi *et al.*, 2003).

Preliminary incubator experiments had shown *I. galbana* to favour a growth temperature of 20 °C and *N. oculata* 15 °C. However, photobioreactor cultures of both were maintained at 23 °C in consideration of other algal species (not investigated in this study) kept in the 'growth room' and was seen as a 'happy medium' (c.f. Figures 4.5 and 5.5). During batch operation of the photobioreactor, mean cell density of *I. galbana* had increased by 24 % over flask cultures under similar conditions. Whereas, the initial batch run of *N. oculata* in the photobioreactor remained within the typical range of 161 – 203 × 10^6 cells/ml seen in earlier flask experiments.

Growth performance of *I. galbana* during continuous culture was initially superior to that of semi-continuous flask cultures (Section 4.1.5) for the same daily renewal rate, before suffering from a rapid decrease in cell density. Despite this, the culture did show a brief but positive sign of its ability to recover, following a 14 % (10 L) semi-continuous replenishment of fresh media. This may be evidence of auto-inhibitory

products of active cell growth, as has been suggested for *N. oculata* (Rodolfi *et al.*, 2003). Meanwhile, *N. oculata* under 10 % continuous media renewal in the photobioreactor produced a generally erratic response. Furthermore, following the decision to double the daily renewal rate, the culture never truly recovered stability. Perhaps if maintained at 10 % daily renewal throughout cell density would have risen further and possibly have reached a steady-state. Yet despite this, cellular dry weight and cell size (to an extent) did increase throughout. Unfortunately without total lipid or FAME analysis for this run, it can only be speculatively suggested that this increase in cell mass was the result of lipid accumulation.

Although there was a persistent loss in cell number during fed-batch production, the mean cell size of *I. galbana*, increased by 1.33 µm and cellular dry weight by 50.88 ng/cell. The opposite was true of *N. oculata*, with mean cell size dropping by 0.25 µm with only negligible changes to cellular dry weight (-0.005 ng/cell) during fed-batch mode. Of the two cultures, *N. oculata* typically achieved higher cell densities but despite this *I. galbana* comparatively maintained the higher levels of chlorophyll *a* per unit volume throughout fed-batch media renewal (10.07, c.f. 7.68 µg/ml, on average). Whilst average oxygen evolution on a cellular level, during fed-batch, was therefore higher in *I. galbana* (1.56, c.f. 0.4 nmol $O_2/10^6$ cell), *N. oculata* on average produced more oxygen per unit chlorophyll *a* (6.92, c.f. 3.50 nmol O_2/µg Chl *a*) under similar conditions (i.e. higher photosynthetic capacity, P_{max}). Despite a steady loss in cell number during 10 % fed-batch growth, the DW of *I. galbana* remained between 0.79 and 1.13 g/L. *N. oculata* by comparison, for the most part of identical fed-batch conditions, maintained biomass levels in the region of 1.3 to 1.5 g/L DW.

Regarding the balance between irradiance levels and impact upon cell density. The terms low-light and high-light regimes are relative to the current photoadaptive state of a culture, and is often a source of confusion between authors. There is evidence that low-light adapted cultures are regarded as being more photosynthetically efficient. Subsequently, this results in an increase in either PSU size or number (two strategies which vary between species). Therefore, from reviewing the data of other authors, in theory maintenance of low-light conditions aids photosynthetic efficiency, increasing GL (contributing towards total lipid, and possibly PUFA) could be commercially more desirable by reducing overheads (using less energy on lighting).

7.1.2: FAME profiles and productivities

Comparison between the initial flask experiments of both *I. galbana* and *N. oculata* (Sections 4.1.7 and 5.1.7, respectively) shows that *N. oculata* on average yielded 24 % more total lipid than *I. galbana*. In terms of mean volumetric yield, *N. oculata* also generally accumulated 40 % more total FAME, however when expressed as a proportion of total volumetric FAME, PUFA was marginally higher (8 %) in *I. galbana*. From an individual cell perspective, both total FAME and PUFA were significantly higher (306 % and 480 %, respectively) in *I. galbana*, when mean values are compared. This might well be explained by the fact that on the whole mean cell size and consequently cell volume of *I. galbana* was the larger of the two algae. Despite the relatively poor cellular accumulation in *N. oculata*, similar volumetric yields can be accounted for due to the significantly higher cell densities achieved over *I. galbana*. The total FAME profile of *N. oculata* flask cultures, on average, consisted predominantly (37 % of total FAME) of EPA (the sole n-3 PUFA detected in this species), which was altogether undetected in *I. galbana*. *I. galbana* was also found to lack any n-6 PUFAs, whereas in *N. oculata* the only n-6 PUFA detected was ARA (with a mean contribution of 3 % of total FAME), but was present only in full-strength artificial sea-water. The dominant n-3 PUFA in *I. galbana* was OTA (30 % of total FAME), which was conversely absent from *N. oculata*. DHA in *I. galbana* provided the second highest concentration of n-3 PUFAs in this species (contributed, on average, 18 % of total FAME), but was altogether lacking from *N. oculata*.

The data obtained from these FAME profiles was combined with earlier results of the media renewal experiments for both *I. galbana* and *N. oculata* (Table 4.7 with Figure 54.7 and Table 5.7 with Figure 5.7, respectively), in an effort to project potential productivities of the larger working volume (70 L) of the photobioreactor (see Table 7.1) from small scale flask experiments. On average, general PUFA accumulation is shown to be higher from *I. galbana* cultures. Despite 'steady-state' cell densities of *I. galbana* being inversely proportional to renewal rates, Table 7.1 shows less than 8 mg/day difference in DHA production between 10 and 30 % media renewal rates. By comparison, EPA productivity in *N. oculata* would typically vary by 29 mg/day. Media renewal rates greater than 10 % greatly affected 'steady-state' cell densities in *N. oculata*. Whilst 'steady-state' cell growth of *I. galbana* would appear to favour a renewal rate of 10 %, the loss in cell density at 20 % media renewal is justified in terms of harvested cells and subsequent PUFA productivity. Meanwhile, it is

suggested that *N. oculata* would be more productive at 10 % media renewal. Although this would half the harvest volume, compared to *I. galbana* at 20 % media renewal, overall PUFA productivity would be only 16 mg/day lower. Furthermore, in comparison to DHA productivity from *I. galbana*, *N. oculata* would produce 2.5 times more EPA.

		Media renewal rate (% v/v/day): *Semi-continuous flask model*							
		I. galbana				*N. oculata*			
		10	20	30	40	10	20	30	40
Data derived from results of Sections 4.1.5 and 5.1.5	Daily harvest (L) based on 70L working volume	7	14	21	28	7	14	21	28
	Mean 'steady-state' cell density ($\times 10^9$ cells/L)	2.35 ± 0.20	1.46 ± 0.21	0.88 ± 0.15	0.32 ± 0.10	11.00 ± 1.50	3.80 ± 0.20	2.75 ± 0.45	1.80 ± 0.20
	Mean daily cell harvest ($\times 10^9$ cells/day)	16.45 ± 1.40	20.44 ± 2.94	18.48 ± 3.15	8.96 ± 2.80	77.00 ± 10.50	53.20 ± 2.80	57.75 ± 9.45	50.40 ± 5.60
	Mean volumetric cell yield ($\times 10^8$ cells/L/day)	2.35 ± 0.20	2.92 ± 0.42	2.64 ± 0.45	1.28 ± 0.40	11.00 ± 1.50	7.60 ± 0.40	8.25 ± 1.35	7.20 ± 0.80
Data calculated from above and cellular yields from 32 ‰ sf/2 batch cultures (Section 4.1.7 and 5.1.7)	Mean daily total FAME harvest (mg/day)	29.17 ± 2.48	36.24 ± 5.21	19.68 ± 5.59	9.54 ± 4.97	26.52 ± 3.62	18.32 ± 0.96	19.89 ± 3.26	17.36 ± 1.93
	Mean daily PUFA harvest (mg/day)	16.63 ± 1.41	20.66 ± 2.97	18.68 ± 3.18	9.06 ± 2.83	11.08 ± 1.51	7.65 ± 0.40	8.31 ± 1.36	7.25 ± 0.81
	Mean daily DHA / EPA harvest (mg/day)	6.24 ± 0.53	7.76 ± 1.12	7.02 ± 1.20	3.40 ± 1.06	9.41 ± 1.28	6.50 ± 0.34	7.05 ± 1.15	6.16 ± 0.68
	Mean volumetric DHA / EPA yield (µg/L/day)	89.14 ± 7.57	110.86 ± 16.00	100.29 ± 17.14	48.59 ± 15.04	134.43 ± 18.29	92.86 ± 4.86	100.71 ± 16.43	88.00 ± 9.71

Table 7.1: Projected productivities of *I. galbana* and *N. oculata* in a 70L tubular photobioreactor based on results of flask data. Assumes that cultures grown in a tubular photobioreactor will reach identical cell densities and FAME profiles as flask cultures. Mean values derived from cellular FAME yields (Tables 4.7 and 5.7), *assuming profile remained constant regardless of media renewal rate.*

The productivity *estimates* derived from flask experiments (Table 7.1, above) provide a useful 'bench-mark' with which to compare PUFA productivities of the photobioreactor (Table 7.2, below), used in the later half of this study. Total lipid and FAME analysis for photobioreactor-grown cultures was only provided for fed-batch runs; therefore the values shown in Table 7.2 for continuous cultures were again estimated (from fed-batch results) to make relative comparisons. From which it can be seen that productivities of photobioreactor cultures (both *I. galbana* and *N. oculata*) were overall higher, in terms of total PUFA accumulation (both volumetric and cellular) and PUFA enrichment (specifically DHA or EPA), than estimated from flask results. This may possibly be attributed towards the physical characteristics of the photobioreactor (discussed in Section 7.2).

I. galbana when cultivated in the photobioreactor yielded a three-fold increase in total cellular lipid accumulation over 50 days of fed-batch media renewal, reaching 4.18 pg/cell. However, decreases in cell density lead to a cumulative volumetric loss of 14 mg/L total lipid for this period. Whilst this also resulted in net loss in total FAME content per unit volume, cellular content had risen by ~45 % which was attributed to PUFAs in general (~7 % increase of total FAME), but not DHA (refer to Table 4.12). Fed-batch results of *N. oculata*, by comparison, showed remarkable stability in cell number whilst total lipid also saw a three-fold increase (the total FAME profile of which was more than doubled) over 28 days. However, this was in favour of SAT accumulation and a decrease in PUFAs (as percentage of total FAME- refer to Table 5.13), including 10 % decline in EPA. Having used FAME profiling data from fed-batch cultures, the approximated PUFA accumulation under continuous media renewal calculated to be marginally lower (but not significantly) for both *I. galbana* and *N. oculata* alike. Between the two algal species examined, *I. galbana* did on average produced more PUFA on a daily basis, although *N. oculata* produced double the amount of EPA compared with averaged daily DHA production in *I. galbana*, regardless of media renewal method (Table 7.2). However, it should be noted that DHA synthesis has a higher metabolic cost since additional chain elongation and desaturation is required, which may justify this comparison.

Photobioreactor culture	*I. galbana*		*N. oculata*	
Media renewal method *70 L working volume (area = 1.13 m^2)*	**Continuous**	**Fed-batch**	**Continuous**	**Fed-batch**
Harvest production period				
Total run time (days)	127	66	110	50
Active media renewal (days)	90	43	46	28
Harvest period (% of total run time)	71	65	42	56
Media renewal rate				
(% working volume)	10	10 - 20	10 - 20	10
(L/day)	7	7 - 14	7 - 14	7
(L/hr)	0.29	1.75 - 3.5	0.29 - 0.58	1.75
Total harvest volume				
Volume (L)	630	343	455	196
Total cellular / biomass harvest				
Cell density (× 10^{12} cells)	25.19	12.34	47.54	31.44
Biomass (g DW)	865.38	331.64	347.53	266.33
Mean harvest volume				
Daily volume (L/day)	7 ± *0.00*	7.98 ± *0.52*	9.89 ± *0.51*	7 ± *0.00*
Areal volume (L/m^2/day)	6.19 ± *0.00*	7.06 ± *0.46*	8.75 ± *0.45*	6.19 ± *0.00*
Mean cellular / biomass harvest				
Cell density (× 10^9 cells/L)	39.99 ± *1.51*	35.98 ± *2.46*	104.50 ± *16.61*	160.41 ± *1.70*
Daily cell harvest (× 10^{10} cells/day)	27.99 ± *1.06*	28.71 ± *1.28*	103.35 ± *8.47*	112.29 ± *1.19*
Areal cell yield (× 10^{10} cells/m^2/day)	24.77 ± *0.94*	25.40 ± *1.13*	91.46 ± *7.50*	99.37 ± *1.05*
Volumetric cell yield (× 10^9 cells/L/day)	4.00 ± *0.15*	4.10 ± *0.18*	14.76 ± *1.21*	16.04 ± *0.17*
Areal volumetric cell yield (× 10^9 cells/L/m^2/day)	3.54 ± *0.13*	3.63 ± *0.16*	13.07 ± *1.07*	14.19 ± *0.15*
Volumetric biomass (g/L)	1.37 ± *0.03*	0.97 ± *0.06*	0.76 ± *0.05*	1.36 ± *0.02*
Daily biomass harvest (g/day)	9.62 ± *0.24*	7.71 ± *0.48*	7.55 ± *0.47*	9.51 ± *0.16*
Areal biomass yield (g/m^2/day)	8.51 ± *0.21*	6.82 ± *0.42*	6.68 ± *0.42*	8.42 ± *0.14*
Volumetric biomass yield (mg/L/day)	137.43 ± *3.43*	110.14 ± *6.86*	107.86 ± *6.71*	135.86 ± *2.29*
Areal volumetric biomass yield (mg/L/m^2/day)	121.62 ± *3.04*	97.46 ± *6.07*	95.45 ± *5.94*	120.23 ± *2.03*
Mean PUFA				
Cellular PUFA yield (fg/cell)	791.19 *	791.19 *	184.95 **	184.95 **
Total PUFA harvest (g)	19.93	9.76	8.79	5.81
Biomass PUFA (mg/g DW)	23.03	29.43	25.29	21. 82
Volumetric PUFA (mg/L)	31.63	28.45	19.32	29.64
Daily PUFA harvest (mg/day)	221.45 ± *8.39*	227.07 ± *10.13*	191.14 ± *15.67*	207.50 ± *22.01*
Areal PUFA yield (mg/m^2/day)	195.97 ± *7.42*	200.95 ± *8.96*	169.15 ± *13.87*	183.63 ± *19.48*
Volumetric PUFA yield (mg/L/day)	3.16 ± *0.12*	3.24 ± *0.14*	2.73 ± *0.22*	2.96 ± *0.31*
Areal volumetric PUFA yield (mg/L/m^2/day)	2.80 ± *0.12*	2.87 ± *0.13*	2.42 ± *0.20*	2.62 ± *0.28*
Mean DHA (*I. galbana*) / EPA (*N. oculata*)				
Cellular DHA/EPA yield (fg/cell)	214.70 *	214.70 *	119.88 **	119.88 **
Total DHA/EPA harvest (g)	5.41	2.64	5.70	3.77
Biomass DHA/EPA (mg/g DW)	6.25	7.96	16.40	14.16
Volumetric DHA/EPA (mg/L)	8.59	7.70	12.53	19.23
Daily DHA/EPA harvest (mg/day)	60.09 ± *2.28*	61.62 ± *2.75*	123.90 ± *10.15*	134.64 ± *0.05*
Areal DHA/EPA yield (mg/m^2/day)	53.17 ± *2.02*	54.53 ± *2.43*	109.65 ± *8.98*	119.15 ± *0.04*
Volumetric DHA/EPA yield (µg/L/day)	858.84 ± *32.57*	880.29 ± *39.29*	1770.00 ± *145*	1923.43 ± *0.71*
Areal volumetric DHA/EPA yield (µg/L/m^2/day)	760.04 ± *28.86*	779.00 ± *34.71*	1566.43 ± *128*	1702.15 ± *0.57*
Annual harvest production period (days/yr)	259	237	153	204
Annual harvest volume				
Annual volume (L/yr)	1813	1891	1513	1428
Areal volume (L/m^2/yr)	1604	1673	1339	1264
Annual biomass harvest				
Annual cell density (× 10^{12} cells/yr)	72.49 ± *2.75*	68.01 ± *3.03*	158.13 ± *12.96*	229.07 ± *2.42*
Areal cell density (× 10^{12} cells/m^2/yr)	64.15 ± *2.43*	60.19 ± *2.68*	139.94 ± *11.47*	202.72 ± *2.14*
Annual DW (kg/yr)	2.49 ± *0.06*	1.83 ± *0.11*	1.16 ± *0.07*	1.94 ± *0.03*
Areal DW (kg/m^2/yr)	2.20 ± *0.05*	1.62 ± *0.10*	1.03 ± *0.06*	1.72 ± *0.03*
PUFA				
Annual harvest (g/yr)	57.36 ± *2.17*	53.82 ± *2.40*	29.24 ± *2.40*	42.33 ± *4.49*
Areal harvest (g/m^2/yr)	50.76 ± *1.92*	47.63 ± *2.12*	25.88 ± *2.12*	37.46 ± *3.97*
DHA (*I. galbana*) / EPA (*N. oculata*)				
Annual harvest (g/yr)	15.56 ± *0.59*	14.60 ± *0.65*	18.96 ± *1.55*	27.47 ± *0.01*
Areal harvest (g/m^2/yr)	13.77 ± *0.52*	12.92 ± *0.58*	16.78 ± *1.37*	24.31 ± *0.01*

Table 7.2: Estimated productivity summary of 70 L tubular photobioreactors. 24Hr illuminated indoor cultures. Comparisons made between continuous and fed-batch operations for both *I. galbana* and *N. oculata* based on values from Table 4.11 (*) and 5.12 (**), respectively (*assuming values remained constant*). Annual projection derived assuming cultures are ran consecutively throughout the year.

The commercial viability of cultivating microalgae depends not only upon cellular or volumetric yields, but should also account for area of land required to obtain these yields. Traditional open pond cultures have been known to require large acres of land in order to produce the volumes required for successful commerce (see Section 1.6.1). This can be expensive in terms of both initial capital outlay and subsequent maintenance. Thus culture productivity should also consider yield in terms of areal harvests in order to calculate a cost efficient use of space (Richmond, 2000).

The work of Miron *et al.* (1999) featured the use of a 200 L tubular photobioreactor (with windings arranged in a horizontally stacked geometry) with a footprint area of 12 m^2. Having cultivated *Phaeodactylum tricornutum*, Miron and co-workers (1999) report an areal EPA productivity in the region of 1.2 $kg/m^2/yr$. Whilst productivities herein are a fraction of this, this may be due to comparatively low biomass concentrations (4 g/L c.f. an optimum 1.37 g/L in this study- see Table 7.2), rather than a difference in cellular EPA levels between species. Yet in terms of making an efficient use of space, the helical geometry featured in this study is calculated to hold 61.95 L/m^2, compared with 16.67 L/m^2 of land in Miron's design. Provided cell densities can be improved for the same footprint area (1.13 m^2), areal yields of this helical photobioreactor could therefore be highly competitive. Indeed, higher cell densities for *N. oculata* during this study have been achieved by either increasing phosphate concentrations, reducing growth temperature, removing auto-inhibitory particulates (see Section 5.3.1) or modifying the photobioreactor design (discussed in Section 7.2). Nonetheless, the helical geometry of this photobioreactor remains a more compact and efficient use of space, which provided volumetric yields are increased, could be a more commercially attractive feature of its design.

7.1.3: Cultivation strategies and recommendations

In *I. galbana*, there was little difference in terms of PUFA productivity between continuous and fed-batch media renewal methods. However, the continuous method can be seen as more favourable since the photobioreactor showed a longer harvestable lifespan (71 % of the total run-time), offering greater stability. Conversely, *N. oculata* would appear to favour fed-batch media renewal both in terms of harvestable lifespan and daily/ annual PUFA production. That said, it should be noted that loss of cell numbers during continuous production began directly after media renewal rate was doubled. Perhaps, *N. oculata* may have been more productive if maintained at 10% under continuous media renewal.

Culturing strategies, focusing upon either cellular or volumetric yields, must be specifically targeted towards the market. For example, the use of phytoplankton as an aquaculture feed would focus upon cellular quality since predation rate is limited to mouth and gut size (can only eat so many before full). Volumetric yields are meaningless if the predator (zooplankton or fish larvae) can not eat enough to achieve it's nutritional needs. Although cell numbers of *I. galbana* generally declined under both media renewal regimes of photobioreactor cultures, causing reduced volumetric yields, individual cell quality did significantly improve with respect to PUFAs. Pharmaceutical applications however would be more concerned with volumetric yields, since cells would require extraction of specific fatty acids (namely ARA, OTA, EPA and DHA- refer to Table 1.1). In this respect, *I. galbana* would perhaps not appear to be a suitable source of fatty acids to be used in refined health food supplements. *N. oculata*, due to high volumetric yields, would however appear to be a more suitable organism for pharmaceutical production of EPA. While *N. oculata* may be too small in size to satisfy the predatory habits of juvenile fish (compared to smaller larval stages), it may provide significant nutritional benefits indirectly via enrichment of zooplankton (preferred prey items of larger Juvenile stages). Therefore, of the two microalga featured in this study for commercial purposes, *N. oculata* may potentially be more applicable towards a broader range of markets.

Based upon the current data, growth conditions for increasing cell density and PUFA accumulation are generally antagonistic. Specific lipid fractions were not analysed within this study but were reviewed to better understand the behaviour of total lipid

accumulation and quality (FAME profiles). For the purpose of this study, four lipid classes (ST, GL, PL and TAG) have been discussed, based upon similar work of other authors. It is recommended that future studies should preferably include analysis of specific lipid fractions. For example, the methodologies employed by Alonso *et al.* (1998) identified the presence of twelve specific lipid fractions (each with separate FAME profiles). However, based upon the data reviewed during the course of this study the following considerations regarding DHA (in *I. galbana*) and EPA (in *N. oculata*) accumulation are noted as follows:

(1) DHA and EPA accumulation during exponential growth can be attributed to cell membranes (PL), but is mainly associated to GL bound to the thylakoid membrane of chloroplasts. Therefore, higher chlorophyll *a* could be used as a general indicator of GLs. Due to photoadaptive response of chloroplasts towards changes to irradiance, low-light conditions ($I_{av} < I_k$) would be preferable for DHA/ EPA synthesis since Photoadaptation results in increased PSU number/ size.

(2) Stationary phase cultures store lipid as TAGs. As conditions become N-limited carbon flow is redirected towards carbohydrate and lipid accumulation. For example, sf/2 produced higher cell density due to excess nitrate levels over f/2, however total lipid accumulation was higher in f/2 as result of nitrate depletion (likely to be attributed to the presence of TAGs). If aeration is supplemented with CO_2, specifically at onset of nitrate limitation this should further aid the carbon supply chain necessary for elongation of fatty acids within TAG portion of the total lipid.

(3) High light intensities during stationary growth phase are also believed to act as a trigger for PUFA accumulation, possibly acting to absorb excess thermal energy much like a filter to protect the chloroplasts in the GL lipid fraction. Therefore, low-light conditions can be applied during exponential phase growth to promote an increase in PSU (and therein thylakoids). Once a maximum cell density is reached, light intensity could be increased to 'stress' chloroplasts, triggering the photo-protective role from GLs by way of PUFA

synthesis as a whole. Although this may be exclusive of DHA and EPA, which are reported to respond in opposition (refer to Sections 4.3.4 and 5.3.4).

(4) Reducing temperature appears to increase desaturation rather than chain elongation, within the FAME profile of PLs, for increased membrane fluidity. Therefore lowering growth temperature alone may be insufficient to increase PUFA accumulation.

(5) Raising salinity did not increase cellular DHA/ EPA yields, but inadvertently did boost volumetric yields by increasing cell density.

8.2: PHOTOBIOREACTOR DESIGN

Although the use of sf/2 growth medium may be a key factor towards the comparatively high cell densities in this study (discussed in Sections 4.3.1 and 5.3.1), nonetheless cultivation within the photobioreactor encouraged still further cell growth compared to flask cultures, in the case of *I. galbana* at least. The fact that *N. oculata* failed to follow this trend could be due to various reasons. This may be a reflection of differences in shear (as a result of bubble formation at the sparge plate, coalescence in the riser and break-up in the header tank) tolerances between the two alga (Vandanjon *et al.*, 1999), or that the photobioreactor had reached it's biological capacity in terms of g/L (typically higher in *N. oculata*) affecting rheology (hydrodynamic characteristics). The photostage and lighting regime of the photobioreactor may also be sub-optimal for this particular culture's photosynthetic capacity (compared in Section 7.1.1). Furthermore, an inadequate supply of dissolved CO_2 would equally limit growth, as would any oxygen build-up due to inefficient gaseous mixing (mass transfer) or removal. The physical characteristics of any photobioreactor are therefore critical and must meet the needs of individual species. Figure 7 highlights how the interrelated processes of design parameters combine to affect cell density and ultimately productivity. A change to any one of the seven key variables (shown to the left of Figure 7) of the current design can impact directly upon one parameter along with indirect consequences to others.

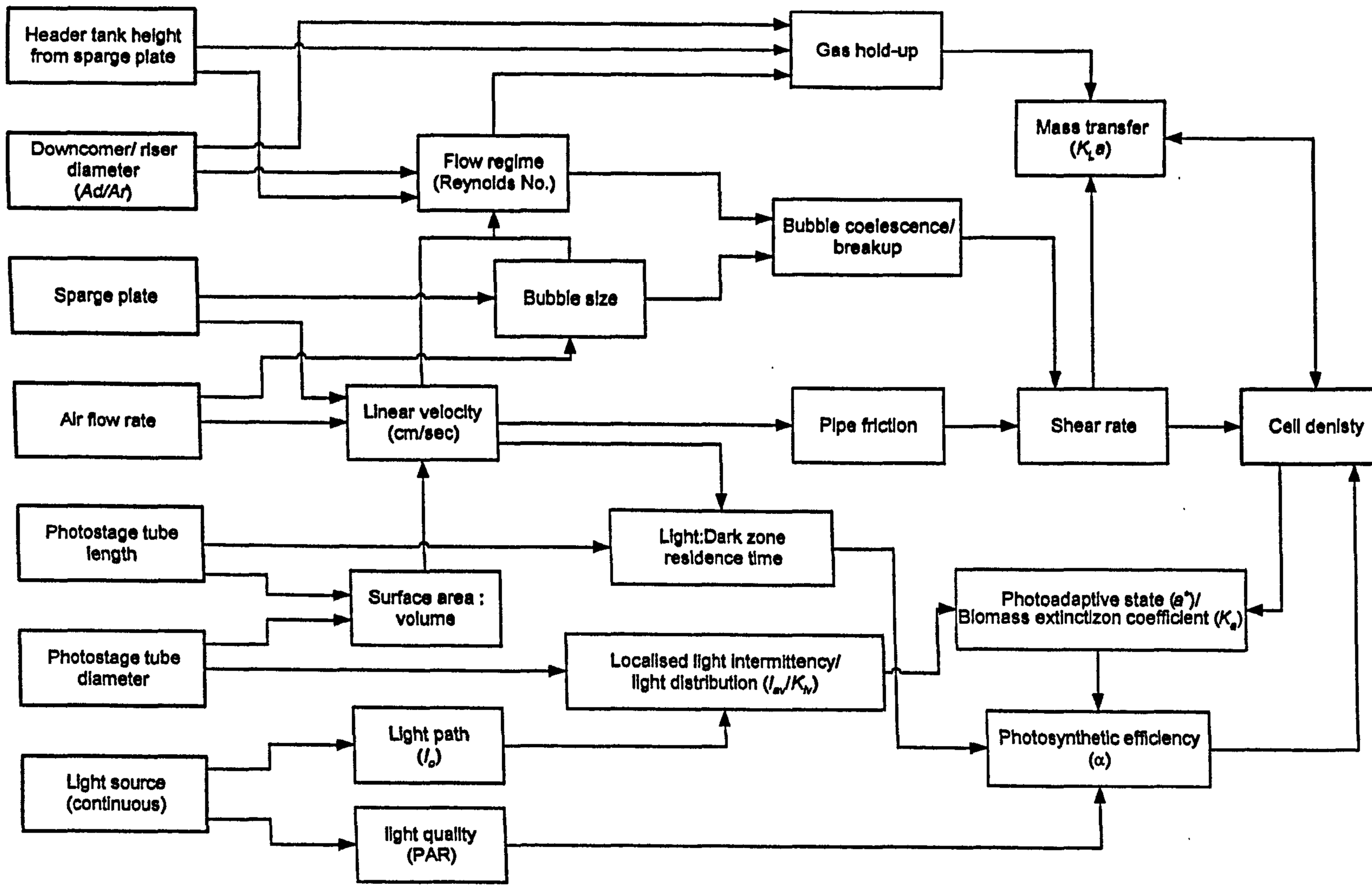

Figure 7: Interrelated process of photobioreactor design affecting cell density. Changes to key system variables (on the left) can impact directly or indirectly upon essential operational parameters and ultimately cell density (on the right). A cultures preference for each parameter may also be species specific.

7.2.1: Mixing efficiency

Poor gas transfer is known to inhibit growth rate and overall productivity. Mass transfer of the current photobioreactor was found to be subordinate to similar systems, and is therefore an area for improvement. Sparge plate configuration was the only physical aspect of the current design to be tested regarding mass transfer, from which it was shown that the 'standard' configuration used was optimal during operation with the two cultures. In respect to enriching aeration with supplementary CO_2, the injection point used during culture runs (at the 'U-bend') was found to be the worst location when tested. This may have hindered photosynthesis potentials (P_{max}) and/ or PUFA synthesis (acting as 'carbon sinks' in TAGs). Five main strategies are proposed for improving overall mass transfer within the riser:

(1) Since mass transfer is the result of shear forces, determining the tolerance of cultures to shear would be beneficial in order to further maximise mass transfer efficiency within a known shear threshold.

(2) Investigation into effects of changing height ratio of header tank height to photostage on flow parameters, as highlighted by Fernandez *et al.* (2001).

(3) Investigate changes towards riser and/ or downcomer diameters on flow characteristics. The ratio of the two cross-sections is known to affect linear velocity, gas hold-up and bubble residence time within the riser (Fraser *et al.*, 1994; Merchuk, 1990; Chisti *et al.*, 1988).

(4) The use of a converging-diverging riser to generate eddy formation within the riser (turbulent flow) maintaining a high Reynolds number at lower linear velocities, thus making air lift more energetically efficient (Data of Ghosh *et al.*, 1993 reveals an average K_La increased 188 % comparatively, for same linear velocities). Furthermore, possibly increasing culture residence time within light zones (beneficial for light intermittency in dense cultures).

(5) Sparge plate fabrication. Whilst reducing pore size in a solid plate aided mass transfer, there is evidence (Fregapane *et al.*, 1999; Hebrard *et al.*, 1996) that a flexible membrane sparge plate may increase mass transfer still further.

7.2.2: Photostage development

Lighting regime is also a prime concern, which has not been directly investigated here, however key areas have been discussed (see Section 6.6.2) in order to allow a general awareness of the methods and terms used within this field. Although lighting provided continuous irradiance to the photostage surface, cells would receive light intermittently due to both self-shading or as a result of recirculating between sections of the photobioreactor. Based upon the estimated residence times of cells through each section of the photobioreactor (Table 6.1), the ratio of light to dark zones was 16:1 (or 9:1 if the photostage is the only light zone). Therefore increasing/ decreasing translucent areas of the photobioreactor may aid photosynthetic efficiency of cultures (Grobbelaar, 1994; 1989). More detailed analysis of specific light models would also be highly recommended for future research. In regard to photostage development, the following changes to the current design are proposed with a view to increasing biomass productivities:

(1) Doubling photostage height (number of windings) would add 44 L to the current working volume and could potentially increase overall productivity for same footprint area by 61 %. Although this would increase residence time within the light zone affecting low frequency light intermittency, which should also be considered.

(2) Although reducing tubing diameter of the photostage coil may increase volumetric yields (Richmond *et al.*, 1993), increasing diameter, although possibly reducing cell density due to increasing photolimitation, (from self-shading), has been found to increase overall areal productivity ($g/m^2/day$) (Fernandez *et al.*, 2001; Molina Grima, 2001; Richmond, 2000; Kobayashi and Fujita, 1997). However, this would also change linear velocity and residence time within the photostage, affecting light intermittency (see Figure 7).

(3) Tubing could be 'basket-weaved' around vertical coil supports to increase turbulence within the photostage in order to prevent biofouling. Added turbulence within this section could also increase light intermittency. This would also provide a marginal increase in culture volume due to increased length for same diameter tubing and 'footprint'.

(4) Removal of stainless steal mesh altogether this acts to block/ reflect light from ~12 % of internal surface area of the photostage. Instead could support coil windings between two concentric circles made from transparent acrylic (also cheaper and easier to fabricate).

(5) Testing of alternative light sources, such as LEDs.

(6) Incorporation of a variable resistor to, and calibration of, light source. If optimal light levels (I_{av}) for known biomass cell densities (or more specifically biomass extinction coefficients) can be determined then possible to automate (Efe *et al.*, 1999; Pavlou, 1999) and ensure further cost saving to light source.

8.2.3: General recommendations

As a result of general operational experience gained during this study, minor recommendations regarding everyday maintenance include:

(1) Online analysis of vent gas from header tank to measure culture respiration. Also referred to as a dynamic method of gassing-out (Chisti *et al.*, 1988).

(2) Revision of the header tank shape to remove 'dead spaces' of mixing, reducing no. seals/ inlets and possible contamination sites.

(3) Examination and sourcing of alternative NRV designs. Those used within this study on occasion suffered from minor leaks. Although cultures remained monoalgal throughout, this is of concern regarding achieving axenic conditions.

(4) Addition of taps to manifold outlets would allow for gradual increase in culture volume in steps (as cell density becomes photolimited). Also push-fit connections between manifolds and coil windings, rather than use of jubilee clips (show in Figure 3.4) would be generally labour saving.

7.2.4: Potential for scale-up

The major obstacle for successful commercial use of such a photobioreactor is of course scale-up. Although tubular systems are generally easier to scale-up compared to bubble columns and ALRs (Borowitzka, 1994; Molina Grima *et al.*, 1999), height is still a restrictive factor since K_La is known to decrease with increasing riser height (Ghosh *et al.*, 1993; Jones and Benyahia, 1996). This is primarily because static pressure increases with height, reducing gaseous solubility between the bottom and top of riser (Dhauadi *et al.*, 1997). Alternative methods of recirculation should therefore be considered, taking into account the relatively poor shear tolerances of microalgal cultures. Alternative wet pumps such as centrifugal (glandless/ canned, dry-motor, monoblock) or peristaltic should therefore be investigated.

During the course of this study attempts were made to run a 2000 L photobioreactor (Plate 12- data not shown). Ultimately, the outdoor conditions made inoculation difficult, which resulted in contamination from protozoa in this instance. However, scale-up may be not necessarily the product of proportional increased of a single unit. As well as possibly resulting in a loss of mass transfer efficiency (Section 7.2.1) this can restrict usage to outdoor environments due to scalability of height- the 2000 L system shown in Plate 12 being ~ 7 m tall. As mentioned previously, the main advantage of the helical geometry of this tubular photobioreactor is its small footprint area. For just over the same footprint area used by the 2000 L system (27.56 m^2, coil windings alone), twenty-five 70 L systems could be placed making a total working volume of 1750 L. Based upon the above productivities (Table 7.2) for a fed-batch culture of *N. oculata*, an annual EPA harvest of 0.69 – 0.71 kg/yr can be calculated. Doubling photostage height would raise this combined volume to 2818 L (see Section 7.2.2), producing 1.12 – 1.14 kg/yr of EPA (based on calculations). This would allow for maintenance/ repair to individual subunits without disruption to the overall harvest, as well as isolating any possible contamination. However, this strategy is a more labour intensive means of management, requiring the operating of twenty-five units instead of one. Alternatively the subunits could be interconnected as one for pre-sterilisation in order to reduce labour time, and isolated by valves during actual operation.

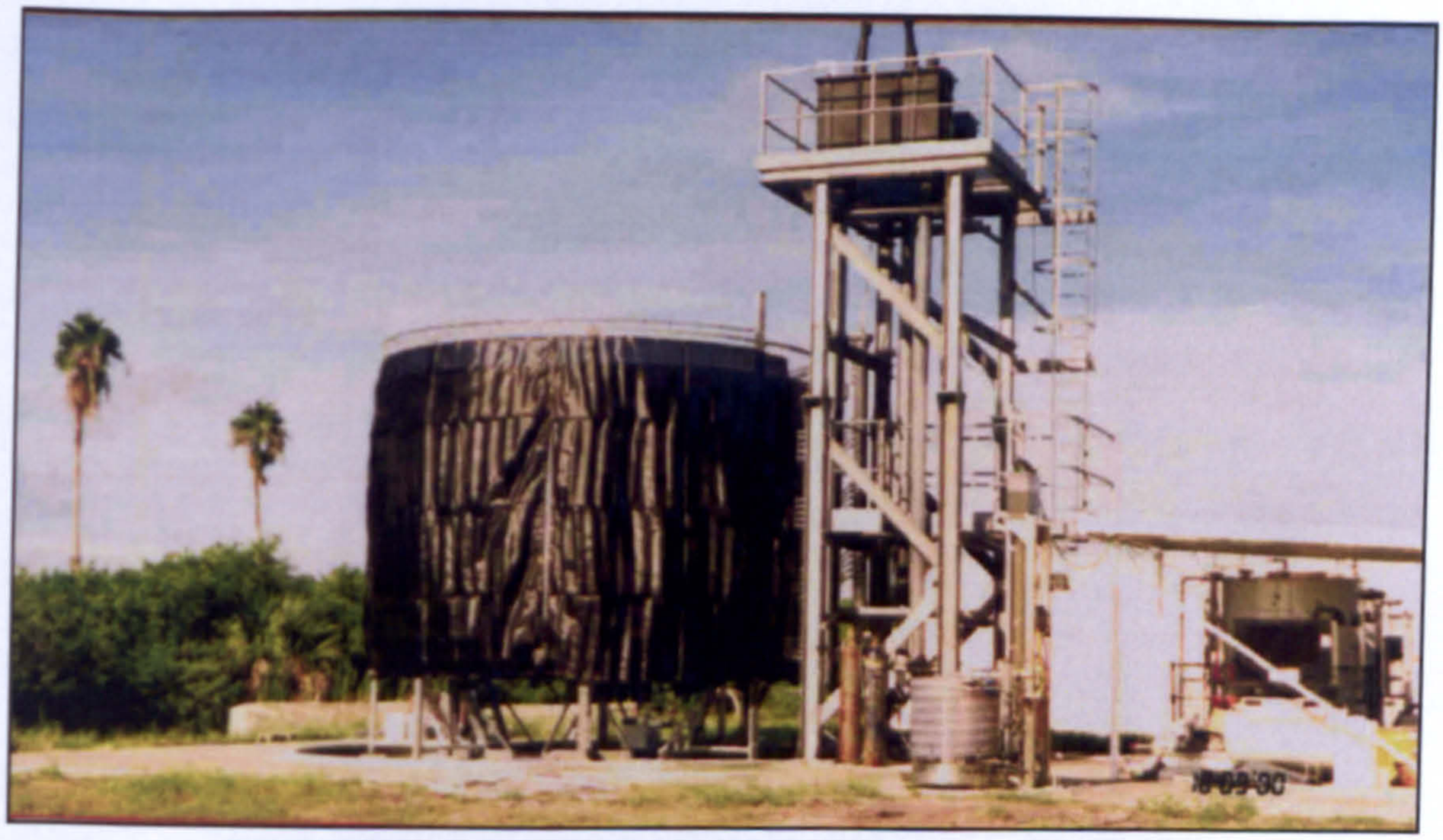

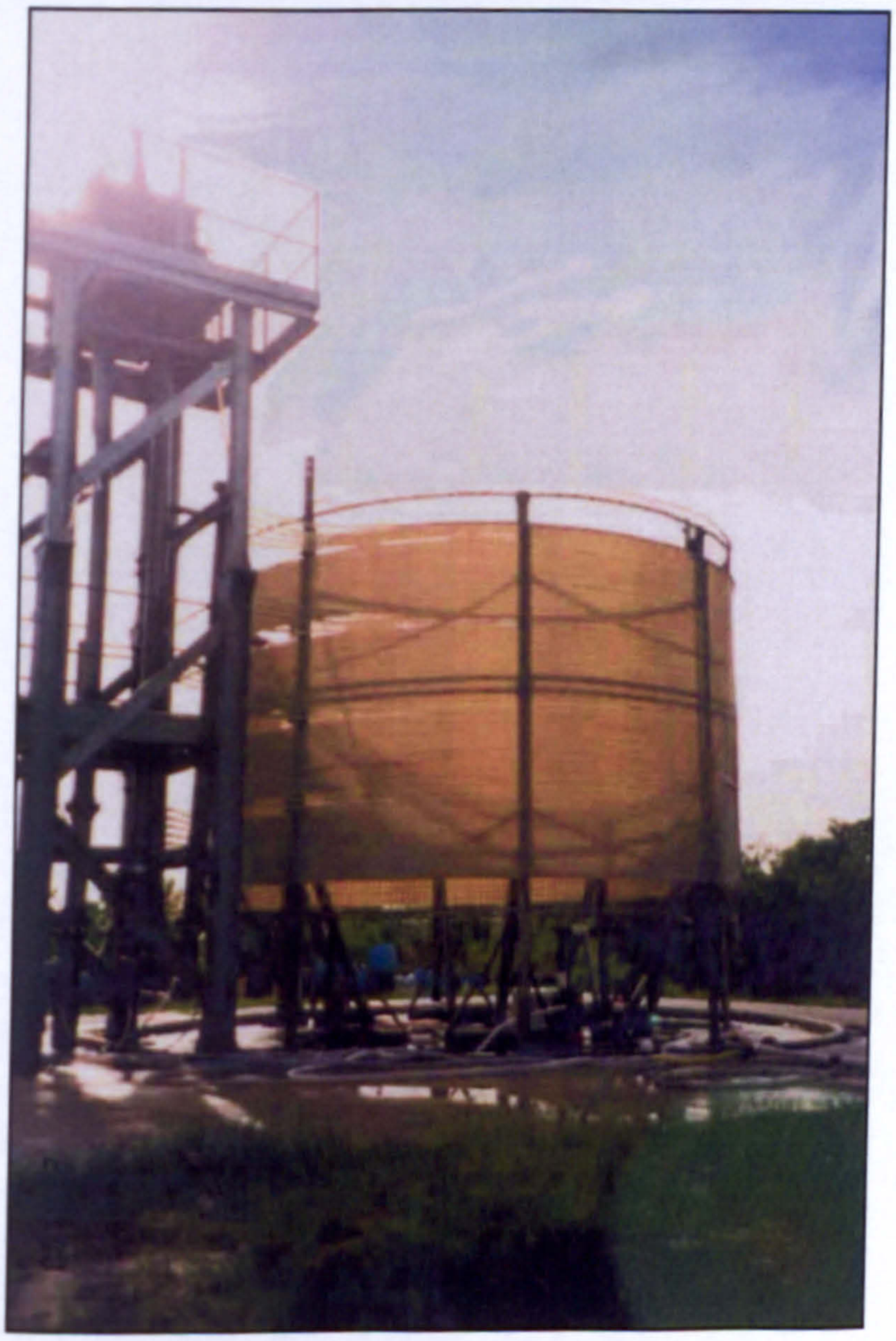

Plates 12: A 2000 L helical photobioreactor. A 70L culture to the bottom right showing comparative scale (top). Inner diameter of the 2000 L photostage is 5.25 m. A covering was used during inoculation with *I. galbana* (data not shown) to prevent photoinhibition during early growth. This was removed once cell density had risen (bottom). Location: Harbour Branch Oceanographic Institute (Fort Pierce, Florida, USA).

7.3: SUMMARY

From the flask experiments it is apparent that the modified f/2 (sf/2) medium (containing 7.12 mM $NaNO_3$ and 0.10 mM $NaH_2PO_4.H_2O$) used in this study extended the linear growth phases of both cultures (as also demonstrated in N and P limiting experiments with 32 ‰ sf/2), with a more notable affect on *N. oculata*. Yet, neither changes to medium formulation (f/2 or sf/2) or salinity (16 or 32 ‰) made any statistical difference towards the overall cell densities of either algae. Both *I. galbana* and *N. oculata* especially, favoured a lower growth temperature (20 and 15 °C, respectively) over the standard growth temperature of 23 °C. The mean cell size of *N. oculata* was smaller than that of *I. galbana* and therefore possibly less metabolically demanding, hence the comparatively higher cell densities achieved. Photobioreactor-grown cultures of *I. galbana* (but not *N. oculata*) achieved higher cell densities over flask experiment controls. However, photobioreactor cultures had benefited from 10 % (v/v) CO_2 to supplement aeration, but this was too impractical to apply to flask cultures. Furthermore, discrepancies in inoculation densities between, and within, cultures of *I. galbana* and *N. oculata* were a major source of experimental error throughout.

Again due to impracticality, continuous and fed-batch methods of media renewal were not applied to flask cultures. Instead, semi-continuous flask cultures of *I. galbana* and *N. oculata* indicated cellular yields were optimal at media renewal rates of 20 and 10 % (v/v/day), respectively. *I. galbana* when grown in the photobioreactor under continuous media renewal at 10 % (v/v/day) did show some stability in terms of cell density (but not at 20 % v/v/day). Unfortunately, media renewal at the same rate for fed-batch production lead to continued loss in cell numbers. While *N. oculata* displayed relative stability for both continuous and fed-batch production methods in the photobioreactor during 10 % (v/v/day) media renewal.

Oxygen evolution data showed that the irradiance at the surface of the photobioreactor (I_o = 107 µmol/m^2/s using light setup D- Table 6.3) was well below mean I_k values for both *I. galbana* and *N. oculata* (175 and 294 µmol/m^2/s, respectively). Increasing irradiance levels may therefore increase cell densities in the photobioreactor further, although such light levels are still relatively low when compared to other authors. Whilst it is apparent that both cultures were low-light adapted, the data suggests that *I. galbana* and *N. oculata* employed different methods photoadaptation (in terms of PSU

size or number) since the typically lower cell densities of *I. galbana* displayed higher net P-I curve values on a cellular basis (α, P_{max} and I_o/cell) as a result of a higher Chlorophyll *a* content. Although, *N. oculata* cultures recorded the lower Chlorophyll *a* levels between the two (both cellular and volumetric) they achieved higher cell densities over *I. galbana*. However, despite the lower Chlorophyll *a* levels, *N. oculata* showed greater metabolic efficiency with respect to net Chlorophyll *a*-based oxygen evolution rates (α) and P_{max}.

The higher total lipid accumulation in f/2 grown cultures (of both *I. galbana* and *N. oculata*, regardless of salinity) may be attributed to the fact that f/2 cultures entered stationary phase growth earlier than sf/2 cultures due to nitrate limitation, allowing carbon uptake to be diverted away from protein synthesis (requiring a nitrogen source, which became limited from the media with growth). With regard to FAME analysis of flask cultures, salinity did not affect cellular accumulation in either algae, but did positively influence volumetric DHA levels in *I. galbana* (independently of other PUFAs- refer to Appendix D). Whilst *N. oculata* accumulated more total lipid when grown in f/2 medium, the PUFA content was half of that found in sf/2 grown cultures. Overall, volumetric PUFA yields compared between stationary phase flask samples and the photobioreactor fed-batch samples were similar. However on a per cell basis, PUFA content was higher in cells grown in the photobioreactor for both algae.

While an air flow rate of 15 L/min gave a 'perfect bubbly' riser dynamic during algal cultivation, when mass transfer was measured (i.e. in the absence of cells) with the same sparge plate and air flow rate, the riser dynamic was 'imperfect bubbly'. Without cells, 10 L/min provided the 'perfect bubbly' conditions for mass transfer measurements with the 'standard sparge plate'. In situ measurements would have offered a truer representation of mass transfer, but this was avoided mainly due to potential contamination problems during setup (see Figure 3.6) and biofouling (shown to occur with *I. galbana*) of the probe. Physical characterisation of the photobioreactor did prove that reducing the pore size (and not pore density) of the sparge plate significantly increased linear fluid velocity, Reynolds number and mass transfer. Data also suggest that relocating the CO_2 injection point will aid solubility, increasing the metabolic CO_2 supply needed for photosynthesis by algal cells which, under nutrient limited conditions, may result in an increase total FAME accumulation or chain length. Regarding the 'light regime' it is suggested that irradiance levels are

too low (see above) and it is also calculated that during recirculation around the photobioreactor cells are exposed to irradiance (I_o) 90 % of the time. It is suggested that by reducing this (i.e. light intermittency times from light to dark zones) will prevent cell damage by allowing more time for photosystems (PSI and II) to return to their ground states.

It is hoped that this thesis has gone some way to help integrate knowledge of the cellular processes/ needs of photosynthesis and FAME accumulation in microalgae with the physical parameters offered by the photobioreactor with a view to balancing metabolic supply and demand, to meet with the larger world of commercial demand. Hopefully through continued demand this work may help shed some light on how to keep our elusive little friends happy, so that they may one day return the favour.

REFERENCES

Acheson, D.J. (1990). Elementary Fluid Dynamics. Oxford, Clarendon press.

Ackman, R.G. and Tocher, C.S. (1968). "Marine phytoplankter fatty acids." Fisheries Research Board of Canada **25** (8): 1603-1620.

Al-Masry, W.A. and Dukkan, A.R. (1997). "The role of gas disengagement and surface active agents on hydrodynamic and mass transfer characteristics of airlift reactors." Chemical Engineering Journal **65**: 263-271.

Alonso, D.G. *et al.* (1998). "Acyl Lipids in three microalgae." Phytochemistry **47** (8): 1473-1481.

Babarro, J.M.F. *et al.* (2001). "Influence of preservation techniques and freezing storage time on biochemical composition and spectrum of fatty acids of *Isochrysis galbana* clone T-iso." Aquaculture Research **32**: 565-572.

Bannister, T.T. and Weidemann, A.D. (1984). "The maximum quantum yield of phytoplankton photosynthesis *in situ*." Journal of Plankton Research **6** (2): 275-294,

Bannister, T.T. (1974). "Production equations in terms of chlorophyll concentration, quantum yield, and upper limit to production." Limnology and Oceanography **19**(1): 1-12.

Becker, E.W. (1994). Large-scale cultivation. Microalgae: biotechnology and microbiology. E. W. Becker. London, Cambridge university press: 63-95.

Behrens, P.W. and Kyle, D.J. (1996). "Microalgae as a source of fatty acids." Journal of Food Lipids **3**: 259-279.

Bello, R.A. *et al.* (1985). "Gas holdup and overall volumetric oxygen transfer coefficient in airlift contactors." Biotechnology and Bioengineering **27**: 369-381.

Ben-Amotz, A. *et al.* (1987). "Chemical composition of dietary species of marine unicellular algae and rotifers with emphasis on fatty acids." Marine Biology **95**: 31-36.

Benemann, J.R. (1990). "Microalgae products and production: an overview." Journal of Industrial Microbiology (5): 247-256.

Bentrifraouine, C. *et al.* (1997). "An experimental study of the hydrodynamic characteristics of external loop airlift contactors." *Journal of Chemical Technology and Biotechnology* **69**: 345-349.

Benyahia, F. and Jones, L. (1997). "Scale effects on hydrodynamic and mass transfer characteristics of external loop airlift reactors." Journal of Chemical Technology and Biotechnology **69**: 301-308.

Bernhard, K. (1990). "Synthetic Astaxanthin- the route from research to commercialisation." Carotenoids: Chemistry and Biology: 337-362.

Bligh, E.G. and Dyer, W.J. (1959). "A rapid method of total lipid extraction and purification." Canadian Journal of Biochemistry and Physiology **37**(8): 911-917.

Bonalberti, E. and Croatto, U. (1985). Use of algal systems as a source of fuels and chemicals. Energy from Biomass. Proceedings of the International Conference on Biomass, E.C. Conference, Elsevier Applied Science Publishing, London & New York.

Borowitzka, M.A. (1999). "Commercial production of microalgae: ponds, tanks, tubes and fermentors." Journal of Biotechnology **70**: 313-321.

Borowitzka, M.A. (1997). "Microalgae for aquaculture: Opportunities and constraints." Journal of Applied Phycology **9**: 393-401.

Borowitzka, M.A. (1994). "Large-scale algal culture systems: The next generation." Australian Biotechnology **4**: 212-215.

Borowitzka, L.J. (1991). "Development of Western Biotechnology's algal ß-carotene plant." Bioresource Technology **38**: 251-251.

Bott, T.R. (2000). "Biofouling control with ultrasound." Heat Transfer Engineering **21** (3): 43-49.

Brown, M.R. *et al.* (1996). "Effects of harvest stage and light on the biochemical composition of the diatom *Thalassiosira pseudomona*." Journal of Phycology **32**: 64-73.

Brown, M.R. *et al.* (1993). "The influence of irradiance on the biochemical composition of the Prymnesiophyte *Isochrysis* sp. (clone T.iso)." Journal of Phycology **29**: 601-612.

Bryhn, M. (2001). "Omega-3: A vast range of applications." http://www.triomega.com/index.php?ID=Articles&ID2=Show&ID3=Articles&Cat=5&counter=27 (last access date 20/07/2005).

Callow, M.E. and Callow, J.A. (2002). "Marine biofouling: a sticky problem." The Biologist 49 (1): 10-14.

Carlozzi, P. and Torzillo, G. (1996). "Production of *Spirulina* in a strongly curved outdoor tubular photobioreactor." Applied Microbiology and Biotechnology 45: 18-23.

Cederholm, T. (2004). "Does fish fat protect against Alzheimer's disease? ", Pronova Biocare. http://www.pronovabiocare.com/index.php?ID=Artikler&ID2=Vis&ID3=Articles&Cat=4&counter=119&topp=heading4.jpg&topplogo=logo4.jpg (last access date 20/07/2005).

Cheng-Wu, Z. *et al.* (2001). "An industrial-size flat plate glass reactor for mass production of *Nannochloropsis* sp. (Eustigmatophyceae)." Aquaculture 195: 35-49.

Chisti, M.Y. *et al.* (1988). "Liquid circulation in airlift reactors." Chemical Engineering Science 43 (3): 451-457.

Cho, J.Y. *et al.* (1999). "Growth activation of the microalga *Isochrysis galbana* by the aqueous extract of the seaweed *Monostroma nitidum*." Journal of Applied Phycology 10: 561-567.

Chrismadha, T. and Borowitzka, M.A. (1994). Growth and lipid production of *Phaeodactylum tricornutum* in a tubular photobioreactor. Algal Biotechnology in the Asia-Pacific Region: Proceedings of the first Asia-Pacific Conference on Algal Biotechnology, Institute of Advances Studies, University of Malaya, Kuala Lumpur.

Clayton, R.K. (2002). "Research on photosynthetic reaction centers from 1932 to 1987." Photosynthesis Research 73: 63-71.

Connor, W. (1999). "Fish oil prevents death from heart disease: Guest Editorial." PUFA Newsletter 3 (3): 1-12.

Contreras, A. *et al.* (1998). "Interaction between CO_2 mass transfer, light availability and hydrodynamic stress in the growth of *Phaeodactylum tricornutum* in a concentric tube airlift photobioreactor." Biotechnology and Bioengineering 60: 317-325.

Das, U.N. *et al.* (2001). "Effect of corticosteroids and eicosapentaenoic acid/ docosahexaenoic acid on pro-oxidant and anti-oxidant status and metabolism of essential fatty acids in patients with glomerular disorders." Prostaglandins, Leukotrienes and Essential Fatty Acids 65(4): 197-203.

Degen, J. *et al.* (2001). "A novel airlift photobioreactor with baffles for improved light utilization through the flashing light effect." Journal of Biotechnology 92: 89-94.

Denys, A. *et al.* (2001). "Eicosapentaenoic acid and docosahexaenoic acid modulate MAP kinase (ERK1/ ERK2) signalling in human T cells." Journal of Lipid Research 42: 2015-2020.

Dhauadi, H. *et al.* (1997). "Mass transfer in an external-loop airlift reactor: experiments and modeling." Chemical Engineering Science 52 (21/22): 3909-3917.

Droop, M.R. (1955). "Some new suppra-littoral protista." Journal of the Marine Biological Association, United Kingdom 34: 233-245.

Duerr, E.O. *et al.* (1998). "Cultured microalgae as aquaculture feeds." Journal of Marine Biotechnology 7: 65-70.

Duray, M.M. *et al.* (1997). "Larval rearing of the grouper *Epinephelus suillus* under laboratory conditions." Aquaculture 150: 63-76.

Efe, M.O. *et al.* (1999). "A novel analysis and design of a neural network assisted nonlinear controller for a bioreactor." International Journal of Robust and Nonlinear Control 9: 799-815.

Eriksen, N.T. *et al.* (1998). "Dual sparging laboratory scale photobioreactor for continuous production of microalgae." Journal of Applied Phycology 10: 377-382.

Eugster, C.H. (1995). Isolation and Analysis. Carotenoids. Britton, G; Liaaen-Jensen, S; Pfander, H. Birkhäuser Verlag, Basel. 1A: 71.

Evjemo, J.O. and Olsen, Y. (1999). "Effect of food concentration on the growth and production rate of *Artemia franciscana* feeding on algae (*T.iso*)." Journal of experimental Marine Biology and Ecology 242: 273-296.

Fabregas, J. *et al.* (1985). "Growth, chlorophyll *a* and protein of the marine microalgae *Isochrysis galbana* in batch cultures with different salinities and high nutrient concentrations." Aquaculture 50: 1-11.

Fernandez, F.G. *et al.* (2001). "Airlift-driven external-loop tubular photobioreactors for outdoor production of microalgae: assessment of design and performance." Chemical Engineering Science **56**: 2721-2732.

Fernandez, F.G. *et al.* (1997). "A model for light distribution and average solar irradiance inside outdoor tubular photobioreactors for the microalgal mass culture." Biotechnology and Bioengineering **55** (5): 701-714.

Fernandez-Reiriz, M.J. and Labarta, U. (1996). "Lipid classes and fatty acid composition of rotifers (*Brachionus plicatilis*) fed two algal diets." Hydrobiologia **330**: 73-79.

Fidalgo, J. *et al.* (1998). "Effects of nitrogen source and growth phase on proximate biochemical composition, lipid classes and fatty acid profile of the marine microalga *Isochrysis galbana*." Aquaculture **166**: 105-116.

Fisher, T. *et al.* (1998). "The kinetics of the photoacclimation response of *Nannochloropsis* Sp. (Eustigmatophyceae): A study of changes in ultrastructure and PSU density." Journal of Phycology **34**: 818-824.

Fisher, T. *et al.* (1996). "Photoacclimation in the marine alga *Nannochloropsis* Sp. (Eustigmatophyte): a kinetic study." Journal of Plankton Research **18** (10): 1797-1818.

Flynn, K.J. *et al.* (1992). "Changes in fatty acids, amino acids and carbon/ nitrogen biomass during nitrogen starvation of ammonium- and nitrate-grown *Isochrysis galbana*." Journal of Applied Phycology **4**: 95-104.

Fraser, R.D. *et al.* (1994). "Dynamic mixing and oxygen transfer in small, airlift loop bioreactors : Model and experimental verification." Biotechnology Progress **10**(5): 543-547.

Fredrickson, A.G. and Tsuchiya, H.M. (1970). Utilization of the effects of intermittent illumination on photosynthetic microoganisms. Prediction and measurement of photosynthetic productivity. Proceeding of the IBP/PP technical meeting, Trebon, Wageningen, Centre for Agricultural Publishing and Documentation.

Fregapane, G. *et al.* (1999). "Wine vinegar production using a non-commercial 100-litre bubble column reactor equipped with a novel type of dynamic sparger." Biotechnology and Bioengineering **63**: 141-146.

Gavrilescu, M. and Tudose, R.Z. (1996). "Bubble column reactors of small dimensions II. Mass transfer in gas/ liquid dispersions." Hungarian Journal of Industrial Chemistry Veszprem **24**: 81-86.

Geel, C. *et al.* (1997). "Estimation of oxygen evolution by marine phytoplankton from measurement of the efficiency of photosystem II electron flow." Photosynthesis Research **51**: 61-70.

Ghosal, S. *et al.* (2000). "The turbulent life of phytoplankton." Centre for Turbulence Research: Proceedings of the Summer Program 2000: 31-45.

Ghosh, T.K. *et al.* (1993). "Studies on mass transfer characteristics of a modified airlift fermenter." Bioprocess Engineering **9**: 239-244.

Gilbert, M. *et al.* (2000). "Bio-optical modelling of oxygen evolution using *in vivo* fluorescence: Comparison of measured and calculated photosynthesis/ irradiance (P-I) curves in four representative phytoplankton species." Journal of Plant Physiology **157**: 307-314.

Gill, I. and Valivety, R. (1997). "Polyunsaturated fatty acids, part 1: Occurrence, biological activities and applications." Tibtech **15** (October): 401-409.

GISSI (1999). "Dietary supplementation with n-3 polyunsaturated fatty acids and vitamin E after myocardial infarction: results of the GISSI-Prevenzione trial." The Lancet **354** (August 7th): 447-455.

Goldman, J.C. *et al.* (1982). "Effect of nitrogen-mediated changes in alkalinity on pH control and CO_2 supply in intensive microalgal cultures." Biotechnology & Bioengineering **24**: 619-631.

Graham, L.E. and Wilcox, L.W. (2000). Algae. London, Prentice-Hall International (UK) Limited.

Grobbelaar, J.U. (1989). "Do light/ dark cycles of medium frequency enhance phytoplankton productivity?" Journal of Applied Phycology **1**: 333-340.

Grobbelaar, J.U. (1994). "Turbulence in mass algal cultures and the role of light/ dark fluctuations." Journal of Applied Phycology **6**: 331-335.

Guttman, B.S. (1999). Biology. London, WCB McGraw-Hill.

Hall, D.O. *et al.* (2002). "Outdoor helical tubular photobioreactors for microalgal production: Modelling of fluid-dynamics and mass transfer and assessment of biomass productivity." Biotechnology and Bioengineering **82** (1): 62-73.

Harris, W.S. (2001). "Omega-3 long chain PUFA and triglyceride lowering: Minimum effective intakes." European Heart Journal Supplements **3D**: 59-61.

Hebrard, G. *et al.* (1996). "Influence of the gas sparger on the hydrodynamic behaviour of bubble columns." Institute of Chemical Engineering 74 (A): 406-414.

Henley, W. (1993). "Measurement and interpretation of photosynthetic light-response curves in algae in the context of photoinhibition and diel changes." Journal of Phycology 29: 729-739.

Herzig, R. and Dubinsky, Z. (1992). "Photoacclimation, photosynthesis, and growth in phytoplankton." Israel Journal of Botany 41: 199-211.

Hibberd, D.J and Leedale, G.F. (1972). "Observations on the cytology and ultrastructure of the new algal class, Eustigmatophyceae." Annual of Botany 36: 49-71.

Ho, H.P. *et al.* (2001). "Application of white light emitting diode to surface plasmon resonance sensors." Sensors and Actuators B80: 89-94.

Hodgson, P.A. *et al.* (1991). "Patterns of variation in the lipid class and fatty acid composition of *Nannochloropsis oculata* (Eustigmatophyceae) during batch culture." Journal of Applied Phycology 3: 169-181.

Humphrey, G.F. (1979). "Photosynthetic characteristics of algae grown under constant illumination and light-dark regimes." Journal of Experimental Marine Biology and Ecology 40: 63-70.

Jeffery, B.G. *et al.* (2001). "The role of docosahexaenoic acid in retinal function." Lipids 36 (9): 859-871.

Jeffrey, S. *et al.* (1997). Phytoplankton pigments in oceanography. Paris, Unesco publishing.

Jones, L. and Benyahia, F. (1996). Hydrodynamics and mass transfer studies in external loop airlift reactors. The 1996 ICHEME Research Event/ Second European Conference for Young Researchers.

Kaplan, D. *et al.* (1986). "Optimal growth conditions for *Isochrysis galbana*." Biomass 9: 37-48.

Kim, Y.J. *et al.* (1996). "Desulfurization in a plate-type gas-lift photobioreactor using light emitting diodes." Korean Journal of Chemical Engineering 13 (6): 606-611.

Kobayashi, K. and Fujita, K. (1997). "Tube diameter on tubular photobioreactor for microalgal culture and its biomass productivity." Journal of Chemical Engineering of Japan 30 (2): 339-341.

Krause, G.H. and Weis, E. (1991). "Chlorophyll fluorescence and photosynthesis: the basics." Annual review of Plant Physiology and Plant Molecular Biology 42: 313-349.

Kureshy, N. *et al.* (1999). "Effect of ozone-treatment on cultures of *Nannochloropsis oculata, Isochrysis galbana* and *Chaetoceros gracilis*." Journal of the World Aquaculture Society 30 (4): 473-480.

Kyle, D.J. (1997). "Production and use of a single cell oil highly enriched in arachidonic acid." Lipid Technology 9 (September): 116-121.

Kyle, D.J. (1996). "Production and use of a single cell oil which is highly enriched in docosaxahexaenoic acid." Lipid Technology (September): 107-110.

Lavens, P. and Sorgeloos, P. (1996). Manual on the production and use of live food for aquaculture, Laboratory of Aquaculture & Artemia Reference Centre, University of Gent (Belgium): 1-99.

Lee, C.-G. and Palsson, B.O. (1994a). "High-density algal photobioreactors using light-emitting diodes." Energy Conservation 44: 1161-1167.

Lepage, G. and Roy, C.C. (1984). "Improved recovery of fatty acid through direct transesterification without prior extraction or purification." Journal of Lipid Research 25: 1391-1396.

Lewin, R. (1987). The Biology of the Algae and Diverse Other Verses. Pacific grove, California, USA, The Boxwood Press.

Lin, C.H. *et al.* (1976). "Oxygen transfer and mixing in a tower cycling fermentor." Biotechnology and Bioengineering 18: 1557-1572.

Liu, C-P. and Lin, L-P. (2001). "Ultrastructural study and lipid formation of *Isochrysis sp.* CCMP1324." Bot. Bull. Acad. Sin 42: 207-214.

Lu, Y.T and Blake, N.J (1997). "Clearance and ingestion rates of *Isochrysis galbana* by larval and juvenile bay scallops, *Argopecten irradians concentricus* (SAY)." Journal of Shellfish Research 16: 47-54.

Livne, A. and Sukenik, A. (1992). "Lipid synthesis and abundance of Acetyl Co A carboxylase in *Isochrysis galbana* (Prymnesiophyceae) following nitrogen starvation." Plant Cell Physiology 33 (8): 1175-1181.

Lubzens, E. *et al.* (1985). "De novo synthesis of fatty acids in the rotifer, *Brachionus plicatilis*." Aquaculture 47: 27-37.

Markl, H. and Mather, M. (1985). "Mixing and aeration of shallow open ponds." *Arch. Hydrobiol. Beih. Ergebn. Limnol* **20**: 85-93.

Markl, H. (1977). "CO_2 transport and photosynthetic productivity of a continuous culture of algae." Biotechnology and Bioengineering **19**: 1851-1862.

Martekbio (2005)."Nutritional Products". http://www.martekbio.com/nutritional_products/introduction.asp (last access date 20/07/2005).

Martinez-Jerónimo, F. and Espinosa-Chávez, F. (1994). "A laboratory scale system for mass culture of freshwater microalgae in polyethylene bags." Journal of Applied Phycology **6**: 423-425.

Maruyama, I. *et al.* (1997). "Application of unicellular *Chlorella vulgaris* for the mass-culture of marine rotifer *Brachionus*." Hydrobiologia **358**: 133-138.

Maruyama, I. *et al.* (1986). "Identification of the alga known as 'marine *Chlorella*' as a member of the Eustigmatophyceae." Japanese Journal of Phycology **34**: 319-325.

Mazzeo, M. *et al.* (2002). "White light from blue: white emitting organic LEDs based on spin coated blends of blue-emitting molecules." Physica **E13**: 1243-1246.

McStay, D. *et al.* (1995). "Sea trials of an optical fibre marine fluorosensor." Measurement Science and Amplitude Technology **6**: 1309-1316.

Medev (2002). "Save your brain: Eat fish! " http://www.usaweekend.com/food/carper_archive/961117carper_eatsmart.html (last accessed 10/07/2005).

Merchuk, J.C. (1988). "Shear effects on suspended cells." Advances in Biochemical Engineering Biotechnology **44**: 65-95.

Merchuk, J.C. and Berzin, I. (1995). "Distribution of energy dissipation in airlift reactors." Chemical Engineering Science **50**: 2225-2233.

Merchuk, J.C. (1990). "Why use air-lift bioreactors?" Tibtech **8**(March): 66-71.

Michaels, J.D. *et al.* (1996). "Sparging and agitation - Induced injury of cultured animal cells: Do cell to bubble interactions in the bulk liquid injure cells?" Biotechnology and Biotechnology **51**: 399-409.

Minoda, A. *et al.* (2002). "Role of sulfoquinovosyl diacylglycerol for the maintenance of photosystem II in *Chlamydomonas reinhardtii*." European Journal of Biochemistry **269**: 2353 - 2358.

Miron, A.S. *et al.* (1999). "Comparative evaluation of compact photobioreactors for large-scale monoculture of microalgae." Journal of Biotechnology 70: 249-270.

Molina Grima, E. *et al.* (2001). "Tubular photobioreactor design for algal cultures." Journal of Biotechnology 92: 113-131.

Molina Grima, E. *et al.* (1999). "Photobioreactors: light regime, mass transfer and scaleup." Journal of Biotechnology 70: 231-247.

Molina Grima, E. *et al.* (1997a). "Evaluation of photosynthetic efficiency in microalgal cultures using averaged irradiance." Enzyme and Microbial Technology 21: 375-381.

Molina Grima, E. *et al.* (1997b). "Growth yield determination in a chemostat culture of the marine microalga *Isochrysis galbana*." Journal of Applied Phycology 8: 529-534.

Molina Grima, E. *et al.* (1996). "A study on simultaneous photolimitation and photoinhibition in dense microalgal cultures taking into account incident and averaged irradiances." Journal of Biotechnology 45: 59-69.

Molina Grima, E. *et al.* (1994a). "A mathematical model of microalgal growth in light-limited chemostat culture." Journal of Chemical Technology and Biotechnology 61: 167-173.

Molina Grima, E. *et al.* (1994b). "Outdoor culture of *Isochrysis galbana* ALII -4 in a closed tubular photobioreactor." Journal of Biotechnology 37(2): 159-166.

Molina Grima, E. *et al.* (1994c). "Effect of growth rate on the eicosapentaenoic acid and docosahexaenoic acid content of *Isochrysis galbana* in chemostat culture." Applied Microbiology and Biotechnology 41: 23-27.

Molina Grima, E. *et al.* (1992). "EPA from *Isochrysis galbana*. Growth conditions and productivity." Process Biochemistry 27: 299-305.

Mori, K. (1986). "Photoautotrophic bioreactor using visible solar rays condensed by frensel lenses and transmitted through optical fibers." Biotechnology and Bioengineering 15: 331-345.

Morris, P. (2000). "Essential feed additives and why they are needed." Fish Farmer(January/ February): 9-10.

Nakamura, S. (1997). "Present and future aspects of blue light emitting devices." Applied surface Science 113/114: 689-697

Nakajima, Y. and Ueda, R. (1997). "Improvement of photosynthesis in dense microalgal suspension by reduction of light harvesting pigments." Journal of Applied Phycology 9: 503-510.

Nickell, D. and Bromage, N. (1997). "Problems of pigmentation." Fish Farmer (January/ February): 48-51.

NREL (1996). A look back at the U.S. department of energy's Aquatic Species Program: Biodiesel from algae (close-out report), NREL: 1-291.

Ogbonna, J.C. *et al.* (1999). "An integrated solar and artificial light system for internal illumination of photobioreactors." Journal of Biotechnology 70: 289-287.

Ogbonna, J.C. *et al.* (1995a). "Kinetic study on light-limited batch cultivation of photosynthetic cells." Journal of fermentation and Bioengineering 80 (3): 259-264.

Ogbonna, J.C. *et al.* (1995b). "Light supply coefficient: A new engineering parameter for photobioreactor design." Journal of Fermentation and Bioengineering 80 (4): 369-376.

Olaizola, M. (2003). "Commercial development of microalgal biotechnology: from the test tube to the marketplace." Biomolecular Engineering 20: 459-466.

Olson, J.A. *et al.* (1989). "Symposium: Biological actions of carotenoids." *American Institute of Nutrition*: 94-137.

Oswald, W.J. (1963). "The high-rate pond in waste disposal." Developments in Industrial Microbiology 4: 112-125.

Otero, A. *et al.* (1997a). "Factors controlling eicosapentaenoic acid production in semicontinuous cultures of marine microalgae." Journal of Applied Phycology 9: 465-469.

Otero, A. *et al.* (1997b). "Manipulation of the biochemical composition of the eicosapcntaenoic acid-rich microalga *Isochrysis galbana* in semicontinuous cultures." Biotechnology and Applied Biochemistry 26: 171-177.

Parke, M. (1949). "Studies on marine flagellates." Journal of the Marine Biological Association of the United Kingdom 28: 255-286.

Parrish, C.C. (1999). Determination of total lipid, lipid classes, and fatty acids in aquatic samples. Lipids in freshwater ecosytems. Arts, M.T. and Wainman, B.C. New York, Springer-Verlag: 4-20.

Parrish, C.C. *et al.* (1998). "Growth and lipid composition of scallop juveniles, *Placopecten magellanicus,* fed the flagellate *Isochrysis galbana* with varying lipid composition and the diatom *Chaetoceros muelleri.*" Marine Biology **133**: 461-471.

Pavlou, S. (1999). "Computing operating diagrams of bioreactors." Journal of Biotechnology **71**: 7-16.

Perez, J.A.S. (1994). "n-3 Polyunsaturated fatty acid productivity of the marine microalga *Isochrysis galbana.* Growth conditions and phenotypic selection." Journal of Applied Phycology **6**: 475-478.

Phatarpekar, P.V. *et al.* (2000). "A comparative study on growth performance and the biochemical composition of mixed culture of *Isochrysis galbana* and *Chaetoceros calcitrans* with monocultures." Aquaculture **181**: 141-155.

Pielke, R. (1995). "Phytoplankton and the biological pump" Reviews of Geophysics **33**: Supplement 1995. http://www.agu.org/revgeophys/chisho00/node2.html (last access date 20/07/2005).

Poisson, L. and Ergan, F. (2001). "Docosahexaenoic acid ethyl esters from *Isochrysis galbana.*" Journal of Biotechnology **91**: 75-81.

Politi, L. *et al.* (2001). "Effects of docosahexaenoic acid on retinal development: cellular and molecular aspects." Lipids **36** (9): 927-935.

Pulz, O. and Scheibenbogen, K. (1998). "Photobioreactors: Design and performance with respect to light energy input." Advances in Biochemical Engineering/ Biotechnology **59**: 124-152.

Pulz, O. *et al.* (1995). "Light supply in plate-type and light diffusing optical fibre bioreactors." Journal of Applied Phycology **7**: 145-149.

Qi, B. *et al.* (2003). "The varient 'his-box' of the C18-Δ^9-PUFA-specific elongase IgASE1 from *Isochrysis galbana* is essentisal for optimum enzyme activity." Feberation of European Biochemical Societies Letters **547**: 137-139.

Qi, B. *et al.* (2002). "Indentification of a cDNA endcoding a novel C18-Δ^9 polyunsaturated fatty acid-specific elongating activity from the docosahexaenoic acid (DHA)-producing microalga, *Isochrysis galabana.*" Federation of European Biochemical Societies Letters **510**: 159-165.

Qiang, H. and Richmond, A. (1994). "Optimizing the population density in *Isochrysis galbana* grown outdoors in a glass column photobioreactor." Journal of Applied Phycology **6**: 391-396.

Rainuzzo, J.R. *et al.* (1994). "Effect of short- and long-term lipid enrichment on total lipids, lipid class and fatty acid composition in rotifers." Aquaculture International 2: 19-32.

Ratledge, C. (1998). Opportunities for marine microorganisms for the production of polyunsaturated fatty acids. Marine microorganisms for industry : Proceedings of the meeting held in Brest-France on the 17-19th of September 1997. Le Gal, Y. and Muller-Feuga, A. Plouzané, France, IF REMER: 18-25.

Reitan, K. *et al.* (1997). "A review of the nutritional effects of algae in marine fish larvae." Aquaculture 155: 207-221.

Renaud, S.M. (2002). "Effect of temperature on growth, chemical composition and fatty acid composition of tropical Australian microalgae grown in batch cultures." Aquaculture 211: 195-214.

Renaud, S.M. *et al.* (1999). "The gross chemical composition and fatty acid composition of 18 tropical Australian microalgae for possible use in mariculture." Aquaculture 170: 147-159.

Renaud, S.M. *et al.* (1995). "Effect of temperature on the growth, total lipid content and fatty acid composition of recently isolated tropical microalgae *Isochrysis* sp, *Nitzschia closterium, Nitzschia paleacea,* and commercial species *Isochrysis* sp. (clone T.ISO)." Journal of Applied Phycology 7: 595-602.

Richmond, A. *et al.* (2003). "Efficient use of strong light for high photosynthetic productivity: interrelationships between the optical path, the optimal population density and cell-growth inhibition." Biomolecular Engineering 20: 229-236.

Richmond, A. (2000). "Microalgal biotechnology at the turn of the millennium: a personal view." Journal of Applied Phycology 12: 441-451.

Richmond, A. and Zou, N. (1999). "Efficient utilisation of high photon irradiance for mass production of photoautrophic micro-organisms." Journal of Applied Phycology 11: 123-127.

Richmond, A. *et al.* (1993). "A new tubular reactor for mass production of microalgae products." Journal of Applied Phycology 5: 327-332

Rimmer, M. (2000). "Review of grouper hatchery technology." Secretariat of the Pacific Community (SPC) Live Reef Fish Information Bulletin 7 (May): 14-19.

Rodolfi, L. *et al.* (2003). "Growth medium recycling in *Nannochloropsis* sp. mass cultivation." Biomolecular Engineering 20: 243-248.

Rorrer, G.L. and Mullikin, R.K. (1999). "Modelling and simulation of a tubular recycle photobioreactor for macroalgal cell suspension cultures." Chemical Engineering Sciences **54**: 3153-3162.

Ryer, A. (1997). "Light measurement handbook." International Light. Http://www.intl-light.com/handbook (last access date 20/07/05).

Sakshaug, E. *et al.* (1997). "Parameters of photosynthesis: definitions, theory and interpretation of results." Journal of Plankton Research **19** (11): 1637-1670.

Sanchez, S. *et al.* (2000). "Biomass production and biochemical variability of the marine microalgae *Isochrysis galbana* in relation to culture medium." Biochemical Engineering Journal **6**: 13-18.

Sargent, J. *et al.* (1999a). "Recent developments in the essential fatty acid nutrition of fish." Aquaculture **177**: 191-199.

Sargent, J. *et al.* (1999b). "Lipid nutrition of marine fish during early development: current status and future directions." Aquaculture **179**: 217-229.

Sevilla, J.M.F. *et al.* (1998). "Photolimitation and photoinhibition as factors determining optimal dilution rate to produce eicosapentaenoic acid from cultures of the microalga *Isochrysis galbana*." Applied Microbiology and Biotechnology **50**: 199-205.

Schlotter, P. *et al.* (1999). "Fabrication and characterization of GaN/ InGaN/ AlGaN double heterostructure LEDs and their application in luminescence conversion LEDs." Materials Science and Engineering **B59**: 390-394.

Schopf, J.W. (1996). "Cyanobacteria: Pioneers of early Earth." Nova Hedwigia **112**: 13-32.

Scragg, A.H. *et al.* (2002). "Growth of microalgae with increased calorific values in a tubular bioreactor." Biomass and Bioenergy **23**: 67-73.

Sevilla, J.M.F. *et al.* (1998). "Photolimitation and photoinhibition as factors determining optimal dilution rate to produce eicosapentaenoic acid from cultures of the microalga *Isochrysis galbana*." Applied Microbiology and Biotechnology **50**: 199-205.

Shaish, A. *et al.* (1992). "Biosynthesis of ß-carotene in *Dunaliella*." *Methods in Enzymology* **213**: 439-444.

Sinnot, R. (1988). "Fish pigmentation." *Trout News* 7: 8-11.

Stuchlík, M. and Zák, S. (2002). "Vegetable lipids as components of functional foods." Biomedical Papers **146** (2): 3-10.

Suen, Y.H. *et al.* (1987). "Total lipid production of the green alga *Nannochloropsis* sp. QII under different nitrogen regimes." Journal of Phycology **23**: 289-296.

Sukenik, A. (1991a). "Ecophysiological considerations in the optimization of Eicosapentaenoic Acid production by *Nannochloropsis* sp. (Eustigmatophyceae)." Bioresource Technology **35**: 263-269.

Sukenik, A. *et al.* (1989). "Regulation of fatty acid composition by irradiance levels in the eustigmatophyte *Nannochloropsis sp.*" Journal of Phycology **25**: 686-692.

Tapiero, H. *et al.* (2002). "Polyunsaturated fatty acids (PUFA) and eicosandoids in human health and pathologies." Biomedicine and Pharmacotherapy **56**: 215-222.

Tonon, T.H. *et al.* (2002). "Long chain polyunsaturated fatty acids production and partitioning to triacylglycerols in four microalgae." Phytochemistry **61**: 15-24.

Tramper, J. *et al.* (2003). "What to do in marine biotechnology?" Biomolecular Engineering **20**: 467-471

Tsavalos, A.J; Harker, M. and Young, A.J. (1993). "Analysis of carotenoids using HPLC with diode-array detection" Chromatography and Analysis (April/ May): 9-11.

Tsavalos, A. (1995). "Production of microalgal secondary carotenoids" Ph.D thesis, Liverpool John Moores University.

Tzovenis, I. *et al.* (2003). "Optimisation of T-ISO biomass production rich in essential fatty acids: I. Effect of different light regimes on growth and biomass production." Aquaculture **216**: 203-222.

Tzovenis, I. *et al.* (1997). "Effect of different light regimes on the docosahexenoic acid (DHA) content of *Isochrysis* aff. *galbana* (clone T.ISO)." Aquaculture International **5**: 489-507.

Uauy, R. *et al.* (2001). "Essential fatty acids in visual and brain development." Lipids **36** (9): 885-895.

Valenzuela-Espinoza, E. *et al.* (2002). "Protein, carbohydrate, lipid and chlorophyll a content of *Isochrysis aff. galbana (T.iso)* cultures with a low-cost alternative to the F/2 medium." Aquacultural Engineering **25**: 207-216.

Venkatraman, J.T. and Meksawan, K. (2002). "Effects of dietary w3 and w6 lipids and vitamin E on chemokine levels in autoimmune-prone MRL/MpJ- Ipr/Ipr mice." Journal of Nutritional Biochemistry 13: 479-486.

Vandanjon, L.R. *et al.* (1999). "Effects of shear on two microalgae species. Contribution of pumps and valves in tangential flow filtration systems." Biotechnology and Bioengineering **63** (1): 1-9.

Walker, D. (1988). The use of the oxygen electrode and fluorescence probes in simple measurements of photosynthesis. Sheffield, Packard Publishing Ltd.

Watanabe, Y. and Hall, D.O. (1996). "Photosynthetic CO_2 conversion technologies using a photobioreactor incorporating microalgae: energy and material balances." Energy Conservation Management **37** (6-8): 1321-1326

Watanabe, T. *et al.* (1983). "Nutritional values of live organisms used in Japan for mass propagation of fish: a review." Aquaculture **34**: 115-143.

Wen, Z-Y. and Chen, F. (2003). "Heterotrophic production of eicosapentaenoic acid by microalgae." Biotechnology Advances **21**: 273-297.

Whyte, J.N.C. and Nagata, W.D. (1990). "Carbohydrate and fatty acid composition of the rotifer *Brachionus plicatilis,* fed on monospecific diets of yeast or phytoplankton." Aquaculture **89**: 263-273.

Whyte, J.N.C. (1987). "Biochemical composition and energy composition of six species of phytoplankton used in mariculture of bivalves." Aquaculture **60**: 231-241.

Wozniak, B. and Dera, J. (2000). "Luminescence and photosynthesis of marine phytoplankton- a brief presentation of new results." Oceanologia 42(2): 137-156.

Yamaguchi, K. (1997). "Recent advances in microalgal bioscience in Japan, with special reference to utilization of biomass and metabolites: A review." Journal of Applied Phycology **8**: 487-502.

Young, A.J. and Britton, G. (1993). Carotenoids in Photosynthesis, Chapman & Hall, London.

Youngblood, J.P. *et al.* (2003). "Coatings Based on Side-chain Ether-linked Poly(ethylene glycol) and Fluorocarbon Polymers for the Control of Marine Biofouling." Biofouling **19**: 91–98.

Zhu, C.J. *et al.* (1997a). "Diurnal changes in gross chemical composition and fatty acid profiles of *Isochrysis galbana* TK1 in outdoor closed tubular photobioreactors." Journal of Marine Biotechnology **5**: 153-157.

Zhu, C.J. *et al.* (1997b). "Effects of temperature and growth phase on lipid and biochemical composition of *Isochrysis galbana* TK1." Journal of Applied Phycology **9**: 451-457.

Zittelli, G.C. *et al.* (1999). "Production of eicosapentaenoic acid by *Nannochloropsis* sp. cultures in outdoor tubular photobioreactors." Journal of Biotechnology **70**: 299-312.

Zou, N. and Richmond, A. (2002). "Light-path length and population density in photoacclimation of *Nannochloropsis sp.* (Eustigmatophyceae)." Journal of Applied Phycology **12**: 349-354.

Zou, N. *et al.* (2000). "Production of cell mass and eicosapentaenoic acid (EPA) in ultrahigh cell density cultures of *Nannochloropsis sp.* (Eustigmatophyceae)." European Journal of Phycology **35**: 127-133.

ACKNOWLEDGEMENTS

Thanks first of all to Andy Young and the Carotenoid research team of 1996 for taking me under their wings last minute and actually teaching me some science, such as how to use a pipette and a microscope. Thanks also to everyone who joined ranks in the 6th floor lab along the way too. It's been a long road, but the scenery was all worth it.

My main thanks goes out to family and friends for their continued patience and support. Especially for still being my friends, having effectively becoming a hermit for the past couple of years. Much thanks also to Abolfazl Saajedi who, just in passing, allowed me to use his office to print off this dreadnought of documented ditch-water on a less than brilliant day. You helped save the day, and what little remained of my sanity- well what ever form it usually takes anyways.

Final respects goes to my long suffering and fatigued computer, which has sorely earnt it's place in silicon heaven ("where all the calculators go") after putting me through hell..... its payback time!

APPENDIX A:

GLOSSARY OF TERMS & ABBREVIATIONS

ABS	Acrylonitrile Butadiene Styrene. An amorphous translucent plastic
AFDW	Ash-free dry weight
ALR	Air Lift Reactor. A bioreactor mixed and recirculated using an air-pump. Generates low shearing, which would otherwise damage cultures with weak cell calls/ membranes (such as microalgae)
ARA	Arachidonoic acid (20:4n-6). An intermediate in omega-6 PUFA pathway. Refer to figures 1.6, 3.5 and table 3.1
ARC	Artemia Reference Centre
ASP	Aquatic Species Program
Aspect ratio	Height : Diameter. Used to describe general shape of a bioreactor. High aspect ratio refers to tall thin bioreactors.
Atherogenesis	Process leading to the formation of a plaque (atheroma) within the smooth muscle of blood vessels
Biotic	Biological conditions. Effects of predation and competition from other organisms.
CCAP	Culture Collection of Alga and Protozoa
CCMP	Centre for the Culture of Marine Phytoplankton
CSTR	Conventional Stirred Tank Reactor. A traditional style of bioreactor used for various industrial microbial fermentations
DART	Diet And Reinfarction Trial
DHA	Docasahexaenoic acid (22:6 n-3). Refer to figures 1.6, 3.5 and table 3.1
DW	Dry weight
EDA	Refer to figures 1.6, 3.5 and table 3.1
EFA	Essential Fatty Acids. Those which are unable to be synthesised, but which must be ingested. Namely omega-3 fatty acids, particularly PUFAs
EPA	Eicosapentaenoic acid (20:5 n-3). An intermediate in the omega-3 PUFA pathway. Refer to figures 1.6, 3.5 and table 3.1
FAME	Fatty Acid Methyl Ester
GC	Gas chromatography- analytical method which vapourises liquid compounds, moved across a matrix using a carrier gas. A temperature gradient. Retention time on the matrix complex compounds

GISSI	Gruppo Italiano per lo Studio della Sopravvivenza nell'Infarto miocardio (Italian group for the study of infarct survival).
GL	Galactolipid. A class of polar lipids associated with thylakoid membranes
HDA	An external standard used to calibrate. Refer to figure 3.5 and table 3.1
HDL	High-Density Lipoprotein
HIMB	Hawaii Institute of Marine Biology
Laminar flow	Fluid dynamic expression for unidirectional parallel flow. Antonym, turbulent flow.
LAU	Refer to figures 1.6, 3.5 and table 3.1
LDL	Low-Density Lipoprotein
LHP	Light harvesting pigments. Pigment-protein complexes which act as antennae to harvest light energy and channel electrons towards photosystems (PSI and PSII)
LIN	Linoleic acid (18:2 n-6). Refer to figures 1.6, 3.5 and table 3.1
LKLL	Lake Kinneret Limnological Laboratory
LON	Linolenic acid (18:3 n-3). Refer to figures 1.6, 3.5 and table 3.1
MUFA	Mono-unsaturated fatty acids- containing only one double bond between two carbon atoms along the hydrocarbon tail. Includes PML and OLE.
MYR	Refer to figures 1.6, 3.5 and table 3.1
NREL	National Renewable Energy Laboratory
NRV	Non-return valve. Allows one-way flow and prevents backflow of liquid/ gases
OLE	Refer to figures 1.6, 3.5 and table 3.1
Omega-3 PUFA	A group of PUFAs, with double bonds beginning from the 3rd carbon atom of the methyl end group (n-3)
Omega-6 PUFA	A group of PUFAs, with double bonds beginning from the 6th carbon atom of the methyl end group (n-6)
Opsin/ Rhodopsin	Visual pigments in eyes. When opsin (a protein) becomes bound to the pigment 11 *cis*-retinal, it forms rhodopsin. In the presence of light it is converted to all-*trans*-retinal activating signal transduction pathways
OTA	Refer to figures 1.6, 3.5 and table 3.1
PAL	Refer to figures 1.6, 3.5 and table 3.1

PAR	Photosynthetically Active Radiation. Spectral range of light available for photosynthetic pigments (400 – 700nm)
PBR	Plate-type Bioreactor
PEMBS	Port Erin Marine Biological Station
PFD	Photon Flux Density. An expression derived from the field of photobiology used to express I_o within PAR, measured as µmol/m^2/s. This term is commonly used with reference towards determining photosynthetic efficiency.
Photoautotrophic	Able to grow in the presence of light which generates the energy (via photosynthesis) required to assimilate atmospheric carbon
Photoinhibition	The cessation of growth due to cell stress invoked by excess light (cell damaged by over excitation of pigments)- producing free radicals within the cell. Typical of 'dilute'/ optically thin algal cultures (low cell density).
Photolimitation	The cessation of growth due to insufficient lighting (average irradiance) necessarily for optimal photosynthesis, or as a result of self-shading. Typical of dense cultures.
PL	Phospholipid. A class of polar lipids associated with cell membranes
PML	Refer to figures 1.6, 3.5 and table 3.1
PS I	Photosystem I. See also PSU (below)
PS II	Photosystem II. See also PSU (below)
PSU	Photosynthetic unit. Includes PS I and II, reaction centres and LHCPs bound to thylakoid membrane. Refer to section 1.9.2. There are two strategies of Photoadaptation: (a) change number of PSUs or (b) change the size of PSUs.
PTFE	Polytetrafluoroethylene
PUFA (HUFA / LC-PUFA)	Polyunsaturated Fatty Acid. Unsaturated (containing double bonds) fatty acids with hydrocarbon chain lengths greater than 18 carbon atoms. Also referred to as Highly Unsaturated Fatty Acids or Long Chain –PUFA. Includes LIN, LON, OTA, EDA, ARA, EPA and DHA
PVC-U	Poly Vinyl Chloride- Unplastisized
RuBP	Ribulose bisphosphate. A 5C sugar that binds to CO_2 to form the enzyme RuBP carboxylase, used in the Calvin cycle of photosynthesis to fix carbon for cell metabolism. Oxygen is a competitive inhibitor of RuBP, leading to inefficient photosynthesis (photorespiration)
SAT	Saturated fatty acids- single bonds between carbon atoms. Includes LAU, MYR, PAL and STE
SCOR	Scientific Committee on Oceanic Research
Self-shading	In dense culture, the cells furthest from the light source receive less light energy than those immediately in front.

SERI	Solar Energy Research Institute
ST	Sterol. A class of cyclic unsaturated lipids.
STE	Refer to figures 1.6, 3.5 and table 3.1
TAG	Triacylglycerol. A class of neutral (non-polar) lipid acting as a storage compound
TBR	Tubular Photobioreactor
TML	Tungkang Marine Laboratory
Triacylglycerides	Dietary fats (neutral and phospolipids from foods) re-synthesised by intestinal epithelial cells
Turbulent flow	Fluid dynamic expression for erratic/ chaotic flow patterns producing eddies (flow in opposite direction). Antonym, laminar flow.
UNESCO	United Nations Educational, Scientific and Cultural Organization
Xanthophylls	Sub-class of >600 carotenoids (secondary pigments). Derivatives of Lycopene ($C_{40}H_{56}$ carotenoid pre-cursor) with oxygenated (cyclic or non-cyclic) end groups. Help dissipate thermal energy instead of transferring to reaction centres of PSU.
‰	Salinity concentration, expressed as parts per thousand (ppt)

APPENDIX B: GROWTH MEDIA

All medium was formulated using artificial sea-salt ("Coral Reef Red", Red Sea Pharmaceuticals: Israel) dissolved in distilled water at a density of 32 ‰ (unless otherwise stated). At this concentration, this commercially available artificial sea-salt is known to contain the following elements (expressed in ppb): Manganese (29); Zinc (5); Molybdenum (5.1); Nickel (2.2); Chromium (0.51); Lead (0.37); Antimony (0.18).

f/2 MEDIUM

	Concentration		Amount	Stock solutions	
Major Elements Solution	**M_w**	**mM**	**g/L**	**g/L**	**Add (ml/L)**
$NaNO_3$	85.00	0.882	0.075000	75.000	1
$NaH_2PO_4.H_2O$	156.00	0.036	0.005650	5.650	1
Trace Elements Solution	**M_w**	**µM**	**g/L**	**g/L**	**Add (ml/L)**
EDTA Na_2	372.20	11.714	0.004360	4.360	1
$FeCl_3.6H_2O$	270.30	11.654	0.003150	3.150	1
$MnCl_2.4H_2O$	197.90	0.910	0.000180	0.180	1
$ZnSO_4.7H_2O$	287.54	0.077	0.000022	0.022	1
$CoCl_2.6H_2O$	237.93	0.042	0.000010	0.010	1
$CuSo_4.5H_2O$	249.68	0.040	0.000010	0.010	1
$Na_2MoO_4.2H_2O$	241.95	0.025	0.000006	0.006	1
Vitamin Solution	**M_w**	**nM**	**g/L**	**g/L**	**Add (ml/L)**
Thiamine HCl (Vit. B1)	337.30	296.000	0.0001000	0.1	1
Biotin (Vit. H)	244.31	2.047	0.0000005	0.0005	1
Cyanocobalamin (Vit. B12)	1355.4	0.369	0.0000005	0.0005	1

sf/2 MEDIUM (modified f/2)

	Concentration		Amount	Comparison to	Stock solutions	
Major Elements Solution	**M_w**	**MM**	**g/L**	**f/2 (%)**	**g/L**	**Add (ml/L)**
$NaNO_3$	85.00	7.118	0.605000	+707	605.000	1
$NaH_2PO_4.H_2O$	156.00	0.096	0.014900	+164	14.9.000	1
Trace Elements Solution	**M_w**	**µM**	**g/L**	**± % f/2**	**g/L**	**Add (ml/L)**
EDTA Na_2	372.20	11.177	0.0041600	-5	4.160	1
$FeCl_3.6H_2O$	270.30	11.654	0.0031500	0	3.150	1
$MnCl_2.4H_2O$	197.90	0.910	0.0001800	0	0.180	1
$ZnSO_4.7H_2O$	287.54	-	-	-100	-	-
$CoCl_2.6H_2O$	237.93	-	-	-100	-	-
$CuSo_4.5H_2O$	249.68	-	-	-100	-	-
$Na_2MoO_4.2H_2O$	241.95	-	-	-100	-	-
Vitamins Solution	**M_w**	**nM**	**g/L**	**± % f/2**	**g/L**	**Add (ml/L)**
Thiamine HCl (Vit. B1)	337.30	296.000	0.0001000	0	0.100	1
Biotin (Vit. H)	244.31	-	-	-100	-	-
Cyanocobalamin (Vit. B12)	1355.4	0.369	0.0000005	0	0.0005	1

APPENDIX C:

TUBULAR PHOTOBIOREACTOR, TECHNICAL SPECIFICATIONS

	Material	Height/ Length (mm)	Width/ Diameter (mm)	Depth (mm)	Thickness (mm)	Working Volume (L)
HEADER TANK	Acrylic (transparent)	400	200	400	5	15.92 (minus gas hold-up)
Access port	ABS (grey)	-	160	10	-	-
Sample port	ABS (grey)	-	8	10	-	-
Manifold vent port	ABS (grey)	-	45	10	-	-
Air inlet port	ABS (grey)	-	15	10	-	-
Air outlet port	ABS (grey)	-	15	10	-	-
Overflow port	ABS (grey)	-	34	10	-	-
Water inlet port	ABS (grey)	-	15	10	-	-
Nutrient inlet port	ABS (grey)	-	8	10	-	-
RISER	PVC-U (Transparent)	2116	68 (I.D.) 74 (O.D.)	-	3	4.52
DOWNCOMER	PVC-U (grey)	1752	56 (I.D.) 62 (O.D.)	-	3	3.08
OUTLET MANIFOLD 3 × outlet	PVC-U (grey)	245 45	80 26	-	4 2	0.62
RETURN MANIFOLD 3 × outlet	PVC-U (grey)	245 45	80 26	-	4 2	0.62
U-BEND	PVC-U (grey)	1442	56 (I.D.) 62 (O.D.)	-	3	2.53
PHOTOSTAGE Photostage support	Stainless steel	1139	720 (I.D.) 780 (O.D.)	-	2	-
Photostage tubing (× 3 windings; 8.5 turns)	foodgrade PVC	2262 (57681)	24 (I.D.) 30 (O.D.)	-	3	1.71 (43.49)
SUPPORT MAST	Stainless steel	2294	68	68	3	-
UNION PLATE	Stainless steel	1139	262	-	2	-
CONTROL BOX	ABS (Beige)	400	300	200	3	-
BASE	Stainless steel	231	928	2	3	-

SECTION	Vol (L)/ size (mm)
Header tank (working, minus gas hold-up)	15.92
Riser	4.52
Downcomer	3.08
2 × Manifold	0.62
U-bend	2.53
Photostage:	
Coil winding length	2262
No. coil windings	3
No. turns/ coil winding	8.5
Volume/ winding	1.71
Total volume	43.49
Surface area (inner)	5121
SA : volume	1.18
TOTAL WORKING VOLUME	**70.78**

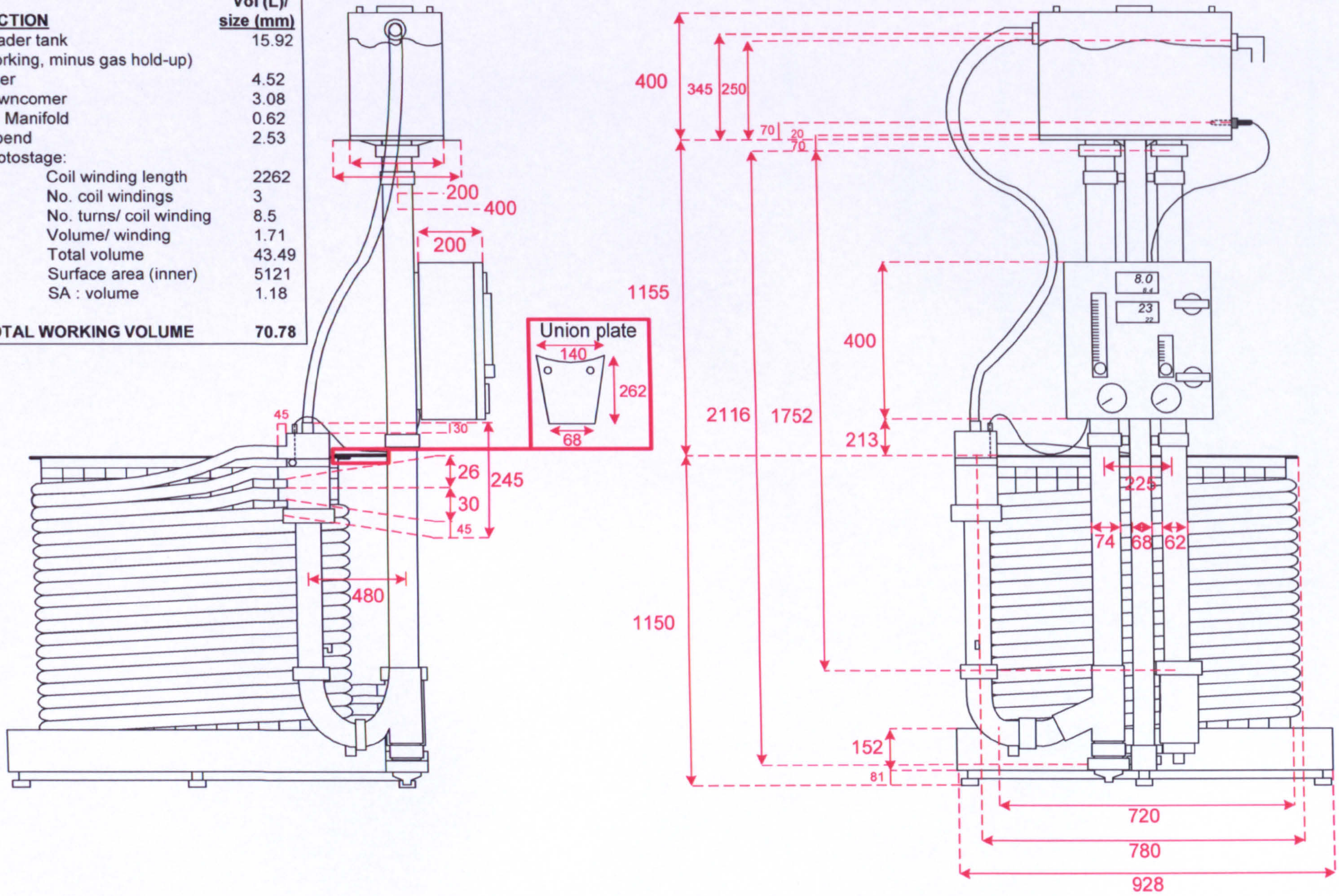

(Not to scale. All measurements in mm)

APPENDIX D:
STATISTICAL DATA

Section 4.1.2: *I. galbana* media conditions (Pages 75 - 77)

Variable	Compare	Relationship	Test statistic	Test Value	d.f.	*p* Value	Significant
Cell/ml	16‰ f/2 V 32‰ f/2	Difference	Mann Whittney (W)	173	13	0.9183	no
	16‰ f/2 V 16‰ sf/2	Difference	Mann Whittney (W)	151	13	0.2184	no
	16‰ f/2 V 32‰ sf/2	Difference	Mann Whittney (W)	169	13	0.7583	no
	32‰ f/2 V 16‰ sf/2	Difference	Mann Whittney (W)	147	13	0.151	no
	32‰ f/2 V 32‰ sf/2	Difference	Mann Whittney (W)	169	13	0.7583	no
	16‰ sf/2 V 32‰ sf/2	Difference	Mann Whittney (W)	190	13	0.4728	no
	All formulations	Difference	Kruskal Wallis (H)	2.26	3	0.521	no
	Cell/ml V salinity	Correlation	Spearman Rank (rs)	-0.087	52	>0.05	no
	Cell/ml V media	Correlation	Spearman Rank (rs)	0.169	52	>0.05	no
Cell size	16‰ f/2 V 32‰ f/2	Difference	Mann Whittney (W)	145	13	0.1239	no
	16‰ f/2 V 16‰ sf/2	Difference	Mann Whittney (W)	191	13	0.4418	no
	16‰ f/2 V 32‰ sf/2	Difference	Mann Whittney (W)	139	13	0.0649	no
	32‰ f/2 V 16‰ sf/2	Difference	Mann Whittney (W)	212	13	0.0649	no
	32‰ f/2 V 32‰ sf/2	Difference	Mann Whittney (W)	174	13	0.9591	no
	16‰ sf/2 V 32‰ sf/2	Difference	Mann Whittney (W)	138.5	13	0.0612	no
	All formulations	Difference	Kruskal Wallis (H)	6.86	3	0.077	no
	Cell size V salinity	Correlation	Spearman Rank (rs)	0.36	52	<0.02	yes
	Cell size V media	Correlation	Spearman Rank (rs)	-0.036	52	>0.05	no

Section 4.1.3: *I. galbana* nitrate limitation (Pages 77 - 79)

Variable	Compare	Relationship	Test statistic	Test Value	d.f.	*p* Value	Significant
Cell/ml	3.56mM V 5.34mM	Difference	Mann Whittney (W)	113	11	0.3933	no
	3.56mM V 7.12mM	Difference	Mann Whittney (W)	112	11	0.3579	no
	3.56mM V 8.90mM	Difference	Mann Whittney (W)	110.5	11	0.3088	no
	3.56mM V 10.68mM	Difference	Mann Whittney (W)	112	11	0.3579	no
	5.34mM V 7.12mM	Difference	Mann Whittney (W)	119	11	0.6458	no
	5.34mM V 8.90mM	Difference	Mann Whittney (W)	118	11	0.5994	no
	5.34mM V 10.68mM	Difference	Mann Whittney (W)	118	11	0.5994	no
	7.12mM V 8.90mM	Difference	Mann Whittney (W)	117	11	0.5545	no
	7.12mM V 10.68mM	Difference	Mann Whittney (W)	118	11	0.5994	no
	8.90mM V 10.68mM	Difference	Mann Whittney (W)	1222	11	0.7928	no
	All Concs	Difference	Kruskal Wallis (H)	2.03	4	0.7310	no
	Cell/ml V conc.	Correlation	Spearman Rank (rs)	0.186	55	>0.05	no
Cell/ml (d 19-29)	3.56mM V 5.34mM	Difference	Mann Whittney (W)	10	4	0.0304	yes
	3.56mM V 7.12mM	Difference	Mann Whittney (W)	10	4	0.0304	yes
	3.56mM V 8.90mM	Difference	Mann Whittney (W)	10	4	0.0304	yes
	3.56mM V 10.68mM	Difference	Mann Whittney (W)	10	4	0.0304	yes
	5.34mM V 7.12mM	Difference	Mann Whittney (W)	12	4	0.1124	no
	5.34mM V 8.90mM	Difference	Mann Whittney (W)	10	4	0.0304	yes
	5.34mM V 10.68mM	Difference	Mann Whittney (W)	10	4	0.0304	yes
	7.12mM V 8.90mM	Difference	Mann Whittney (W)	10	4	0.0304	yes
	7.12mM V 10.68mM	Difference	Mann Whittney (W)	10	4	0.0304	yes
	8.90mM V 10.68mM	Difference	Mann Whittney (W)	13	4	0.1939	no
	All Concs	Difference	Kruskal Wallis (H)	17.33	4	0.002	yes

Section 4.1.3: *I. galbana* nitrate limitation *continued* (Pages 77 - 79)

Variable	Compare	Relationship	Test statistic	Test Value	d.f.	*p* Value	Significant
Cell size	3.56mM V 5.34mM	Difference	Mann Whittney (W)	159.5	11	0.0327	yes
	3.56mM V 7.12mM	Difference	Mann Whittney (W)	160	11	0.0301	yes
	3.56mM V 8.90mM	Difference	Mann Whittney (W)	158.5	11	0.0385	yes
	3.56mM V 10.68mM	Difference	Mann Whittney (W)	163	11	0.018	yes
	5.34mM V 7.12mM	Difference	Mann Whittney (W)	128	11	0.9476	no
	5.34mM V 8.90mM	Difference	Mann Whittney (W)	139	11	0.4302	no
	5.34mM V 10.68mM	Difference	Mann Whittney (W)	139.5	11	0.4114	no
	7.12mM V 8.90mM	Difference	Mann Whittney (W)	140	11	0.3932	no
	7.12mM V 10.68mM	Difference	Mann Whittney (W)	136.5	11	0.5325	no
	8.90mM V 10.68mM	Difference	Mann Whittney (W)	121	11	0.7425	no
	All Concs	Difference	Kruskal Wallis (H)	8.98	4	0.062	no
	Cell size V conc.	Correlation	Spearman Rank (rs)	-0.353	55	<0.05	yes
Cell size (d 19-29)	3.56mM V 5.34mM	Difference	Mann Whittney (W)	57	6	0.005	yes
	3.56mM V 7.12mM	Difference	Mann Whittney (W)	57	6	0.005	yes
	3.56mM V 8.90mM	Difference	Mann Whittney (W)	57	6	0.005	yes
	3.56mM V 10.68mM	Difference	Mann Whittney (W)	56	6	0.0082	yes
	5.34mM V 7.12mM	Difference	Mann Whittney (W)	41	6	0.8085	no
	5.34mM V 8.90mM	Difference	Mann Whittney (W)	51	6	0.0651	no
	5.34mM V 10.68mM	Difference	Mann Whittney (W)	46.5	6	0.2607	yes
	7.12mM V 8.90mM	Difference	Mann Whittney (W)	52	6	0.045	yes
	7.12mM V 10.68mM	Difference	Mann Whittney (W)	47.5	6	0.1986	no
	8.90mM V 10.68mM	Difference	Mann Whittney (W)	33	6	0.3768	no
	All Concs	Difference	Kruskal Wallis (H)	17.64	4	0.002	yes

Section 4.1.4: *I. galbana* temperature (Pages 80 - 81)

Variable	Compare	Relationship	Test statistic	Test Value	d.f.	*p* Value	Significant
Cell/ml	15°C V 20°C	Difference	Mann Whittney (W)	125	15	0	yes
	15°C V 25°C	Difference	Mann Whittney (W)	130	15	0	yes
	15°C V 30°C	Difference	Mann Whittney (W)	154	15	0.0012	yes
	20°C V 25°C	Difference	Mann Whittney (W)	274	15	0.089	no
	20°C V 30°C	Difference	Mann Whittney (W)	322	15	0.0002	yes
	25°C V 30°C	Difference	Mann Whittney (W)	319	15	0.0004	yes
	All temps	Difference	Kruskal Wallis (H)	37.46	3	0	yes
	Cell/ml V temp.	Correlation	Spearman Rank (rs)	0.211	60	<0.05	yes
Cell size	15°C V 20°C	Difference	Mann Whittney (W)	342	15	0	yes
	15°C V 25°C	Difference	Mann Whittney (W)	336	15	0	yes
	15°C V 30°C	Difference	Mann Whittney (W)	288	15	0.0225	yes
	20°C V 25°C	Difference	Mann Whittney (W)	199	15	0.1711	no
	20°C V 30°C	Difference	Mann Whittney (W)	135	15	0.0001	yes
	25°C V 30°C	Difference	Mann Whittney (W)	145	15	0.0003	yes
	All temps	Difference	Kruskal Wallis (H)	37.49	3	0	yes
	Cell size V temp.	Correlation	Spearman Rank (rs)	-0.141	60	>0.05	no

Section 4.1.5: *I. galbana* semi-continuous culture (Pages 82 - 84)

Variable	Compare	Relationship	Test statistic	Test Value	d.f.	*p* Value	Significant
Cell/ml	10% V 20% day 18-46	Difference	Mann Whittney (W)	126	9	0.0004	yes
	10% V 30% day 18-46	Difference	Mann Whittney (W)	126	9	0.0004	yes
	10% V 40% day 18-46	Difference	Mann Whittney (W)	126	9	0.0004	yes
	20% V 30% day 18-46	Difference	Mann Whittney (W)	126	9	0.0004	yes
	20% V 40% day 18-46	Difference	Mann Whittney (W)	126	9	0.0004	yes
	30% V 40% day 18-46	Difference	Mann Whittney (W)	126	9	0.0004	yes
	Daily renewal day 0-14	Difference	Kruskal Wallis (H)	0.34	3	0.952	no
	Daily renewal day 18-46	Difference	Kruskal Wallis (H)	32.84	3	0	yes
	Cell/ml V daily renewal	Correlation	Spearman Rank (rs)	-0.969	36	<0.02	yes
Cell size	10% V 20% day 18-46	Difference	Mann Whittney (W)	100	9	0.2164	no
	10% V 30% day 18-46	Difference	Mann Whittney (W)	96	9	0.3772	no
	10% V 40% day 18-46	Difference	Mann Whittney (W)	112.5	9	0.0192	yes
	20% V 30% day 18-46	Difference	Mann Whittney (W)	83	9	0.8598	no
	20% V 40% day 18-46	Difference	Mann Whittney (W)	99	9	0.251	no
	30% V 40% day 18-46	Difference	Mann Whittney (W)	102	9	0.1577	no
	Daily renewal day 0-14	Difference	Mann Whittney (W)	0.98	3	0.806	no
	Daily renewal day 18-46	Difference	Kruskal Wallis (H)	6.04	3	0.11	no
	Cell size V daily renewal	Correlation	Spearman Rank (rs)	-0.377	36	<0.05	yes

Section 4.1.6: *I. galbana* oxygen evolution (Pages 84 - 85)

Variable	Compare	Relationship	Test statistic	Test Value	d.f.	*p* Value	Significant
Cell/ml	Cell/ml V R_d	Correlation	Spearman Rank (r_s)	1	6	<0.02	yes
	Cell/ml V α	Correlation	Spearman Rank (r_s)	-0.543	6	>0.05	no
	Cell/ml V P_{max}	Correlation	Spearman Rank (r_s)	1	6	<0.02	yes
	Cell/ml V net P_{max}	Correlation	Spearman Rank (r_s)	-0.543	6	>0.05	no
	Cell/ml V I_k	Correlation	Spearman Rank (r_s)	-0.878	6	<0.05	yes
	Cell/ml V PFD I_k	Correlation	Spearman Rank (r_s)	-1	6	<0.02	yes
	Cell/ml V PFD 100	Correlation	Spearman Rank (r_s)	-1	6	<0.02	yes
R_d	R_d V α	Correlation	Spearman Rank (r_s)	-0.543	6	>0.05	no
	R_d V P_{max}	Correlation	Spearman Rank (r_s)	1	6	<0.02	yes
	R_d V net P_{max}	Correlation	Spearman Rank (r_s)	-0.543	6	>0.05	no
	R_d V I_k	Correlation	Spearman Rank (r_s)	-0.878	6	<0.05	yes
	R_d V PFD I_k	Correlation	Spearman Rank (r_s)	-1	6	<0.02	yes
	R_d V PFD 100	Correlation	Spearman Rank (r_s)	-1	6	<0.02	yes
α	α V P_{max}	Correlation	Spearman Rank (r_s)	-0.543	6	>0.05	no
	α V net P_{max}	Correlation	Spearman Rank (r_s)	1	6	<0.02	yes
	α V I_k	Correlation	Spearman Rank (r_s)	0.878	6	<0.05	yes
	α V PFD I_k	Correlation	Spearman Rank (r_s)	0.543	6	>0.05	no
	α V PFD 100	Correlation	Spearman Rank (r_s)	0.543	6	>0.05	no
P_{max}	P_{max} V net P_{max}	Correlation	Spearman Rank (r_s)	-0.543	6	>0.05	no
	P_{max} V I_k	Correlation	Spearman Rank (r_s)	-0.878	6	<0.05	yes
	P_{max} V PFD I_k	Correlation	Spearman Rank (r_s)	-1	6	<0.02	yes
	P_{max} V PFD 100	Correlation	Spearman Rank (r_s)	-1	6	<0.02	yes
Net P_{max}	Net P_{max} V I_k	Correlation	Spearman Rank (r_s)	0.878	6	<0.05	yes
	Net P_{max} V PFD I_k	Correlation	Spearman Rank (r_s)	0.543	6	>0.05	no
	Net P_{max} V PFD 100	Correlation	Spearman Rank (r_s)	0.543	6	>0.05	no
I_k	I_k V PFD I_k	Correlation	Spearman Rank (r_s)	0.878	6	<0.05	yes
	I_k V PFD 100	Correlation	Spearman Rank (r_s)	0.878	6	<0.05	yes

Section 4.1.7: *I. galbana* FAME profile (Pages 86 - 90)

Variable	Compare	Relationship	Test statistic	Test Value	d.f.	*p* Value	Significant
Volumertic FAME (all)	Total V all	Difference	Kruskal Wallis (H)	6.38	3	0.095	no
	SAT V all	Difference	Kruskal Wallis (H)	7.27	3	0.064	no
	MUFA V all	Difference	Kruskal Wallis (H)	8.5	3	0.037	yes
	PUFA V all	Difference	Kruskal Wallis (H)	6.59	3	0.087	no
	DHA V all	Difference	Kruskal Wallis (H)	7.46	3	0.059	no
Volumetric FAME (salinity)	Total V salinity	Difference	Mann Whittney (W)	26	6	0.0453	yes
	SAT V salinity	Difference	Mann Whittney (W)	25	6	0.0303	yes
	MUFA V salinity	Difference	Mann Whittney (W)	35	6	0.5745	no
	PUFA V salinity	Difference	Mann Whittney (W)	29	6	0.1282	no
	DHA V salinity	Difference	Mann Whittney (W)	26	6	0.0453	yes
	Total V salinity	Correlation	Spearman Rank (r_s)	0.628	12	<0.05	yes
	SAT V salinity	Correlation	Spearman Rank (r_s)	0.677	12	<0.05	yes
	MUFA V salinity	Correlation	Spearman Rank (r_s)	0.193	12	>0.05	no
	PUFA V salinity	Correlation	Spearman Rank (r_s)	0.483	12	>0.05	no
	DHA V salinity	Correlation	Spearman Rank (r_s)	0.628	12	<0.05	yes
Volumetric FAME (media)	Total V media	Difference	Mann Whittney (W)	35	6	0.5752	no
	SAT V media	Difference	Mann Whittney (W)	46.5	6	0.2615	no
	MUFA V media	Difference	Mann Whittney (W)	55.5	6	0.0103	yes
	PUFA V media	Difference	Mann Whittney (W)	33	6	0.3785	no
	DHA V media	Difference	Mann Whittney (W)	38	6	0.9362	no
	Total V media	Correlation	Spearman Rank (r_s)	0.193	12	>0.05	no
	SAT V media	Correlation	Spearman Rank (r_s)	-0.363	12	>0.05	no
	MUFA V media	Correlation	Spearman Rank (r_s)	-0.798	12	<0.05	yes
	PUFA V media	Correlation	Spearman Rank (r_s)	0.29	12	>0.05	no
	DHA V media	Correlation	Spearman Rank (r_s)	0.048	12	>0.05	no

Section 4.1.7: *I. galbana* FAME profile *continued* (Pages 86 - 90)

Variable	Compare	Relationship	Test statistic	Test Value	d.f.	*p* Value	Significant
Cellular FAME (all)	Total V all	Difference	Kruskal Wallis (H)	9.58	3	0.023	yes
	SAT V all	Difference	Kruskal Wallis (H)	8.94	3	0.031	yes
	MUFA V all	Difference	Kruskal Wallis (H)	8.84	3	0.032	yes
	PUFA V all	Difference	Kruskal Wallis (H)	9.87	3	0.02	yes
	DHA V all	Difference	Kruskal Wallis (H)	8.76	3	0.033	yes
Cellular FAME (salinity)	Total V salinity	Difference	Mann Whittney (W)	38	6	0.9362	no
	SAT V salinity	Difference	Mann Whittney (W)	33	6	0.3785	no
	MUFA V salinity	Difference	Mann Whittney (W)	35	6	0.5752	no
	PUFA V salinity	Difference	Mann Whittney (W)	30	6	0.1735	no
	DHA V salinity	Difference	Mann Whittney (W)	32	6	0.298	no
	Total V salinity	Correlation	Spearman Rank (r_s)	0.048	12	>0.05	no
	SAT V salinity	Correlation	Spearman Rank (r_s)	0.29	12	>0.05	no
	MUFA V salinity	Correlation	Spearman Rank (r_s)	0.193	12	>0.05	no
	PUFA V salinity	Correlation	Spearman Rank (r_s)	0.435	12	>0.05	no
	DHA V salinity	Correlation	Spearman Rank (r_s)	0.338	12	>0.05	no
Cellular FAME (media)	Total V media	Difference	Mann Whittney (W)	57	6	0.0051	yes
	SAT V media	Difference	Mann Whittney (W)	57	6	0.0051	yes
	MUFA V media	Difference	Mann Whittney (W)	57	6	0.0051	yes
	PUFA V media	Difference	Mann Whittney (W)	39	6	1	no
	DHA V media	Difference	Mann Whittney (W)	41	6	0.8102	no
	Total V media	Correlation	Spearman Rank (r_s)	-0.869	12	<0.02	yes
	SAT V media	Correlation	Spearman Rank (r_s)	-0.869	12	<0.02	yes
	MUFA V media	Correlation	Spearman Rank (r_s)	-0.869	12	<0.02	yes
	PUFA V media	Correlation	Spearman Rank (r_s)	0	12	>0.05	no
	DHA V media	Correlation	Spearman Rank (r_s)	0	12	>0.05	no

Section 4.1.7: *I. galbana* FAME profile *continued* (Pages 86 - 90)

Variable	Compare	Relationship	Test statistic	Test Value	d.f.	*p* Value	Significant
FAME as % Fatty acid (all)	SAT V all	Difference	Kruskal Wallis (H)	7.82	3	0.05	no
	MUFA V all	Difference	Kruskal Wallis (H)	8.08	3	0.045	yes
	PUFA V all	Difference	Kruskal Wallis (H)	6.9	3	0.076	no
	DHA V all	Difference	Kruskal Wallis (H)	8.9	3	0.031	yes
FAME as % Fatty acid (salinity)	SAT V salinity	Difference	Mann Whittney (W)	42	6	0.6889	no
	MUFA V salinity	Difference	Mann Whittney (W)	42	6	0.6889	no
	PUFA V salinity	Difference	Mann Whittney (W)	34	6	0.4712	no
	DHA V salinity	Difference	Mann Whittney (W)	28	6	0.0927	no
	SAT V salinity	Correlation	Spearman Rank (r_s)	-0.483	12	>0.05	no
	MUFA V salinity	Correlation	Spearman Rank (r_s)	-0.724	12	<0.02	yes
	PUFA V salinity	Correlation	Spearman Rank (r_s)	0.579	12	<0.05	yes
	DHA V salinity	Correlation	Spearman Rank (r_s)	-0.048	12	>0.05	no
FAME as % Fatty acid (media)	SAT V media	Difference	*Mann Whittney (W)*	49	6	0.1282	no
	MUFA V media	Difference	Mann Whittney (W)	54	6	0.0202	yes
	PUFA V media	Difference	Mann Whittney (W)	27	6	0.0656	no
	DHA V media	Difference	Mann Whittney (W)	40	6	0.9362	no
	SAT V media	Correlation	Spearman Rank (r_s)	-0.145	12	>0.05	no
	MUFA V media	Correlation	Spearman Rank (r_s)	-0.145	12	>0.05	no
	PUFA V media	Correlation	Spearman Rank (r_s)	0.241	12	>0.05	no
	DHA V media	Correlation	Spearman Rank (r_s)	0.531	12	<0.05	yes

Section 4.1.7: *I. galbana* FAME profile *continued* (Pages 86 - 90)

Variable	Compare	Relationship	Test statistic	Test Value	d.f.	*p* Value	Significant
FAME as % Total lipid (all)	Total V all	Difference	Kruskal Wallis (H)	8.08	3	0.045	yes
	SAT V all	Difference	Kruskal Wallis (H)	10.38	3	0.016	yes
	MUFA V all	Difference	Kruskal Wallis (H)	9.46	3	0.024	yes
	PUFA V all	Difference	Kruskal Wallis (H)	6.59	3	0.087	no
	DHA V all	Difference	Kruskal Wallis (H)	6.69	3	0.083	no
FAME as % Total lipid (salinity)	Total V salinity	Difference	Mann Whittney (W)	24	6	0.0202	yes
	SAT V salinity	Difference	Mann Whittney (W)	21	6	0.0051	yes
	MUFA V salinity	Difference	Mann Whittney (W)	21	6	0.0051	yes
	PUFA V salinity	Difference	Mann Whittney (W)	31	6	0.2298	no
	DHA V salinity	Difference	Mann Whittney (W)	27	6	0.0656	no
	Total V salinity	Correlation	Spearman Rank (r_s)	0.724	12	<0.02	yes
	SAT V salinity	Correlation	Spearman Rank (r_s)	0.869	12	<0.02	yes
	MUFA V salinity	Correlation	Spearman Rank (r_s)	0.869	12	<0.02	yes
	PUFA V salinity	Correlation	Spearman Rank (r_s)	0.386	12	>0.05	no
	DHA V salinity	Correlation	Spearman Rank (r_s)	0.576	12	<0.05	yes
FAME as % Total lipid (media)	Total V media	Difference	Mann Whittney (W)	30	6	0.1735	no
	SAT V media	Difference	Mann Whittney (W)	30	6	0.1735	no
	MUFA V media	Difference	Mann Whittney (W)	36	6	0.6889	no
	PUFA V media	Difference	Mann Whittney (W)	27	6	0.0656	no
	DHA V media	Difference	Mann Whittney (W)	33	6	0.3785	no
	Total V media	Correlation	Spearman Rank (r_s)	0.435	12	>0.05	no
	SAT V media	Correlation	Spearman Rank (r_s)	0.435	12	>0.05	no
	MUFA V media	Correlation	Spearman Rank (r_s)	0.145	12	>0.05	no
	PUFA V media	Correlation	Spearman Rank (r_s)	0.579	12	<0.05	yes
	DHA V media	Correlation	Spearman Rank (r_s)	0.29	12	>0.05	no

Section 4.2.2: *I. galbana* photobioreactor continuous culture (Pages 93 - 97)

Variable	Compare	Relationship	Test statistic	Test Value	d.f.	*p* Value	Significant
Daily renewal	Daily renewal V cell/ml	Correlation	Spearman Rank (r_s)	0.619	20	<0.02	yes
	Daily renewal V cell size	Correlation	Spearman Rank (r_s)	0.529	17	<0.05	yes
	Daily renewal V nitrate	Correlation	Spearman Rank (r_s)	-0.796	20	<0.02	yes
	Daily renewal V DW	Correlation	Spearman Rank (r_s)	0.418	12	>0.05	no
	Daily renewal V AFDW	Correlation	Spearman Rank (r_s)	0.53	12	<0.05	yes
Cell/ml	Cell/ml V cell size	Correlation	Spearman Rank (r_s)	0.403	17	>0.05	no
	Cell/ml V nitrate	Correlation	Spearman Rank (r_s)	-0.877	20	<0.02	yes
	Cell/ml V DW	Correlation	Spearman Rank (r_s)	0.574	12	<0.05	yes
	Cell/ml V AFDW	Correlation	Spearman Rank (r_s)	0.657	12	<0.05	yes
Cell size	Cell size V nitrate	Correlation	Spearman Rank (r_s)	-0.423	17	<0.05	yes
	Cell size V DW	Correlation	Spearman Rank (r_s)	0.403	12	>0.05	no
	Cell size V AFDW	Correlation	Spearman Rank (r_s)	0.618	12	<0.05	yes
Nitrate	Nitrate V DW	Correlation	Spearman Rank (r_s)	-0.748	12	<0.02	yes
	Nitrate V AFDW	Correlation	Spearman Rank (r_s)	-0.818	12	<0.02	yes
DW	DW V AFDW	Correlation	Spearman Rank (r_s)	0.944	12	<0.02	yes

Section 4.2.3: *I. galbana* photobioreactor fed-batch culture (Pages 98 - 109)

Variable	Compare	Relationship	Test statistic	Test Value	d.f.	*p* Value	Significant
Daily renewal	Daily renewal V cell/ml	Correlation	Spearman Rank (r_s)	0.019	21	>0.05	no
	Daily renewal V cell size	Correlation	Spearman Rank (r_s)	0.729	21	<0.02	yes
	Daily renewal V nitrate	Correlation	Spearman Rank (r_s)	0.024	15	>0.05	no
	Daily renewal V phosphate	Correlation	Spearman Rank (r_s)	0.354	15	>0.05	no
	Daily renewal V DW	Correlation	Spearman Rank (r_s)	-0.129	9	>0.05	no
	Daily renewal V AFDW	Correlation	Spearman Rank (r_s)	-0.194	9	>0.05	no
	Daily renewal V vol Chl *a*	Correlation	Spearman Rank (r_s)	-0.284	16	>0.05	no
	Daily renewal V cell Chl *a*	Correlation	Spearman Rank (r_s)	0.664	16	<0.02	yes
Cell/ml	Cell/ml V cell size	Correlation	Spearman Rank (r_s)	-0.433	21	<0.05	yes
	Cell/ml V nitrate	Correlation	Spearman Rank (r_s)	-0.6	5	>0.05	no
	Cell/ml V phosphate	Correlation	Spearman Rank (r_s)	0.1	5	>0.05	no
	Cell/ml V DW	Correlation	Spearman Rank (r_s)	0.471	18	<0.05	yes
	Cell/ml V AFDW	Correlation	Spearman Rank (r_s)	0.501	18	<0.05	yes
	Cell/ml V vol Chl *a*	Correlation	Spearman Rank (r_s)	0.071	8	>0.05	no
	Cell/ml V cell Chl *a*	Correlation	Spearman Rank (r_s)	-0.946	8	<0.02	yes
Cell size	Cell size V nitrate	Correlation	Spearman Rank (r_s)	0.7	5	>0.05	no
	Cell size V phosphate	Correlation	Spearman Rank (r_s)	-0.2	5	>0.05	no
	Cell size V DW	Correlation	Spearman Rank (r_s)	-0.103	18	>0.05	no
	Cell size V AFDW	Correlation	Spearman Rank (r_s)	0.078	18	>0.05	no
	Cell size V vol Chl *a*	Correlation	Spearman Rank (r_s)	0.15	9	>0.05	no
	Cell size V cell Chl *a*	Correlation	Spearman Rank (r_s)	0.711	9	<0.05	yes
Nitrate	Nitrate V phosphate	Correlation	Spearman Rank (r_s)	0.668	15	<0.02	yes
	nitrate V DW	Correlation	Spearman Rank (r_s)	-0.113	14	>0.05	no
	nitrate V AFDW	Correlation	Spearman Rank (r_s)	-0.205	14	>0.05	no
	nitrate V vol Chl *a*	Correlation	Spearman Rank (r_s)	-0.331	16	>0.05	no
	nitrate V cell Chl *a*	Correlation	Spearman Rank (r_s)	0.702	16	<0.02	yes
Phosphate	Phosphate V DW	Correlation	Spearman Rank (r_s)	-0.31	14	>0.05	no
	Phosphate V AFDW	Correlation	Spearman Rank (r_s)	-0.456	14	<0.05	yes
	phosphate V vol Chl *a*	Correlation	Spearman Rank (r_s)	-0.165	16	>0.05	no
	phosphate V cell Chl *a*	Correlation	Spearman Rank (r_s)	0.882	16	<0.02	yes
DW	DW V AFDW	Correlation	Spearman Rank (r_s)	0.74	14	<0.02	yes
	DW V vol Chl *a*	Correlation	Spearman Rank (r_s)	0.196	14	>0.05	no
	DW V cell Chl *a*	Correlation	Spearman Rank (r_s)	-0.322	14	>0.05	no
AFDW	AFDW V vol Chl *a*	Correlation	Spearman Rank (r_s)	0.673	14	<0.02	yes
	AFDW V cell Chl *a*	Correlation	Spearman Rank (r_s)	-0.378	14	>0.05	no
Chl *a*	Vol Chl a V cell Chl *a*	Correlation	Spearman Rank (r_s)	-0.111	14	>0.05	no

Variable	Compare	Relationship	Test statistic	Test Value	d.f.	*p* Value	Significant
Cellular P-I curve	R_d (exp V renewal)	Difference	Mann Whittney (W)	57	6	0.0049	yes
	α (exp V renewal)	Difference	Mann Whittney (W)	21	6	0.0051	yes
	P_{max} (exp V renewal)	Difference	Mann Whittney (W)	33	6	0.3785	no
	Net P_{max} (exp V renewal)	Difference	Mann Whittney (W)	21	6	0.0051	yes
	I_k (exp V renewal)	Difference	Mann Whittney (W)	39	6	1	no
	PFD I_k (exp V renewal)	Difference	Mann Whittney (W)	39	6	1	no
	PFD 100 (exp V renewal)	Difference	Mann Whittney (W)	39	6	1	no
Cell/ml	Cell/ml V R_d	Correlation	Spearman Rank (r_s)	0.085	12	>0.05	no
	Cell/ml V α	Correlation	Spearman Rank (r_s)	-0.116	12	>0.05	no
	Cell/ml V P_{max}	Correlation	Spearman Rank (r_s)	-0.618	12	<0.05	yes
	Cell/ml V net P_{max}	Correlation	Spearman Rank (r_s)	-0.39	12	>0.05	no
	Cell/ml V I_k	Correlation	Spearman Rank (r_s)	0.357	12	>0.05	no
	Cell/ml V PFD I_k	Correlation	Spearman Rank (r_s)	-0.62	12	<0.05	yes
	Cell/ml V PFD 100	Correlation	Spearman Rank (r_s)	-0.997	12	<0.05	yes
Cellular R_d	R_d V α	Correlation	Spearman Rank (r_s)	-0.73	12	<0.02	yes
	R_d V P_{max}	Correlation	Spearman Rank (r_s)	-0.292	12	>0.05	no
	R_d V net P_{max}	Correlation	Spearman Rank (r_s)	-0.782	12	<0.02	yes
	R_d V I_k	Correlation	Spearman Rank (r_s)	0.241	12	>0.05	no
	R_d V PFD I_k	Correlation	Spearman Rank (r_s)	-0.007	12	>0.05	no
	R_d V PFD 100	Correlation	Spearman Rank (r_s)	-0.067	12	>0.05	no
Cellular α	α V P_{max}	Correlation	Spearman Rank (r_s)	0.628	12	<0.05	yes
	α V net P_{max}	Correlation	Spearman Rank (r_s)	0.888	12	<0.02	yes
	α V I_k	Correlation	Spearman Rank (r_s)	0.353	12	>0.05	no
	α V PFD I_k	Correlation	Spearman Rank (r_s)	0.427	12	>0.05	no
	α V PFD 100	Correlation	Spearman Rank (r_s)	0.127	12	>0.05	no
Cellular P_{max}	P_{max} V net P_{max}	Correlation	Spearman Rank (r_s)	0.684	12	<0.05	yes
	P_{max} V I_k	Correlation	Spearman Rank (r_s)	0.369	12	>0.05	no
	P_{max} V PFD I_k	Correlation	Spearman Rank (r_s)	0.94	12	<0.02	yes
	P_{max} V PFD 100	Correlation	Spearman Rank (r_s)	0.64	12	<0.05	yes
Cellular net P_{max}	Net P_{max} V I_k	Correlation	Spearman Rank (r_s)	0.113	12	>0.05	no
	Net P_{max} V PFD I_k	Correlation	Spearman Rank (r_s)	0.434	12	>0.05	no
	Net P_{max} V PFD 100	Correlation	Spearman Rank (r_s)	0.366	12	>0.05	no
Cellular I_k	I_k V PFD I_k	Correlation	Spearman Rank (r_s)	0.495	12	>0.05	no
	I_k V PFD 100	Correlation	Spearman Rank (r_s)	-0.299	12	>0.05	no

Variable	Compare	Relationship	Test statistic	Test Value	d.f.	*p* Value	Significant
Vol chl *a* P-I curve	R_d (exp V renewal)	Difference	Mann Whittney (W)	56	6	0.0082	yes
	α (exp V renewal)	Difference	Mann Whittney (W)	25.5	6	0.0374	yes
	P_{max} (exp V renewal)	Difference	Mann Whittney (W)	29	6	0.1282	no
	Net P_{max} (exp V renewal)	Difference	Mann Whittney (W)	23	6	0.0131	yes
	I_k (exp V renewal)	Difference	Mann Whittney (W)	39	6	1	no
	PFD I_k (exp V renewal)	Difference	Mann Whittney (W)	35	6	0.5752	no
	PFD 100 (exp V renewal)	Difference	Mann Whittney (W)	36	6	0.6889	no
Vol chl *a*	Vol chl *a* V R_d	Correlation	Spearman Rank (r_s)	0.07	12	>0.05	no
	Vol chl *a* V α	Correlation	Spearman Rank (r_s)	0.2	12	>0.05	no
	Vol chl *a* V P_{max}	Correlation	Spearman Rank (r_s)	-0.685	12	<0.05	yes
	Vol chl *a* V net P_{max}	Correlation	Spearman Rank (r_s)	-0.21	12	>0.05	no
	Vol chl *a* V I_k	Correlation	Spearman Rank (r_s)	0.057	12	>0.05	no
	Vol chl *a* V PFD I_k	Correlation	Spearman Rank (r_s)	-0.608	12	<0.05	yes
	Vol chl *a* V PFD 100	Correlation	Spearman Rank (r_s)	-1	12	<0.02	yes
Chl *a* R_d	R_d V α	Correlation	Spearman Rank (r_s)	-0.739	12	<0.02	yes
	R_d V P_{max}	Correlation	Spearman Rank (r_s)	-0.308	12	>0.05	no
	R_d V net P_{max}	Correlation	Spearman Rank (r_s)	-0.594	12	<0.05	yes
	R_d V I_k	Correlation	Spearman Rank (r_s)	0.283	12	>0.05	no
	R_d V PFD I_k	Correlation	Spearman Rank (r_s)	0.112	12	>0.05	no
	R_d V PFD 100	Correlation	Spearman Rank (r_s)	-0.07	12	>0.05	no
Chl *a* α	α V P_{max}	Correlation	Spearman Rank (r_s)	0.424	12	>0.05	no
	α V net P_{max}	Correlation	Spearman Rank (r_s)	0.799	12	<0.02	yes
	α V I_k	Correlation	Spearman Rank (r_s)	0.34	12	>0.05	no
	α V PFD I_k	Correlation	Spearman Rank (r_s)	0.158	12	>0.05	no
	α V PFD 100	Correlation	Spearman Rank (r_s)	-0.2	12	>0.05	no
Chl *a* P_{max}	P_{max} V net P_{max}	Correlation	Spearman Rank (r_s)	0.776	12	<0.02	yes
	P_{max} V I_k	Correlation	Spearman Rank (r_s)	0.523	12	<0.05	yes
	P_{max} V PFD I_k	Correlation	Spearman Rank (r_s)	0.888	12	<0.02	yes
	P_{max} V PFD 100	Correlation	Spearman Rank (r_s)	0.685	12	<0.05	yes
Chl *a* net P_{max}	Net P_{max} V I_k	Correlation	Spearman Rank (r_s)	0.523	12	<0.05	yes
	Net P_{max} V PFD I_k	Correlation	Spearman Rank (r_s)	0.58	12	<0.05	yes
	Net P_{max} V PFD 100	Correlation	Spearman Rank (r_s)	0.21	12	>0.05	no
Chl *a* I_k	I_k V PFD I_k	Correlation	Spearman Rank (r_s)	0.735	12	<0.02	yes
	I_k V PFD 100	Correlation	Spearman Rank (r_s)	-0.057	12	>0.05	no

Section 4.2.3: *I. galbana* photobioreactor fed-batch culture *continued* (Pages 98 - 109)

Variable	Compare	Relationship	Test statistic	Test Value	d.f.	*p* Value	Significant
Volumetric FAME	Total	Difference	Mann Whittney (W)	15	3	0.0809	no
	SAT	Difference	Mann Whittney (W)	15	3	0.0809	no
	MUFA	Difference	Mann Whittney (W)	15	3	0.0809	no
	PUFA	Difference	Mann Whittney (W)	15	3	0.0809	no
	DHA	Difference	Mann Whittney (W)	15	3	0.0809	no
Cellular FAME	Total	Difference	Mann Whittney (W)	6	3	0.0809	no
	SAT	Difference	Mann Whittney (W)	6	3	0.0809	no
	MUFA	Difference	Mann Whittney (W)	6	3	0.0809	no
	PUFA	Difference	Mann Whittney (W)	6	3	0.0809	no
	DHA	Difference	Mann Whittney (W)	6	3	0.0809	no
FAME as % Total fatty acid	SAT	Difference	Mann Whittney (W)	15	3	0.0809	no
	MUFA	Difference	Mann Whittney (W)	15	3	0.0809	no
	PUFA	Difference	Mann Whittney (W)	6	3	0.0809	no
	DHA	Difference	Mann Whittney (W)	11	3	1	no
FAME as % Total lipid	Total	Difference	Mann Whittney (W)	15	3	0.0809	no
	SAT	Difference	Mann Whittney (W)	15	3	0.0809	no
	MUFA	Difference	Mann Whittney (W)	15	3	0.0809	no
	PUFA	Difference	Mann Whittney (W)	15	3	0.0809	no
	DHA	Difference	Mann Whittney (W)	15	3	0.0809	no

Section 5.1.2: *N. oculata* media conditions (Pages 121 - 128)

Variable	Compare	Relationship	Test statistic	Test Value	d.f.	*p* Value	Significant
Cell/ml	16‰ f/2 V 32‰ f/2	Difference	Mann Whittney (W)	173	12	0.1939	no
	16‰ f/2 V 16‰ sf/2	Difference	Mann Whittney (W)	129	12	0.2366	no
	16‰ f/2 V 32‰ sf/2	Difference	Mann Whittney (W)	131	12	0.2855	no
	32‰ f/2 V 16‰ sf/2	Difference	Mann Whittney (W)	121	12	0.0999	no
	32‰ f/2 V 32‰ sf/2	Difference	Mann Whittney (W)	121	12	0.0999	no
	16‰ sf/2 V 32‰ sf/2	Difference	Mann Whittney (W)	160	12	0.5834	no
	All formulations	Difference	Kruskal Wallis (H)	5.06	3	0.168	no
	Cell/ml V salinity	Correlation	Spearman Rank (r_s)	-0.129	48	>0.05	no
	Cell/ml V media	Correlation	Spearman Rank (r_s)	0.295	48	>0.05	no
Cell size	16‰ f/2 V 32‰ f/2	Difference	Mann Whittney (W)	173	12	0.1939	no
	16‰ f/2 V 16‰ sf/2	Difference	Mann Whittney (W)	129	12	0.2366	no
	16‰ f/2 V 32‰ sf/2	Difference	Mann Whittney (W)	152	12	0.931	no
	32‰ f/2 V 16‰ sf/2	Difference	Mann Whittney (W)	177.5	12	0.119	no
	32‰ f/2 V 32‰ sf/2	Difference	Mann Whittney (W)	121	12	0.0999	no
	16‰ sf/2 V 32‰ sf/2	Difference	Mann Whittney (W)	160	12	0.5834	no
	All formulations	Difference	Kruskal Wallis (H)	3.06	3	0.383	no
	Cell size V salinity	Correlation	Spearman Rank (rs)	0.16	48	>0.05	no
	Cellsize V media	Correlation	Spearman Rank (rs)	0	48	>0.05	no

Section 5.1.3: *N. oculata* phosphate limitation (Pages 123 - 125)

Variable	Compare	Relationship	Test statistic	Test Value	d.f.	*p* Value	Significant
Cell/ml	0.05mM V 0.10mM	Difference	Mann Whittney (W)	188	15	0.068	no
	0.05mM V 0.14mM	Difference	Mann Whittney (W)	185	15	0.0512	no
	0.05mM V 0.17mM	Difference	Mann Whittney (W)	185	15	0.0512	no
	0.05mM V 0.19mM	Difference	Mann Whittney (W)	183	15	0.0421	yes
	0.10mM V 0.14mM	Difference	Mann Whittney (W)	209	15	0.3401	no
	0.10mM V 0.17mM	Difference	Mann Whittney (W)	212	15	0.4068	no
	0.10mM V 0.19mM	Difference	Mann Whittney (W)	207	15	0.2998	no
	0.14mM V 0.17mM	Difference	Mann Whittney (W)	226	15	0.8035	no
	0.14mM V 0.19mM	Difference	Mann Whittney (W)	222	15	0.6783	no
	0.17mM V 0.19mM	Difference	Mann Whittney (W)	220	15	0.6187	no
	All Concs	Difference	Kruskal Wallis (H)	7.4	4	0.117	no
	Cell/ml V conc.	Correlation	Spearman Rank (rs)	0.288	75	<0.05	yes
Cell size	0.05mM V 0.10mM	Difference	Mann Whittney (W)	252.5	15	0.4183	no
	0.05mM V 0.14mM	Difference	Mann Whittney (W)	287	15	0.025	yes
	0.05mM V 0.17mM	Difference	Mann Whittney (W)	297.5	15	0.0074	yes
	0.05mM V 0.19mM	Difference	Mann Whittney (W)	285	15	0.031	yes
	0.10mM V 0.14mM	Difference	Mann Whittney (W)	264	15	0.1983	no
	0.10mM V 0.17mM	Difference	Mann Whittney (W)	269.5	15	0.1299	no
	0.10mM V 0.19mM	Difference	Mann Whittney (W)	259.5	15	0.2713	no
	0.14mM V 0.17mM	Difference	Mann Whittney (W)	244.5	15	0.6331	no
	0.14mM V 0.19mM	Difference	Mann Whittney (W)	235.5	15	0.9174	no
	0.17mM V 0.19mM	Difference	Mann Whittney (W)	225	15	0.7713	no
	All Concs	Difference	Kruskal Wallis (H)	9.55	4	0.049	yes
	Cell size V conc.	Correlation	Spearman Rank (rs)	-0.318	75	<0.05	yes

Section 5.1.4: *N. oculata* temperature (Pages 126 - 127)

Variable	Compare	Relationship	Test statistic	Test Value	d.f.	*p* Value	Significant
Cell/ml	15°C V 20°C	Difference	Mann Whittney (W)	259	15	0.2808	no
	15°C V 25°C	Difference	Mann Whittney (W)	261	15	0.2455	no
	15°C V 30°C	Difference	Mann Whittney (W)	339	15	0	yes
	20°C V 25°C	Difference	Mann Whittney (W)	252	15	0.4306	no
	20°C V 30°C	Difference	Mann Whittney (W)	343	15	0	yes
	25°C V 30°C	Difference	Mann Whittney (W)	344	15	0	yes
	All temps	Difference	Kruskal Wallis (H)	32.51	3	0	yes
	Cell/ml V temp.	Correlation	Spearman Rank (rs)	-0.65	60	<0.02	yes
Cell size	15°C V 20°C	Difference	Mann Whittney (W)	189	15	0.0745	no
	15°C V 25°C	Difference	Mann Whittney (W)	173	15	0.0144	yes
	15°C V 30°C	Difference	Mann Whittney (W)	230	15	0.9339	no
	20°C V 25°C	Difference	Mann Whittney (W)	218.5	15	0.5755	no
	20°C V 30°C	Difference	Mann Whittney (W)	270	15	0.1249	no
	25°C V 30°C	Difference	Mann Whittney (W)	275	15	0.0815	no
	All temps	Difference	Kruskal Wallis (H)	7.67	3	0.054	no
	Cell size V temp.	Correlation	Spearman Rank (rs)	0.057	60	>0.05	no

Section 5.1.5: *N. oculata* semi-continuous culture (Pages 128 - 130)

Variable	Compare	Relationship	Test statistic	Test Value	d.f.	*p* Value	Significant
Cell/ml	10% V 20% day 21-45	Difference	Mann Whittney (W)	97	8	0.0028	yes
	10% V 30% day 21-45	Difference	Mann Whittney (W)	100	8	0.0009	yes
	10% V 40% day 21-45	Difference	Mann Whittney (W)	100	8	0.0009	yes
	20% V 30% day 21-45	Difference	Mann Whittney (W)	91	8	0.0181	yes
	20% V 40% day 21-45	Difference	Mann Whittney (W)	97	8	0.0028	yes
	30% V 40% day 21-45	Difference	Mann Whittney (W)	92	8	0.0136	yes
	Daily renewal day 0-17	Difference	Kruskal Wallis (H)	0.2	3	0.978	no
	Daily renewal day 21-45	Difference	Kruskal Wallis (H)	24.66	3	0	yes
	Cell/ml V daily renewal	Correlation	Spearman Rank (r_s)	0.562	28	<0.02	yes
Cell size	10% V 20% day 21-45	Difference	Mann Whittney (W)	49	8	0.052	no
	10% V 30% day 21-45	Difference	Mann Whittney (W)	43.5	8	0.0117	yes
	10% V 40% day 21-45	Difference	Mann Whittney (W)	42	8	0.0074	yes
	20% V 30% day 21-45	Difference	Mann Whittney (W)	64	8	0.7132	no
	20% V 40% day 21-45	Difference	Mann Whittney (W)	65	8	0.7929	no
	30% V 40% day 21-45	Difference	Mann Whittney (W)	72	8	0.7132	no
	10% V 20% day 35-45	Difference	Mann Whittney (W)	10	4	0.0304	yes
	Daily renewal day 0-17	Difference	Kruskal Wallis (H)	0.21	3	0.975	no
	Daily renewal day 21-45	Difference	Kruskal Wallis (H)	9.45	3	0.024	yes
	Cell size V daily renewal	Correlation	Spearman Rank (r_s)	0.949	28	<0.02	yes
day 21-45	Cell/ml V cell size at 10%	Correlation	Spearman Rank (r_s)	-0.321	7	>0.05	no
	Cell/ml V cell size at 20%	Correlation	Spearman Rank (r_s)	-0.75	7	<0.05	yes
	Cell/ml V cell size at 30 %	Correlation	Spearman Rank (r_s)	0	7	>0.05	no
	Cell/ml V cell size at 40%	Correlation	Spearman Rank (r_s)	0	7	>0.05	no

Section 5.1.6: *N. oculata* oxygen evolution (Pages 131 - 132)

Variable	Compare	Relationship	Test statistic	Test Value	d.f.	*p* Value	Significant
Cell/ml	Cell/ml V R_d	Correlation	Spearman Rank (r_s)	0.878	6	<0.05	yes
	Cell/ml V α	Correlation	Spearman Rank (r_s)	-0.543	6	>0.05	no
	Cell/ml V P_{max}	Correlation	Spearman Rank (r_s)	-0.543	6	>0.05	no
	Cell/ml V net P_{max}	Correlation	Spearman Rank (r_s)	-0.543	6	>0.05	no
	Cell/ml V I_k	Correlation	Spearman Rank (r_s)	0.638	6	>0.05	no
	Cell/ml V PFD I_k	Correlation	Spearman Rank (r_s)	-0.029	6	>0.05	no
	Cell/ml V PFD 100	Correlation	Spearman Rank (r_s)	-0.771	6	>0.05	no
R_d	R_d V α	Correlation	Spearman Rank (r_s)	-0.878	6	<0.05	yes
	R_d V P_{max}	Correlation	Spearman Rank (r_s)	-0.878	6	<0.05	yes
	R_d V net P_{max}	Correlation	Spearman Rank (r_s)	-0.878	6	<0.05	yes
	R_d V I_k	Correlation	Spearman Rank (r_s)	0.198	6	>0.05	no
	R_d V PFD I_k	Correlation	Spearman Rank (r_s)	-0.488	6	>0.05	no
	R_d V PFD 100	Correlation	Spearman Rank (r_s)	-0.878	6	<0.05	yes
α	α V P_{max}	Correlation	Spearman Rank (r_s)	1	6	<0.02	yes
	α V net P_{max}	Correlation	Spearman Rank (r_s)	1	6	<0.02	yes
	α V I_k	Correlation	Spearman Rank (r_s)	0.29	6	>0.05	no
	α V PFD I_k	Correlation	Spearman Rank (r_s)	0.829	6	<0.05	yes
	α V PFD 100	Correlation	Spearman Rank (r_s)	0.771	6	>0.05	no
P_{max}	P_{max} V net P_{max}	Correlation	Spearman Rank (r_s)	1	6	<0.02	yes
	P_{max} V I_k	Correlation	Spearman Rank (r_s)	0.29	6	>0.05	no
	P_{max} V PFD I_k	Correlation	Spearman Rank (r_s)	0.829	6	<0.05	yes
	P_{max} V PFD 100	Correlation	Spearman Rank (r_s)	0.771	6	>0.05	no
Net P_{max}	Net P_{max} V I_k	Correlation	Spearman Rank (r_s)	0.29	6	>0.05	no
	Net P_{max} V PFD I_k	Correlation	Spearman Rank (r_s)	0.829	6	<0.05	yes
	Net P_{max} V PFD 100	Correlation	Spearman Rank (r_s)	0.771	6	>0.05	no
I_k	I_k V PFD I_k	Correlation	Spearman Rank (r_s)	0.725	6	>0.05	no
	I_k V PFD 100	Correlation	Spearman Rank (r_s)	-0.232	6	>0.05	no

Section 5.1.7: *N. oculata* FAME profile (Pages 133 - 138)

Variable	Compare	Relationship	Test statistic	Test Value	d.f.	*p* Value	Significant
Volumertic FAME (all)	Total V all	Difference	Kruskal Wallis (H)	9.46	3	0.024	yes
	SAT V all	Difference	Kruskal Wallis (H)	9.46	3	0.024	yes
	MUFA V all	Difference	Kruskal Wallis (H)	9.46	3	0.024	yes
	PUFA V all	Difference	Kruskal Wallis (H)	9.46	3	0.024	yes
	EPA V all	Difference	Kruskal Wallis (H)	8.08	3	0.045	yes
Volumetric FAME (salinity)	Total V salinity	Difference	Mann Whittney (W)	42	6	0.6889	no
	SAT V salinity	Difference	Mann Whittney (W)	36	6	0.6889	no
	MUFA V salinity	Difference	Mann Whittney (W)	39	6	1	no
	PUFA V salinity	Difference	Mann Whittney (W)	39	6	1	no
	EPA V salinity	Difference	Mann Whittney (W)	42	6	0.6889	no
	Total V salinity	Correlation	Spearman Rank (r_s)	-0.145	12	>0.05	no
	SAT V salinity	Correlation	Spearman Rank (r_s)	0.145	12	>0.05	no
	MUFA V salinity	Correlation	Spearman Rank (r_s)	0	12	>0.05	no
	PUFA V salinity	Correlation	Spearman Rank (r_s)	0	12	>0.05	no
	EPA V salinity	Correlation	Spearman Rank (r_s)	-0.145	12	>0.05	no
Volumetric FAME (media)	Total V media	Difference	Mann Whittney (W)	45	6	0.3789	no
	SAT V media	Difference	Mann Whittney (W)	45	6	0.3785	no
	MUFA V media	Difference	Mann Whittney (W)	51	6	0.0656	no
	PUFA V media	Difference	Mann Whittney (W)	27	6	0.0656	no
	EPA V media	Difference	Mann Whittney (W)	30	6	0.1735	no
	Total V media	Correlation	Spearman Rank (r_s)	-0.324	12	>0.05	no
	SAT V media	Correlation	Spearman Rank (r_s)	-0.194	12	>0.05	no
	MUFA V media	Correlation	Spearman Rank (r_s)	-0.518	12	<0.05	yes
	PUFA V media	Correlation	Spearman Rank (r_s)	0.518	12	<0.05	yes
	EPA V media	Correlation	Spearman Rank (r_s)	0.324	12	>0.05	no

Section 5.1.7: *N. oculata* FAME profile *continued* (Pages 133 - 138)

Variable	Compare	Relationship	Test statistic	Test Value	d.f.	*p* Value	Significant
Cellular FAME (all)	Total V all	Difference	Kruskal Wallis (H)	9.67	3	0.022	yes
	SAT V all	Difference	Kruskal Wallis (H)	9.67	3	0.022	yes
	MUFA V all	Difference	Kruskal Wallis (H)	10.38	3	0.016	yes
	PUFA V all	Difference	Kruskal Wallis (H)	8.44	3	0.038	yes
	EPA V all	Difference	Kruskal Wallis (H)	8.13	3	0.044	yes
Cellular FAME (salinity)	Total V salinity	Difference	Mann Whittney (W)	39	6	1	no
	SAT V salinity	Difference	Mann Whittney (W)	39	6	1	no
	MUFA V salinity	Difference	Mann Whittney (W)	39	6	1	no
	PUFA V salinity	Difference	Mann Whittney (W)	37	6	0.8102	no
	EPA V salinity	Difference	Mann Whittney (W)	41	6	0.8102	no
	Total V salinity	Correlation	Spearman Rank (r_s)	0	12	>0.05	no
	SAT V salinity	Correlation	Spearman Rank (r_s)	0	12	>0.05	no
	MUFA V salinity	Correlation	Spearman Rank (r_s)	0	2	>0.05	no
	PUFA V salinity	Correlation	Spearman Rank (r_s)	0.097	12	>0.05	no
	EPA V salinity	Correlation	Spearman Rank (r_s)	-0.097	12	>0.05	no
Cellular FAME (media)	Total V media	Difference	Mann Whittney (W)	55	6	0.0131	yes
	SAT V media	Difference	Mann Whittney (W)	55	6	0.0131	yes
	MUFA V media	Difference	Mann Whittney (W)	57	6	0.0051	yes
	PUFA V media	Difference	Mann Whittney (W)	54	6	0.0202	yes
	EPA V media	Difference	Mann Whittney (W)	51	6	0.0656	no
	Total V media	Correlation	Spearman Rank (r_s)	-0.691	12	<0.05	yes
	SAT V media	Correlation	Spearman Rank (r_s)	-0.691	12	<0.05	yes
	MUFA V media	Correlation	Spearman Rank (r_s)	-0.777	12	<0.02	yes
	PUFA V media	Correlation	Spearman Rank (r_s)	-0.605	12	<0.05	yes
	EPA V media	Correlation	Spearman Rank (r_s)	-0.561	12	<0.05	yes

Section 5.1.7: *N. oculata* FAME profile *continued* (Pages 133 - 138)

Variable	Compare	Relationship	Test statistic	Test Value	d.f.	*p* Value	Significant
FAME as % Fatty acid (all)	SAT V all	Difference	Kruskal Wallis (H)	5.97	3	0.114	no
	MUFA V all	Difference	Kruskal Wallis (H)	9.97	3	0.019	yes
	PUFA V all	Difference	Kruskal Wallis (H)	8.9	3	0.031	yes
	EPA V all	Difference	Kruskal Wallis (H)	8.08	3	0.045	yes
FAME as % Fatty acid (salinity)	SAT V salinity	Difference	Mann Whittney (W)	25	6	0.0306	yes
	MUFA V salinity	Difference	Mann Whittney (W)	39	6	1	no
	PUFA V salinity	Difference	Mann Whittney (W)	40	6	0.9362	no
	EPA V salinity	Difference	Mann Whittney (W)	42	6	0.6889	no
	SAT V salinity	Correlation	Spearman Rank (r_s)	0.676	12	<0.05	yes
	MUFA V salinity	Correlation	Spearman Rank (r_s)	0	12	>0.05	no
	PUFA V salinity	Correlation	Spearman Rank (r_s)	-0.048	12	>0.05	no
	EPA V salinity	Correlation	Spearman Rank (r_s)	-0.145	12	>0.05	no
FAME as % Fatty acid (media)	SAT V media	Difference	Mann Whittney (W)	38	6	0.9362	no
	MUFA V media	Difference	Mann Whittney (W)	56	6	0.0082	yes
	PUFA V media	Difference	Mann Whittney (W)	24	6	0.0202	yes
	EPA V media	Difference	Mann Whittney (W)	24	6	0.0202	yes
	SAT V media	Correlation	Spearman Rank (r_s)	0.345	12	>0.05	no
	MUFA V media	Correlation	Spearman Rank (r_s)	-0.734	12	<0.05	yes
	PUFA V media	Correlation	Spearman Rank (r_s)	0.626	12	<0.05	yes
	EPA V media	Correlation	Spearman Rank (r_s)	0.583	12	<0.05	yes

Variable	Compare	Relationship	Test statistic	Test Value	d.f.	*p* Value	Significant
FAME as % Total lipid (all)	Total V all	Difference	Kruskal Wallis (H)	8.08	3	0.045	yes
	SAT V all	Difference	Kruskal Wallis (H)	9.46	3	0.024	yes
	MUFA V all	Difference	Kruskal Wallis (H)	9.46	3	0.024	yes
	PUFA V all	Difference	Kruskal Wallis (H)	9.26	3	0.027	yes
	EPA V all	Difference	Kruskal Wallis (H)	10.38	3	0.016	yes
FAME as % Total lipid (salinity)	Total V salinity	Difference	Mann Whittney (W)	42	6	0.6889	no
	SAT V salinity	Difference	Mann Whittney (W)	39	6	1	no
	MUFA V salinity	Difference	Mann Whittney (W)	42	6	0.6889	no
	PUFA V salinity	Difference	Mann Whittney (W)	45	6	0.3785	no
	EPA V salinity	Difference	Mann Whittney (W)	48	6	0.1735	no
	Total V salinity	Correlation	Spearman Rank (r_s)	-0.145	12	<0.05	no
	SAT V salinity	Correlation	Spearman Rank (r_s)	0	12	>0.05	no
	MUFA V salinity	Correlation	Spearman Rank (r_s)	-0.145	12	>0.05	no
	PUFA V salinity	Correlation	Spearman Rank (r_s)	-0.29	12	>0.05	no
	EPA V salinity	Correlation	Spearman Rank (r_s)	-0.435	12	>0.05	no
FAME as % Total lipid (media)	Total V media	Difference	Mann Whittney (W)	30	6	0.1735	no
	SAT V media	Difference	Mann Whittney (W)	27	6	0.0656	no
	MUFA V media	Difference	Mann Whittney (W)	45	6	0.3785	no
	PUFA V media	Difference	Mann Whittney (W)	21	6	0.0051	yes
	EPA V media	Difference	Mann Whittney (W)	21	6	0.0051	yes
	Total V media	Correlation	Spearman Rank (r_s)	0.324	12	>0.05	no
	SAT V media	Correlation	Spearman Rank (r_s)	0.518	12	<0.05	yes
	MUFA V media	Correlation	Spearman Rank (r_s)	-0.324	12	>0.05	no
	PUFA V media	Correlation	Spearman Rank (r_s)	0.648	12	<0.05	yes
	EPA V media	Correlation	Spearman Rank (r_s)	0.583	12	<0.05	yes

Section 5.2.2: *N. oculata* continuous culture (Pages 140 -144)

Variable	Compare	Relationship	Test statistic	Test Value	d.f.	*p* Value	Significant
Daily renewal	Daily renewal V cell/ml	Correlation	Spearman Rank (r_s)	0.451	40	<0.02	yes
	Daily renewal V cell size	Correlation	Spearman Rank (r_s)	0.461	40	<0.02	yes
	Daily renewal V nitrate	Correlation	Spearman Rank (r_s)	0.08	15	>0.05	no
	Daily renewal V phosphate	Correlation	Spearman Rank (r_s)	0.187	14	>0.05	no
	Daily renewal V DW	Correlation	Spearman Rank (r_s)	0.385	14	>0.05	no
	Daily renewal V AFDW	Correlation	Spearman Rank (r_s)	0.445	14	>0.05	no
Cell/ml	Cell/ml V cell size	Correlation	Spearman Rank (r_s)	-0.031	40	>0.05	no
	Cell/ml V nitrate	Correlation	Spearman Rank (r_s)	0.008	15	>0.05	no
	Cell/ml V phosphate	Correlation	Spearman Rank (r_s)	-0.099	15	>0.05	no
	Cell/ml V DW	Correlation	Spearman Rank (r_s)	0.874	13	<0.02	yes
	Cell/ml V AFDW	Correlation	Spearman Rank (r_s)	0.901	13	<0.02	yes
Cell size	Cell size V nitrate	Correlation	Spearman Rank (r_s)	-0.423	15	>0.05	no
	Cell size V phosphate	Correlation	Spearman Rank (r_s)	-0.123	15	>0.05	no
	Cell size V DW	Correlation	Spearman Rank (r_s)	-0.5	13	<0.05	yes
	Cell size V AFDW	Correlation	Spearman Rank (r_s)	-0.44	13	>0.05	no
Nitrate	Nitrate V phosphate	Correlation	Spearman Rank (r_s)	0.786	15	<0.02	yes
	Nitrate V DW	Correlation	Spearman Rank (r_s)	-0.233	13	>0.05	no
	Nitrate V AFDW	Correlation	Spearman Rank (r_s)	-0.21	13	>0.05	no
Phosphate	Phosphate V DW	Correlation	Spearman Rank (r_s)	-0.309	13	>0.05	no
	Phosphate V AFDW	Correlation	Spearman Rank (r_s)	-0.277	13	>0.05	no
DW	DW V AFDW	Correlation	Spearman Rank (r_s)	0.991	14	<0.02	yes

Section 5.2.3: *N. oculata* fed-batch culture (Pages 145 -155)

Variable	Compare	Relationship	Test statistic	Test Value	d.f.	*p* Value	Significant
Daily renewal	Daily renewal V cell/ml	Correlation	Spearman Rank (r_s)	0.805	17	<0.02	yes
	Daily renewal V cell size	Correlation	Spearman Rank (r_s)	0.098	17	>0.05	no
	Daily renewal V nitrate	Correlation	Spearman Rank (r_s)	-0.423	13	>0.05	no
	Daily renewal V phosphate	Correlation	Spearman Rank (r_s)	0	13	>0.05	no
	Daily renewal V DW	Correlation	Spearman Rank (r_s)	0.316	7	>0.05	no
	Daily renewal V AFDW	Correlation	Spearman Rank (r_s)	0.474	7	>0.05	no
	Daily renewal V vol Chl *a*	Correlation	Spearman Rank (r_s)	0.314	14	>0.0.5	no
	Daily renewal V cell Chl *a*	Correlation	Spearman Rank (r_s)	-0.334	14	>0.05	no
Cell/ml	Cell/ml V cell size	Correlation	Spearman Rank (r_s)	0.352	16	>0.05	no
	Cell/ml V nitrate	Correlation	Spearman Rank (r_s)	-0.881	8	<0.02	yes
	Cell/ml V phosphate	Correlation	Spearman Rank (r_s)	-0.333	8	>0.05	no
	Cell/ml V DW	Correlation	Spearman Rank (r_s)	0.722	13	<0.02	yes
	Cell/ml V AFDW	Correlation	Spearman Rank (r_s)	0.72	13	<0.02	yes
	Cell/ml V vol Chl *a*	Correlation	Spearman Rank (r_s)	0.571	8	>0.05	no
	Cell/ml V cell Chl *a*	Correlation	Spearman Rank (r_s)	-0.695	8	<0.05	yes
Cell size	Cell size V nitrate	Correlation	Spearman Rank (r_s)	-0.69	8	<0.05	yes
	Cell size V phosphate	Correlation	Spearman Rank (r_s)	-0.214	8	>0.05	no
	Cell size V DW	Correlation	Spearman Rank (r_s)	0.341	13	>0.05	no
	Cell size V AFDW	Correlation	Spearman Rank (r_s)	0.432	13	>0.05	no
	Cell size V vol Chl *a*	Correlation	Spearman Rank (r_s)	0.262	8	>0.05	no
	Cell size V cell Chl *a*	Correlation	Spearman Rank (r_s)	-0.06	8	>0.05	no
Nitrate	Nitrate V phosphate	Correlation	Spearman Rank (r_s)	0.385	13	>0.05	no
	Nitrate V DW	Correlation	Spearman Rank (r_s)	-0.346	11	>0.05	no
	Nitrate V AFDW	Correlation	Spearman Rank (r_s)	-0.342	11	>0.05	no
	Nitrate V vol Chl *a*	Correlation	Spearman Rank (r_s)	-0.282	11	>0.05	no
	Nitrate V cell Chl *a*	Correlation	Spearman Rank (r_s)	0.018	11	>0.05	no
Phosphate	Phosphate V DW	Correlation	Spearman Rank (r_s)	0.497	11	>0.05	no
	Phosphate V AFDW	Correlation	Spearman Rank (r_s)	0.569	11	<0.05	yes
	Phosphate V vol Chl *a*	Correlation	Spearman Rank (r_s)	0.455	11	>0.05	no
	Phosphate V cell Chl *a*	Correlation	Spearman Rank (r_s)	0.105	11	>0.05	no
DW	DW V AFDW	Correlation	Spearman Rank (r_s)	0.856	13	<0.02	yes
	DW V vol Chl *a*	Correlation	Spearman Rank (r_s)	0.481	13	<0.05	yes
	DW V cell Chl *a*	Correlation	Spearman Rank (r_s)	-0.069	13	>0.05	no
AFDW	AFDW V vol Chl *a*	Correlation	Spearman Rank (r_s)	0.462	13	<0.05	yes
	AFDW V cell Chl *a*	Correlation	Spearman Rank (r_s)	-0.047	13	>0.05	no
Vol Chl *a*	Vol Chl *a* V cell Chl *a*	Correlation	Spearman Rank (r_s)	0.681	13	<0.02	yes

Section 5.2.3: *N. oculata* fed-batch culture *continued* (Pages 145 - 155)

Variable	Compare	Relationship	Test statistic	Test Value	d.f.	*p* Value	Significant
Cellular P-I curve	R_d (exp V renewal)	Difference	Mann Whittney (W)	37	6	0.8102	no
	α (exp V renewal)	Difference	Mann Whittney (W)	43.5	6	0.5218	no
	P_{max} (exp V renewal)	Difference	Mann Whittney (W)	50	6	0.0927	no
	Net P_{max} (exp V renewal)	Difference	Mann Whittney (W)	45	6	0.3785	no
	I_k (exp V renewal)	Difference	Mann Whittney (W)	23	6	0.0131	yes
	PFD I_k (exp V renewal)	Difference	Mann Whittney (W)	50	6	0.0927	no
	PFD 100 (exp V renewal)	Difference	Mann Whittney (W)	57	6	0.0051	yes
Cell/ml	Cell/ml V R_d	Correlation	Spearman Rank (r_s)	0.538	12	<0.05	yes
	Cell/ml V α	Correlation	Spearman Rank (r_s)	-0.485	12	>0.05	no
	Cell/ml V P_{max}	Correlation	Spearman Rank (r_s)	-0.685	12	<0.05	yes
	Cell/ml V net P_{max}	Correlation	Spearman Rank (r_s)	-0.622	12	<0.05	yes
	Cell/ml V I_k	Correlation	Spearman Rank (r_s)	0.901	12	<0.02	yes
	Cell/ml V PFD I_k	Correlation	Spearman Rank (r_s)	-0.531	12	<0.05	yes
	Cell/ml V PFD 100	Correlation	Spearman Rank (r_s)	-0.996	12	<0.02	yes
Cellular R_d	R_d V α	Correlation	Spearman Rank (r_s)	-0.728	12	<0.02	yes
	R_d V P_{max}	Correlation	Spearman Rank (r_s)	-0.559	12	<0.05	yes
	R_d V net P_{max}	Correlation	Spearman Rank (r_s)	-0.846	12	<0.02	yes
	R_d V I_k	Correlation	Spearman Rank (r_s)	0.535	12	<0.05	yes
	R_d V PFD I_k	Correlation	Spearman Rank (r_s)	-0.357	12	>0.05	no
	R_d V PFD 100	Correlation	Spearman Rank (r_s)	-0.533	12	<0.05	yes
Cellular α	α V P_{max}	Correlation	Spearman Rank (r_s)	0.914	12	<0.02	yes
	α V net P_{max}	Correlation	Spearman Rank (r_s)	0.84	12	<0.02	yes
	α V I_k	Correlation	Spearman Rank (r_s)	-0.248	12	>0.05	no
	α V PFD I_k	Correlation	Spearman Rank (r_s)	0.833	12	<0.02	yes
	α V PFD 100	Correlation	Spearman Rank (r_s)	0.497	12	>0.05	no
Cellular P_{max}	P_{max} V net P_{max}	Correlation	Spearman Rank (r_s)	0.727	12	<0.02	yes
	P_{max} V I_k	Correlation	Spearman Rank (r_s)	-0.398	12	>0.05	no
	P_{max} V PFD I_k	Correlation	Spearman Rank (r_s)	0.902	12	<0.02	yes
	P_{max} V PFD 100	Correlation	Spearman Rank (r_s)	0.698	12	<0.05	yes
Cellular net P_{max}	Net P_{max} V I_k	Correlation	Spearman Rank (r_s)	-0.468	12	>0.05	no
	Net P_{max} V PFD I_k	Correlation	Spearman Rank (r_s)	0.587	12	<0.02	yes
	Net P_{max} V PFD 100	Correlation	Spearman Rank (r_s)	0.632	12	<0.05	yes
Cellular I_k	I_k V PFD I_k	Correlation	Spearman Rank (r_s)	-0.282	12	>0.05	no
	I_k V PFD 100	Correlation	Spearman Rank (r_s)	-0.887	12	<0.02	yes

Variable	Compare	Relationship	Test statistic	Test Value	d.f.	*p* Value	Significant
Vol chl *a* P-I curve	R_d (exp V renewal)	Difference	Mann Whittney (W)	37	6	0.8102	no
	α (exp V renewal)	Difference	Mann Whittney (W)	48	6	0.1735	no
	P_{max} (exp V renewal)	Difference	Mann Whittney (W)	54.5	6	0.0163	yes
	Net P_{max} (exp V renewal)	Difference	Mann Whittney (W)	47	6	0.2298	no
	I_k (exp V renewal)	Difference	Mann Whittney (W)	23	6	0.0131	yes
	PFD I_k (exp V renewal)	Difference	Mann Whittney (W)	40	6	0.9362	no
	PFD 100 (exp V renewal)	Difference	Mann Whittney (W)	54	6	0.0202	yes
vol chl *a*	Vol chl *a* V R_d	Correlation	Spearman Rank (r_s)	0.594	12	<0.05	yes
	Vol chl *a* V α	Correlation	Spearman Rank (r_s)	-0.469	12	>0.05	no
	Vol chl *a* V P_{max}	Correlation	Spearman Rank (r_s)	-0.511	12	<0.05	yes
	Vol chl *a* V net P_{max}	Correlation	Spearman Rank (r_s)	-0.371	12	>0.05	no
	Vol chl *a* V I_k	Correlation	Spearman Rank (r_s)	0.982	12	<0.02	yes
	Vol chl *a* V PFD I_k	Correlation	Spearman Rank (r_s)	0.245	12	>0.05	no
	Vol chl *a* V PFD 100	Correlation	Spearman Rank (r_s)	-1	12	<0.02	yes
Chl *a* R_d	R_d V α	Correlation	Spearman Rank (r_s)	-0.741	12	<0.02	yes
	R_d V P_{max}	Correlation	Spearman Rank (r_s)	-0.399	12	>0.05	no
	R_d V net P_{max}	Correlation	Spearman Rank (r_s)	-0.664	12	<0.05	yes
	R_d V I_k	Correlation	Spearman Rank (r_s)	0.539	12	<0.05	yes
	R_d V PFD I_k	Correlation	Spearman Rank (r_s)	0.545	12	<0.05	yes
	R_d V PFD 100	Correlation	Spearman Rank (r_s)	-0.594	12	<0.05	yes
Chl *a* α	α V P_{max}	Correlation	Spearman Rank (r_s)	0.865	12	<0.02	yes
	α V net P_{max}	Correlation	Spearman Rank (r_s)	0.972	12	<0.02	yes
	α V I_k	Correlation	Spearman Rank (r_s)	-0.458	12	>0.05	no
	α V PFD I_k	Correlation	Spearman Rank (r_s)	-0.224	12	>0.05	no
	α V PFD 100	Correlation	Spearman Rank (r_s)	0.469	12	>0.05	no
Chl *a* P_{max}	P_{max} V net P_{max}	Correlation	Spearman Rank (r_s)	0.876	12	<0.02	yes
	P_{max} V I_k	Correlation	Spearman Rank (r_s)	-0.554	12	<0.05	yes
	P_{max} V PFD I_k	Correlation	Spearman Rank (r_s)	-0.042	12	>0.05	no
	P_{max} V PFD 100	Correlation	Spearman Rank (r_s)	0.511	12	<0.05	yes
Chl *a* net P_{max}	Net P_{max} V I_k	Correlation	Spearman Rank (r_s)	-0.373	12	>0.05	no
	Net P_{max} V PFD I_k	Correlation	Spearman Rank (r_s)	-0.189	12	>0.05	no
	Net P_{max} V PFD 100	Correlation	Spearman Rank (r_s)	0.371	12	>0.05	no
Chl *a* I_k	I_k V PFD I_k	Correlation	Spearman Rank (r_s)	0.31	12	>0.05	no
	I_k V PFD 100	Correlation	Spearman Rank (r_s)	-0.982	12	<0.02	yed

Variable	Compare	Relationship	Test statistic	Test Value	d.f.	*p* Value	Significant
Volumetric FAME	Total	Difference	Mann Whittney (W)	6	3	0.0809	no
	SAT	Difference	Mann Whittney (W)	6	3	0.0809	no
	MUFA	Difference	Mann Whittney (W)	6	3	0.0809	no
	PUFA	Difference	Mann Whittney (W)	6	3	0.0809	no
	EPA	Difference	Mann Whittney (W)	6	3	0.0809	no
Cellular FAME	Total	Difference	Mann Whittney (W)	6	3	0.0809	no
	SAT	Difference	Mann Whittney (W)	6	3	0.0809	no
	MUFA	Difference	Mann Whittney (W)	6	3	0.0809	no
	PUFA	Difference	Mann Whittney (W)	6	3	0.0809	no
	EPA	Difference	Mann Whittney (W)	7	3	0.1904	no
FAME as % Total fatty acid	SAT	Difference	Mann Whittney (W)	7	3	0.1904	no
	MUFA	Difference	Mann Whittney (W)	7	3	0.1904	no
	PUFA	Difference	Mann Whittney (W)	15	3	0.0809	no
	EPA	Difference	Mann Whittney (W)	15	3	0.0809	no
FAME as % Total lipid	Total	Difference	Mann Whittney (W)	14	3	0.1904	no
	SAT	Difference	Mann Whittney (W)	13	3	0.3827	no
	MUFA	Difference	Mann Whittney (W)	14	3	0.1904	no
	PUFA	Difference	Mann Whittney (W)	15	3	0.0809	no
	EPA	Difference	Mann Whittney (W)	15	3	0.0809	no

Section 6.1: (i) Linear fluid velocity (Pages 163 -166)

Variable	Compare	Relationship	Test statistic	Test Value	d.f.	*p* Value	Significant
Individual sparge plates	25s V 25L	Difference	Mann Whittney (W)	21	4	0.4705	no
	25s V 49s	Difference	Mann Whittney (W)	16	4	0.665	no
	25s V 49L	Difference	Mann Whittney (W)	21	4	0.4705	no
	25s V 69s	Difference	Mann Whittney (W)	15	4	0.4705	no
	25L V 49s	Difference	Mann Whittney (W)	15	4	0.4705	no
	25L V 49L	Difference	Mann Whittney (W)	17	4	0.8852	no
	25L V 69s	Difference	Mann Whittney (W)	12	4	0.1124	no
	49s V 49L	Difference	Mann Whittney (W)	22	4	0.3123	no
	49s V 69s	Difference	Mann Whittney (W)	16	4	0.665	no
	49L V 69L	Difference	Mann Whittney (W)	13	4	0.1939	no
	All plates	Difference	Kruskal Wallis (H)	4.26	4	0.373	no
Pore size	Pore size at 5L/min	Difference	Mann Whittney (W)	40	5	0.0109	yes
	Pore size at 10L/min	Difference	Mann Whittney (W)	40	5	0.0109	yes
	Pore size at 15L/min	Difference	Mann Whittney (W)	40	5	0.0109	yes
	Pore size at 20L/min	Difference	Mann Whittney (W)	40	5	0.0109	yes
	Overall pore size	Difference	Kruskal Wallis (H)	610	20	0	yes
	Fluid flow V pore size	Correlation	Spearman Rank (r_s)	-0.425	20	<0.05	yes
Pore no.	Pore no. at 5L/min	Difference	Kruskal Wallis (H)	2	2	0.368	no
	Pore no. at 10L/min	Difference	Kruskal Wallis (H)	2.4	2	0.302	no
	Pore no. at 15L/min	Difference	Kruskal Wallis (H)	2	2	0.368	no
	Pore no. at 20L/min	Difference	Kruskal Wallis (H)	2.4	2	0.302	no
	Overall pore no.	Difference	Kruskal Wallis (H)	2.4	2	0.302	no
	Fluid flow V pore no.	Correlation	Spearman Rank (r_s)	0.31	20	>0.05	no
Air flow rate	All plates at 5L/min	Difference	Kruskal Wallis (H)	9.48	4	0.051	no
	All plates at 10L/min	Difference	Kruskal Wallis (H)	12.83	4	0.031	yes
	All plates at 15L/min	Difference	Kruskal Wallis (H)	12.02	4	0.018	yes
	All plates at 20L/min	Difference	Kruskal Wallis (H)	11.41	4	0.023	yes
	All flow rates	Difference	Kruskal Wallis (H)	14.22	3	0.003	yes
	5L/min V 10L/min	Difference	Mann Whittney (W)	17	5	0.0367	yes
	5L/min V 15L/min	Difference	Mann Whittney (W)	15	5	0.0122	yes
	5L/min V 20L/min	Difference	Mann Whittney (W)	15	5	0.0122	yes
	10L/min V 15L/min	Difference	Mann Whittney (W)	18	5	0.0601	no
	10L/min V 20L/min	Difference	Mann Whittney (W)	16	5	0.0216	yes
	15L/min V 20L/min	Difference	Mann Whittney (W)	23	5	0.4034	no
	Fluid flow V air flow	Correlation	Spearman Rank (r_s)	0.853	20	<0.02	yes

Section 6.1: (ii) Riser dynamics (Pages 163 - 166)

Variable	Compare	Relationship	Test statistic	Test Value	d.f.	*p* Value	Significant
Individual sparge plates	25s V 25L	Difference	Mann Whittney (W)	18	4	1	no
	25s V 49s	Difference	Mann Whittney (W)	17	4	0.8809	no
	25s V 49L	Difference	Mann Whittney (W)	16	4	0.6532	no
	25s V 69s	Difference	Mann Whittney (W)	20	4	0.6532	no
	25L V 49s	Difference	Mann Whittney (W)	17	4	0.8809	no
	25L V 49L	Difference	Mann Whittney (W)	16	4	0.6532	no
	25L V 69s	Difference	Mann Whittney (W)	20	4	0.6532	no
	49s V 49L	Difference	Mann Whittney (W)	16.5	4	0.76	no
	49s V 69s	Difference	Mann Whittney (W)	21.5	4	0.3529	no
	49L V 69L	Difference	Mann Whittney (W)	23	4	0.172	no
	All plates	Difference	Kruskal Wallis (H)	2.21	4	0.698	no
Pore size	Pore size at 5L/min	Difference	Mann Whittney (W)	25	5	0.6312	no
	Pore size at 10L/min	Difference	Mann Whittney (W)	27.5	5	1	no
	Pore size at 15L/min	Difference	Mann Whittney (W)	18.5	5	0.0573	no
	Pore size at 20L/min	Difference	Mann Whittney (W)	15	5	0.0086	yes
	Overall pore size	Difference	Mann Whittney (W)	314	20	0.0057	yes
	Riser dynamics V pore size	Correlation	Spearman Rank (r_s)	0.21	20	>0.05	no
Pore no.	Pore no. at 5L/min	Difference	Kruskal Wallis (H)	4	2	0.136	no
	Pore no. at 10L/min	Difference	Kruskal Wallis (H)	0.67	2	0.717	no
	Pore no. at 15L/min	Difference	Kruskal Wallis (H)	4	2	0.136	no
	Pore no. at 20L/min	Difference	Kruskal Wallis (H)	4	2	0.136	no
	Overall pore no.	Difference	Kruskal Wallis (H)	1.6	2	0.449	no
	Riser dynamics V pore no.	Correlation	Spearman Rank (r_s)	0.224	20	>0.05	no
Air flow rate	All plates at 5L/min	Difference	Kruskal Wallis (H)	4	4	0.407	no
	All plates at 10L/min	Difference	Kruskal Wallis (H)	4	4	0.407	no
	All plates at 15L/min	Difference	Kruskal Wallis (H)	4	4	0.407	no
	All plates at 20L/min	Difference	Kruskal Wallis (H)	4	4	0.407	no
	All flow rates	Difference	Kruskal Wallis (H)	13.12	3	0.005	yes
	5L/min V 10L/min	Difference	Mann Whittney (W)	21	5	0.1213	no
	5L/min V 15L/min	Difference	Mann Whittney (W)	19	5	0.0766	no
	5L/min V 20L/min	Difference	Mann Whittney (W)	15	5	0.0122	yes
	10L/min V 15L/min	Difference	Mann Whittney (W)	22	5	0.2482	no
	10L/min V 20L/min	Difference	Mann Whittney (W)	15.5	5	0.0101	yes
	15L/min V 20L/min	Difference	Mann Whittney (W)	17	5	0.0209	yes
	Riser dynamics V air flow	Correlation	Spearman Rank (r_s)	0.816	20	<0.02	yes

Section 6.2: (i) Gas hold-up (Pages 167 - 168)

Variable	Compare	Relationship	Test statistic	Test Value	d.f.	*p* Value	Significant
Individual sparge plates	25s V 25L	Difference	Mann Whittney (W)	20	4	0.665	no
	25s V 49s	Difference	Mann Whittney (W)	18	4	1	no
	25s V 49L	Difference	Mann Whittney (W)	14	4	0.3123	no
	25s V 69s	Difference	Mann Whittney (W)	14	4	0.3123	no
	25L V 49s	Difference	Mann Whittney (W)	16	4	0.665	no
	25L V 49L	Difference	Mann Whittney (W)	12	4	0.1124	no
	25L V 69s	Difference	Mann Whittney (W)	13	4	0.1939	no
	49s V 49L	Difference	Mann Whittney (W)	14	4	0.3123	no
	49s V 69s	Difference	Mann Whittney (W)	14	4	0.3123	no
	49L V 69L	Difference	Mann Whittney (W)	18	4	1	no
	All plates	Difference	Kruskal Wallis (H)	3.49	4	0.48	no
Pore size	Pore size at 5L/min	Difference	Mann Whittney (W)	15	5	0.0109	yes
	Pore size at 10L/min	Difference	Mann Whittney (W)	24	5	0.5245	no
	Pore size at 15L/min	Difference	Mann Whittney (W)	34	5	0.2031	no
	Pore size at 20L/min	Difference	Mann Whittney (W)	37	5	0.0539	no
	Overall pore size	Difference	Mann Whittney (W)	410	20	1	no
	Gas hold-up V pore size	Correlation	Spearman Rank (r_s)	-0.018	20	>0.05	no
Pore no.	Pore no. at 5L/min	Difference	Kruskal Wallis (H)	1.4	2	0.497	no
	Pore no. at 10L/min	Difference	Kruskal Wallis (H)	1.4	2	0.497	no
	Pore no. at 15L/min	Difference	Kruskal Wallis (H)	3.6	2	0.166	no
	Pore no. at 20L/min	Difference	Kruskal Wallis (H)	3.6	2	0.166	no
	Overall pore no.	Difference	Kruskal Wallis (H)	3.01	2	0.222	no
	Gas hold-up V pore no.	Correlation	Spearman Rank (r_s)	0.397	20	>0.05	no
Air flow rate	All plates at 5L/min	Difference	Kruskal Wallis (H)	11.1	4	0.026	yes
	All plates at 10L/min	Difference	Kruskal Wallis (H)	11.1	4	0.026	yes
	All plates at 15L/min	Difference	Kruskal Wallis (H)	12.9	4	0.012	yes
	All plates at 20L/min	Difference	Kruskal Wallis (H)	13.5	4	0.009	yes
	All flow rates	Difference	Kruskal Wallis (H)	13.65	3	0.004	yes
	5L/min V 10L/min	Difference	Mann Whittney (W)	16	5	0.0216	yes
	5L/min V 15L/min	Difference	Mann Whittney (W)	15	5	0.0122	yes
	5L/min V 20L/min	Difference	Mann Whittney (W)	15	5	0.0122	yes
	10L/min V 15L/min	Difference	Mann Whittney (W)	21	5	0.2101	no
	10L/min V 20L/min	Difference	Mann Whittney (W)	17	5	0.0367	yes
	15L/min V 20L/min	Difference	Mann Whittney (W)	21	5	0.2101	no
	Gas hold-up V air flow	Correlation	Spearman Rank (r_s)	0.884	20	<0.002	yes

Section 6.2: (ii) Reynolds number (Pages 167 - 168)

Variable	Compare	Relationship	Test statistic	Test Value	d.f.	*p* Value	Significant
Individual sparge plates	25s V 25L	Difference	Mann Whittney (W)	21	4	0.4705	no
	25s V 49s	Difference	Mann Whittney (W)	16	4	0.665	no
	25s V 49L	Difference	Mann Whittney (W)	21	4	0.4651	no
	25s V 69s	Difference	Mann Whittney (W)	14.5	4	0.3836	no
	25L V 49s	Difference	Mann Whittney (W)	15	4	0.4705	no
	25L V 49L	Difference	Mann Whittney (W)	17	4	0.8852	no
	25L V 69s	Difference	Mann Whittney (W)	12	4	0.1124	no
	49s V 49L	Difference	Mann Whittney (W)	21.5	4	0.3836	no
	49s V 69s	Difference	Mann Whittney (W)	16	4	0.665	no
	49L V 69L	Difference	Mann Whittney (W)	13	4	0.1886	no
	All plates	Difference	Kruskal Wallis (H)	4.27	4	0.372	no
Pore size	Pore size at 5L/min	Difference	Mann Whittney (W)	40	5	0.0107	yes
	Pore size at 10L/min	Difference	Mann Whittney (W)	40	5	0.0109	yes
	Pore size at 15L/min	Difference	Mann Whittney (W)	40	5	0.0109	yes
	Pore size at 20L/min	Difference	Mann Whittney (W)	40	5	0.0109	yes
	Overall pore size	Difference	Mann Whittney (W)	610	20	0	yes
	Reynolds No. V pore size	Correlation	Spearman Rank (r_s)	-0.417	20	<0.05	yes
Pore no.	Pore no. at 5L/min	Difference	Kruskal Wallis (H)	2.11	2	0.349	no
	Pore no. at 10L/min	Difference	Kruskal Wallis (H)	2.4	2	0.302	no
	Pore no. at 15L/min	Difference	Kruskal Wallis (H)	2	2	0.368	no
	Pore no. at 20L/min	Difference	Kruskal Wallis (H)	2.4	2	0.308	no
	Overall pore number	Difference	Kruskal Wallis (H)	2.57	2	0.277	no
	Reynolds No. V pore no.	Correlation	Spearman Rank (r_s)	0.322	20	>0.05	no
Air flow rate	All plates at 5L/min	Difference	Kruskal Wallis (H)	4	4	0.407	no
	All plates at 10L/min	Difference	Kruskal Wallis (H)	4	4	0.407	no
	All plates at 15L/min	Difference	Kruskal Wallis (H)	4	4	0.407	no
	All plates at 20L/min	Difference	Kruskal Wallis (H)	4	4	0.407	no
	All flow rates	Difference	Kruskal Wallis (H)	4.27	4	0.372	mo
	5L/min V 10L/min	Difference	Mann Whittney (W)	16.5	5	0.0273	yes
	5L/min V 15L/min	Difference	Mann Whittney (W)	15	5	0.0119	yes
	5L/min V 20L/min	Difference	Mann Whittney (W)	15	5	0.0119	yes
	10L/min V 15L/min	Difference	Mann Whittney (W)	19	5	0.0927	no
	10L/min V 20L/min	Difference	Mann Whittney (W)	16.5	5	0.0278	yes
	15L/min V 20L/min	Difference	Mann Whittney (W)	22.5	5	0.3457	no
	Reynolds No. V air flow	Correlation	Spearman Rank (r_s)	0.848	20	<0.02	yes

Section 6.3: Mass transfer (Pages 168 - 169)

Variable	Compare	Relationship	Test statistic	Test Value	d.f.	*p* Value	Significant
Individual sparge plates	25s V 25L	Difference	Mann Whittney (W)	11	3	1	no
	25s V 49s	Difference	Mann Whittney (W)	7	3	0.1904	no
	25s V 49L	Difference	Mann Whittney (W)	15	3	0.0809	no
	25s V 69s	Difference	Mann Whittney (W)	6	3	0.0809	no
	25L V 49s	Difference	Mann Whittney (W)	6	3	0.0809	no
	25L V 49L	Difference	Mann Whittney (W)	15	3	0.0809	no
	25L V 69s	Difference	Mann Whittney (W)	6	3	0.0809	no
	49s V 49L	Difference	Mann Whittney (W)	15	3	0.0809	no
	49s V 69s	Difference	Mann Whittney (W)	10	3	1	no
	49L V 69L	Difference	Mann Whittney (W)	6	3	0.0809	no
	All plates	Difference	Kruskal Wallis (H)	11.63	4	0.021	yes
Pore size	Overall pore size	Difference	Mann Whittney (W)	40	5	0.0109	yes
	Mass transfer V pore size	Correlation	Spearman Rank (r_s)	-0.866	5	>0.05	no
Pore no.	Overall pore number	Difference	Kruskal Wallis (H)	2	2	0.368	no
	Mass transfer V pore no.	Correlation	Spearman Rank (r_s)	0.542	5	>0.05	no
Salinity	32‰ V 0‰	Difference	Kruskal Wallis (H)	15	4	0.4705	no

Section 6.4: pH control/ CO_2 solubility (Pages 169 - 171)

Variable	Compare	Relationship	Test statistic	Test Value	d.f.	*p* Value	Significant
CO_2 Injection point (see Figure 3.6)	1 V 2	Difference	Mann Whittney (W)	2499	61	0	yes
	1 V 3	Difference	Mann Whittney (W)	4195	61	0.0228	yes
	1 V 4	Difference	Mann Whittney (W)	4780.5	61	0	yes
	1 V 5	Difference	Mann Whittney (W)	4927	61	0	yes
	2 V 3	Difference	Mann Whittney (W)	5152	61	0	yes
	2 V 4	Difference	Mann Whittney (W)	4363	61	0.0017	yes
	2 V 5	Difference	Mann Whittney (W)	4813.5	61	0	yes
	3 V 4	Difference	Mann Whittney (W)	4849	61	0	yes
	3 V 5	Difference	Mann Whittney (W)	5101	61	0	yes
	4 V 5	Difference	Mann Whittney (W)	2742.5	61	0	yes

Section 6.5: Light regime (Pages 172 - 173)

Variable	Compare	Relationship	Test statistic	Test Value	d.f.	*p* Value	Significant
Light source	A V B	Difference	Mann Whittney (W)	100.5	10	0.7613	no
	A V C	Difference	Mann Whittney (W)	71.5	10	0.0124	yes
	A V D	Difference	Mann Whittney (W)	55	10	0.0002	yes
	B V C	Difference	Mann Whittney (W)	74.5	10	0.0233	yes
	B V D	Difference	Mann Whittney (W)	55.5	10	0.0002	yes
	C V D	Difference	Mann Whittney (W)	59.5	10	0.0007	yes
	No tubes V light intensity	Difference	Mann Whittney (W)	0.798	40	<0.02	yes